Soil-Structure Interaction Effects on the Seismic Response of Steel Structures

By

Humam Al-Ghabawi

A thesis submitted to the Graduate Faculty of
Auburn University
in partial fulfillment of the
requirements for the Degree of
Master of Science in Civil Engineering

Auburn, Alabama
Aug 7, 2021

Keywords: Earthquake Engineering, Soil-Structure Interaction, Steel Moment Frame, Buckling Restrained Braced frame

Approved by

Justin D. Marshall, Ph.D., P.E., Chair, Associate Professor of Civil and Environmental Engineering.
Jack Montgomery, Ph.D., Assistant Professor of Civil and Environmental Engineering.
Kadir Sener, Ph.D., P.E., Assistant Professor of Civil and Environmental Engineering.

Abstract

Significant earthquakes are one of the most damaging events for structures. Much research has been done to mitigate the effect of earthquakes on structures. Soil-structure interaction can have a significant impact on the seismic response and gives more realistic results for the structures' seismic response. Previous work has shown that soil-structure interaction could have beneficial or detrimental effects on the seismic response of the structures.

In this study, the seismic response of the three buildings (4-, 8-, and 16-story buildings) with two different lateral force resisting systems (SMF and BRBF) was investigated with the inclusion of the soil-structure interaction using OpenSeesPy. The foundation was modeled using idealized conditions (pin and fixed support) and using the Beam-on-Nonlinear-Winkler-Foundation (BNWF) concept. The soil-structure interaction was considered through modeling springs to represent the soil flexibility. Three types of foundations were considered (isolated, combined, and pile foundation). The same clay soil was utilized for all buildings in this study.

Nonlinear Response history analysis (NRHA) was conducted for a suite of scaled earthquake records. The response was evaluated based on the maximum displacement, residual displacement, maximum drift, residual drift, maximum acceleration, maximum base shear, and the energy dissipation in the BRB element and RBS and columns' springs. The results indicate that the soil-structure interaction has more pronounced effects on the SMF than BRBF and on 4-story than 8-story and 16-story buildings.

In general, the amount of change is not very high to the degree that cause concern. So, it can be concluded that neglecting the soil-structure interaction is acceptable in the BRBF and SMF,

especially in raft foundation case. But in the SMF of the 4-story building it is recommended to include the SSI because it leads to reduction in the floor shear.

Acknowledgment

I want to thank my advisor, Dr. Marshall, for his support and encouragement through my study at Auburn University. His knowledge and skills are valuable to me. I want to thank my co-advisor Dr. Montgomery for all his information and support during the foundation modeling.

A special thanks to my parents and my siblings who supported me through my life to be where I am now. Also, I would like to thank my friend Dr. Wael Baldawi for his continuous support and encouragement since my undergrad. I am glad to have him as my teacher and friend. I want to thank my friend Rania Aziz for all her support, her knowledge and skills in computer are valuable to me.

I want to thank my Fulbright advisors for giving me the opportunity to do my master's degree in the US.

I want to thank all my professors, friends, and classmates at Auburn University for their supports during my life in Auburn.

Table of Contents

Abstract ii

Acknowledgment iv

List of Tables viii

List of Figures xiv

Chapter 1 Introduction 1

1.1 Defining the Problem 1
1.2 Proposed Solution 2
1.3 Scope of Work 2
1.4 Organization of Thesis 3

Chapter 2 Literature Review 4

2.1 background 4
2.2 Types of Soil-Structure Interaction Modeling: 9
2.2.1 Direct Analysis Approach 9
2.2.2 Substructure Approach 10
2.3 Situations Where SSI is Important 11
2.3.1 Building Footprint Area 12
2.3.2 Foundation Embedment 12
2.3.3 Structure-to-Soil Stiffness Ratio 13
2.3.4 Foundation Rocking Impacts Superstructure Behavior 14
2.4 Period Lengthening 15
2.5 Foundation Damping 19
2.6 Summary 23

Chapter 3 Development of the OpenSeesPy Model 24

3.1 Building Description 24

3.2 Load Calculation 32
3.3 Lateral Load Calculations: 34
3.4 Mass Calculations 37
3.5 Modal Analysis of the Center-to-Center model 39
3.6 Footing Design 41
3.6.1 Modeling of Isolated Footing 43
3.6.2 Modeling of Raft Footing 46
3.6.3 Modeling of Pile Foundation 47
3.7 Modeling of the Panel Zone 48
3.8 Reduced Beam Section (RBS) Modeling 50
3.9 Column Modeling 51
3.10 SMF verification 52
3.11 BRB Nonlinear Modeling. 54
3.12 Modal Analysis for the Nonlinear Modeling 56
3.13 Pushover Analysis: 57
3.14 Damping 69
3.15 Earthquake Records 69
3.16 Summary 74
Chapter 4 Results and Discussion of Nonlinear Response History Analysis 75

4.1 Introduction 75
4.2 4-story Building Seismic Response 75
4.2.1 SMF 75
4.2.2 BRBF 88
4.3 8-Story Building Seismic Response 97
4.3.1 SMF 97
4.3.2 BRBF 110
4.4 16-Story Building Seismic Response 119
4.4.1 SMF 119
4.4.2 BRBF 136
4.5 Summary 151
Chapter 5 Summary, Conclusions, and Future Work 155

5.1 Summary 155
5.2 Conclusions 156
5.3 Future Work 158
References 159

Appendix A: Isolated footing modeling routine 164

Appendix B: Raft footing modeling routine 171

Appendix C: Pile foundation modeling routine 184

List of Tables

Table 2.5-1 Soil Hysteretic Damping Ratio, β_s (table 19.3.3 from ASCE/SEI 7-16) 23

Table 3.2-1. Design gravity loads (Harris & Speicher, 2015). 32

Table 3.3-1. ELF for the 4-story building 35

Table 3.3-2. ELF for the 8-story building 35

Table 3.3-3. ELF for the 16-story building 36

Table 3.4-1. A comparison between the calculated effective seismic weight and the effective seismic weight from (Harris & Speicher, 2015) report for the 4-story building. 38

Table 3.4-2. A comparison between the calculated effective seismic weight and the effective seismic weight from (Harris & Speicher, 2015) for the 8-story Building 38

Table 3.4-3. A comparison between the calculated effective seismic weight and the effective seismic weight from (Harris & Speicher, 2015) for the 16-story Building 39

Table 3.5-1. A summary of the vibration periods for the 4-Story Building. 40

Table 3.5-2. A summary of the vibration periods for the 8-Story Building 40

Table 3.5-3. A summary of the vibration periods for the 16-Story Building 40

Table 3.12-1. OpenSeesPy vibration periods for the 4-story building with ideal supports. 56

Table 3.12-2. OpenSeesPy vibration periods for the 8-story building with ideal supports. 57

Table 3.12-3. OpenSeesPy vibration periods for the 16-story building with ideal supports. 57

Table 3.15-1 Earthquake, scale factor, and time step for the 4-story building in both BRBF and SMF directions 70

Table 3.15-2 Earthquake, scale factor, and time step for the 8-story building in both BRBF and SMF directions 70

Table 3.15-3 Earthquake, scale factor, and time step for the 16-story building in both BRBF and SMF directions 71
Table 4.2-1 Difference in maximum story displacement (inch) for the SMF direction of the 4-story building. 77
Table 4.2-2 Difference in residual displacement (inch) for the SMF direction of the 4-story building. 78
Table 4.2-3 Average maximum drift for the SMF direction of the 4-story building. 79
Table 4.2-4 Difference in residual drift for the SMF direction of the 4-story building ($*10^{-3}$). ... 80
Table 4.2-5 Percentage change in maximum total acceleration for the SMF direction of the 4-story building. 82
Table 4.2-6 Percentage change in maximum floor shear/weight for the SMF direction of the 4-story building. 83
Table 4.2-7 Average energy dissipation at the selected RBS springs of the 4-story building. 85
Table 4.2-8 Average of maximum rotation at the selected RBS springs of the 4-story building. 86
Table 4.2-9 Energy dissipation at the selected column springs of the 4-story building. 87
Table 4.2-10 Energy dissipation at the selected column springs of the 4-story building for each earthquake. 87
Table 4.2-11 Average of the maximum rotation at the selected column springs of the 4-story building. 88
Table 4.2-12 Difference in maximum story displacement (inch) at each floor for the BRBF direction of the 4-story building. 89
Table 4.2-13 Difference in residual displacement (inch) for the BRBF direction of the 4-story building. 90

Table 4.2-14 Difference in maximum drift for the BRBF direction of the 4-story building (10*$^{-3}$). 91
Table 4.2-15 Difference in residual drift for the BRBF direction of the 4-story building (*10^{-3}).92
Table 4.2-16 Percentage change in maximum total acceleration for the BRBF direction of the 4-story building. 94
Table 4.2-17 Percentage change in the maximum floor shear/ weight for the BRBF direction of the 4-story building. 95
Table 4.2-18 Percentage of change in the energy dissipation in the BRB elements of the 4-story building. 96
Table 4.2-19 Maximum strain at the selected BRB elements..... 96
Table 4.3-1 Difference in maximum story displacement (inch) for the SMF direction of the 8-story building. 98
Table 4.3-2 Difference in residual displacement (inch) for the SMF direction of the 8-story building. 99
Table 4.3-3 Difference in average maximum drift for the SMF direction of the 8-story building (*10^{-3})..... 100
Table 4.3-4 Difference in residual drift for the SMF direction of the 8-story building (*10^{-3}).. 102
Table 4.3-5 Percentage change in maximum acceleration for the SMF direction of the 8-story building. 103
Table 4.3-6 Percentage change in average floor shear for the SMF direction of the 8-story building. 104
Table 4.3-7 Average energy dissipation at the selected RBS springs of the 8-story building.... 107
Table 4.3-8 Average maximum rotation at the selected RBS springs of the 8-story building. .. 108

Table 4.3-9 Energy dissipation at the selected column springs of the 8-story building. 109
Table 4.3-10 Energy dissipation (kip*in) at the selected column springs of the 8-story building for each earthquake. 109
Table 4.3-11 Percentage change in energy dissipation at the selected column springs of the 8-story building. 110
Table 4.3-12 Maximum rotation at the selected column springs of the 8-story building. 110
Table 4.3-13 Difference in maximum displacement (inch) for the BRBF direction of the 8-story building. 111
Table 4.3-14 Difference in the residual displacement (inch) for the BRBF direction for the 8-story building. 112
Table 4.3-15 Difference in maximum drift for the BRBF direction of the 8-story building (10^{-3}). 113
Table 4.3-16 Difference in residual drift for the BRBF direction of the 8-story building (10^{-3}).115
Table 4.3-17 Percentage change in the maximum acceleration at each floor for the BRBF direction of the 8-story building. 116
Table 4.3-18 change in the base and floor shear for the BRBF direction of the 8-story building. 117
Table 4.3-19 Percentage change in the energy dissipation in the BRB elements of the 8-story building. 119
Table 4.3-20 Maximum strain at the selected BRB elements..... 119
Table 4.4-1 Difference in maximum story displacement (inch) for the SMF direction of the 16-story building. 121

Table 4.4-2 Difference in residual story displacement (inch) for the SMF direction of the 16-story building. 123
Table 4.4-3 Difference in maximum drift for the SMF direction of the 16-story building ($*10^{-3}$). 125
Table 4.4-4 Difference in residual drift for the SMF direction of the 16-story building ($*10^{-3}$). 127
Table 4.4-5 Percentage change in maximum acceleration for the SMF direction of the 16-story building. 129
Table 4.4-6 Percentage change in maximum floor shear for the SMF direction of the 16-story building. 131
Table 4.4-7 Average energy dissipation at the selected RBS springs of the 16-story building.. 133
Table 4.4-8 Average maximum rotation at the selected RBS springs of the 16-story building. 134
Table 4.4-9 Energy dissipation at the selected column springs. 135
Table 4.4-10 Maximum rotation at the selected column springs 136
Table 4.4-11 Difference in the maximum BRBF displacement (inch) of the 16-story building. 138
Table 4.4-12 Difference in residual displacement (inch) of the BRBF direction of the 16-story building. 140
Table 4.4-13 Difference in maximum drift of the BRBF direction of 16-story building ($*10^{-3}$). 142
Table 4.4-14 Percentage change in residual drift of the BRBF direction of the 16-story building. 144
Table 4.4-15 Percentage of change in maximum total story acceleration of the BRBF direction of the 16-story building. 146

Table 4.4-16 Percentage of change in maximum story shear of the BRBF direction of the 16-story building. 148

Table 4.4-17 Percentage change in the energy dissipation in the BRB elements of the 16-story building. 150

Table 4.4-18 Maximum strain at the selected BRB elements..... 150

List of Figures

Figure 2.1-1: Illustration of inertial SSI effects on spectral acceleration (base shear) associated with period lengthening and change in damping (NIST, 2012)..... 5

Figure 2.1-2. The significant impact of the soil flexibility on a coupled braced frame system (FEMA, 2018)..... 6

Figure 2.1-3. Foundation types that were considered in Raychowdhury's study (Raychowdhury, 2011). 7

Figure 2.2-1. Schematic illustration of a direct analysis of soil-structure interaction using continuum modeling by finite elements (NIST, 2012). 10

Figure 2.2-2. Schematic illustration of a substructure approach to perform an analysis of soil-structure interaction using either: (i) rigid foundation; or (ii) flexible foundation assumptions (NIST, 2012). 11

Figure 2.3-1. Building footprint area example (FEMA, 2020). 12

Figure 2.3-2 Foundation embedment example (FEMA, 2020)..... 13

Figure 2.3-3 The significant impact of soil flexibility on a reinforced concrete shear wall system (FEMA, 2020). 15

Figure 2.4-1 Example of acceleration and displacement spectra (FEMA, 2020). 16

Figure 2.4-2 Design Response Spectrum (Adopted from (ASCE, 2017a)). 19

Figure 3.1-1. Isometric view of the 4-story archetype building (Bldg. ID: MB4). 25

Figure 3.1-2. Isometric view of the 8-story archetype building (Bldg. ID: MB8). 26

Figure 3.1-3. Isometric view of the 16-story archetype building (Bldg. ID: MB16). 27

Figure 3.1-4. Typical floor framing plan for the 4- and 8-story archetype buildings(Speicher & Harris, 2020). 28
Figure 3.1-5. Typical floor framing plan for the 16-story archetype building (Speicher & Harris, 2020). 28
Figure 3.1-6. BRBF and SMF elevations for the 4-story Building (Speicher & Harris, 2020) and (Harris & Speicher, 2015). 29
Figure 3.1-7. BRBF and SMF elevations for the 8-story Building (Speicher & Harris, 2020)and (Harris & Speicher, 2015). 29
Figure 3.1-8. BRBF and SMF elevations for the 16-story Building (Speicher & Harris, 2020) and (Harris & Speicher, 2015). 30
Figure 3.2-1. A tributary area for W14X22 beams (Speicher & Harris, 2020). 33
Figure 3.2-2. A tributary area for the main girders (Speicher & Harris, 2020). 34
Figure 3.4-1. Tributary areas of some side and middle nodes in the plane. 37
Figure 3.6-1. Plan view of the 4- and 8-story foundation system. 42
Figure 3.6-2. Isometric for the 8- story building foundation system. 42
Figure 3.6-3. Isometric for the 16- story building foundation system. 43
Figure 3.6-4. An isometric view showing the spring distribution under an isolated footing. 45
Figure 3.6-5. A top view for the tributary area around the grid elements 46
Figure 3.6-6. An isometric view showing the spring distribution under the raft footing. 47
Figure 3.6-7. An isometric view showing the pile group, pile cap, and spring distribution. 48
Figure 3.7-1. Panel zone example. 49
Figure 3.7-2. An isometric view that shows how the panel zone is connected to the other elements. 50

Figure 3.8-1 Typical beam model in the SMF. 51
Figure 3.9-1 Typical column model in the SMF 52
Figure 3.10-1 Model assemblage in OpenSeesPy 53
Figure 3.10-2 Comparison between the OpenSeesPy results and the experimental results (Popov et al., 1997). 54
Figure 3.11-1 conceptual behavior of BRB element. 55
Figure 3.11-2. Comparison of BRB inelastic model to experimental results from data reported in (Merritt et al., 2003)(Star Seismic) and (Newell et al., 2006) (CoreBrace). 55
Figure 3.11-3 BRBF brace-to-beam / column subassembly analytical schematic. 56
Figure 3.13-1. Pushover curve in the SMF direction for the 4-Story building. 58
Figure 3.13-2. Plastic hinges development sequence for the OpenSeesPy, PDelta, Idealized and Flexible support analysis of the 4-story building (Bold are the idealized foundation result, nonbold are the flexible foundation result). 59
Figure 3.13-3. Pushover curve in the SMF direction for the 8-Story building. 60
Figure 3.13-4. Plastic hinges development sequence for the OpenSeesPy, PDelta, Idealized and the Flexible support analysis of the 8-story building (Bold are the idealized foundation result, nonbold are the flexible foundation result). 61
Figure 3.13-5. Pushover curve in the SMF direction for the 16-Story building. 62
Figure 3.13-6.Plastic Hinges development sequence for the OpenSeesPy, PDelta, Idealized support analysis of the 16-story building. 63
Figure 3.13-7. Pushover curve in the BRBF direction for the 4-Story building. 64
Figure 3.13-8. BRB yielding sequence for the OpenSeesPy, PDelta, Idealized and Flexible support analysis of the 4-story building. 65

Figure 3.13-9. Pushover curve in the BRBF direction for the 8-Story building..... 65
Figure 3.13-10. BRB yielding sequence for the OpenSeesPy, PDelta, Idealized support analysis of the 8-story building..... 66
Figure 3.13-11. Pushover curve in the BRBF direction for the 16-Story building..... 67
Figure 3.13-12. BRB yielding sequence for the OpenSeesPy, PDelta, Idealized and flexible support analysis of the 16-story building..... 68
Figure 3.15-1 Scaled earthquakes for the 4-story building in the SMF and BRBF direction..... 72
Figure 3.15-2 Scaled earthquakes for the 8-story building in the SMF and BRBF direction..... 72
Figure 3.15-3 Scaled earthquakes for the 16-story building in the SMF direction..... 73
Figure 3.15-4 Scaled earthquakes for the 16-story building in the BRBF direction. 73
Figure 4.2-1 Average of maximum displacements for the SMF direction of the 4-story building. 76
Figure 4.2-2 Average residual displacement for the SMF direction of the 4-story building..... 77
Figure 4.2-3 Average maximum drift for the SMF direction of the 4-story building. 79
Figure 4.2-4 Average residual drift for the SMF direction of the 4-story building..... 80
Figure 4.2-5 Average maximum total acceleration for the SMF direction of the 4-story building. 81
Figure 4.2-6 Average maximum floor shear and base shear for the SMF direction..... 83
Figure 4.2-7 Selected RBS for energy calculation in the SMF direction of the 4-story building. 85
Figure 4.2-8 Selected column springs for the 4-story building. 87
Figure 4.2-9 Maximum average displacement BRBF direction 89
Figure 4.2-10 Average residual deformation in the BRBF direction of the 4-story building..... 90
Figure 4.2-11 Average of the maximum drift for the BRBF direction of the 4-story building.... 91

Figure 4.2-12 Average of the residual drift for the BRBF direction of the 4-story building..... 92
Figure 4.2-13 average maximum roof acceleration for the BRBF direction of the 4-story building. 93
Figure 4.2-14 Average maximum shear force for the BRBF direction of the 4-story building. .. 94
Figure 4.2-15 Selected BRB element for dissipated energy calculations. 96
Figure 4.3-1 Average of the maximum displacement for the SMF direction of the 8-story building. 97
Figure 4.3-2 Average residual displacement for the SMF direction of the 8-story building. 99
Figure 4.3-3 Average maximum drift for the SMF direction of the 8-story building. 100
Figure 4.3-4 Average residual drift for the SMF direction of the 8-story building. 101
Figure 4.3-5 Average maximum acceleration for the SMF direction. 103
Figure 4.3-6 Average maximum floor shear and base shear for the SMF direction of the 8-story building. 104
Figure 4.3-7 Selected RBS for energy calculation in the SMF direction of the 8-story building. 106
Figure 4.3-8 Selected column's springs for the SMF of the 8-story building. 109
Figure 4.3-9 Average maximum displacement for the BRBF direction of the 8-story building. 111
Figure 4.3-10 Average residual displacement for the BRBF direction of the 8-story building.. 112
Figure 4.3-11 Average of the maximum drift for the BRBF direction of the 8-story building. . 113
Figure 4.3-12 Average of the residual drift for the BRBF direction of the 8-story building..... 114
Figure 4.3-13 Average maximum roof acceleration for the BRBF direction of the 8-story building. 115
Figure 4.3-14 Average maximum shear force for the BRBF direction of the 8-story building. 117

Figure 4.3-15 Selected BRB elements for dissipated energy calculations for the 8-story building. 118
Figure 4.4-1 Average of the maximum displacement for the SMF direction of the 16-story building. 120
Figure 4.4-2 Average residual story displacement for the SMF direction of the 16-story building. 122
Figure 4.4-3 Average maximum drift for the SMF direction of the 16-story building. 124
Figure 4.4-4 Average residual drift for the SMF direction of the 16-story building. 126
Figure 4.4-5 Average maximum acceleration for the SMF direction of the 16-story building.. 128
Figure 4.4-6 Average maximum floor shear and base shear for the SMF direction of the 16-story building. 130
Figure 4.4-7 Selected RBS for energy calculation in the SMF direction of the 16-story building. 132
Figure 4.4-8 Selected column's springs. 135
Figure 4.4-9 Average maximum displacement BRBF direction of the 16-story building..... 137
Figure 4.4-10 Average residual displacement of the BRBF direction of the 16-story building. 139
Figure 4.4-11 Average maximum drift of the BRBF direction of the 16-story building..... 141
Figure 4.4-12 Average residual drift of the BRBF direction of the 16-story building. 143
Figure 4.4-13 average maximum total story acceleration for the BRBF of the 16-story building. 145
Figure 4.4-14 Average maximum story shear of the BRBF direction of the 16-story building. 147
Figure 4.4-15 Selected BRB elements for dissipated energy calculations. 149

Chapter 1 Introduction

1.1 Defining the Problem

The current building code's primary goal is to design buildings and structures to provide the required life safety. Most current seismic design is built upon the assumption of the idealized foundation. This assumption can be conservative in certain cases and unsafe in others. Therefore, including soil-structure interaction in seismic analysis is essential because it gives more realistic results, which in turn allows for more safe and economic structures. The effects of soil-structure interaction can be very significant on the structure's behavior during earthquakes. Additionally, soil-structure interaction can affect the structure's energy dissipation capability. The current design codes like ASCE/SEI 7-16 (ASCE, 2017a) and ASCE/SEI 41-17 (2017b) allow practicing engineers to include or neglect the effects of soil-structure interaction during design.

Including soil-structure interaction in the design is important. However, the effect of soil-structure interaction is not fully understood. It is not included in the curriculum most of civil engineering schools, so practicing engineers are not very familiar with soil-structure interaction behavior. Soil-structure interaction behavior depends on many factors, like the stiffness of the structure, the soil properties, and the foundation type, which make it a complex topic to be understood.

1.2 Proposed Solution

This research aims to provide more information and results about the effect of soil-structure interaction on the structure's seismic response to help understand the behavior of the structure and the foundation during earthquakes with the presence of the soil flexibility. A three-dimensional model with different lateral force-resisting systems in each orthogonal direction, explicit modeling of the foundation stiffness, and the soil stiffness using the Beam-on-Nonlinear-Winkler-Foundation (BNWF) approach has been done in this study. Two different lateral systems (steel special moment frame and buckling restrained braced frame) were selected to assess the impact of the lateral system on the impact of soil-structure interaction. Nonlinear Response History Analysis (NRHA) was conducted to capture the effect of soil-structure interaction on the structure's seismic response.

1.3 Scope of Work

The seismic response of structures is significantly affected by soil-structure interaction (SSI). The impact of the soil-structure interaction can be positive or negative, which depends on the stiffness of the structure, stiffness and type of the foundation, and the soil's stiffness. For that reason, three buildings (4-, 8-, and 16-story) were adopted to study the effect of the soil-structure interaction on the structure's seismic response. The buildings used in this study were designed for a previous research effort as case study buildings and had been designed in accordance with the appropriate design codes and reference standards.

The Open System for Earthquake Engineering Simulation (OpenSees) framework, python version (OpenSeesPy), was used to build a 3D nonlinear analysis model for the three buildings with and without the foundations modeled explicitly. NRHA for a suite of earthquakes was conducted to examine the effect of soil-structure interaction on the structure's seismic response

including acceleration, velocity, displacement and structural actions. In addition, the effect on the hysteretic response of the lateral system elements and residual deformation of the structure was examined.

1.4 Organization of Thesis

Chapter 1 introduces this research by defining the problem, introducing the proposed solution, and discussing the work scope and the approach used during this research.

Chapter 2 includes an extensive literature review designed to provide background on the previous research on soil-structure interaction to enable a thorough understanding of the conceptual changes and improvements undertaken in this study.

Chapter 3 presents an overview of the prototype buildings and the lateral force-resisting systems. Information about the special steel moment frame (SMF) and buckling restrained brace frame (BRBF) modeling in OpenSeesPy is presented. Verification of the structural analysis model is presented in this chapter.

Chapter 4 presents the results of the dynamic analysis to a suite of earthquakes. The effects of soil-structure interaction on the structure's response, including acceleration, displacement, element hysteretic response, and residual deformation are presented.

Chapter 5 summarizes the research and provides recommendations for future studies.

Chapter 2 Literature Review

2.1 background

Soil-structure interaction has been a highly researched topic over the last few decades. It leads to a more realistic dynamic response of structural response. However, it is not commonly used by practicing engineers. Soil-structure interaction (SSI) or soil foundation structure interaction (SFSI) refers to the overall effects of the response of the structure, the foundation, and the soil below and around the foundation (NIST, 2012). The soil's seismic response directly affects the structure's seismic response, such as the displacement, the residual displacement, the drift, residual drift, the acceleration, vibration period, and the structure's damping. Soil-structure interaction has three general effects: (1) increasing the vibration period of the structure compared to the vibration period of the rigid base structure, (2) dissipating part of the vibration energy by the wave radiation into foundation medium, (3) modifying the base motion of the structure in comparison to free-field motion (Jennings & Bielak, 1973). Some studies indicate that increasing the vibration period does not always decrease the demands (Mylonakis & Gazetas, 2000), meaning that neglecting SSI is not always a conservative assumption.

Much research has been done to investigate the effect of SSI on the structure's seismic behavior. Some research reported a beneficial effect where the SSI enhances the structure's seismic behavior, like decreasing the displacement, the residual displacement, the drift, and the acceleration, while others reported detrimental effects where the SSI worsens the structure's seismic behavior, like increasing the displacement, the residual displacement, the drift, and the acceleration. As illustrated below.

In general, the SSI effect increases the period of vibration by decreasing the overall stiffness of the structure, thereby reducing the base shear. However, there is a particular case

where including the SSI increases the base shear. This occurs if the vibration period of the structure is small. Including the effect of SSI increases the period of vibration, which causes climbing up the acceleration spectrum, thereby increasing the base shear. Figure 2.1-1 shows how the increase in vibration period affects the base shear demands. This case appears in low-rise buildings (Dutta et al., 2004).

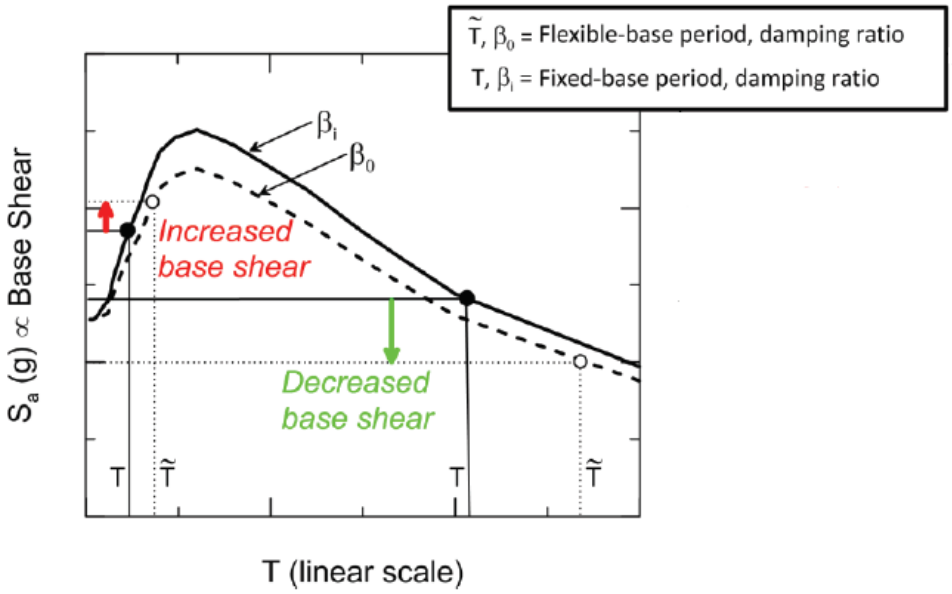

Figure 2.1-1: Illustration of inertial SSI effects on spectral acceleration (base shear) associated with period lengthening and change in damping (NIST, 2012)

When the structure is stiff relative to the soil, including the SSI can have a more pronounced effect on the structure's seismic response. Conversely, SSI effects are less apparent on the structure's seismic response when the soil is relatively stiff related to the structure (FEMA, 2020).

Including SSI can change the structure's behavior, especially for structures with concentrated coupled vertical and lateral force resistance (FEMA, 2020). Figure 2.1-2 shows that there is more stress on the braces in the fixed base case; thereby, the flexible base case has more capability to resist the lateral force.

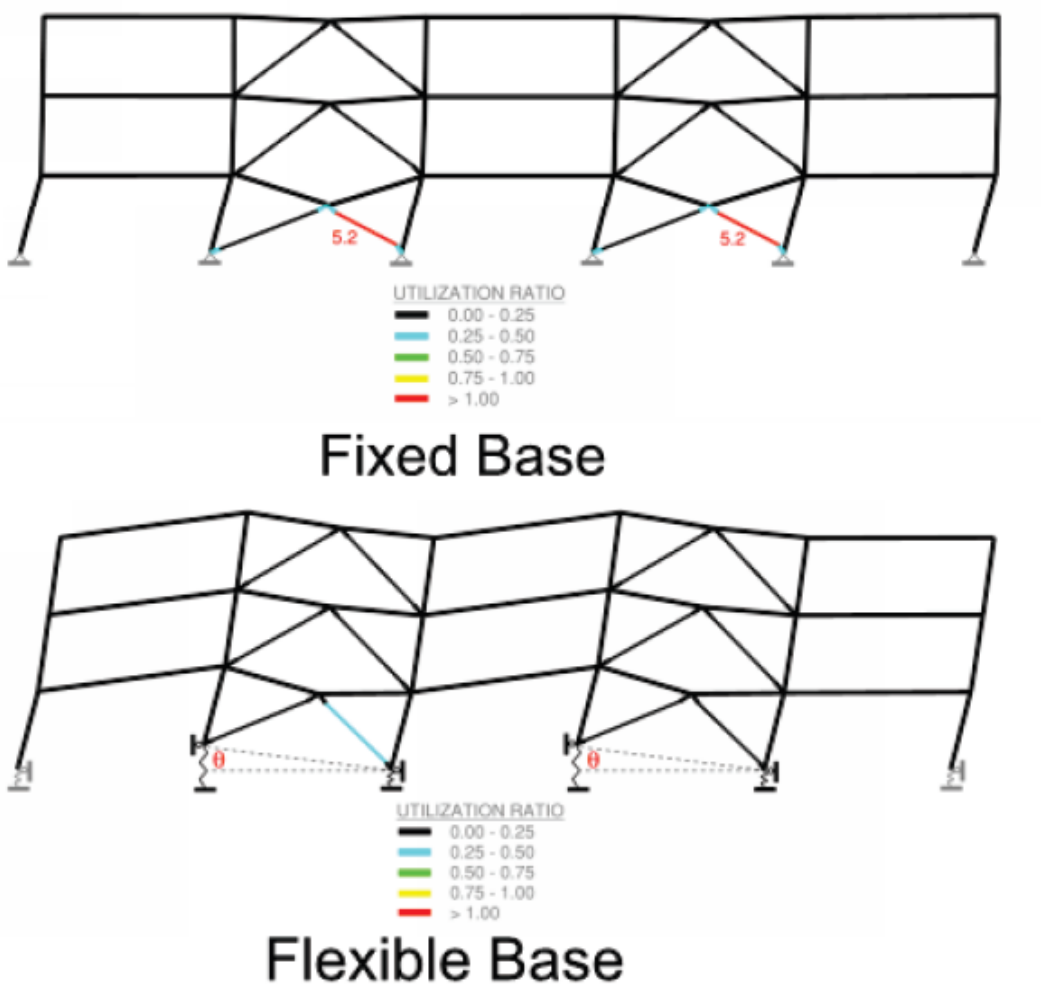

Figure 2.1-2. The significant impact of the soil flexibility on a coupled braced frame system (FEMA, 2018).

SSI does not only affect the deformation and the demands of the earthquake, it also affects the damping. Damping of structures resting on flexible foundations is affected by SSI in two ways: (1) the structure gains damping through energy dissipation in soil, and (2) the damping the structure would have on a rigid foundation is reduced (Novak & Hifnawy, 1983). Veletsos and Meek (1974) describe the principal effects of interaction as reducing the resonant frequency of the structure and to modifying its effective damping. The net result may be a reduction or increase in the structure's maximum deformation.

Raychowdhury (2011) studied the effect of nonlinear soil-structure interaction on the seismic response of a four-story steel moment-resisting frame structure by using the beam-on-nonlinear-Winkler-foundation (BNWF) approach to model the footing. The study states that the force and displacement demands were reduced significantly when the foundation nonlinearity is included. Raychowdhury used OpenSees in his study and considered different cases of foundation: (1) fixed base, (2) elastic Winkler-based SSI model, and (3) nonlinear Winkler-based SSI model. Figure 2.1-3 shows the different types of the foundation that were considered in Raychowdhury's study.

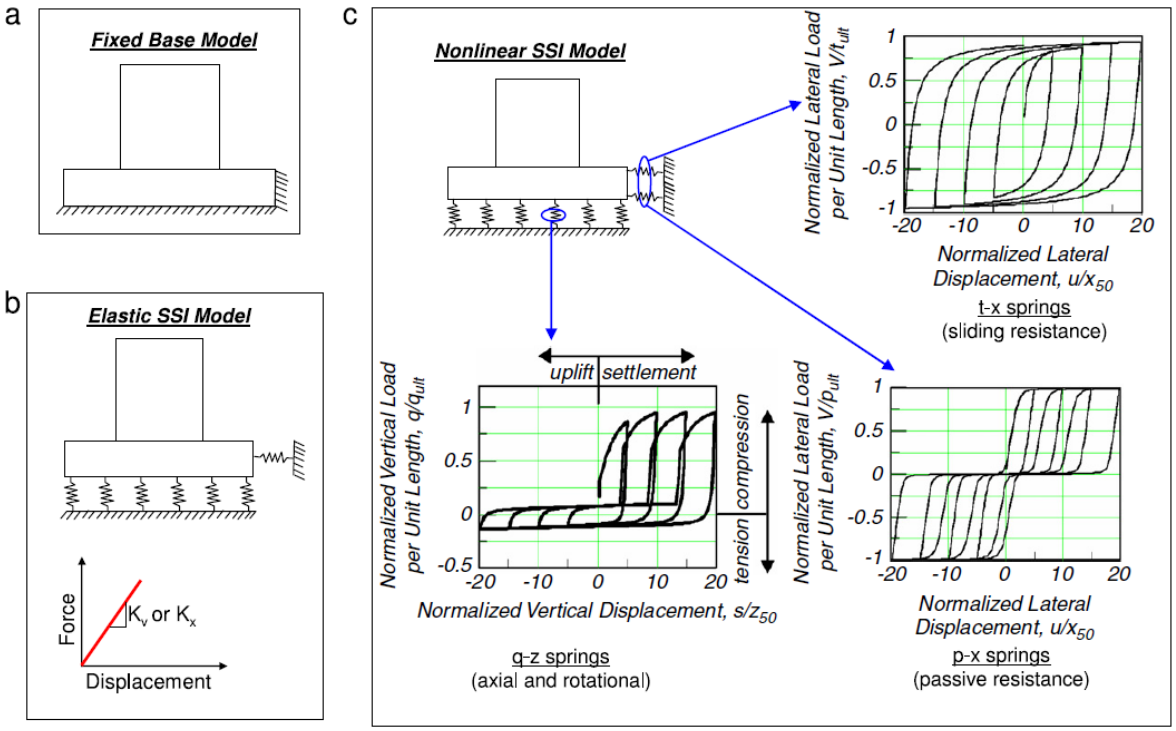

Figure 2.1-3. Foundation types that were considered in Raychowdhury's study (Raychowdhury, 2011).

Tabatabaiefar et al. (2013) did an investigation on the effect of the SSI on the reinforced concrete (RC) moment-resistant frame of a 10-story building. Three types of soil (Ce, De, and Ee, according to the Australian Standard) were adopted in this study. The results indicate that soil class

Ce's effect on the structure's behavior is minimal, while the soil classes De's and Ee's effects are significant. That indicates that neglecting the SSI for soil classes De and Ee results in a nonconservative design of RC moment-resisting frames. The same results were reported in Fatahi et al. (2011), except a fifteen-story building was used in this study.

Lu et al. (2016) did a parametric study to investigate the effect of SSI on the seismic performance of a multi-story shear building. The effects of soil stiffness, design lateral load pattern, fundamental period, number of stories, structure slenderness ratio, and site condition were investigated in this study. The results indicated that the strength and ductility demand can be reduced by up to 60%, which depends significantly on the slenderness ratio and ductility demands.

Vivek and Raychowdhury (2020) did an experimental study on 3 and 6-story steel moment-resisting frame structures and did numerical modeling using OpenSees. The results showed a reduction in the roof acceleration and column moments and an increase in the structure deformation, period of vibration, and the damping.

Hokmabadi et al. (2015) did an experimental study on three buildings (5, 10, 15-story) supported by a pile group. The results showed an increase in the building's lateral displacement due to the rocking of the piles. The effect of SSI also changed the performance level of the structure to near collapse or even collapse levels in performance-based design methods.

Ismail et al. (2020) investigated the effect of SSI on midrise structures. Based on their results, the structures were divided into two categories depending on the number of stories: (1) 5<=N<=10 and (2) 10<=N<=15. The SSI effect was beneficial for the first category and detrimental for the second category.

In conclusion, the effect of SSI can significantly increase or decrease the demands of the earthquake on the structure. Incorporating the SSI in the design of the new buildings or analysis of an existing building is essential. The research presented above shows that the effect of SSI is more significant in the soft soil case rather than the stiff soil. Also, piles have a more detrimental effect on the seismic response of the structure. The impact of SSI depends on many factors, like the soil's stiffness, the stiffness and size of the foundation, and the structure.

2.2 Types of Soil-Structure Interaction Modeling:

There are two primary methods to incorporate and evaluate the soil effects on structures' behavior during earthquakes. They are the direct analysis and the substructure approach.

2.2.1 Direct Analysis Approach

In this approach, the structure, the foundation, and the soil are explicitly modeled using the finite element method. The soil elements should be extended below and around the structure's limits to capture the soil behavior. The earthquake excitation should be at the boundary of the soil. Thereby the soil is excited, and in turn, will excite the structure. Figure 2.2-1 shows a schematic drawing of the direct analysis approach. Because of the high computational effort it requires, it is not preferred in practice. It is typically only undertaken on large, critical projects like nuclear power plants or large infrastructure projects such as major bridges, tunnels, subway stations, tanks, and marine structures, and requires specialist expertise (FEMA, 2020). Direct analyses can address all of the SSI effects described above, but incorporation of kinematic interaction is challenging because it requires specification of spatially variable input motions in three dimensions. Evaluation of site response using wave propagation analysis through the soil is important to this approach. Such analyses are most often performed using an equivalent linear representation of soil properties in finite element, finite difference, or boundary element numerical formulations.

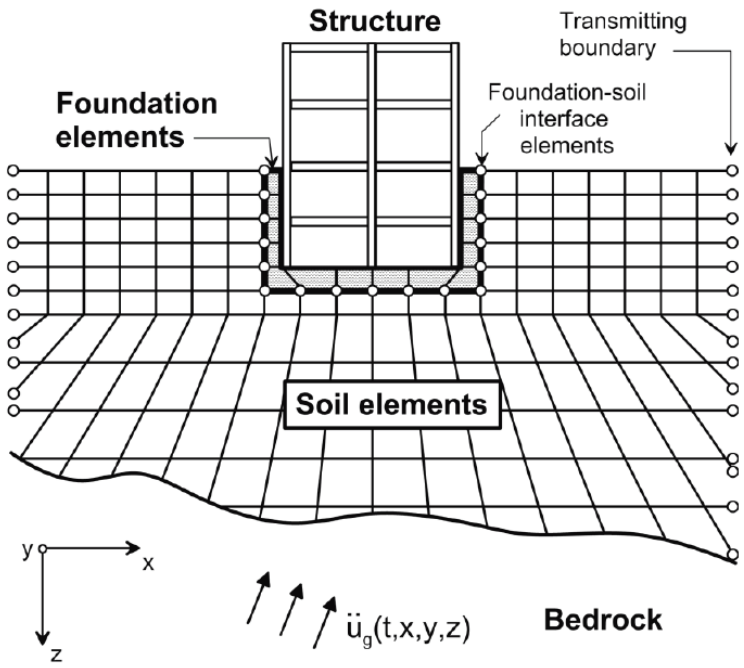

Figure 2.2-1. Schematic illustration of a direct analysis of soil-structure interaction using continuum modeling by finite elements (NIST, 2012).

2.2.2 Substructure Approach

In this approach, the soil is represented by using springs. The springs can be oriented vertically to capture the vertical settlement and the rotation of the footing or oriented vertically and horizontally to capture horizontal displacement as well. Dampers can be included to capture foundation damping (FEMA, 2020). Figure 2.2-2 shows a schematic of using the substructure approach to analyze soil-structure interaction using either: (i) rigid foundation; or (ii) flexible foundation assumptions.

Proper consideration of SSI effects in a substructure approach requires: (i) an evaluation of free-field soil motions and corresponding soil material properties; (ii) an evaluation of transfer functions to convert free-field motions to foundation input motions; (iii) incorporation of springs and dashpots (or more complex nonlinear elements) to represent the stiffness and damping at the soil foundation interface; and (iv) a response analysis of the combined structure spring/ dashpot system with the foundation input motion applied.a

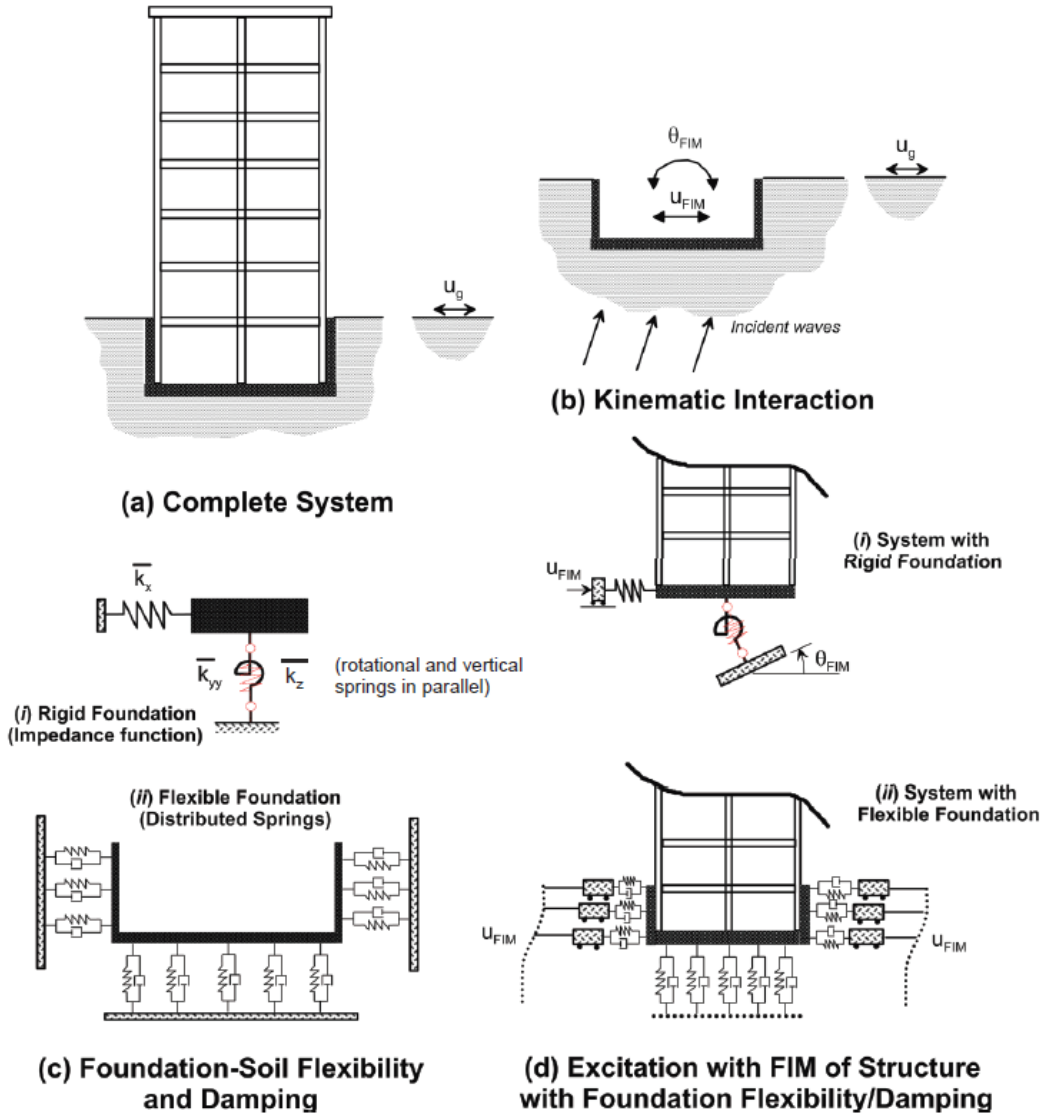

Figure 2.2-2. Schematic illustration of a substructure approach to perform an analysis of soil-structure interaction using either: (i) rigid foundation; or (ii) flexible foundation assumptions (NIST, 2012).

2.3 Situations Where SSI is Important

FEMA P-2091 (FEMA, 2020) summarizes the situations where implementing the effect of SSI is important. A brief discussion about those cases is presented below.

2.3.1 Building Footprint Area

The building footprint size effect is more pronounced in the shorter period range. The larger the building footprint, the greater the reduction in short period spectral response. Figure 2.3-1 shows the illustration of this case. The building on the left with the larger footprint size will have lower design forces than the building with the smaller footprint on the right.

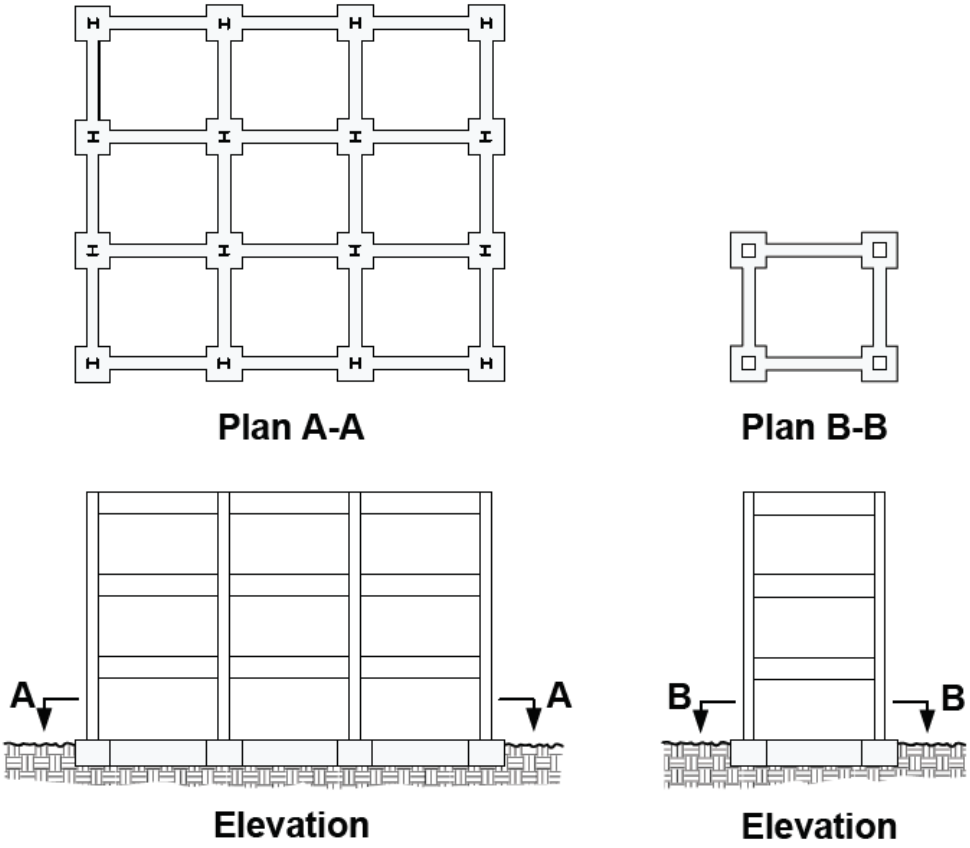

Figure 2.3-1. Building footprint area example (FEMA, 2020).

2.3.2 Foundation Embedment

Foundation embedment has been shown to correlate with spectral demands, primarily in the shorter period range. Typically, the deeper the embedment, the greater the reduction in short period spectral response. This is due to the decrease of ground motion amplitudes with depth, which is a typical feature of site response (FEMA, 2020). Figure 2.3-2 shows the illustration of

this case. The building on the left with a deeper foundation embedment will typically have a greater reduction in design forces than the building on the right.

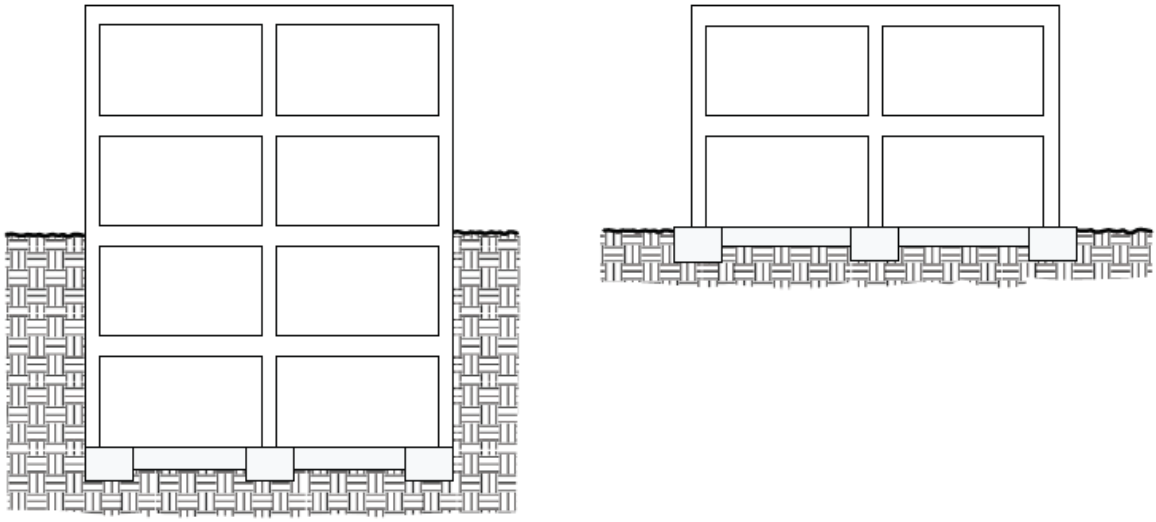

Figure 2.3-2 Foundation embedment example (FEMA, 2020).

2.3.3 Structure-to-Soil Stiffness Ratio

When the structure is relatively stiff compared to the soil, foundation rotation and translation relative to the free-field motion can occur, adding to structural displacements and increasing or lengthening the structure's fundamental period. The increase in period can affect the associated spectral accelerations used in the design. This effect commonly occurs in buildings with a concentrated lateral force-resisting system, such as reinforced concrete shear walls and steel braced frames that are supported on localized foundation elements on flexible soils. Conversely, for a building with wide, stiff foundations on very stiff soils and relatively flexible superstructures, the impact of soil flexibility on the building response is typically relatively small.

2.3.4 Foundation Rocking Impacts Superstructure Behavior

Introducing SSI can change the structure's behavior. Certain elements can have different deformation, and the distribution of the demands is different. Figure 2.1-2 shows a frame with concentrated lateral force resisting system. The figure shows force demand on the brace in the flexible foundation case is less than the idealized foundation case.

Figure 2.3-3 shows a reinforced concrete cantilever shear wall coupled to an adjacent gravity frame of beams and columns (FEMA, 2020). The upper figure shows that a stiff, strong foundation system (represented as a fixed-base condition) can reduce superstructure displacement and protect the adjacent frame from damage, but damage will concentrate in the shear wall base. The lower figure has a more flexible foundation system, which leads to rocking of the shear wall. This increases displacement and damage in the adjacent frame but potentially reduces damage to the shear wall.

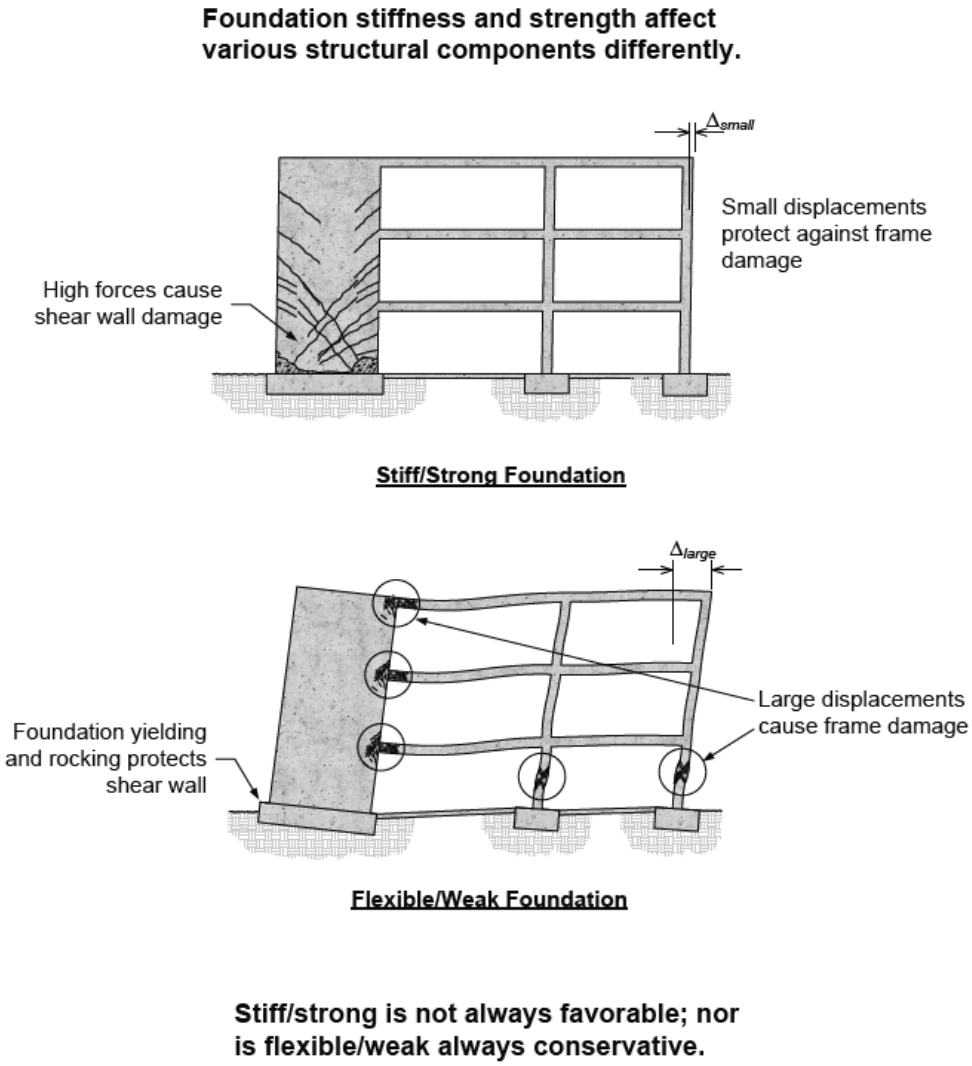

Figure 2.3-3 The significant impact of soil flexibility on a reinforced concrete shear wall system (FEMA, 2020).

2.4 Period Lengthening

Including the foundation flexibility always increases the structure's vibration period and increases the percentage of mass participation factor in the vibration mode. The ratio of the vibration period with a flexible foundation to the vibration period with an idealized foundation is called period lengthening. Increasing the vibration period affects both the spectral displacement and the spectral acceleration. The spectral displacement is increased with the vibration period's increase, and the spectral acceleration is increased or decreased with the increase of the vibration

period. Figure 2.4-1 shows an example of the effect of period lengthening on the acceleration and displacement spectra. Increasing the vibration period increases both the acceleration and the displacement response of building X, while decreasing the acceleration response and increasing the displacement response of building Y (FEMA, 2020).

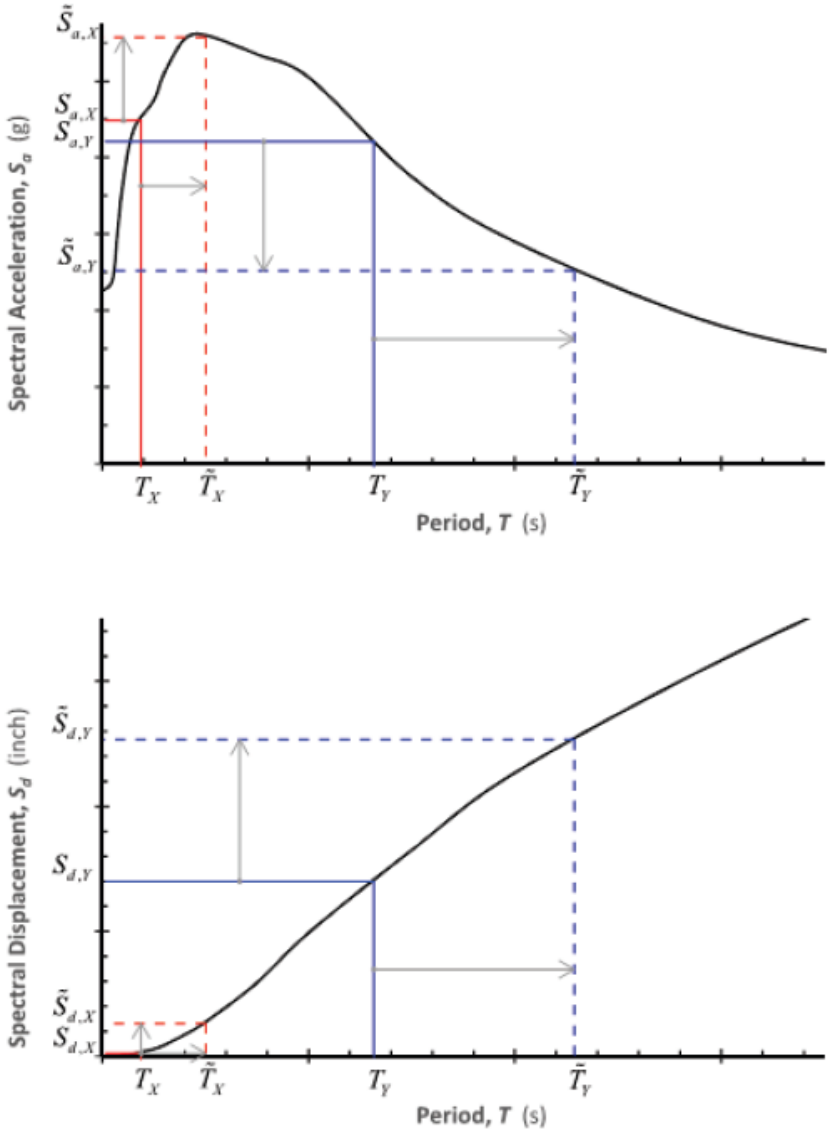

Figure 2.4-1 Example of acceleration and displacement spectra (FEMA, 2020).

Period lengthening also affects the seismic demands. ASCE/SEI 7-16 (ASCE, 2017a) chapter 19 presents a procedure to adjust the seismic design procedures for soil-structure

interaction. Section 19.2.1 presents the adjustment for the Equivalent Lateral Force Procedure by calculating base shear adjustment ΔV, $\Delta v = \left[C_s - \frac{\widetilde{C_s}}{B_{ssI}}\right] \bar{w}$.

Where:

C_s = the seismic response coefficient calculated assuming idealized foundation.

$\widetilde{C_s}$= the seismic response coefficient calculated assuming flexible foundation.

B_{SSI} = the factor to adjust the design response spectrum and MCE_R response spectrum.

W = weight caused by the effective modal mass.

The reduction in the base shear is limited in ASCE/SEI 7-16 because of the limited understanding of how the effects of SSI interact with the R factor. The limited base shear is calculated as follows:

$$\tilde{V} = V - \Delta V \geq \alpha V \qquad \text{(ASCE 7-16 Eq. 19.2-1)}$$

$$\alpha = \begin{cases} 0.7 & \text{for } R \leq 3 \\ 0.5 + R/15 & \text{for } 3 < R < 6 \\ 0.9 & \text{for } R \geq 6 \end{cases} \qquad \text{(ASCE 7-16 Eq. 19.2-3)}$$

Where:

$\tilde{V}$ = the base shear adjusted for soil-structure interaction.

V = the fixed-base structure base shear computed in accordance with ASCE/SEI 7-16 Section 12.8.

α = the coefficient that accounts for the reduction in base shear caused by foundation damping SSI.

R = the response modification coefficient.

Section 19.2.2 presents the adjustment for the Linear Dynamic Analysis. ASCE/SEI 7-16 implements SSI in the Linear Dynamic Analysis by modifying the spectral response acceleration $\tilde{s}_a$ using the BSSI factor as follows. β_0 is defined in section 2.5. T_0, T_S, T_L are defined in Figure 2.4-2.

$T_0 = 0.2*S_{D1}/S_{DS}$

$T_S = S_{D1}/S_{DS}$

T_L = long-period transition period(s) shown in Figs. 22-14 through 22-17 in (ASCE, 2017a).

T = the fundamental period of the building.

$$\tilde{S}_a = \left[\left(\frac{5}{B_{SSI}} - 2\right) \times \frac{T}{T_S} + 0.4\right] \times S_{DS}$$

for $0 < T < T_0$, and

$$\tilde{S}_a = S_{DS}/B_{SSI} \quad \text{for } T_0 \le T \le T_S, \quad \text{and}$$

$$\tilde{S}_a = S_{D1}/(B_{SSI}T), \quad \text{for } T_S < T \le T_L, \quad \text{and}$$

$$\tilde{S}_a = S_{D1}T_L/(B_{SSI}T^2), \quad \text{for } T > T_L$$

$$B_{SSI} = 4/[5.6 - \ln(100\beta_0)]$$

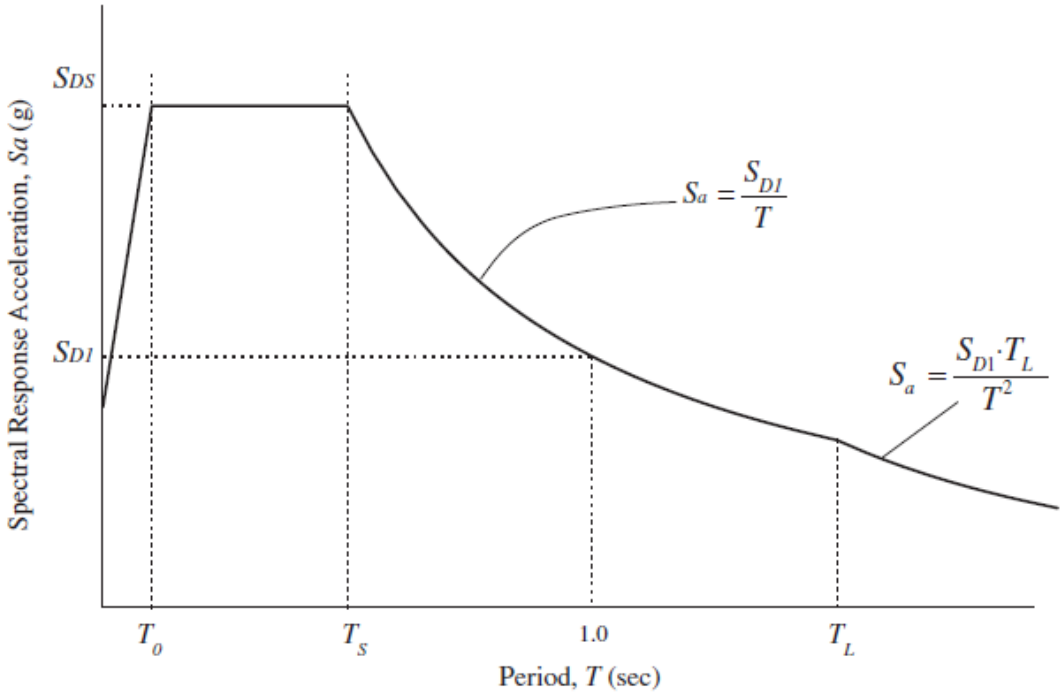

Figure 2.4-2 Design Response Spectrum (Adopted from (ASCE, 2017a)).

2.5 Foundation Damping

Foundation damping consists of two main factors: soil damping and radiation damping. Soil damping is the hysteretic (material) damping of the soil. It is similar to inherent viscous damping in the superstructure, but it is independent of the structure's flexible-base period (FEMA, 2020). Radiation damping is the damping in the soil-structure system caused by the generation and propagation of waves away from the foundation, which is caused by dynamic displacements of the foundation relative to the free-field displacements (FEMA, 2020). Foundation damping is presented in ASCE/SEI 7-16 section 19.3. Foundation damping is represented in ASCE/SEI 7-16 by the Effective Damping Ratio as follows:

$$\beta_0 = \beta_f + \frac{\beta}{\left(\tilde{T}/T\right)^2_{eff}} \leq 0 \cdot 20$$

Where:

β_f = effective viscous damping ratio relating to the foundation–soil interaction.

β= effective viscous damping ratio of the structure, taken as 5% unless otherwise justified by analysis; and

$\left(\tilde{T}/T\right)_{eff}$ = effective period lengthening ratio defined as $\left(\frac{\tilde{T}}{T}\right)_{\text{eff}} = \left\{1 + \frac{1}{\mu}\left[\left(\frac{\tilde{T}}{T}\right)^2 - 1\right]\right\}^{0.5}$ (19.3-2)

μ = expected ductility demand

The foundation damping ratio caused by soil hysteretic damping and radiation damping, β_f , is calculated as follows $\beta_f = \left[\frac{(\tilde{T}/T)^2 - 1}{(\tilde{T}/T)^2}\right]\beta_s + \beta_{rd}$ (19.3-3)

Where:

β_s= soil hysteretic damping ratio determined in accordance with section 19.3.5, and

β_{rd}= radiation damping ratio determined in accordance with Section 19.3.3 or 19.3.4

Radiation damping (β_{rd}) for rectangular foundations is calculated as follows:

$$\beta_{\text{rd}} = \frac{1}{(\tilde{T}/T_y)^2}\beta_y + \frac{1}{(\tilde{T}/T_{xx})^2}\beta_{xx} \qquad (19.3\text{-}5)$$

$$T_y = 2\pi\sqrt{\frac{M^*}{K_y}} \tag{19.3-6}$$

$$T_{xx} = 2\pi\sqrt{\frac{M^*(h^*)^2}{\alpha_{xx}K_{xx}}} \tag{19.3-7}$$

$$K_y = \frac{GB}{2-\nu}\left[6.8\left(\frac{L}{B}\right)^{0.65} + 0.8\left(\frac{L}{B}\right) + 1.6\right] \tag{19.3-8}$$

$$K_{xx} = \frac{GB^3}{1-\nu}\left[3.2\left(\frac{L}{B}\right) + 0.8\right] \tag{19.3-9}$$

$$\beta_y = \left[\frac{4(L/B)}{(K_y/GB)}\right]\left[\frac{a_0}{2}\right] \tag{19.3-10}$$

$$a_0 = \frac{2\pi B}{\tilde{T}v_s} \tag{19.3-11}$$

$$\beta_{xx} = \left[\frac{(4\psi/3)(L/B)a_0^2}{\left(\frac{K_{xx}}{GB^3}\right)\left[\left(2.2-\frac{0.4}{(L/B)^3}\right)+a_0^2\right]}\right]\left[\frac{a_0}{2\alpha_{xx}}\right] \tag{19.3-12}$$

$$\psi = \sqrt{\frac{2(1-\nu)}{(1-2\nu)}} \leq 2.5 \tag{19.3-13}$$

$$\alpha_{xx} = 1.0 - \left[\frac{(0.55 + 0.01\sqrt{(L/B)-1})a_0^2}{\left(2.4-\frac{0.4}{(L/B)^3}\right)+a_0^2}\right] \tag{19.3-14}$$

Where:

M* = effective modal mass for the fundamental mode of vibration in the direction under consideration.

h* = effective structure height taken as the vertical distance from the foundation to the centroid of the first mode shape for multistory structures. Alternatively, h* is permitted to be approximated as 70% of the total structure height for multistory structures or as the full height of the structure for one-story structures.

L = half the larger dimension of the base of the structure.

B = half the smaller dimension of the base of the structure.

v_s = the average effective shear wave velocity over a depth of B below the base of the structure determined using v_{so} and Table 19.3-1 or a site-specific study.

v_{so} = the average low strain shear wave velocity over a depth of B below the base of the structure.

G = effective shear modulus derived or approximated based on G_0 and Table 19.3-2.

$G_0 = \gamma v_{so}^2/g$, the average shear modulus for the soils beneath the foundation at small strain levels.

γ = the average unit weight of the soils over a depth of B below the base of the structure.

ν = Poisson's ratio; it is permitted to use 0.3 for sandy and 0.45 for clayey soils.

Soil damping is calculated from table 19.3-3 from ASCE/SEI 7-16.

Table 2.5-1 Soil Hysteretic Damping Ratio, β_s (table 19.3.3 from ASCE/SEI 7-16)

	Effective Peak Acceleration, $S_{DS}/2.5$[a]			
Site Class	$S_{DS}/2.5=0$	$S_{DS}/2.5=0.1$	$S_{DS}/2.5=0.4$	$S_{DS}/2.5 \geq 0.8$
C	0.01	0.01	0.03	0.05
D	0.01	0.02	0.07	0.15
E	0.01	0.05	0.20	[b]
F	[b]	[b]	[b]	[b]

[a] Use straight-line interpolation for intermediate values of $S_{DS}/2.5$.
[b] Site-specific geotechnical investigation and dynamic site response analyses shall be performed.

2.6 Summary

In this chapter, a general review of the previous work is presented to understand the research that has already been done on this topic along with a brief discussion about the methodology of SSI modeling. The methods of SSI modeling are the direct analysis method and the substructure method. To get a clearer picture of the SSI, a summary of where the SSI is expected to impact the seismic response significantly is presented. Finally, a brief summary of how the ASCE/SEI 7-16 account for the SSI impact on the base shear, period lengthening, and foundation damping is presented.

Chapter 3 Development of the OpenSeesPy Model

3.1 Building Description

In this study, three buildings with different heights (4-, 8- and 16-stories) were modeled in OpenSeesPy. The buildings were designed by NIST according to the International Building Code 2012 (IBC) (Speicher & Harris, 2018). Two types of lateral resisting systems were used to resist the earthquake forces. The first one is a special moment frame (SMF) that works in the east-west (E-W) direction, and the second is a buckling restrained braced frame (BRBF) that works in the north-south (N-S) direction. Those lateral force resisting systems (LFRS) are placed at the perimeter of the building. The SMF information is found in NIST Technical Note 1863-1 (Harris & Speicher, 2015). The information for the BRBF is found in (Speicher & Harris, 2018). The building's floor system consists of steel wide flange sections, metal deck, and 3.25-inches light-weight concrete thickness. The building has a façade along the perimeter. Figure 3.1-1, Figure 3.1-2, and Figure 3.1-3 show isometric views of the three buildings. Figure 3.1-4 shows the typical floor system of the 4- and 8-story buildings. Figure 3.1-5 shows the typical floor system of the 16-story building. Figure 3.1-6, Figure 3.1-7, and Figure 3.1-8 show the BRBF and the SMF elevations of the buildings.

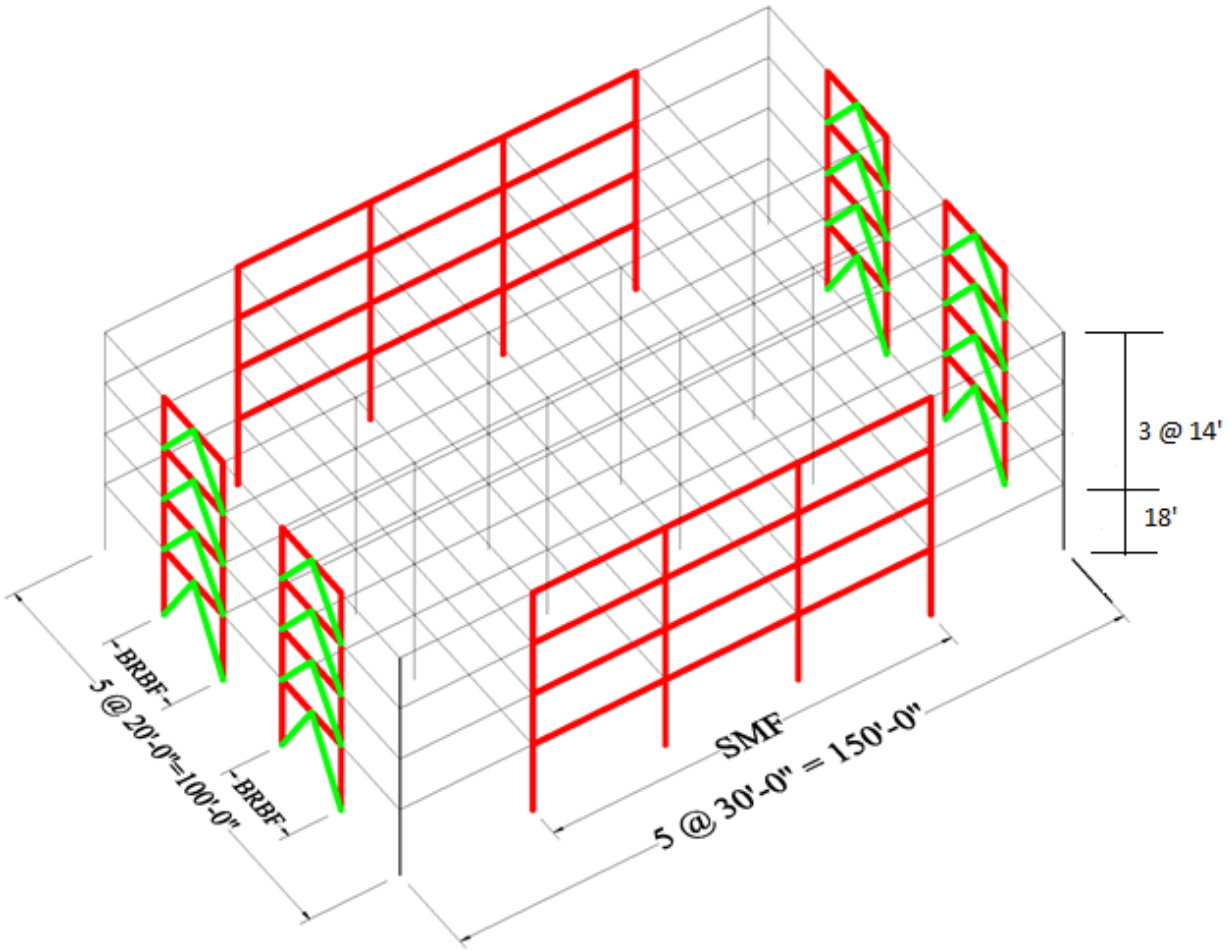

Figure 3.1-1. Isometric view of the 4-story archetype building (Bldg. ID: MB4).

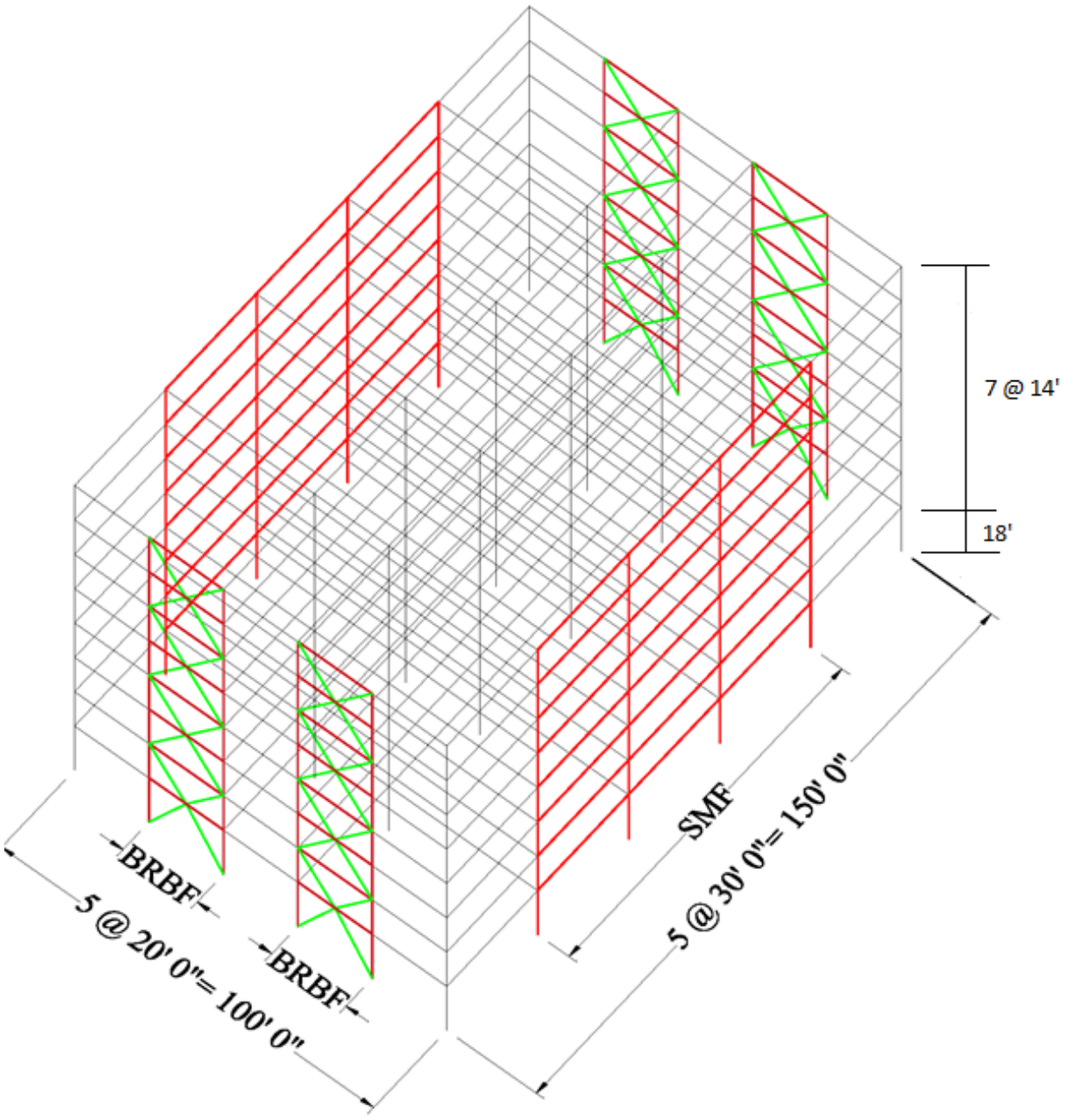

Figure 3.1-2. Isometric view of the 8-story archetype building (Bldg. ID: MB8).

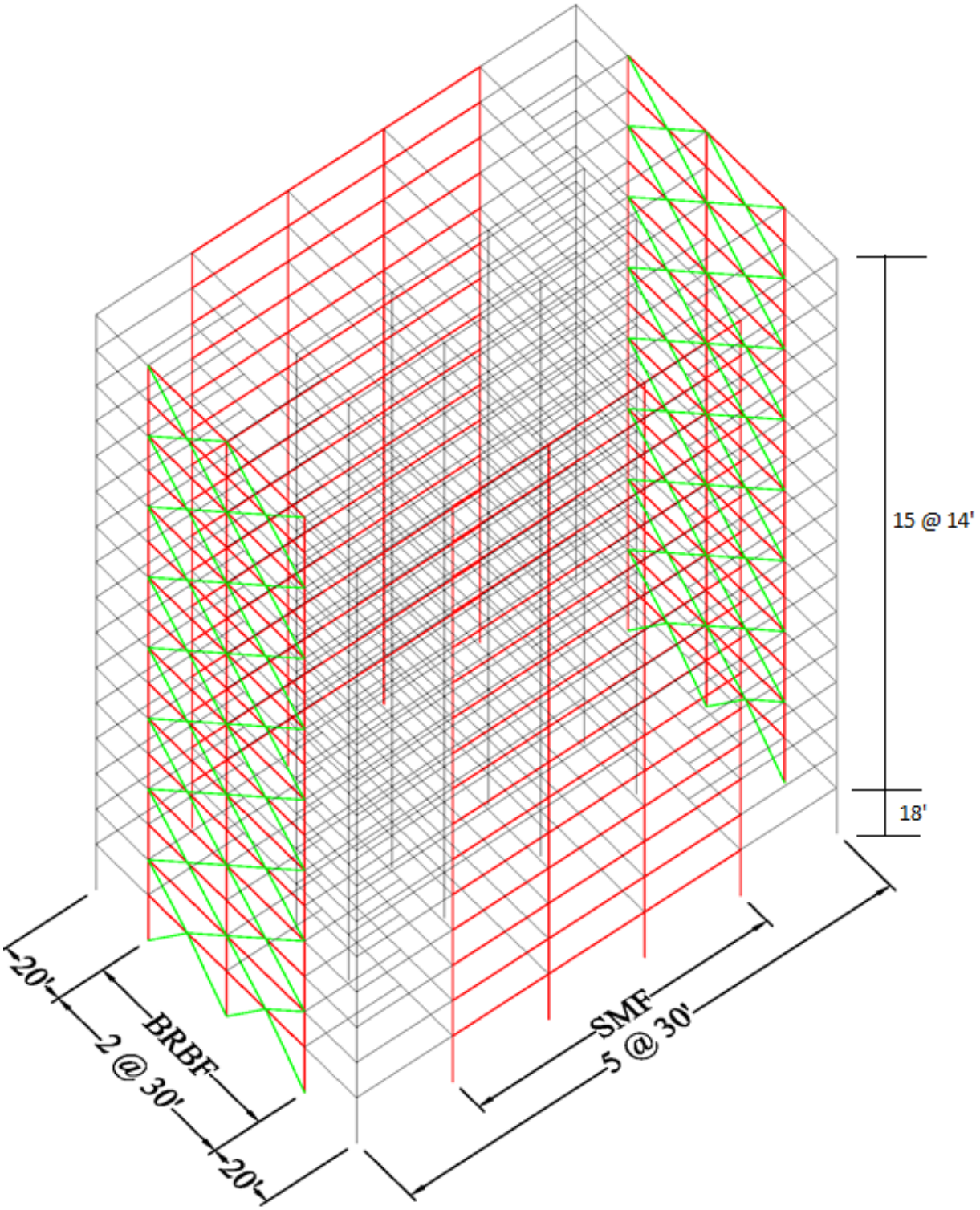

Figure 3.1-3. Isometric view of the 16-story archetype building (Bldg. ID: MB16).

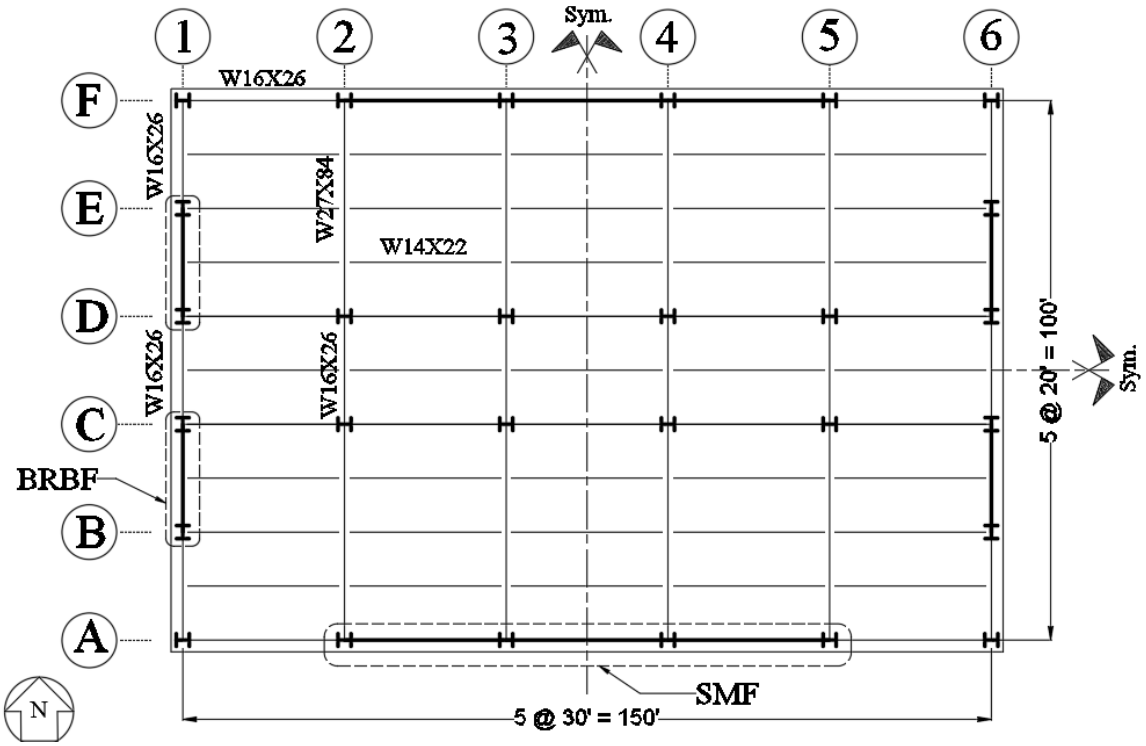

Figure 3.1-4. Typical floor framing plan for the 4- and 8-story archetype buildings(Speicher & Harris, 2020).

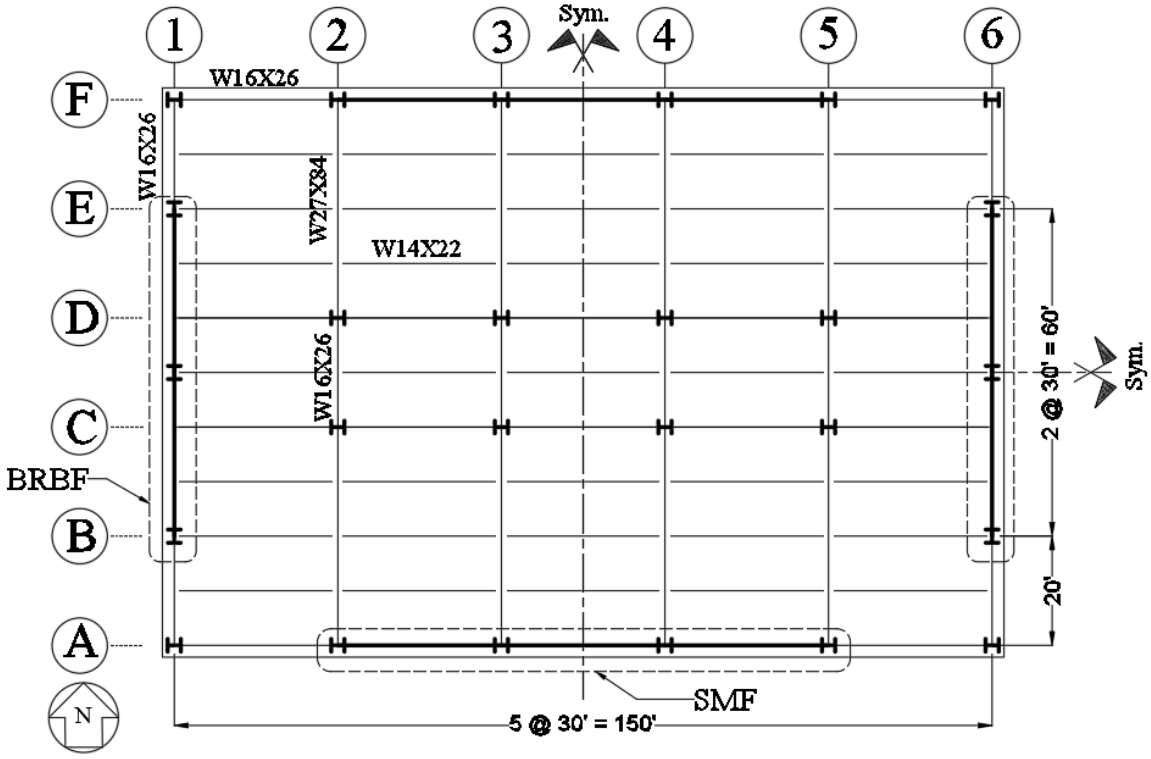

Figure 3.1-5. Typical floor framing plan for the 16-story archetype building (Speicher & Harris, 2020).

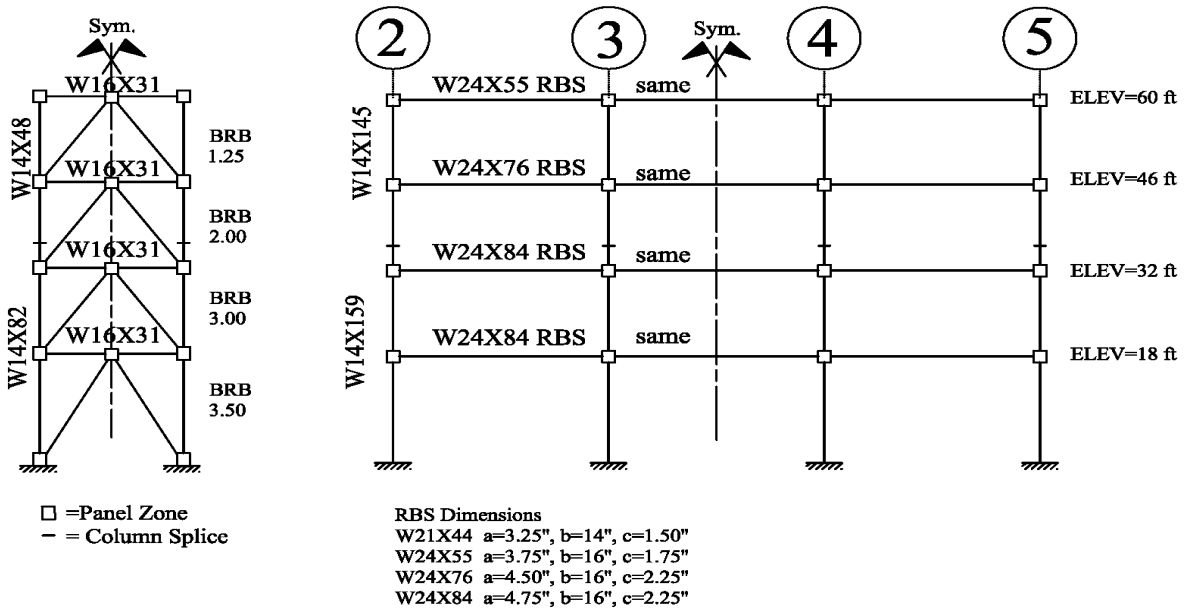

Figure 3.1-6. BRBF and SMF elevations for the 4-story Building (Speicher & Harris, 2020) and (Harris & Speicher, 2015).

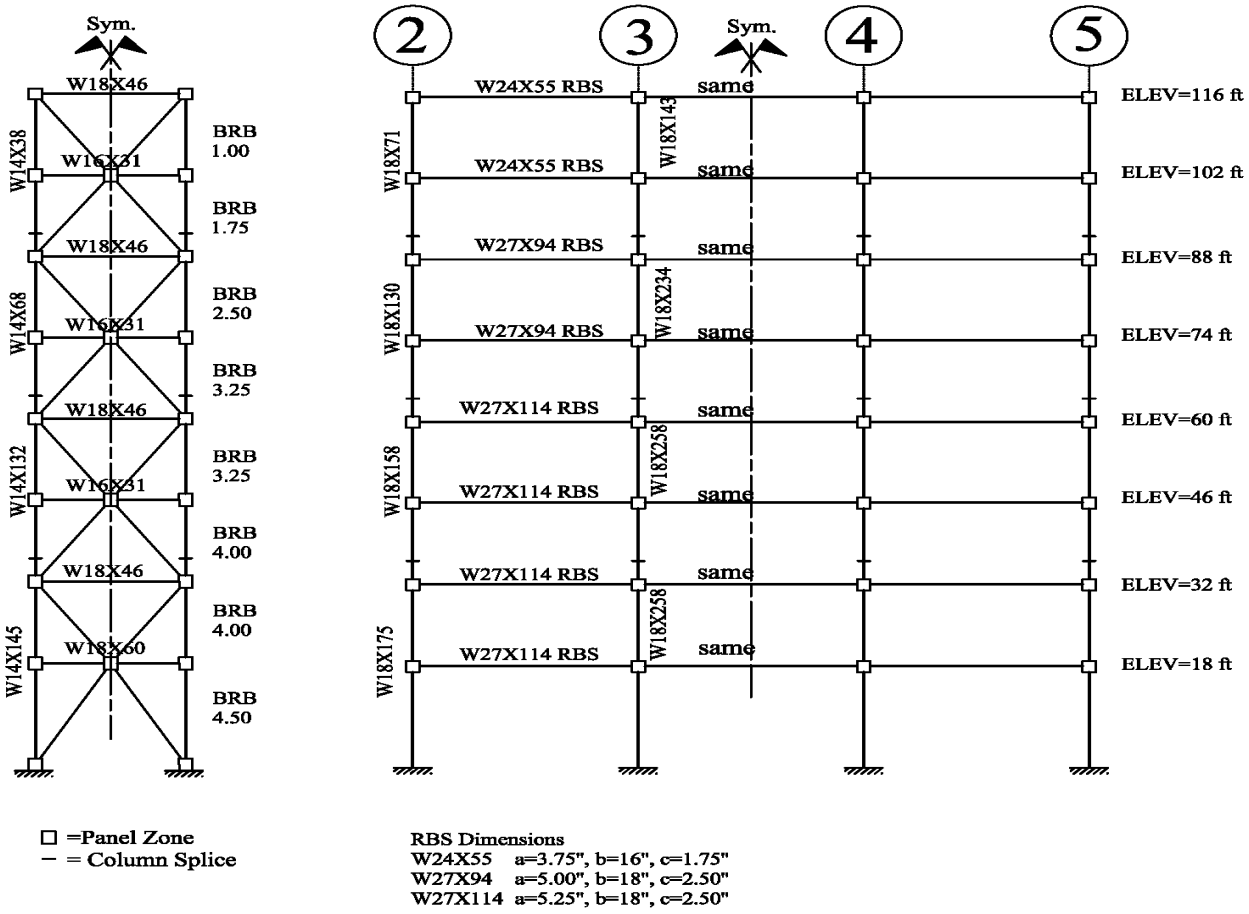

Figure 3.1-7. BRBF and SMF elevations for the 8-story Building (Speicher & Harris, 2020)and (Harris & Speicher, 2015).

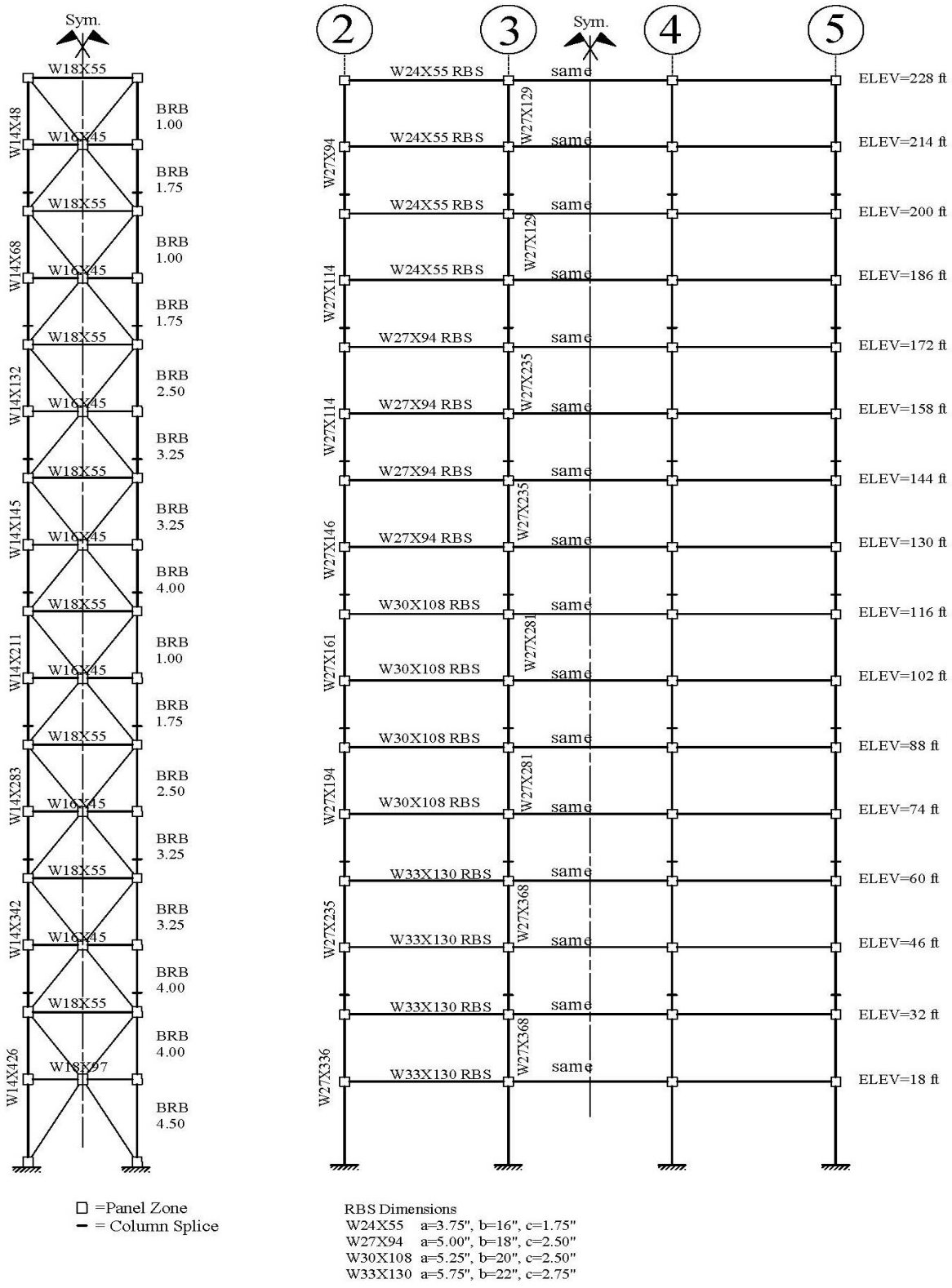

Figure 3.1-8. BRBF and SMF elevations for the 16-story Building (Speicher & Harris, 2020) and (Harris & Speicher, 2015).

Two programs were used for modeling, SAP2000 and OpenSeesPy. Each building was modeled two times. The first model was constructed using the center-to-center methodology, where the center of the beam is connected directly to the center of the column. In the second model, the panel zone, the reduced beam section (RBS), and the columns' lumped plasticity were added to the model to capture the structure's inelastic response in the SMF direction. The inelastic response in the BRBF direction was captured by using a fiber section to model the BRBF's columns. More information about the panel zone's modeling methodology, reduced beam section (RBS), lumped plasticity of the columns, and fiber section of the BRBF's columns are presented later in this paper. The interior columns and beams were the same in both the first and the second model. The interior beams and girders were modeled using elastic beam-column elements. The interior and the BRBF beam-column connections were modeled as a pinned connection, While the SMF beam-column connections were modeled as a rigid connection using the panel zone. The beams attached to the BRB were modeled as continuous beams at the BRB and beam connection. The BRB's were modeled as a truss element with modified stiffness in both SAP2000 and OpenSeesPy. The BRB's modified stiffness is equal to the BRB core elastic stiffness (Es) times the modification factor (KF). The average modification factor (KF) was found to be 1.48 (Speicher & Harris, 2018).

The supports that are part of the lateral force resisting system (SMF and BRBF) were modeled as fixed (Moment resisting) in the primary load resistance direction of the SMF or BRBF and as pin (No moment resistance) in the direction that is perpendicular to the primary load resistance direction of the SMF or BRBF. All the other supports that are not part of the lateral force resisting system were modeled as pin support.

3.2 Load Calculation

The floor dead load consists of the steel members' self-weight, metal deck, and 3.25 inches of light-weight concrete. In addition, 20% of the live load was used to account for the weight of partitions. Table 3.2-1shows a summary of all types of dead and live load.

Table 3.2-1. Design gravity loads (Harris & Speicher, 2015).

Load	Load Type	Magnitude
Dead, D	Dead	46 psf [1]
Floor Superimposed Dead, SD	Dead	15 psf
Roof Superimposed Dead, SD	Dead	10 psf
Façade Dead (Curtain Wall), SD	Dead	250 plf
Unreduced Design Floor Live, L_o	Floor Live	50 psf (Office)
Unreduced Design Roof Live, L_o	Roof Live	30 psf [2]

[1] Weight of slab and metal deck only. Self-weight of steel components are included automatically in the structural analysis.
[2] 10 psf was added to the roof live load to represent non-inertial service equipment weight.

According to AISC 7 -16, the effective seismic weight for computing the earthquake forces is equal to dead load + superimposed dead load + 20% of the live load. This load combination was used to calculate the linear distributed load for each beam and the mass for each node using the tributary area method, as explained in the following:

Load calculation for the roof:

Total Dead Load = Dead Load + Roof Superimposed Dead Load

To calculate the element's linear distributed load, a tributary area was assigned to the W14X22 beams to calculate the linear distributed load along the W14X22 beams. Then the beam's linear distributed load converted to an equivalent linear distributed load on the girders. W14x22 beams that are located between the main grids were omitted from the model. However, the effect of their weight was considered. The procedure below shows how the load per each girder was calculated. Figure 3.2-1shows how the tributary area was taken around the W14X22 beams.

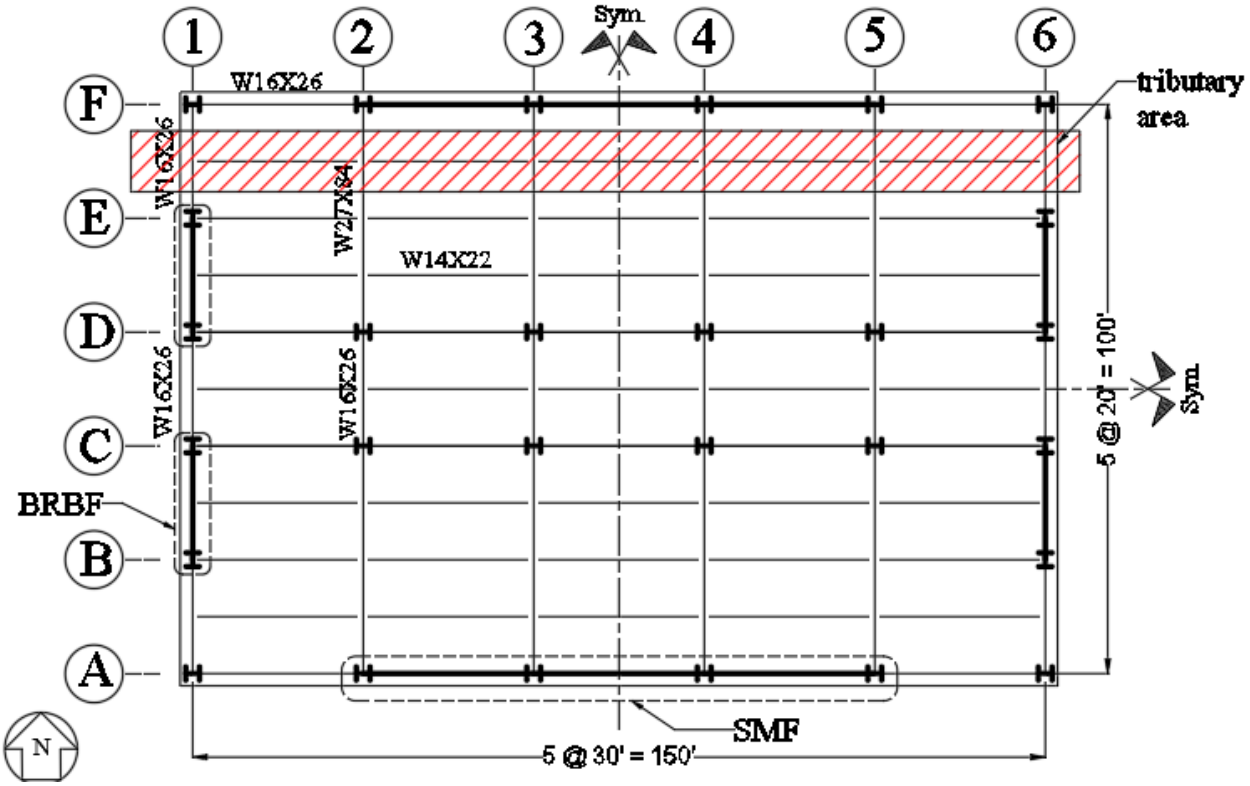

Figure 3.2-1. A tributary area for W14X22 beams (Speicher & Harris, 2020).

A tributary area with width (W) equal to 10 ft was assigned around W14x22 beams. The linear distributed load for each W14x22 was calculated according to the following equation:

W14x22 Total Dead Load= W14x22 Self-Weight + W* (Superimposed Dead Load + Dead Load)

The load of those beams transferred to the main girder. The reactions of the simply supported beams act as point reactions on the girders. Those point reactions have been modeled as linear distributed load on the girders (W_{girder}).

Example of the calculation of the total dead load acting on girder W27x84.

Self-weight of W27x84 girder designate as (W_G).

Total Dead Load on W27x84 Girder = W_G + W14x22 Total Dead Load*(30 ft/2) * the number of W14x22 beams action on the girder *2.

The columns' self-weight was directly assigned to the columns as linearly distributed axial load along the columns. The weight of the cladding is assigned to the beams and girders around the perimeter. Figure 3.2-2 shows how the tributary area is assigned around the internal girders.

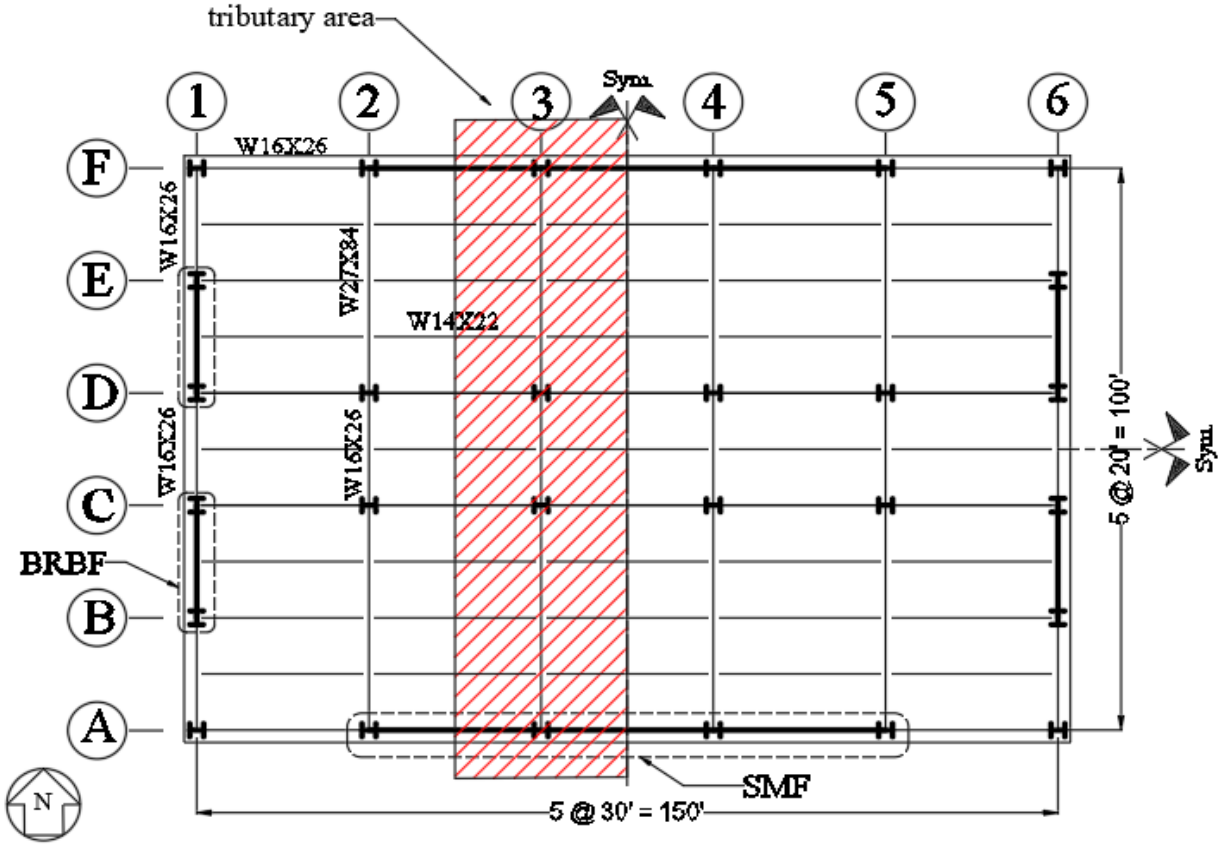

Figure 3.2-2. A tributary area for the main girders (Speicher & Harris, 2020).

3.3 Lateral Load Calculations:

The three buildings' lateral forces were computed according to the equivalent lateral force (ELF) method from ASCE 7- 16 Section 12.8. Table 3.3-1,

Table 3.3-2, Table 3.3-3 show the calculation of ELF forces.

Table 3.3-1. ELF for the 4-story building

BRBF

T (Second)= 0.99 V (kip)= 426 k= 1.245

Floor	W (kip)	h (ft)	$W*h^k$	C_{vx}	Fx (kip)
R (4)	1095	60	179148.2	0.366	156.0
3	1345	46	158072.3	0.323	137.7
2	1359	32	101655.6	0.208	88.5
1	1377	18	50320.88	0.103	43.8
∑	5176		489196.9	1	426

SMF

T (Second)= 1.77 V (kip)= 374 k= 1.635

Floor	W (kip)	h (ft)	$W*h^k$	C_{vx}	Fx (kip)
R (4)	1095	60	884486.9	0.414	154.9
3	1345	46	703608.9	0.329	123.2
2	1359	32	392771.2	0.184	68.8
1	1377	18	155347.6	0.073	27.2
∑	5176		2136215	1	374

Table 3.3-2. ELF for the 8-story building

BRBF

T (Second)= 2.01 V (kip)= 531 k= 1.755

Floor	W (kip)	h (ft)	$W*h^k$	C_{vx}	F_x (kip)
R (9)	1084	116	4551484.345	0.242	128.36
8	1328	102	4449296.792	0.236	125.48
7	1346	88	3480263.682	0.185	98.15
6	1355	74	2584883.435	0.137	72.90
5	1364	60	1800817.966	0.096	50.79
4	1368	46	1132990.04	0.060	31.95
3	1380	32	604529.2213	0.032	17.05
2	1402	18	223743.929	0.012	6.31
	10627		18828009.41	1	531

SMF

T (Second)= 2.79 V (kip)= 467 k= 2

Floor	W (kip)	h (ft)	$W*h^k$	C_{vx}	F_x (kip)
R (9)	1084	116	14586304	0.261	121.82
8	1328	102	13816512	0.247	115.39
7	1346	88	10423424	0.186	87.05
6	1355	74	7419980	0.133	61.97
5	1364	60	4910400	0.088	41.01
4	1368	46	2894688	0.052	24.17
3	1380	32	1413120	0.025	11.80
2	1402	18	454248	0.008	3.79
	10627		55918676	1	467

Table 3.3-3. ELF for the 16-story building

BRBF

T (Second)= 2.55 V (kip)= 963 k= 2

Floor	W (kip)	h (ft)	$W*h^k$	C_{vx}	F_x (kip)
R(17)	1083	228	56298672	0.139	134.10
16	1327	214	60771292	0.150	144.75
15	1342	200	53680000	0.133	127.86
14	1349	186	46670004	0.115	111.16
13	1357	172	40145488	0.099	95.62
12	1360	158	33951040	0.084	80.87
11	1366	144	28325376	0.070	67.47
10	1370	130	23153000	0.057	55.15
9	1379	116	18555824	0.046	44.20
8	1384	102	14399136	0.036	34.30
7	1389	88	10756416	0.027	25.62
6	1394	74	7633544	0.019	18.18
5	1402	60	5047200	0.012	12.02
4	1410	46	2983560	0.007	7.11
3	1425	32	1459200	0.004	3.48
2	1462	18	473688	0.001	1.13
	21799		404303440	1.000	963

SMF

T (Second)= 4.15 V (kip)= 958 k= 2

Floor	W (kip)	h (ft)	$W*h^k$	C_{vx}	F_x (kip)
R(17)	1083	228	56298672	0.139	133.40
16	1327	214	60771292	0.150	144.00
15	1342	200	53680000	0.133	127.20
14	1349	186	46670004	0.115	110.58
13	1357	172	40145488	0.099	95.13
12	1360	158	33951040	0.084	80.45
11	1366	144	28325376	0.070	67.12
10	1370	130	23153000	0.057	54.86
9	1379	116	18555824	0.046	43.97
8	1384	102	14399136	0.036	34.12
7	1389	88	10756416	0.027	25.49
6	1394	74	7633544	0.019	18.09
5	1402	60	5047200	0.012	11.96
4	1410	46	2983560	0.007	7.07
3	1425	32	1459200	0.004	3.46
2	1462	18	473688	0.001	1.12
	21799		404303440	1.000	958

3.4 Mass Calculations

The effective mass was distributed among the beam-column joints in each floor and assigned as a lumped mass to the beam-column joint. The distribution of the effective mass was according to the tributary area method. Each node takes the mass of the structural elements around it. The tributary area around each node was half the adjacent span in each direction, half the column and half the façade, and half the partition masses above and below the considered node. Anything located within the tributary area was considered in the mass calculation like concrete deck mass, structure elements, partitions mass, and façade mass. Figure 3.4-1shows a top view for a tributary area of some internal and side nodes.

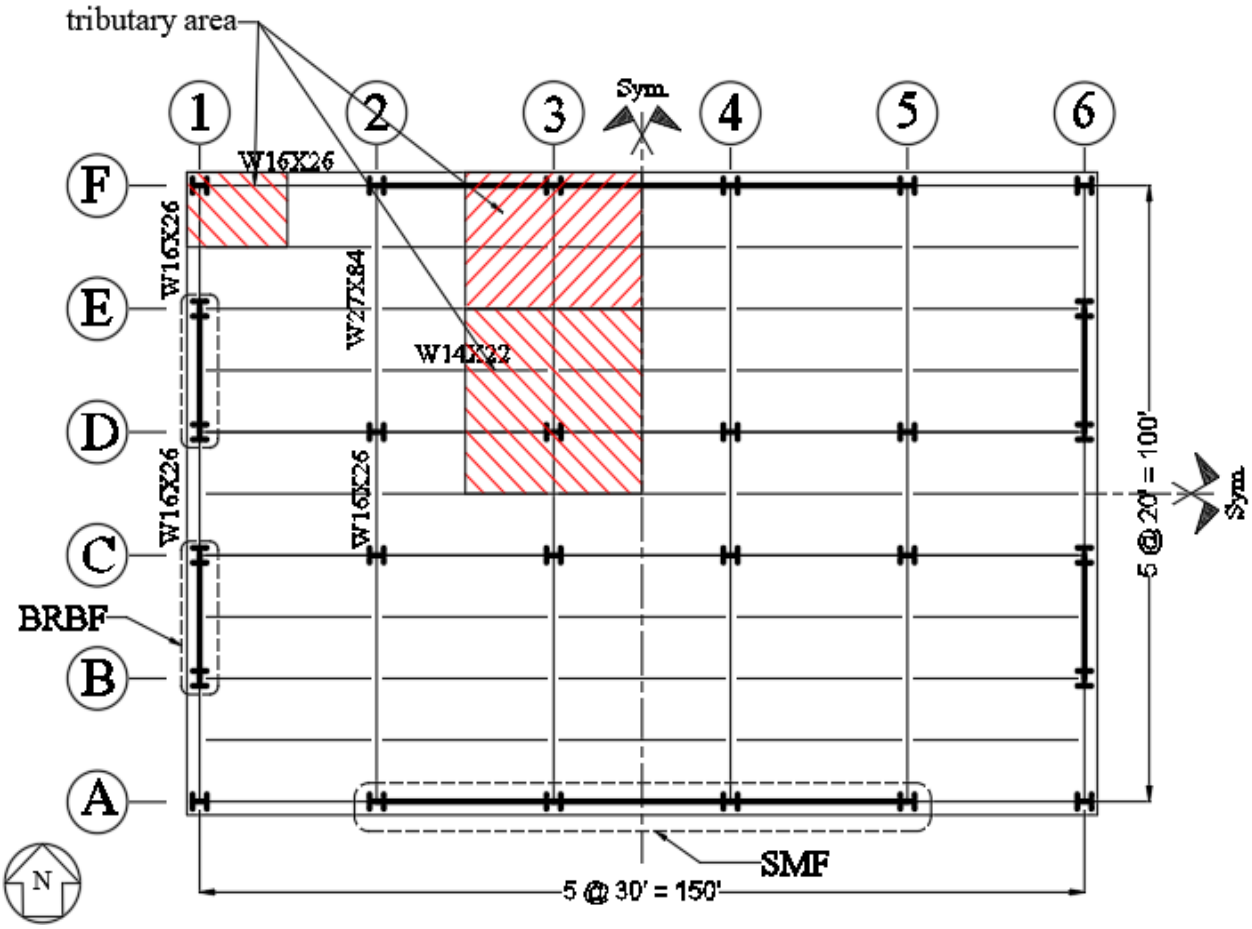

Figure 3.4-1. Tributary areas of some side and middle nodes in the plane.

Table 3.4-1, Table 3.4-2, and Table 3.4-3 below illustrate a comparison between each floor's effective seismic weights with the values mentioned in (Harris & Speicher, 2015). A percentage of error was calculated for the floors, roof, and the total effective seismic weight of the building.

Table 3.4-1. A comparison between the calculated effective seismic weight and the effective seismic weight from (Harris & Speicher, 2015) report for the 4-story building.

Level, X	W_x [NIST Report] (kip)	W_x (kip)	Percentage of error
Roof	1095	1101	0.55
4	1345	1334.3	-0.80
3	1359	1339	-1.47
2	1377	1350	-1.96
total	5176	5124.3	-1.00

Table 3.4-2. A comparison between the calculated effective seismic weight and the effective seismic weight from (Harris & Speicher, 2015) for the 8-story Building

Level, X	W_x [NIST Report] (kip)	W_x (kip)	Percentage of error
Roof	1084	1098	1.28
8	1328	1335	0.52
7	1346	1344	-0.14
6	1355	1351	-0.28
5	1364	1366	0.18
4	1368	1376	0.56
3	1380	1379	-0.06
2	1402	1392	-0.72
total	10627	10641	0.14

Table 3.4-3. A comparison between the calculated effective seismic weight and the effective seismic weight from (Harris & Speicher, 2015) for the 16-story Building

Level, X	W_x [NIST Report] (kip)	W_x (kip)	Percentage of error
Roof	1083	1090	0.69
16	1327	1316	-0.80
15	1342	1331	-0.84
14	1349	1336	-1.00
13	1357	1349	-0.59
12	1360	1358	-0.18
11	1366	1361	-0.34
10	1370	1363	-0.53
9	1379	1378	-0.04
8	1384	1388	0.28
7	1389	1399	0.74
6	1394	1408	1.03
5	1402	1421	1.35
4	1410	1431	1.49
3	1425	1448	1.65
2	1462	1470	0.53
total	21799	21848	0.22

3.5 Modal Analysis of the Center-to-Center model

Modal analysis was conducted in both OpenSeesPy and SAP2000 to find the vibration period and mass participation percentages. The results were close to each other. Table 3.5-1, Table 3.5-2, and Table 3.5-3 show a summary of the results mentioned in the NIST report and the results obtained using SAP2000 and OpenSeesPy.

Table 3.5-1. A summary of the vibration periods for the 4-Story Building.

Mode	Direction	SAP2000	OpenSeesPy	% Difference	Modal period NIST report	% Difference between NIST and OpenSeesPy
1	SMF	1.71	1.757	2.75	1.77	-0.73
2	BRBF	0.98	1.01	3.06	0.99	2.02
3	TORSION	0.70	0.716	2.29		
4	SMF	0.53	0.549	3.58		

Table 3.5-2. A summary of the vibration periods for the 8-Story Building

Mode	Direction	SAP2000	OpenSeesPy	% Difference	Modal period NIST report	% Difference between NIST and OpenSeesPy
1	SMF	2.68	2.80	4.48	2.79	0.36
2	BRBF	2.03	2.07	1.97	2.01	2.99
3	TORSION	1.38	1.39	0.72		
4	SMF	0.97	1.00	3.09		
5	BRBF	0.68	0.69	1.47		
6	SMF	0.54	0.56	3.70		
7	TORSION	0.48	0.48	0.00		
8	BRBF	0.38	0.39	2.63		

Table 3.5-3. A summary of the vibration periods for the 16-Story Building

Mode	Direction	SAP2000	OpenSeesPy	% Difference	Modal period NIST report	% Difference between NIST and OpenSeesPy
1	SMF	4.00	4.17	4.25	4.15	0.48
2	BRBF	2.50	2.54	1.60	2.55	-0.39
3	TORSION	1.80	1.78	-1.11		
4	SMF	1.50	1.52	1.33		
5	BRBF	0.88	0.88	0.00		
6	SMF	0.86	0.88	2.33		
7	TORSION	0.63	0.63	0.00		
8	SMF	0.59	0.60	1.69		

3.6 Footing Design

Three types of footings were used in this study, which are isolated, raft, and piles. The foundations of all the columns that are not part of the lateral force resisting system are isolated footings, while the foundations of the lateral force systems are different. For the 4- and 8-story buildings, the SMF foundations are isolated footings, and the BRBF foundations are raft footings. The raft footing was extended to include the exterior column in order to prevent the overturning of the building. For the 16-story building, the SMF foundations are a raft footing, and the BRBF foundations are piles, As shown in Figure 3.6-1, Figure 3.6-2, and Figure 3.6-3.

Foundations were adequately designed to resist the reactions that are resulting from the primarily linear analysis mentioned above. The load combination that has been used to calculate the reactions on the footing is Dead Load+ 0.25* Live Load (Harris & Speicher, 2015) plus the lateral forces resulted from the equivalent lateral force method ELF. The bearing capacity of the soil was calculated using Meyerhof method.

The isolated foundation was used in the SMF of the 4- and 8-story building because it provided the required bearing capacity to resist the applied load, while the raft foundation was used for the SMF of the 16-story building because the eccentricity of the applied load exceeded B/6, which is the limit for using the isolated footing. A raft foundation used for the BRBF of the 4- and 8-story building to prevent the overturning. For the 16-story building the pile foundation was required to prevent the overturning. The factor of safety was included during the design of the foundation but was not included during the modeling of the foundation in OpenSeesPy for conduction the nonlinear analysis. Clay soil with Shear Strength of 2089 lb/ft^2 (100 kPa) (site class C, very dense soil and soft rock) was adopted in this study for all the buildings.

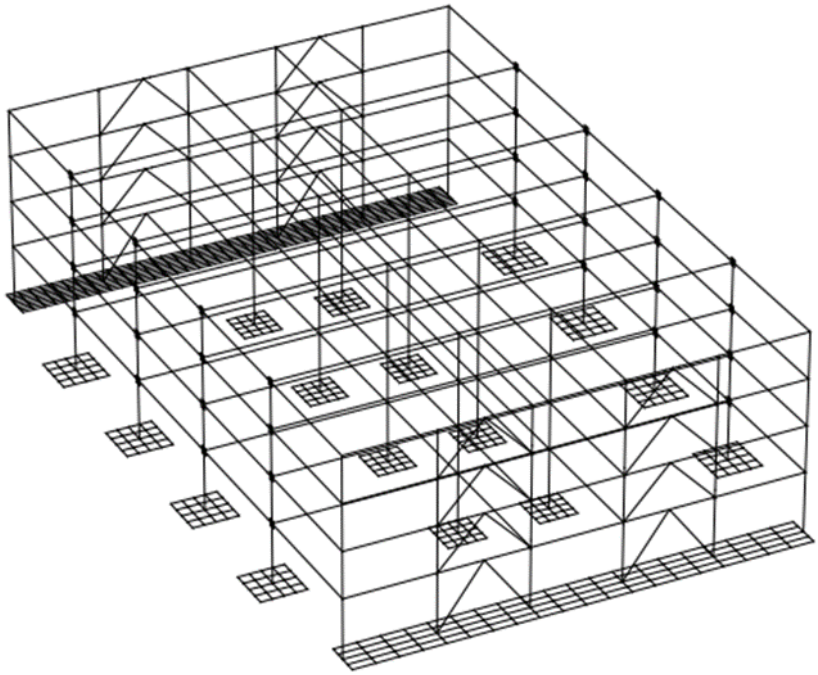

Figure 3.6-1. Plan view of the 4- and 8-story foundation system.

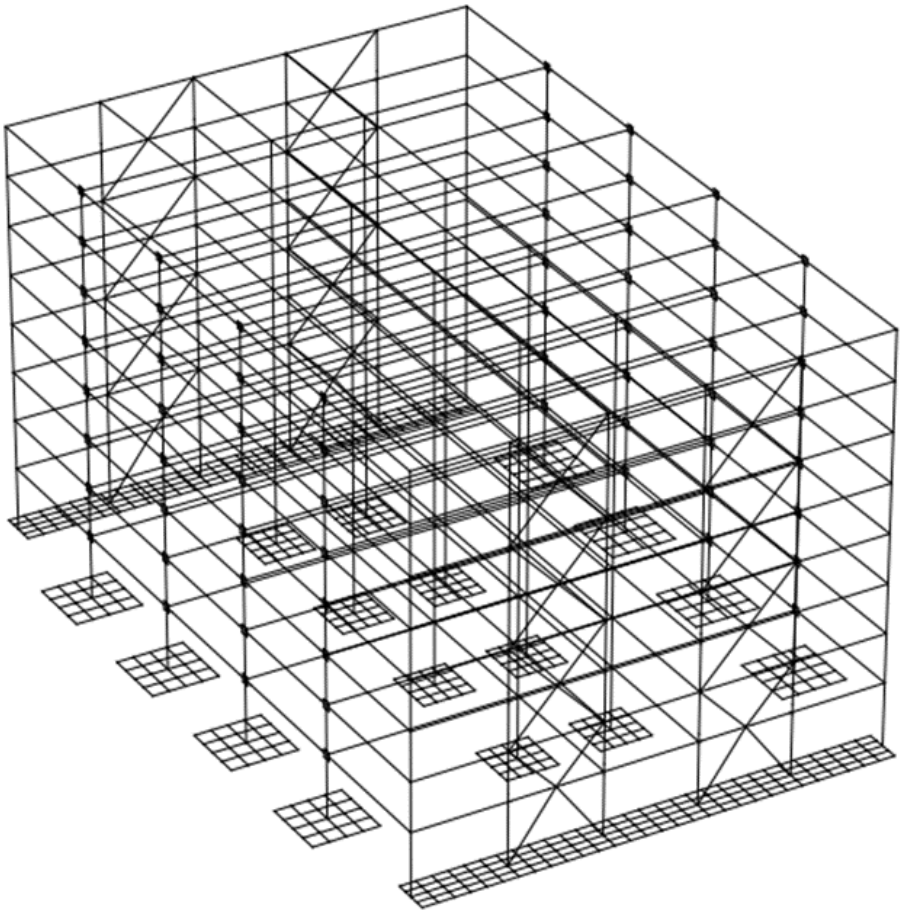

Figure 3.6-2. Isometric for the 8- story building foundation system.

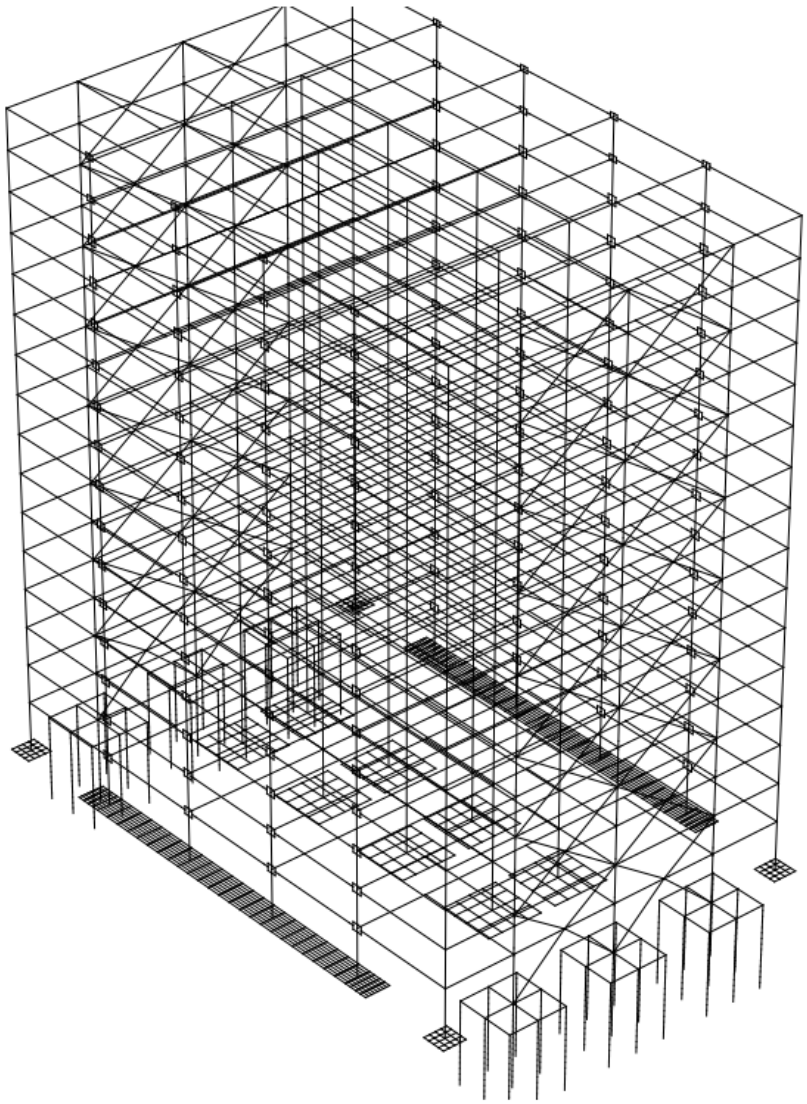

Figure 3.6-3. Isometric for the 16- story building foundation system.

3.6.1 Modeling of Isolated Footing

There is no command or tool to model a 3D isolated footing in OpenSeesPy directly. Thereby, a routine was written to model a 3D isolated footing in OpenSeesPy. The routine works as follows. The footing is divided into a grid. Two layers of the nodes are generated at the same location, let us assume one above the other, but they are at the same location. The bottom layer is constrained in all 6 degrees of freedom, while the top layer does not have any constraint. A group

of springs that connects the bottom and the top layer of nodes represents the soil. The sub-direct method of soil modeling was used in this study. A Q_z Spring (QzSimple1 Material) is used to represent the vertical resistance of the soil. The strength of each Q_z spring was calculated by multiplying the Meyerhof bearing capacity by the tributary area. T_z Spring (TzSimple1 Material) represents the frictional resistance between the soil and the foundation, horizontal resistance in the case of shallow foundations. The strength of each T_z spring was calculated by multiplying the $T_{friction}$ from equation (1) by the tributary area. P_y Spring (PySimple1 material) represents the soil's passive resistance, which is also horizontal resistance. The strength of each P_y spring was calculated by multiplying the $P_{passive}$ from equation 2 by the tributary area at the side of the footing (Gajan et al., 2008) and (Harden et al., 2005). The python routine for modeling the isolated foundation is in appendix A. Figure 3.6-4 shows the spring distribution under an isolated footing. The springs' length is zero, but they are drawn with a finite length for illustration purposes. The grid elements are modeled using Elastic Timoshenko Beam-Column Elements to account for the shear deformation in the footing. Those elements' properties like the moment of inertia and the area were calculated based on the tributary area method. The concrete modulus of elasticity was assigned to those elements because the footings are generally made of concrete. Figure 3.6-5 shows how the tributary areas were assigned around the grid elements in the Y direction. Tributary area 1 was assigned for element 1, tributary area 2 for element 2, and tributary area 3 for element 3. The same conceptual procedure was assigned for the grid element in the X direction. The number of the grids in each direction was 6 grids not 3 as shown in Figure 3.6-4 and Figure 3.6-5. They were drawn as 3 grids for illustration purposes.

$$T_{friction} = W_g \tan \delta + A_b c \qquad (1)$$

$T_{friction}$ = frictional resistance per unit area of foundation (kip).

W_g = weight on the foundation from the structure (kip).

δ = angle of friction between foundation and soil, which typically varies from 1/3φ to 2/3φ.

φ= angle of internal friction of soil.

A_b = the area of the base of footing in contact with the soil (=L x B).

c= shear strength of the soil.

$$P_{passive} = 0.5\gamma K_p D_f^2 \quad (2)$$

$P_{passive}$ = passive earth pressure per unit length of footing.

γ = unit weight of soil.

D_f = depth of embedment.

K_p = passive earth pressure coefficient is calculated using Coulomb (1776).

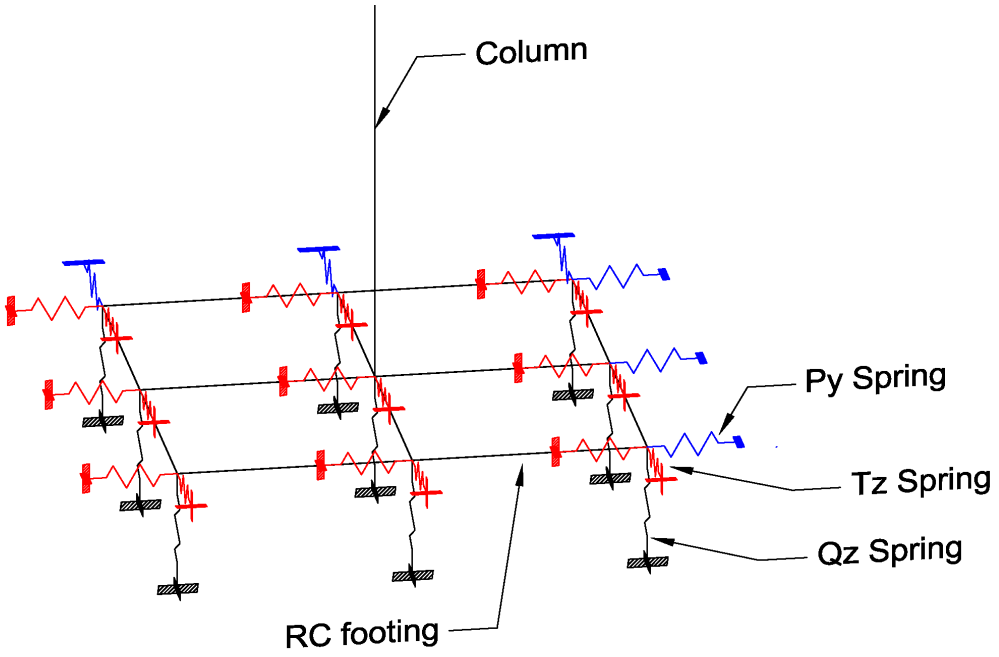

Figure 3.6-4. An isometric view showing the spring distribution under an isolated footing.

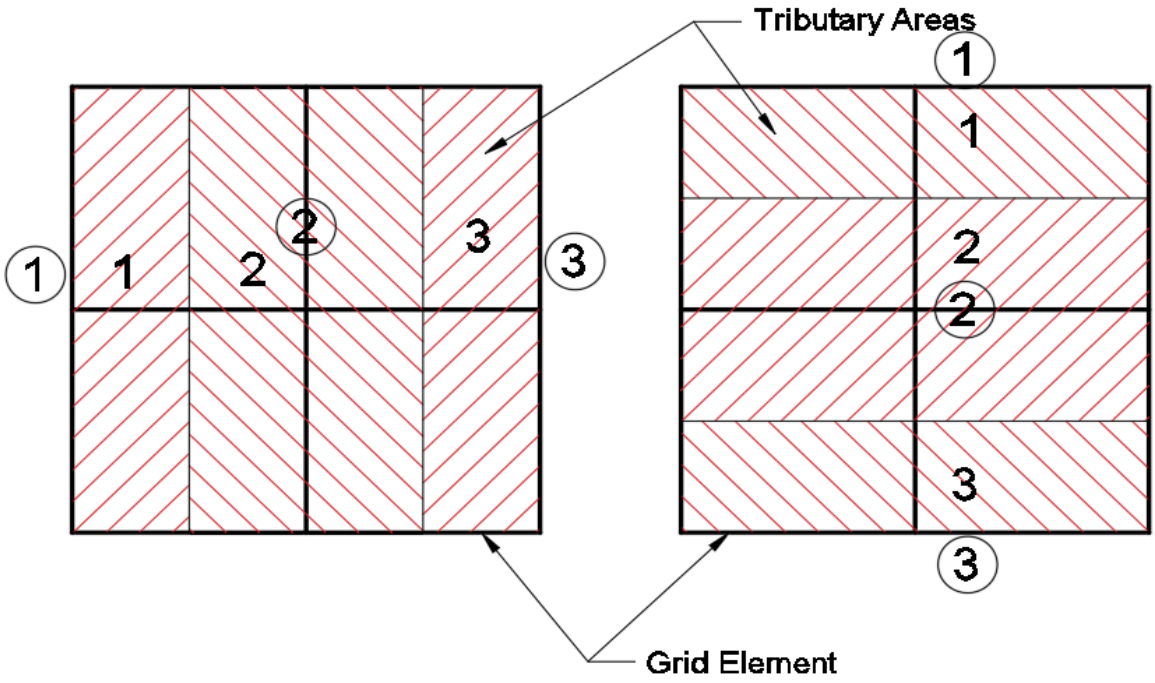

Figure 3.6-5. A top view for the tributary area around the grid elements

3.6.2 Modeling of Raft Footing

The raft modeling methodology in OpenSeesPy was precisely the same as the one used for modeling the isolated footing. Figure 3.6-6 show the springs' distribution under the raft foundation. The python routine for modeling the raft footing is in appendix B.

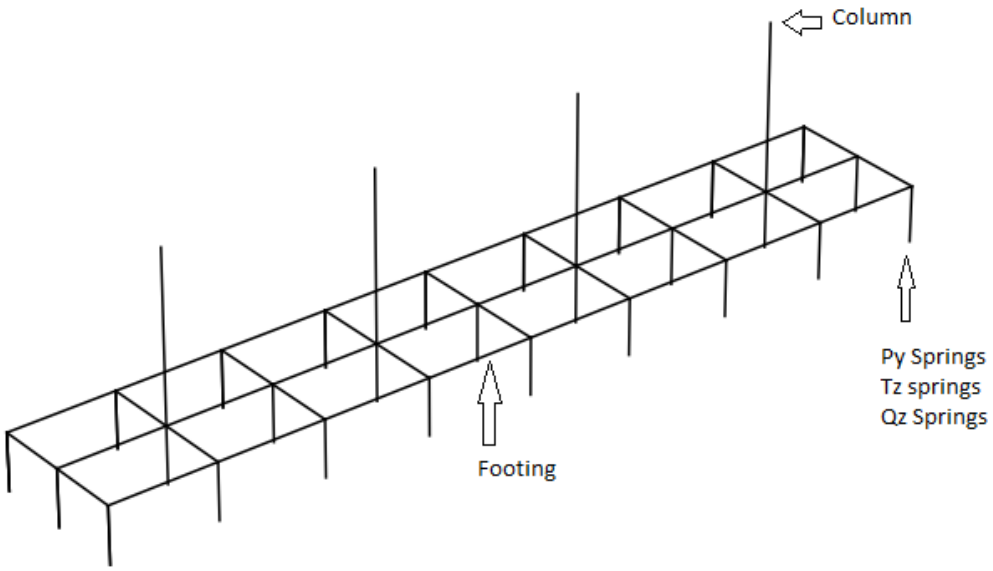

Figure 3.6-6. An isometric view showing the spring distribution under the raft footing.

3.6.3 Modeling of Pile Foundation

The differences between the modeling of the isolated footing and the piles' modeling is the spring distribution. Q_z Spring (QzSimple1 Material) is used to represent the end bearing of the pile. The strength of each Q_z spring was calculated using equation (3). The T_z Spring (TzSimple1 Material) represents the frictional resistance between the soil and the foundation, works along the pile length, and contributes to its vertical resistance. The strength of each T_z spring was calculated using equation (4). P_y Spring (PySimple1 material) represents the soil's passive resistance, which is horizontal resistance. The strength of each P_y spring was calculated using the smallest of equation (5) and equation (6) (Rocscience, 2018a) and (Rocscience, 2018b). Figure 3.6-7 shows an isometric view showing the pile group, pile cap, and spring distribution. The python routine for modeling the pile foundation is in appendix C.

$$q_{ult\_Qz}=9*c*b^2 \quad (3)$$

b= width of the pile cross section (in).

$$q_{ult\_Tz}=0.5*c*b^4 \quad (4)$$

$$p_{ult} = \left[3 + \frac{\gamma'}{c_a} z + \frac{J}{b} z\right] c_a b \tag{5}$$

$$p_{ult} = 9 c_u b \tag{6}$$

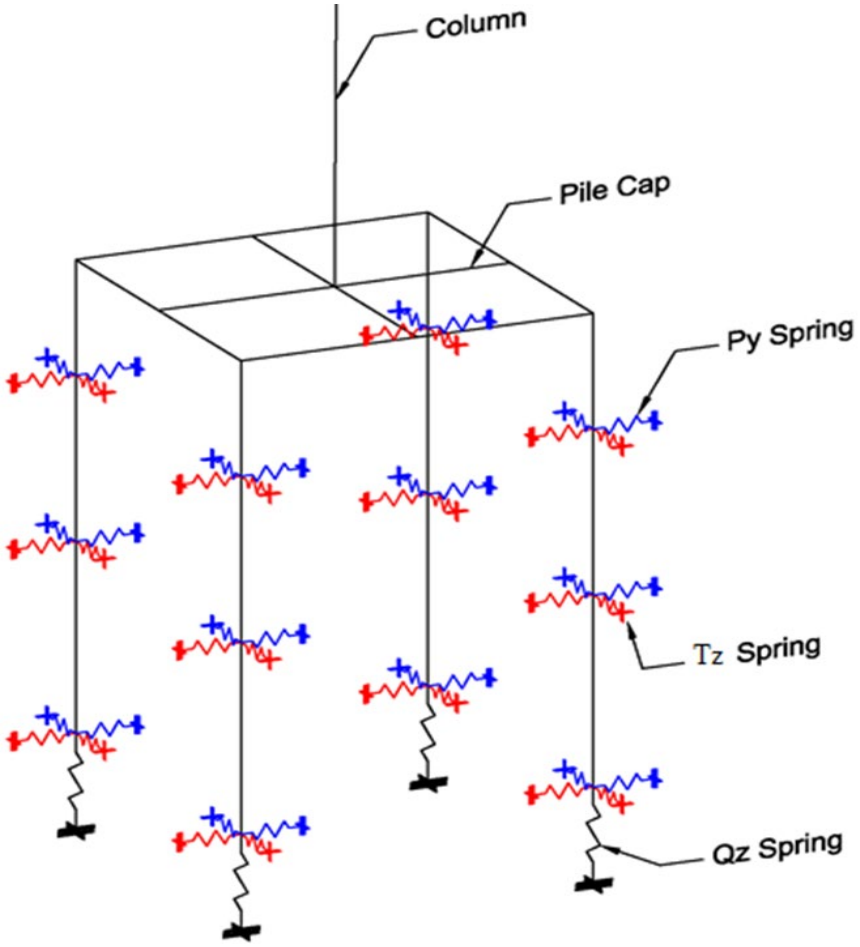

Figure 3.6-7. An isometric view showing the pile group, pile cap, and spring distribution.

3.7 Modeling of the Panel Zone

The lumped plasticity and the panel zone approach was used to capture the nonlinear and the inelastic behavior of the structure. The panel zone dimensions were set up to be equal to the column depth and beam depth that are connected to the panel. The panel zone was modeled using the Gupta and Krawinkler (1999) approach. Each panel zone consists of eight elastic beam-column elements with a moment of inertia ($I=10^4$ in^4) higher than the beams and the columns. At the four corners, the elements are connected as a pinned connection (no rotation resistance). A spring

element modeled using Hysteretic material was assigned to one corner to capture the panel zone stiffness and strength. Figure 3.7-1 below shows a panel zone for a beam-column joint.

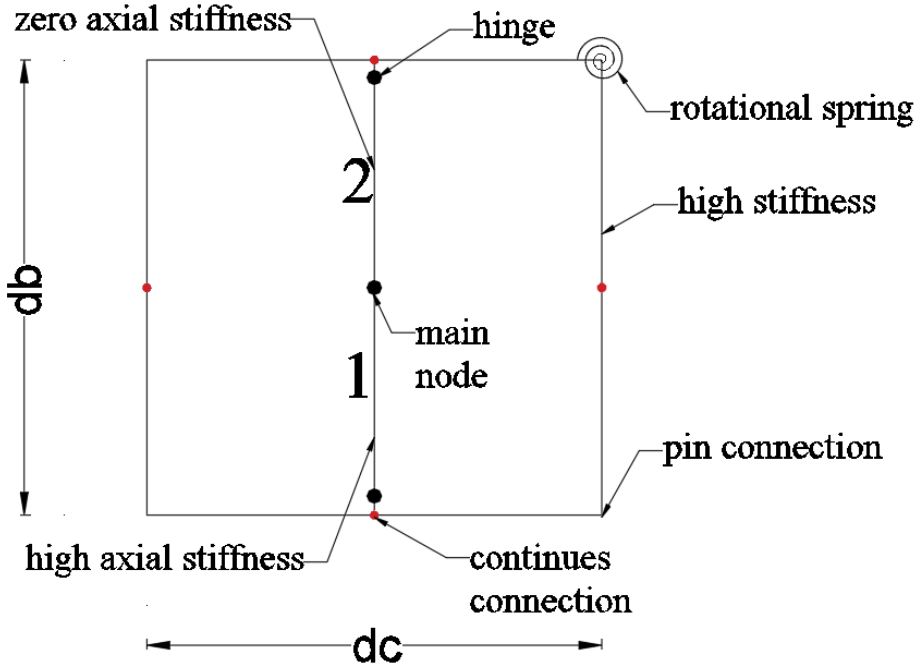

Figure 3.7-1. Panel zone example.

The joints at the corners are connected as a pinned connection. The rotational spring element (at the right top corner) represents the nonlinear force-deformation response of the panel zone. The purpose of element 1 and element 2 is to connect the panel zone with the beam element in the other direction, the beam perpendicular to the plane. The axial stiffness of element 2 is approximately zero and the flexural resistance of the element is high (The area of this element is 0.00001 in^2), while element 1 has high resistance in both the axial and the flexural resistance. Simultaneously, both elements are released in the flexural resistance at one end, the end that is far away from the center of the panel zone. Figure 3.7-2 below shows an isometric view of how the panel zone was connected to the beams and columns.

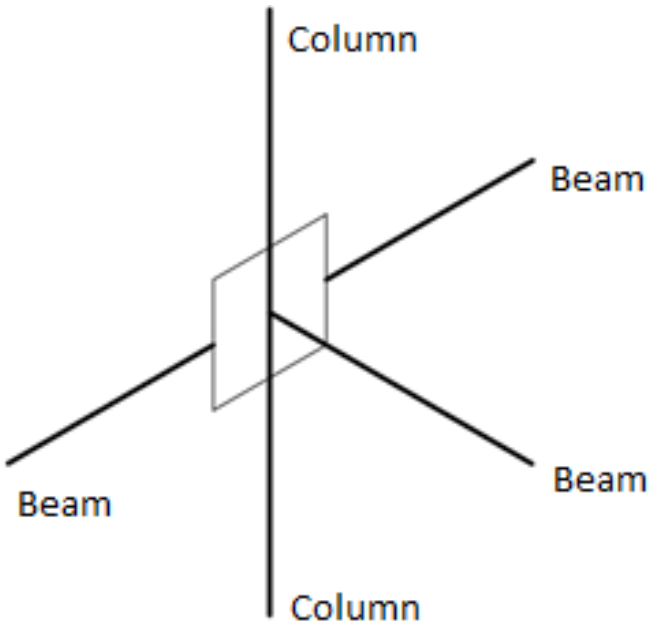

Figure 3.7-2. An isometric view that shows how the panel zone is connected to the other elements.

3.8 Reduced Beam Section (RBS) Modeling

The RBS in the beams was modeled using the modified Ibarra-Krawinkler deterioration model. The RBS is used only in the SMF. The modified Ibarra-Krawinkler spring is located at the center of the RBS. The moment capacity of the modified Ibarra-Krawinkler spring was calculated based upon the reduced cross section of the beam. Because the modified Ibarra-Krawinkler material does not account for the cyclic hardening, the moment capacity calculated based upon the reduced cross section was increased by 1.07 to account for the strain hardening (Lignos, 2008). The stiffnesses of the beam segment between the two RBS and the RBS were modified as recommended in (Gupta & Krawinkler, 1998). The rotational stiffness of the spring was n (n=10) times higher than the rational stiffness of the beam. The rotational stiffness of the beam is $\frac{6EImod}{L_2}$, I_{mod} is $I * \frac{n+1}{n}$, thereby the rotational stiffness of the RBS spring is $n * \frac{6EImod}{L_2}$. The element between the face of the column and the RBS spring was modeled as an elastic beam-column

element with an average stiffness, average of the stiffness at the face of the column and the stiffness at the RBS. Figure 3.8-1 shows the typical beam with RBS model in OpenSeesPy. For more information about panel zone and RBS modeling, see (Lignos, 2008) and (Ibarra & Krawinkler, 2005).

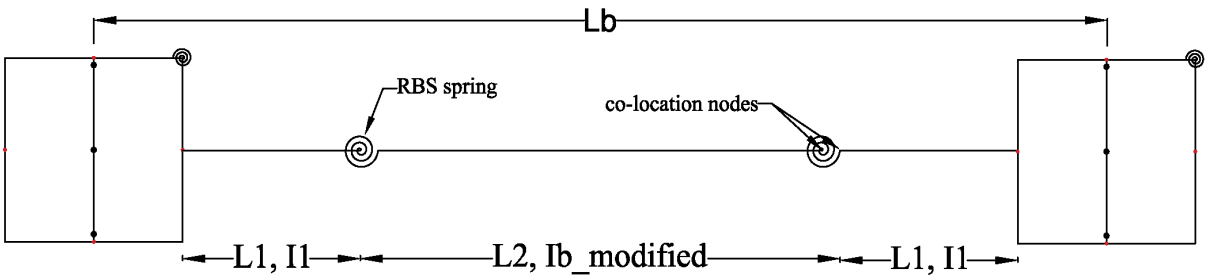

Figure 3.8-1 Typical beam model in the SMF.

3.9 Column Modeling

To capture the nonlinear behavior in the column, springs have been added to the ends of the column. The modified Ibarra-Krawinkler material was used to model the springs. The flexural strength of the springs was calculated based on the column moment of inertia. The flexural strength of the spring was multiplied by 1.17 to account for the cyclic hardening (Lignos, 2008). The stiffnesses of the springs and the column element were modified using the same procedure described in RBS modeling. Figure 3.9-1 shows the typical beam with RBS model in OpenSeesPy.

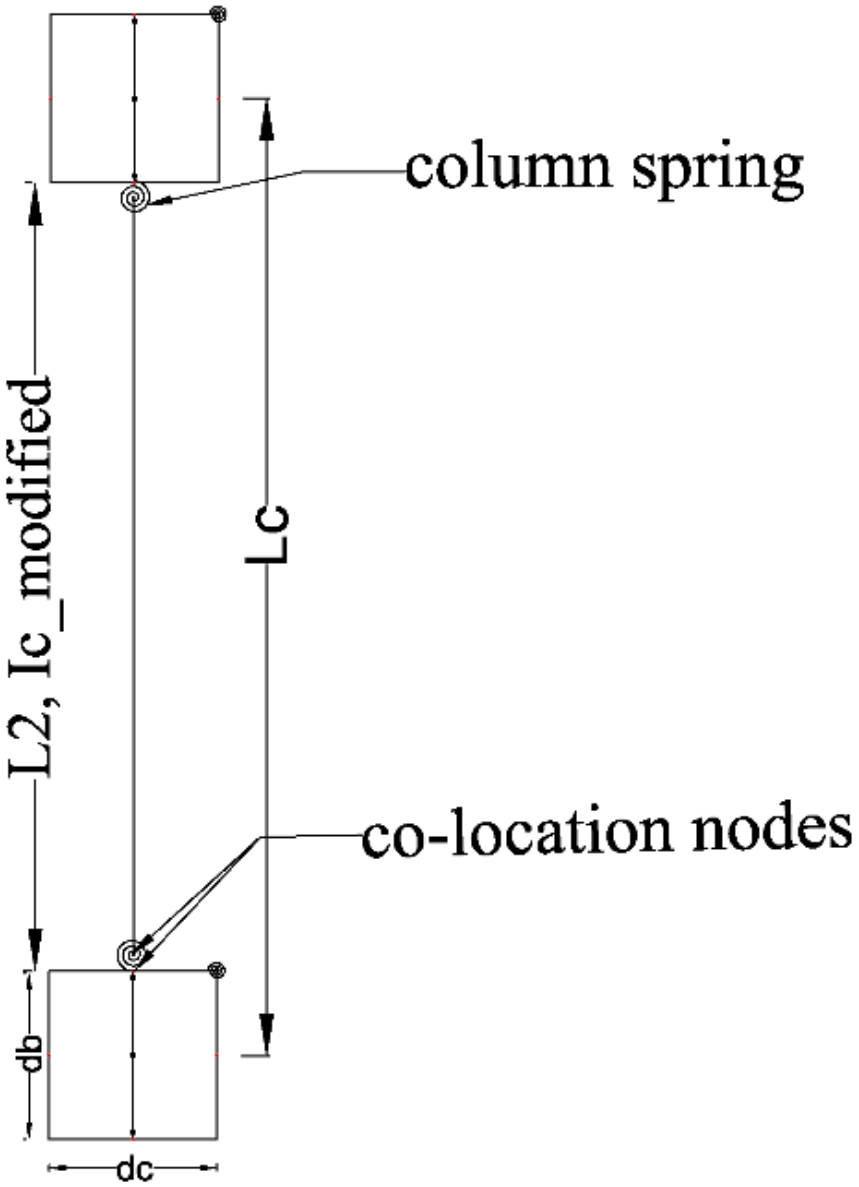

Figure 3.9-1 Typical column model in the SMF.

3.10 SMF verification

The nonlinearity of the SMF was modeled as described in sections 3.8 and 3.9. To verify the factors that were used to model the modified Ibarra-Krawinkler material, an experimental test was modeled and analyzed in OpenSeesPy using the technique described in sections 3.8 and 3.9. the experimental test was done in the University of California, Berkeley (Popov et al., 1997). The test specimen consisted of a W33xl30 beam and a W36x280 column, as shown in Figure 3.10-1.

The strength of the beam was reduced by reducing the flange width (RBS). The center of the RBS was 30” away from the face of the column. The actuator load was applied at the free end of the beam. The end of the two columns were simply supported. Figure 3.10-2 shows a comparison between the OpenSeesPy results and the experimental results. The results show that the general trend of strength degradation and hysteresis in the BRB spring is properly captured.

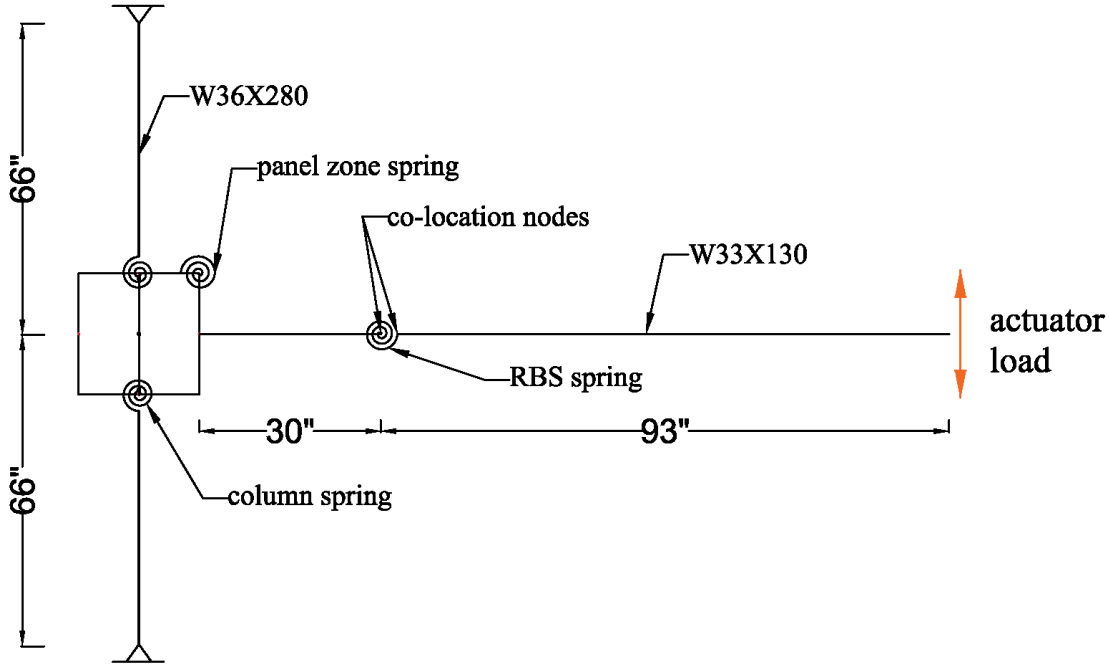

Figure 3.10-1 Model assemblage in OpenSeesPy.

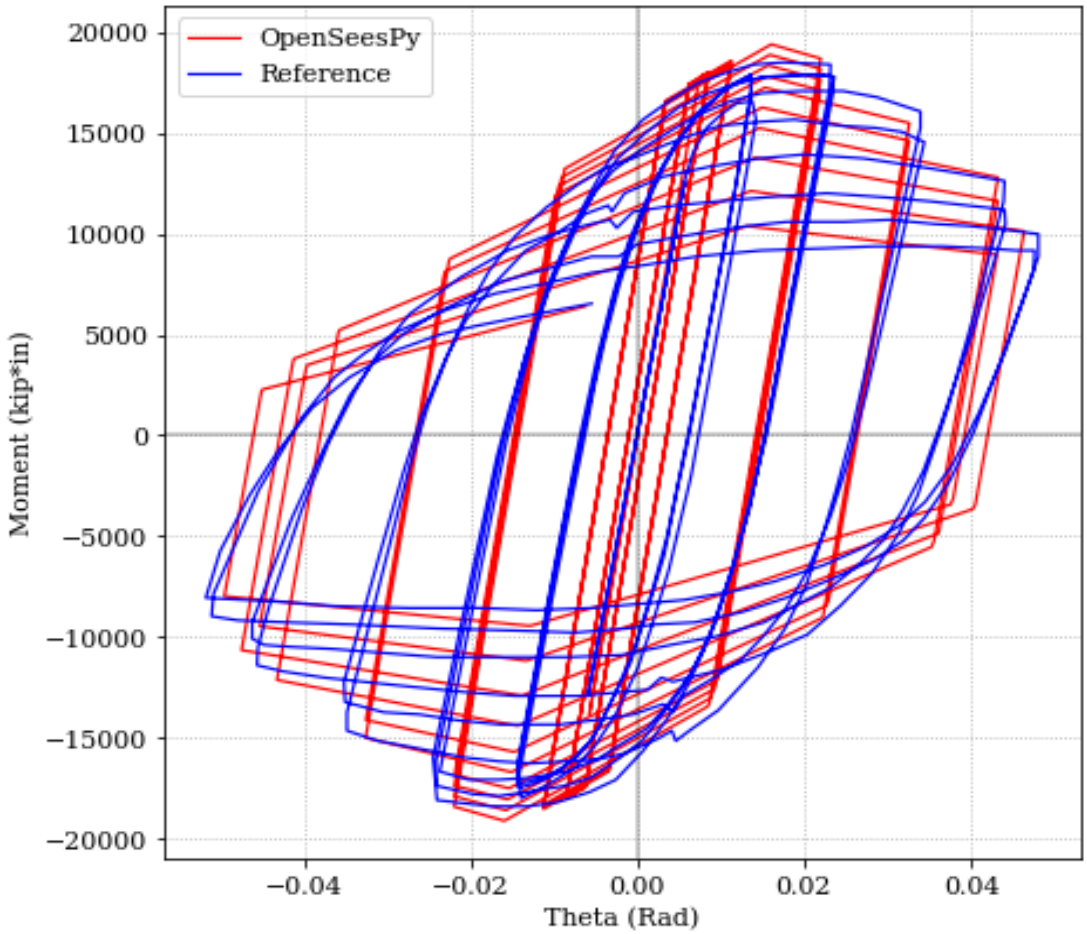

Figure 3.10-2 Comparison between the OpenSeesPy results and the experimental results (Popov et al., 1997).

3.11 BRB Nonlinear Modeling.

Steel02 and Pinching4 materials were used to model the BRB's nonlinear behavior. A BRB yields in tension and compression, but the compression force is higher than the tension force because of friction that develops between the BRB steel core and the surrounding mortar. To account for this additional force in compression Pinching4 material was used in parallel with Steel02. The tension strength of the Pinching4 was zero and the compression force was non-zero. The amount of the compression force that is provided by Pinching4 was quantified based upon experimental data. This modeling technique was adopted from Upadhyay et al. (2019). The behavior of the BRB under cyclic load has been verified with two experimental data sets, (Merritt

et al., 2003) and (Newell et al., 2006). Figure 3.11-1 shows the conceptual behavior of the BRB element. Figure 3.11-2 shows a comparison between the experimental data and the modeling results. The model of BRB matches well with the experimental data.

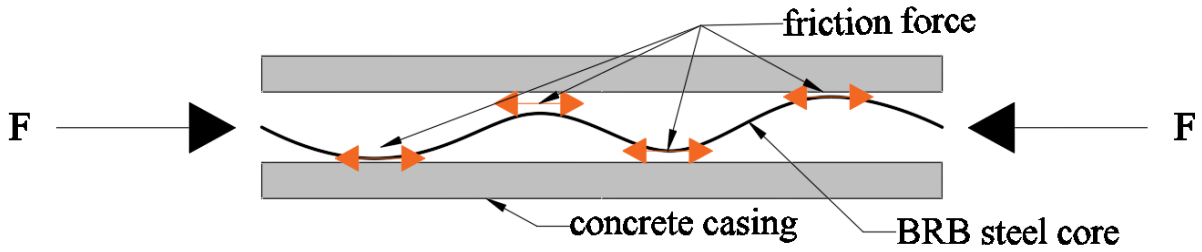

Figure 3.11-1 conceptual behavior of BRB element.

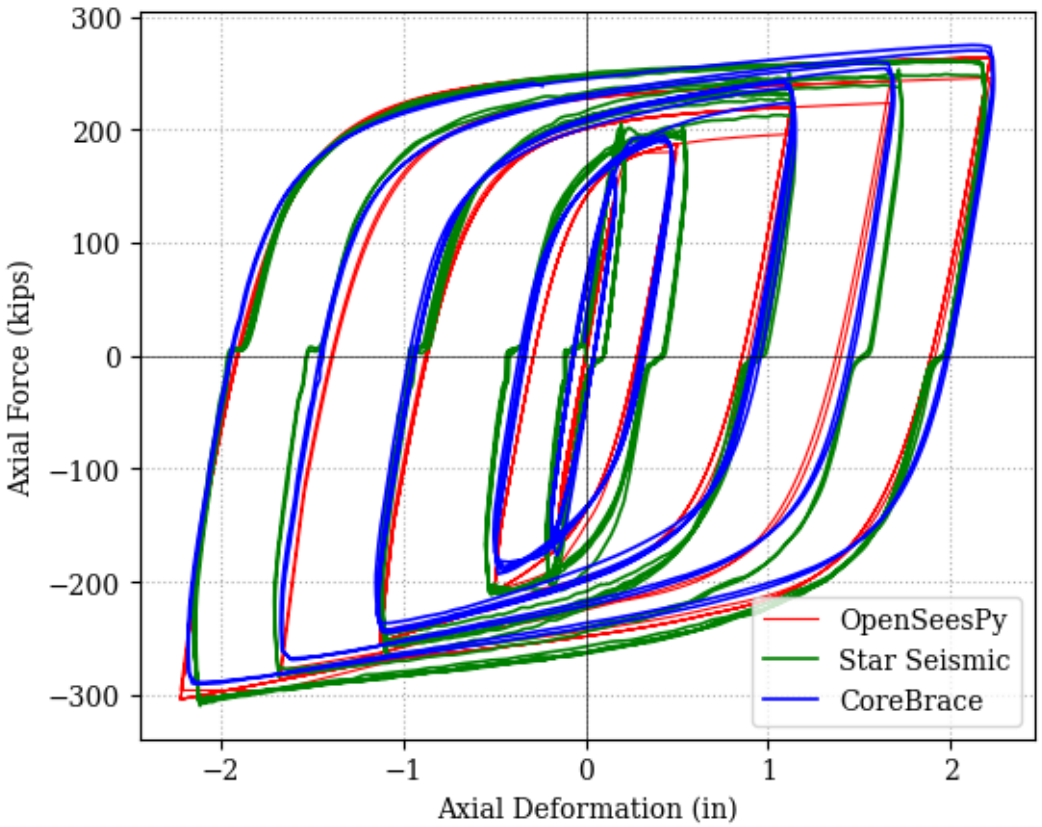

Figure 3.11-2. Comparison of BRB inelastic model to experimental results from data reported in (Merritt et al., 2003)(Star Seismic) and (Newell et al., 2006) (CoreBrace).

The BRB element has been modeled as one truss element and to account for the effect of the gusset plate on the beam and the column, the stiffness of the beam and the column in the

gusset plate region have been multiplied by 2 (Speicher & Harris, 2019), as shown in Figure 3.11-3.

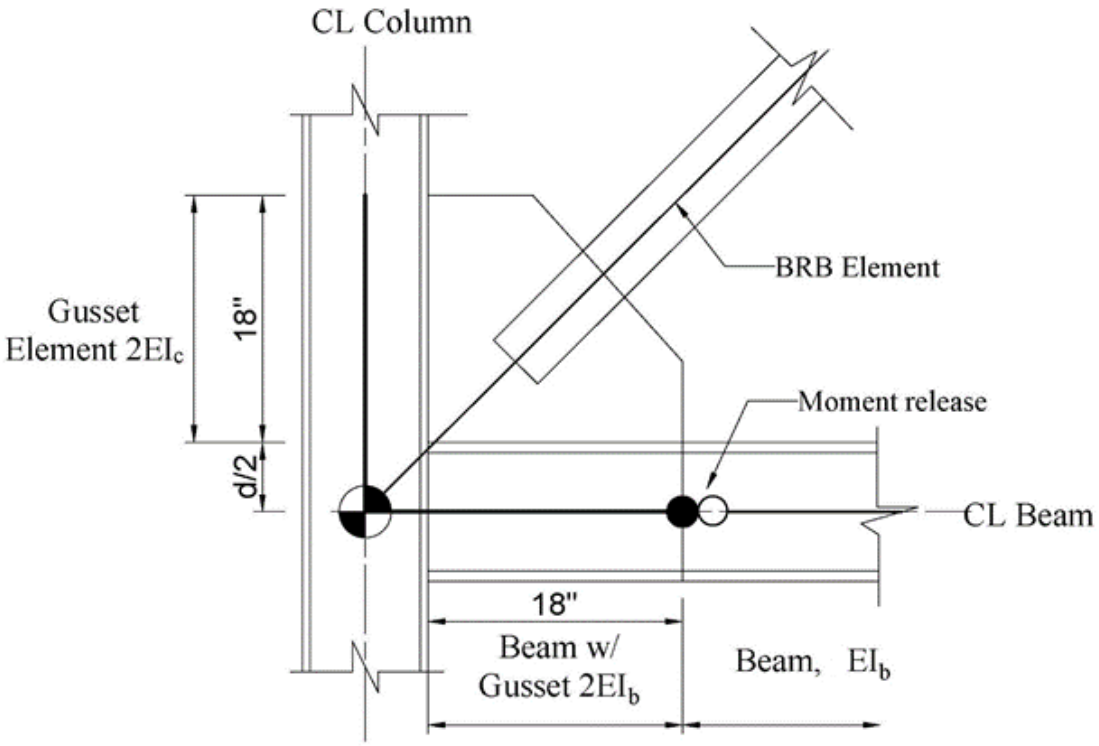

Figure 3.11-3 BRBF brace-to-beam / column subassembly analytical schematic.

3.12 Modal Analysis for the Nonlinear Modeling

Modal analysis was conducted to find the vibration periods for the building modeled with lumped plasticity to capture the nonlinearity. Table 3.12-1, Table 3.12-2, and Table 3.12-3 show a comparison between the nonlinear model vibration periods and the linear elastic vibration period.

Table 3.12-1. OpenSeesPy vibration periods for the 4-story building with ideal supports.

Mode	Linear Model Period of Vibration (s)	Nonlinear Model Period of Vibration (s)	% Difference
1	1.757	1.721	-2.05
2	1.01	0.829	-17.92
3	0.716	0.599	-16.34
4	0.549	0.519	-5.46

Table 3.12-2. OpenSeesPy vibration periods for the 8-story building with ideal supports.

Mode	Linear Model Period of Vibration (s)	Nonlinear Model Period of Vibration (s)	% Difference
1	2.798	2.377	-15.05
2	2.065	1.949	-5.62
3	1.389	1.289	-7.20
4	0.997	0.902	-9.53
5	0.688	0.647	-5.96
6	0.558	0.504	-9.68
7	0.477	0.447	-6.29
8	0.388	0.341	-12.11

Table 3.12-3. OpenSeesPy vibration periods for the 16-story building with ideal supports.

Mode	Linear Model Period of Vibration (s)	Nonlinear Model Period of Vibration (s)	% Difference
1	4.172	3.759	-9.90
2	2.535	2.313	-8.76
3	1.781	1.627	-8.65
4	1.521	1.381	-9.20
5	0.884	0.814	-7.92
6	0.881	0.799	-9.31
7	4.172	3.759	-9.90
8	2.535	2.313	-8.76

3.13 Pushover Analysis:

Pushover analysis was conducted in OpenSeesPy in both directions, SMF and BRBF. Figure 3.13-1, Figure 3.13-3, and Figure 3.13-5 show a comparison between the OpenSeesPy pushover curves and the NIST report pushover curves in the SMF direction (Harris & Speicher, 2015). For each building, the pushover analysis was conducted three times in each direction. The first one was conducted with Idealized foundation and linear transformation, the second with Idealized foundation and PDelta transformation, and the third with flexible foundation and PDelta transformation. There is a reduction in the building's stiffness and strength as expected. 4-story building shows the highest reduction in the building's stiffness and strength compared to 8- and

16-story building. Figure 3.13-2, Figure 3.13-4, and Figure 3.13-6 show the plastic hinges' development sequence for the PDelta Analysis with an idealized and flexible foundation. The numbers above the plastic hinge represents the idealized foundation results, and the numbers below the plastic hinge represents the flexible foundation results. The results are the order of the plastic hinge development and the roof displacement when the plastic hinge developed. The sequence of plastic hinges development changed between the idealized foundation and the flexible foundation case. For the 4-story building, three of the columns did not yield in the flexible foundation case, while the same columns yielded in the idealized foundation case, as shown in Figure 3.13-2. Overall, the plastic hinges developed at higher roof displacement in the flexible foundation case than the idealized foundation case. The plastic hinge development starts from the first floor and ends at the fourth floor. The base of the columns yielded before the RBS on the fourth floor.

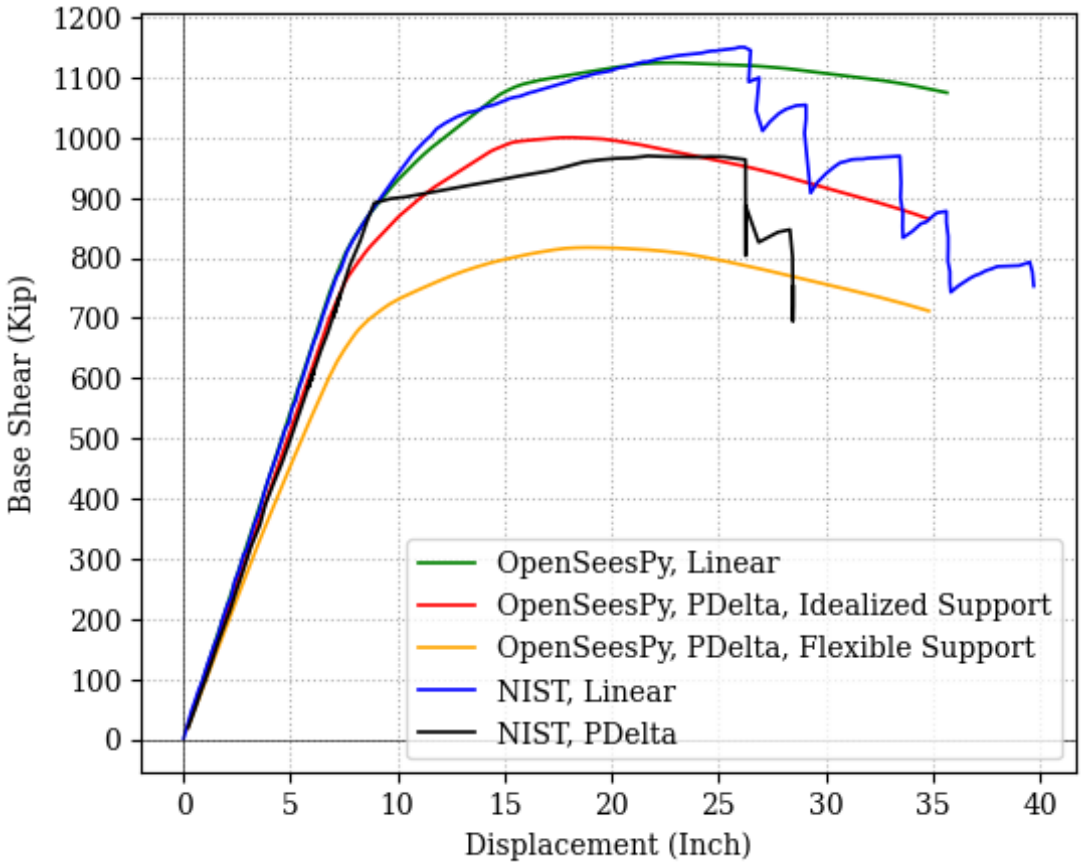

Figure 3.13-1. Pushover curve in the SMF direction for the 4-Story building.

Figure 3.13-2. Plastic hinges development sequence for the OpenSeesPy, PDelta, Idealized and Flexible support analysis of the 4-story building (Bold are the idealized foundation result, nonbold are the flexible foundation result).

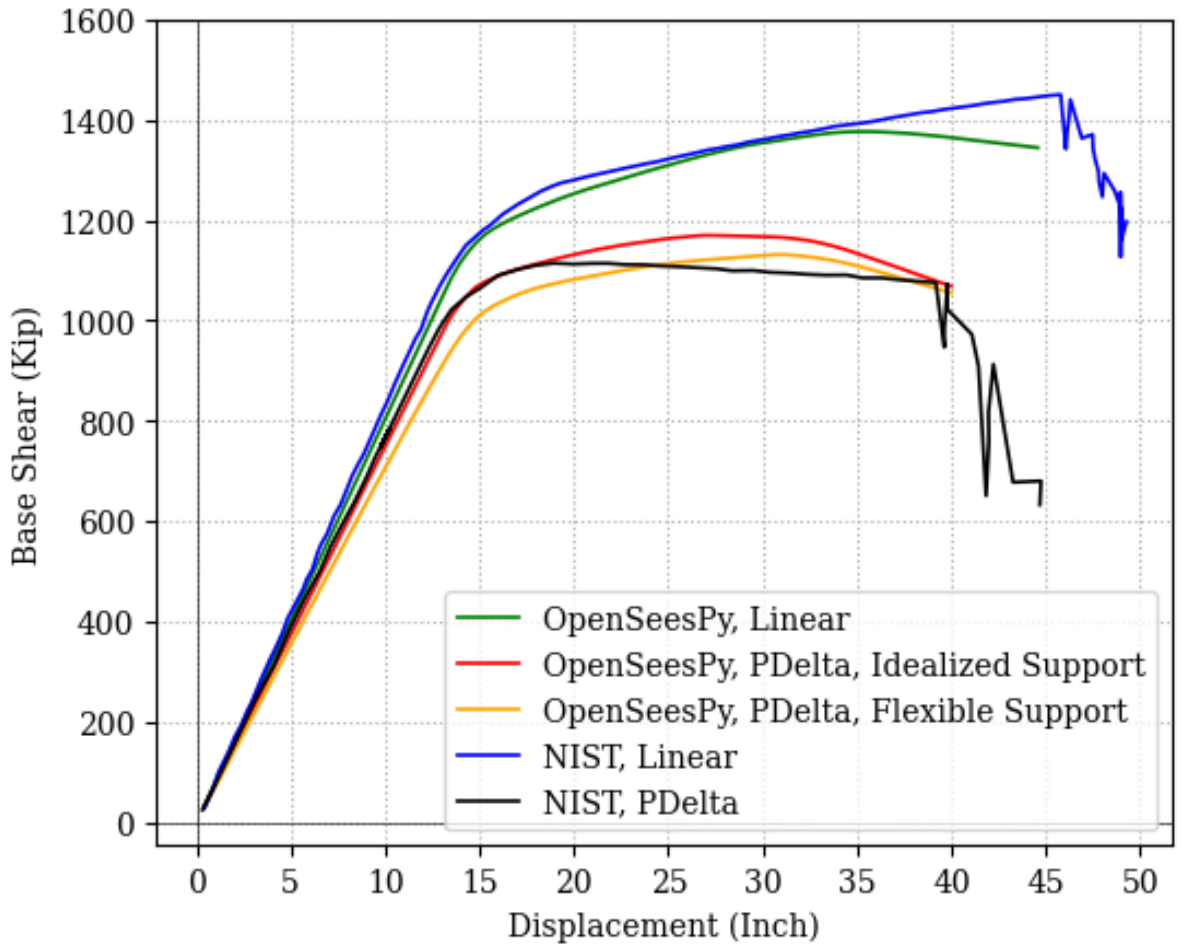

Figure 3.13-3. Pushover curve in the SMF direction for the 8-Story building.

In the 8-story building, the plastics hinges start at the first floor and end at the columns. One column did not yield in the flexible case, as shown in Figure 3.13-4.

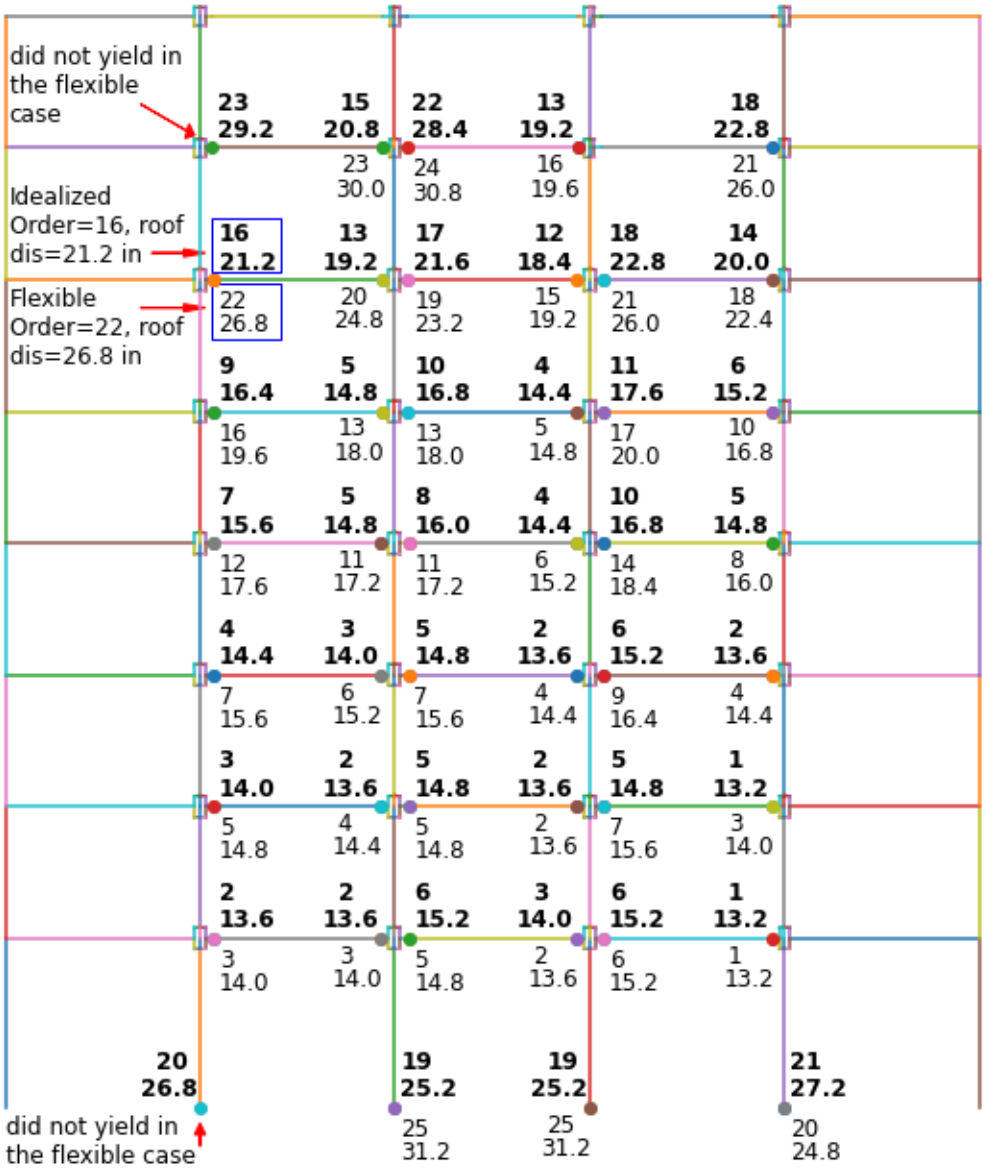

Figure 3.13-4. Plastic hinges development sequence for the OpenSeesPy, PDelta, Idealized and the Flexible support analysis of the 8-story building (Bold are the idealized foundation result, nonbold are the flexible foundation result).

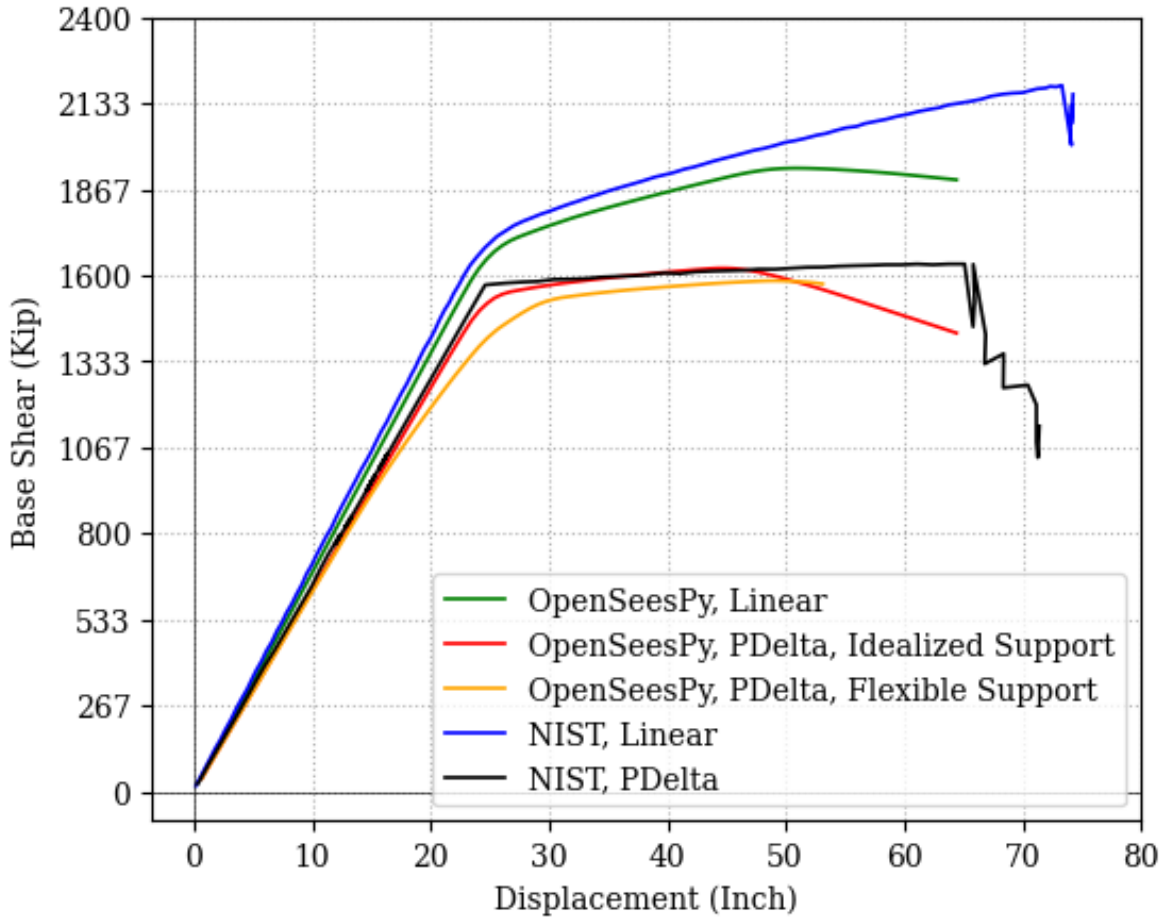

Figure 3.13-5. Pushover curve in the SMF direction for the 16-Story building.

In the 16-story building, the plastics hinges start at the mid of the building and end at the 15th floor. The column did not yield in the idealized and flexible cases, as shown in Figure 3.13-6.

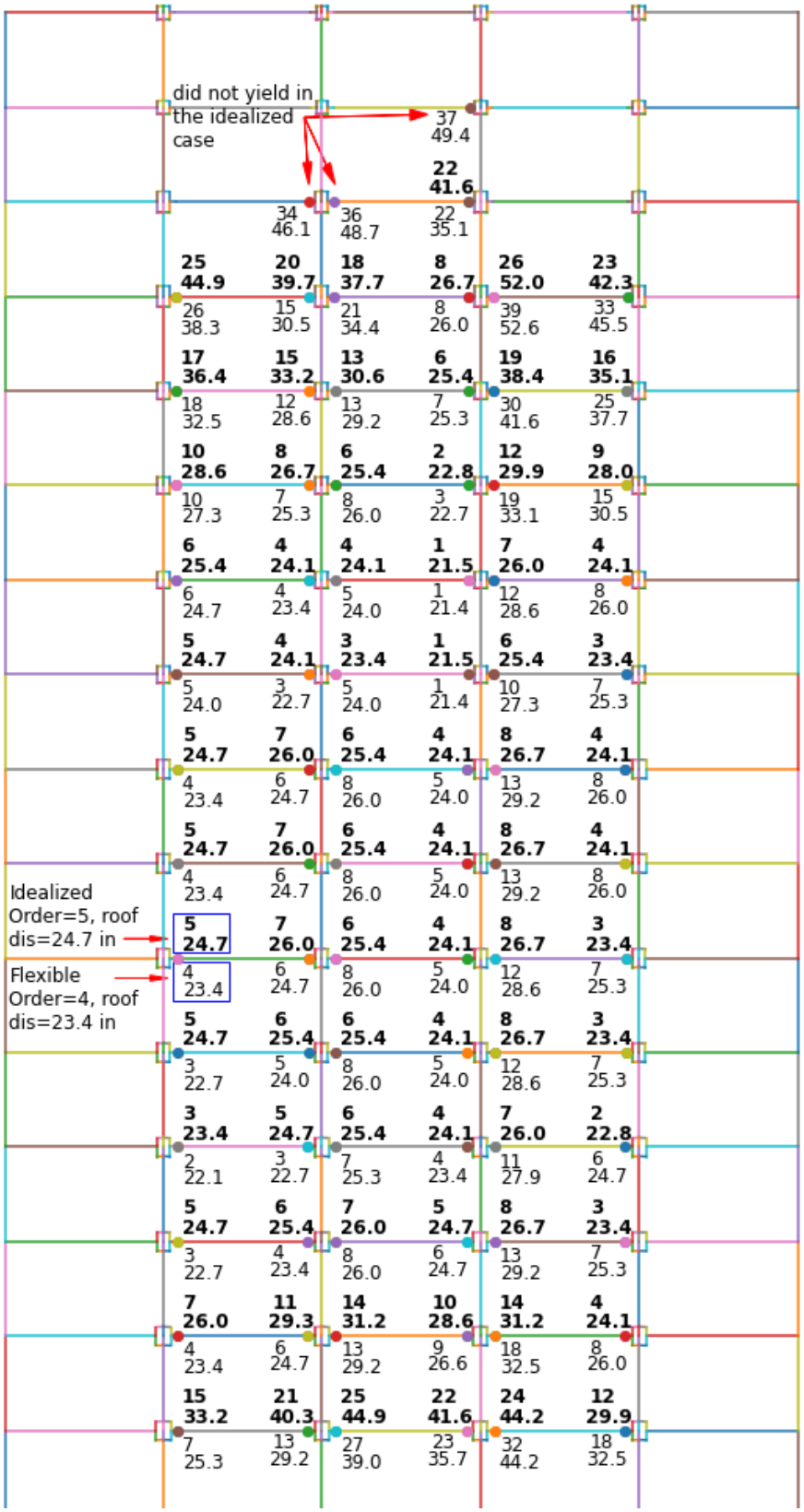

Figure 3.13-6.Plastic Hinges development sequence for the OpenSeesPy, PDelta, Idealized support analysis of the 16-story building.

Figure 3.13-7, Figure 3.13-9, and Figure 3.13-11 show a comparison between the OpenSeesPy pushover curve and the reference pushover curve in the BRBF direction (Speicher & Harris, 2018). Overall, the stiffness and strength of the buildings have been decreased. Figure 3.13-8, Figure 3.13-10, and Figure 3.13-12 show the sequence of BRB yielding. The yielding of the BRB element is at higher roof displacement because of the flexibility of the foundation. This is because of the displacement at the foundation. For the 4-story building, the BRB yielding starts at the third floor and ends at the first floors. For the 8-story building, the BRB yielding starts at the floors from 4th to 7th and ends at the first floors. For the 16-story building, the BRB yielding starts at the tenth floor and ends at the first floors. the results of the pushover analysis showed a lot of simultaneous yielding occurring in the BRB elements.

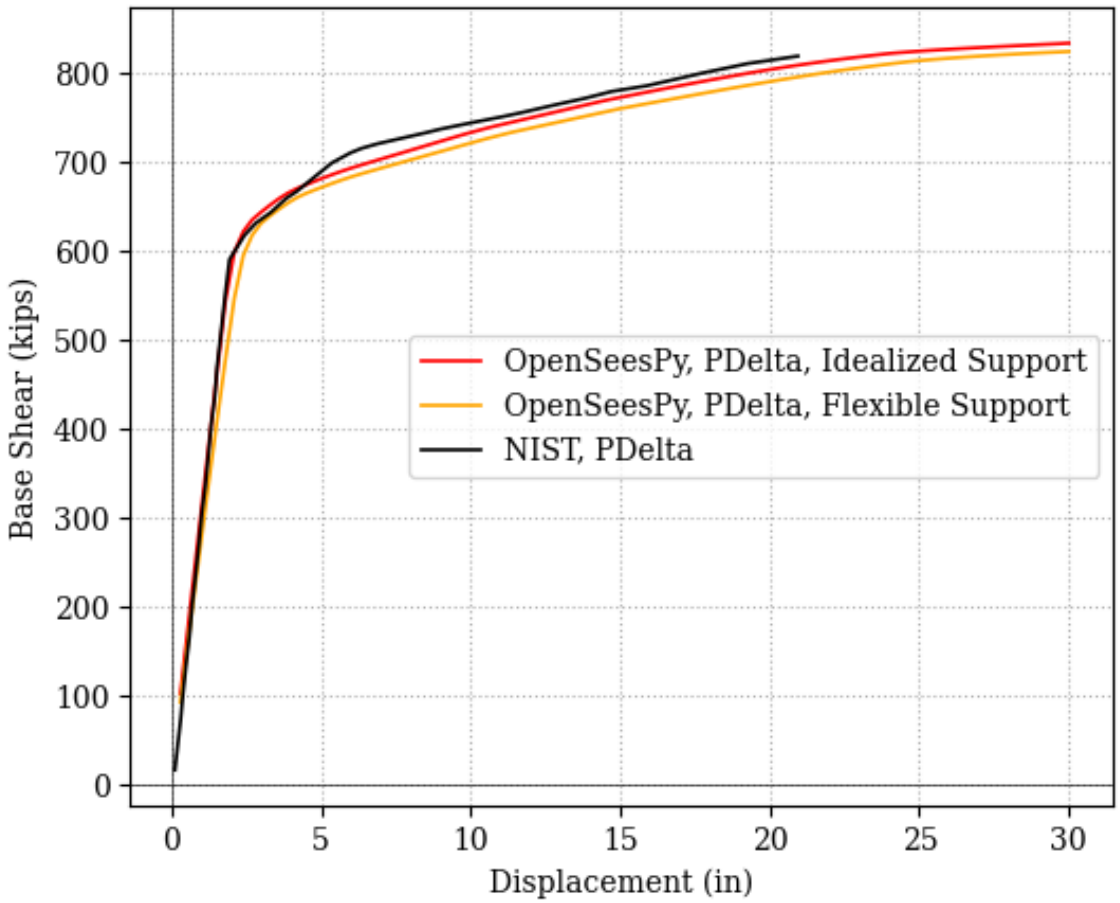

Figure 3.13-7. Pushover curve in the BRBF direction for the 4-Story building.

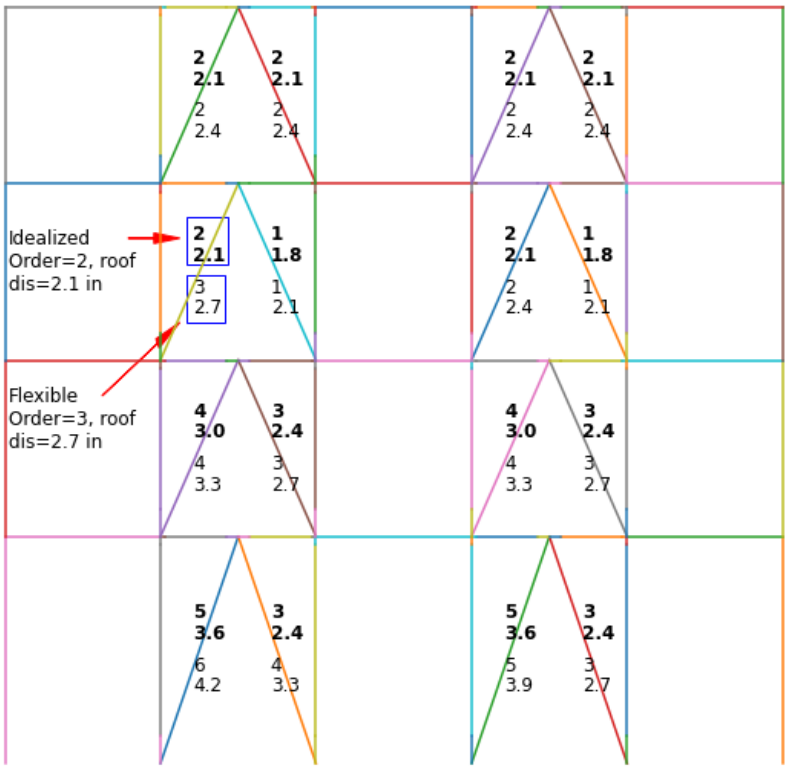

Figure 3.13-8. BRB yielding sequence for the OpenSeesPy, PDelta, Idealized and Flexible support analysis of the 4-story building.

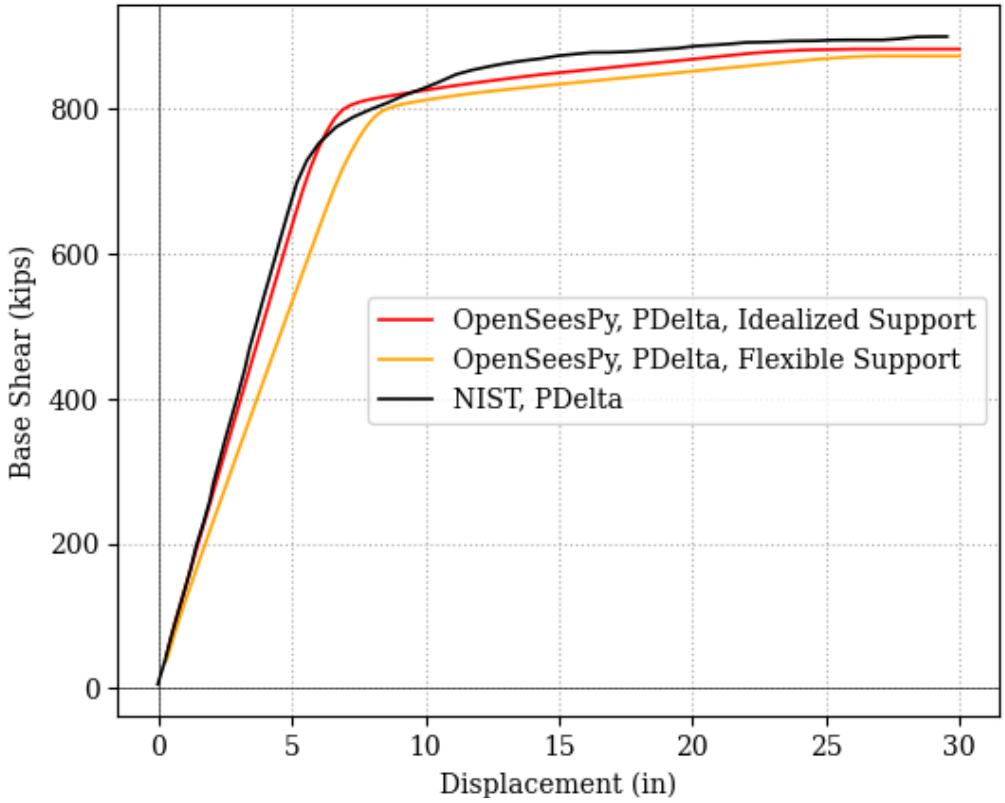

Figure 3.13-9. Pushover curve in the BRBF direction for the 8-Story building.

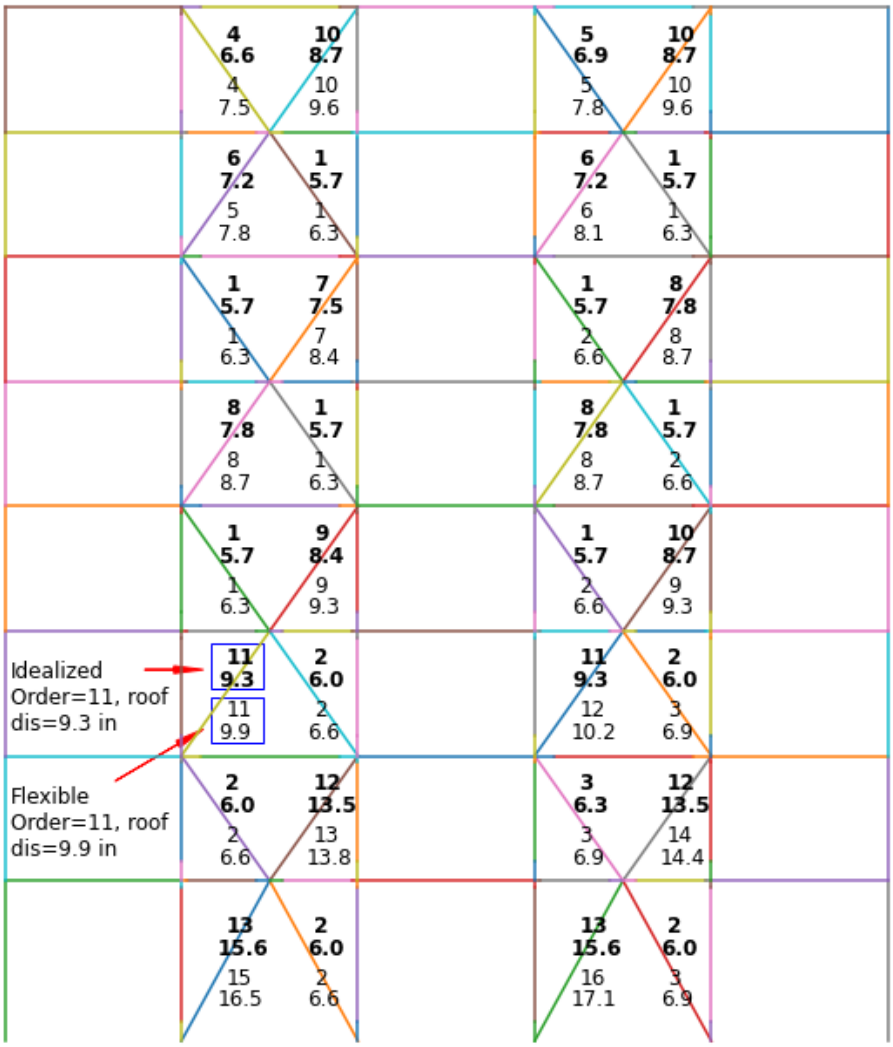

Figure 3.13-10. BRB yielding sequence for the OpenSeesPy, PDelta, Idealized support analysis of the 8-story building.

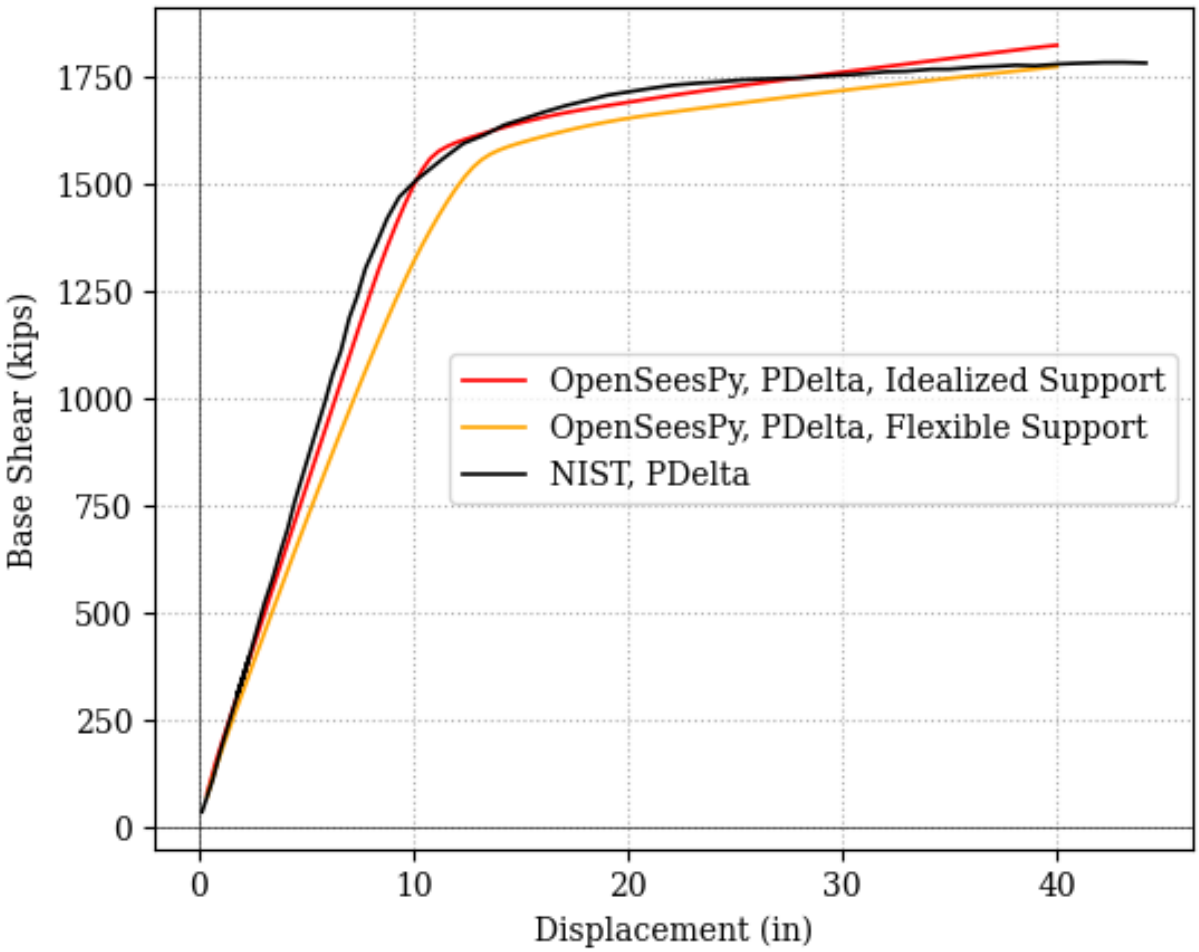

Figure 3.13-11. Pushover curve in the BRBF direction for the 16-Story building.

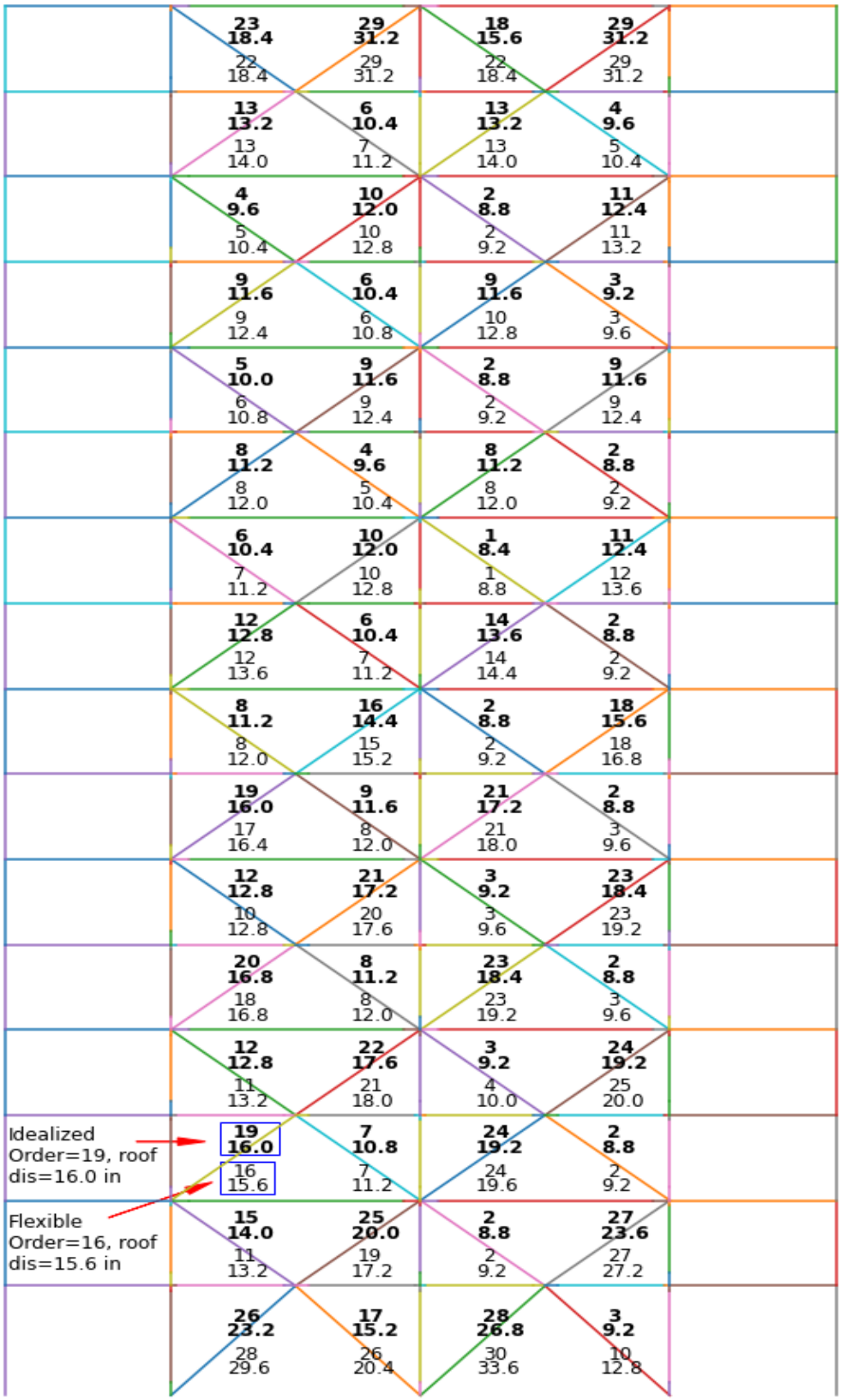

Figure 3.13-12. BRB yielding sequence for the OpenSeesPy, PDelta, Idealized and flexible support analysis of the 16-story building.

3.14 Damping

A damping ratio of 2.5% was assigned to all three buildings using the Rayleigh command. The two modes chosen for Rayleigh damping were the first mode (SMF direction) and the mode that capture more than 95% of the effective modal mass. The coefficients were assigned to the mass matrix and current stiffness matrix.

3.15 Earthquake Records

The ground motion records for the analysis came from the Far Field record set from the FEMA P695 document (FEMA, 2009).The earthquake records were selected by evaluating the suite of 22 earthquake records; 11 earthquakes were selected based upon using the records with the least squares error when compared to the MCE spectrum. The selected earthquakes were scaled to ensure that the mean value of the scaled suite is at least 90% of the MCE response spectrum or higher over the period range from $0.2*T_{1,ave}$ and $1.5* T_{1,ave}$. $T_{1,ave}$ is the average of the fundamental vibration period of the idealized and flexible foundation building models.

NRHA was conducted for the earthquake records in Table 3.15-1, Table 3.15-2, and Table 3.15-3 after applying the gravity load. Thirty seconds of zero excitation was added to the end of each earthquake record to capture the residual deformations. The plots of the scaled earthquakes and the mean along with design spectrum for the three buildings are shown in Figure 3.15-1, Figure 3.15-2, Figure 3.15-3, and Figure 3.15-4. the buildings were modeled in 3D, the NRHA was conducted in one direction.

Table 3.15-1 Earthquake, scale factor, and time step for the 4-story building in both BRBF and SMF directions

Order	P695 Number	Record Name	Event	Station	Scale Factor	Time Step (s)
1	FF02-1	LOS000	Northridge-1994	Canyon Country-West Lost Canyon	2.80	0.01
2	FF04-1	HEC000	Hector Mine-1999	Hector	4.00	0.01
3	FF05-1	H-DLT262	Imperial Valley-1979	Delta	3.62	0.01
4	FF06-1	H-E11140	Imperial Valley-1979	El Centro Array #11	2.11	0.005
5	FF08-1	SHI000	Kobe, Japan-1995	Shin-Osaka	2.27	0.01
6	FF09-1	DZC180	Kocaeli, Turkey-1999	Duzce	2.09	0.005
7	FF10-2	ARC090	Kocaeli, Turkey-1999	Arcelik	5.49	0.005
8	FF11-2	YER360	Landers-1992	Yermo Fire Station	3.36	0.02
9	FF16-1	B-ICC000	Superstition Hills-1987	El Centro Imp. Co. Center	3.34	0.005
10	FF19-2	CHY101-N	ChiChi, Taiwan-1999	CHY101-N	0.94	0.005
11	FF21-1	PEL090	San Fernando-1971	LA-Hollywood Stor Lot	4.25	0.01

Table 3.15-2 Earthquake, scale factor, and time step for the 8-story building in both BRBF and SMF directions

Order	P695 Number	Record Name	Event	Station	Scale Factor	Time Step (s)
1	FF04-1	HEC000	Hector Mine-1999	Hector	6.57	0.01
2	FF05-1	H-DLT262	Imperial Valley-1979	Delta	3.46	0.01
3	FF06-1	H-E11140	Imperial Valley-1979	El Centro Array #11	4.06	0.005
4	FF09-1	DZC180	Kocaeli, Turkey-1999	Duzce	1.92	0.005
5	FF10-2	ARC090	Kocaeli, Turkey-1999	Arcelik	3.17	0.005
6	FF11-2	YER360	Landers-1992	Yermo Fire Station	3.83	0.02
7	FF15-2	ABBAR-T	Manjil, Iran-1990	Manjil-Transverse	1.67	0.02
8	FF16-1	B-ICC000	Superstition Hills-1987	El Centro Imp. Co. Center	3.47	0.005
9	FF17-2	B-POE360	Superstition Hills-1987	Poe Road	4.80	0.01
10	FF19-2	CHY101-N	ChiChi, Taiwan-1999	CHY101-N	0.73	0.005
11	FF21-2	PEL180	San Fernando-1971	LA-Hollywood Stor Lot	6.82	0.01

Table 3.15-3 Earthquake, scale factor, and time step for the 16-story building in both BRBF and SMF directions

BRBF Direction						
Order	**P695 Number**	**Record Name**	**Event**	**Station**	**Scale Factor**	**Time Step (s)**
1	FF05-1	H-DLT262	Imperial Valley-1979	Delta	3.88	0.01
2	FF06-2	H-E11230	Imperial Valley-1979	El Centro Array #11	3.17	0.005
3	FF08-2	SHI090	Kobe, Japan-1995	Shin-Osaka	6.00	0.01
4	FF09-1	DZC180	Kocaeli, Turkey-1999	Duzce	1.56	0.005
5	FF10-2	ARC090	Kocaeli, Turkey-1999	Arcelik	3.21	0.005
6	FF11-2	YER360	Landers-1992	Yermo Fire Station	3.60	0.02
7	FF15-2	ABBAR-T	Manjil, Iran-1990	Manjil-Transverse	1.43	0.02
8	FF16-1	B-ICC000	Superstition Hills-1987	El Centro Imp. Co. Center	2.61	0.005
9	FF17-2	B-POE360	Superstition Hills-1987	Poe Road	4.26	0.01
10	FF19-2	CHY101-N	ChiChi, Taiwan-1999	CHY101-N	1.12	0.005
11	FF21-1	PEL090	San Fernando-1971	LA-Hollywood Stor Lot	3.73	0.01
SMF Direction						
Order	**P695 Number**	**Record Name**	**Event**	**Station**	**Scale Factor**	**Time Step (s)**
1	FF05-2	H-DLT352	Imperial Valley-1979	Delta	3.22	0.01
2	FF06-2	H-E11230	Imperial Valley-1979	El Centro Array #11	3.02	0.005
3	FF09-1	DZC180	Kocaeli, Turkey-1999	Duzce	2.69	0.005
4	FF10-2	ARC090	Kocaeli, Turkey-1999	Arcelik	3.09	0.005
5	FF11-2	YER360	Landers-1992	Yermo Fire Station	2.44	0.02
6	FF12-1	CLW-LN	Landers-1992	Coolwater-LN	3.58	0.025
7	FF15-2	ABBAR-T	Manjil, Iran-1990	Manjil-Transverse	2.08	0.02
8	FF16-1	B-ICC000	Superstition Hills-1987	El Centro Imp. Co. Center	2.45	0.005
9	FF19-1	CHY101-E	ChiChi, Taiwan-1999	CHY101-E	2.16	0.005
10	FF20-1	TCU045-E	ChiChi, Taiwan-1999	TCU045 E	1.97	0.005
11	FF21-1	PEL090	San Fernando-1971	LA-Hollywood Stor Lot	4.69	0.01

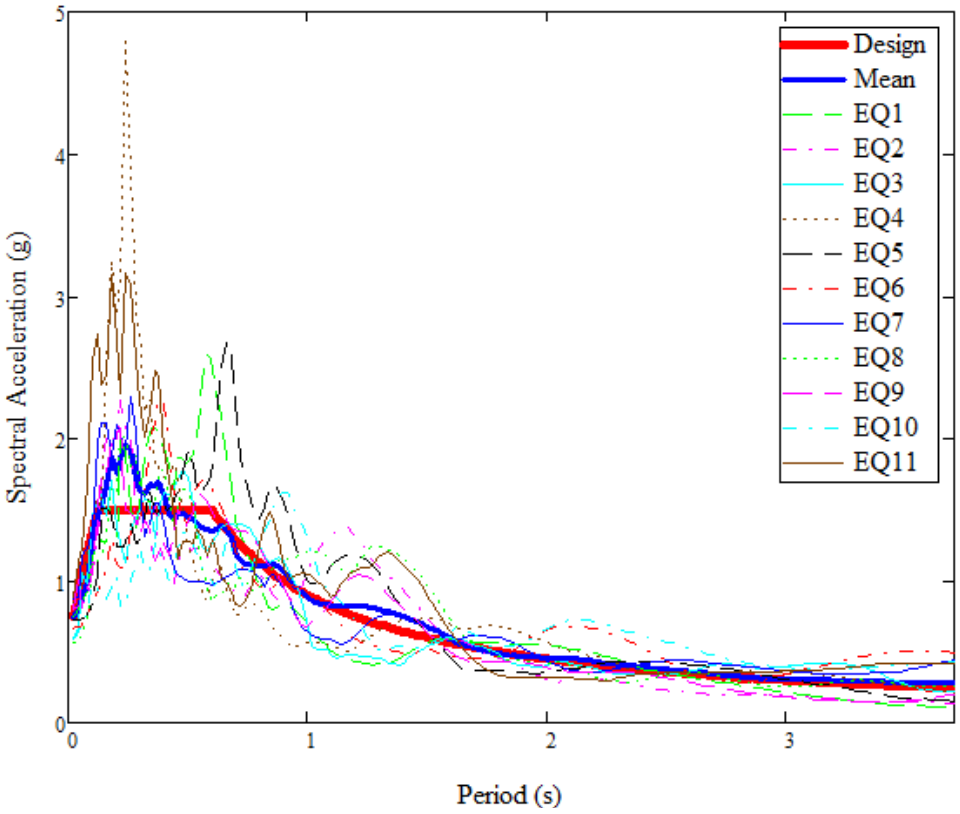

Figure 3.15-1 Scaled earthquakes for the 4-story building in the SMF and BRBF direction.

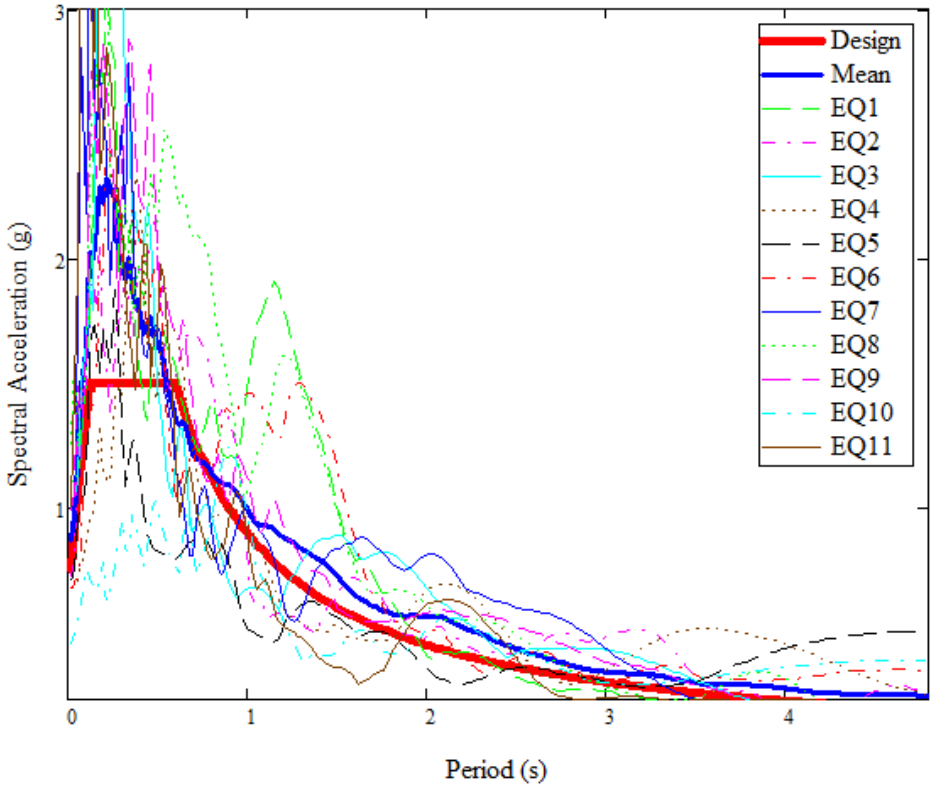

Figure 3.15-2 Scaled earthquakes for the 8-story building in the SMF and BRBF direction.

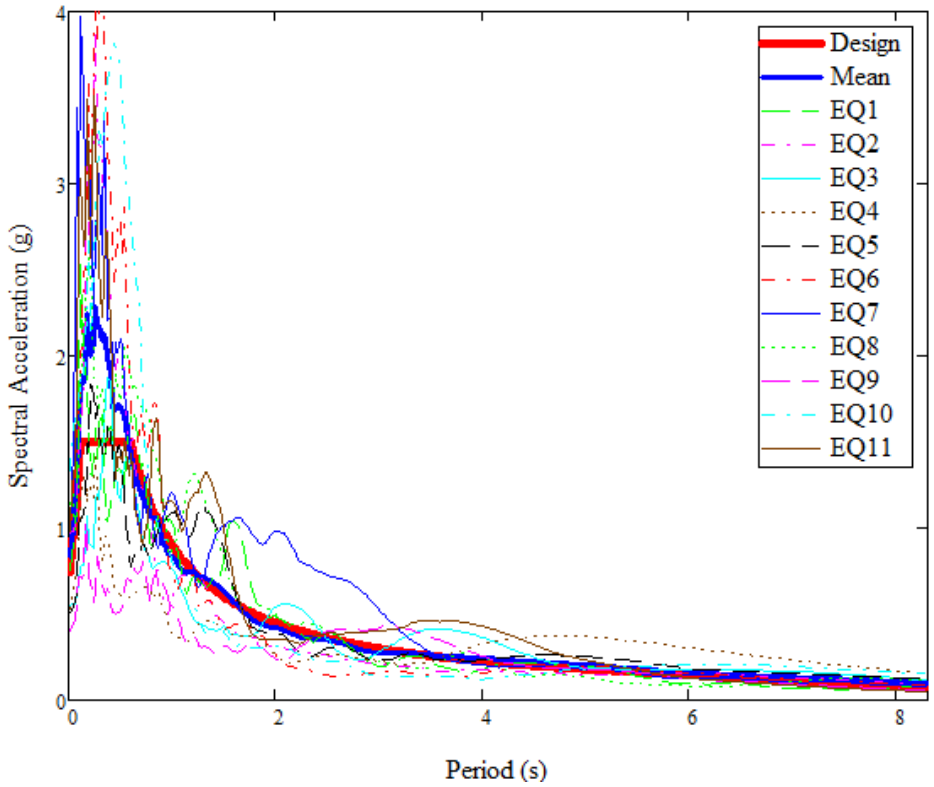

Figure 3.15-3 Scaled earthquakes for the 16-story building in the SMF direction.

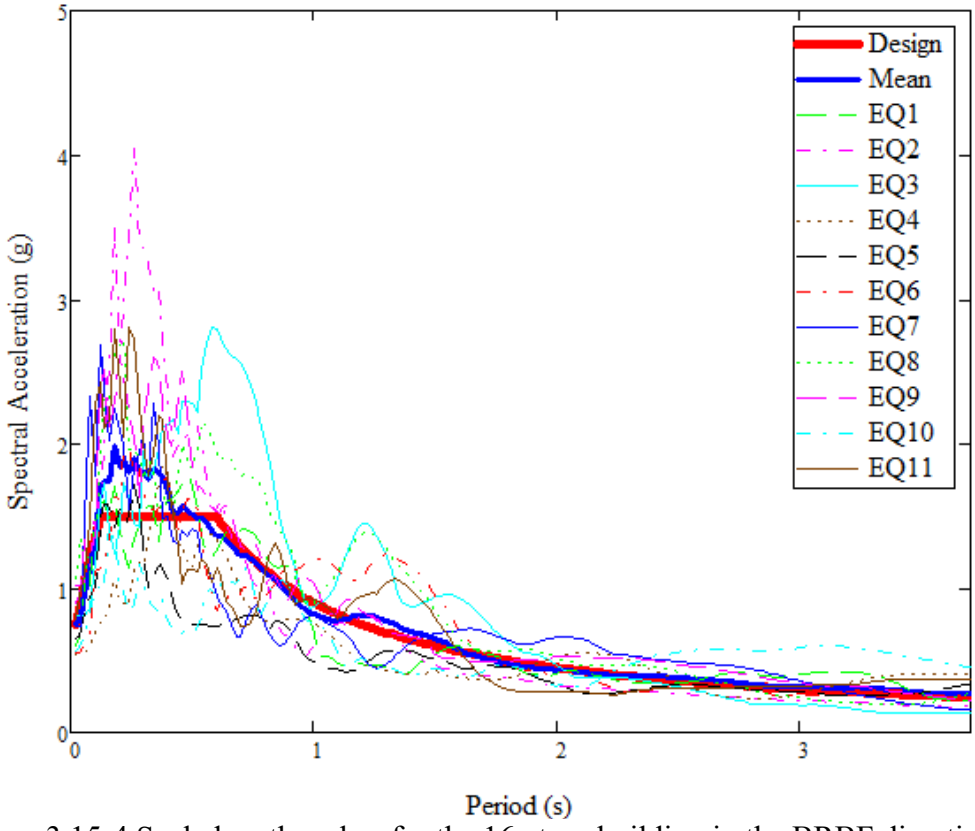

Figure 3.15-4 Scaled earthquakes for the 16-story building in the BRBF direction.

3.16 Summary

In this chapter, a detailed presentation about the building and the modeling methodology in OpenSeesPy is presented. The chapter starts with the building description to explain the dimensions, the layouts, and the lateral force-resisting systems of the buildings followed by the gravity, lateral, and mass calculations. Modal analysis results are presented and compared to the modal analysis results from the NIST report to verify the OpenSeesPy model. Information about the isolated, raft, and pile foundations modeling methodology is presented in detail along with the modeling of the panel zone, RBS, and the column lumped plasticity, and the procedure was verified against experimental data from the University of California. The BRB nonlinear modeling methodology is presented and verified against experimental data from Star Seismic and CoreBrace.

Pushover analysis was conducted for the three buildings in each direction for idealized and flexible foundations and the results are presented and compared with results from the NIST report. The sequence of element yielding (springs and BRB elements) is also presented for the idealized and flexible foundations cases. Finally, the damping ratio of the structure is presented, and the earthquake records that were used for the Dynamic analysis of the buildings are presented.

Chapter 4 Results and Discussion of Nonlinear Response History Analysis

4.1 Introduction

In this chapter, the results of the dynamic analysis are presented. Nonlinear response history analysis (NRHA) was conducted for eleven different earthquakes. The earthquakes were applied using a uniform excitation at the base of the buildings. The buildings were analyzed with flexible and idealized supports. The quantities that were captured during the analysis are (1) displacements and accelerations at each floor and at the base, (2) column forces and moments, (3) moment and rotation at the RBS and columns' springs, and (4) stress and strain in the BRB elements. The displacements and accelerations of the floors were recorded at the center of the rigid diaphragm (main node of the rigid diaphragm), while the displacement and acceleration at the base (for flexible support conditions) were recorded at the individual foundation then the average displacement and acceleration were calculated. The drift was calculated by dividing the floor displacement by the height of the floor. In the following comparison, the idealized foundation is considered the reference, so the increment or decrement ratios are with respect to the idealized foundation case. The plots are between the mean of the idealized footing results and the flexible footing results, plus and minus of standard deviation is also added to the plots. The tables show the percentage of change between the flexible footing results and the idealized footing results. Positive percentage means that the flexible footing response is higher than the idealized footing response and vice versa.

4.2 4-story Building Seismic Response

4.2.1 SMF

The results of the 4-story building dynamic analysis in the SMF direction are presented in this section along with a comparison between the idealized and flexible foundation. The results

show an increase in the maximum absolute displacement, as shown in Figure 4.2-1. The reason for this increase is because of the flexibility that the foundation added to the structure. Only EQ8 and EQ11 showed a decrease in the maximum displacement, while all the other earthquakes showed an increase in the displacement by different amounts, as shown in Table 4.2-1. EQ6 showed the highest increase in the displacement. The increase or decrease in the displacement depends on the nature of the earthquake but the overall trend is to increase the displacement of the structure by modeling the flexibility of the foundation.

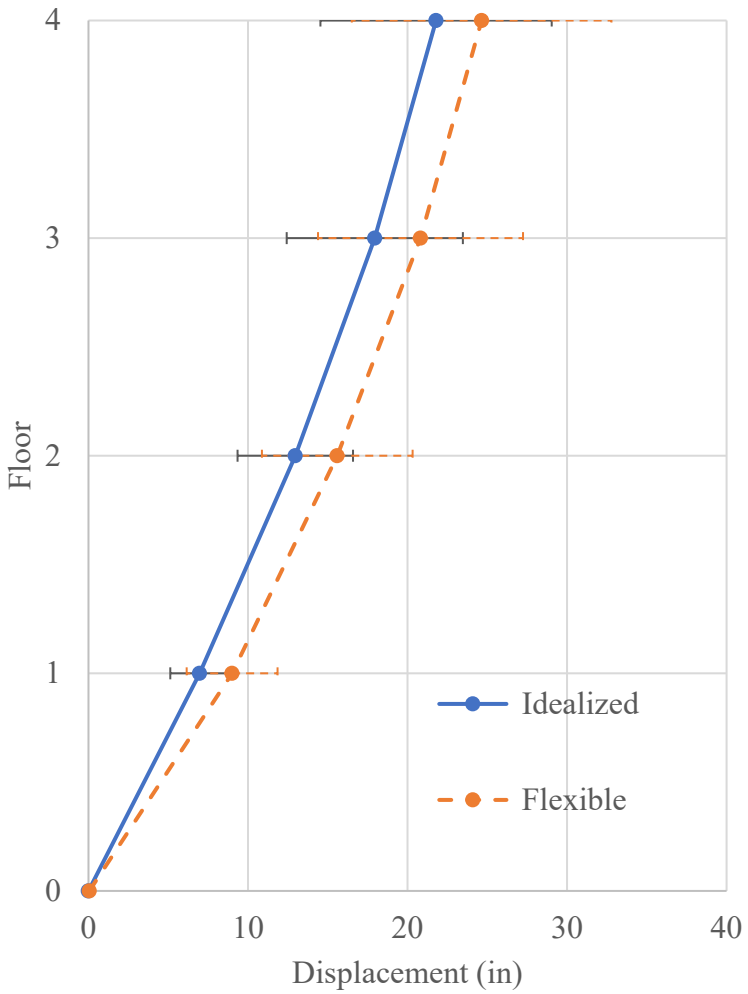

Figure 4.2-1 Average of maximum displacements for the SMF direction of the 4-story building.

Table 4.2-1 Difference in maximum story displacement (inch) for the SMF direction of the 4-story building.

Story	EQ1	EQ2	EQ3	EQ4	EQ5	EQ6	EQ7	EQ8	EQ9	EQ10	EQ11	Average
1	3.8	2.2	0.7	2.1	0.6	6.2	1.7	-0.4	4.3	1.3	-0.2	2.0
2	4.4	1.9	1.1	2.0	1.8	8.8	2.6	-1.3	6.2	2.4	-1.1	2.6
3	3.5	2.3	1.7	1.4	3.4	9.9	3.6	-2.5	6.7	3.4	-2.0	2.9
4	1.7	2.0	2.8	-0.3	4.0	11.2	4.5	-3.1	6.8	4.2	-2.4	2.9

Overall, the residual displacement decreased for the SMF direction as shown in Figure 4.2-2. EQ5, EQ7, EQ9, and EQ10 showed an increase in the residual displacement, as shown in Table 4.2-2. The other earthquakes showed a decrease in the residual displacement. The average reduction in residual displacement for each story ranged from 0.8 to 1.9 inches.

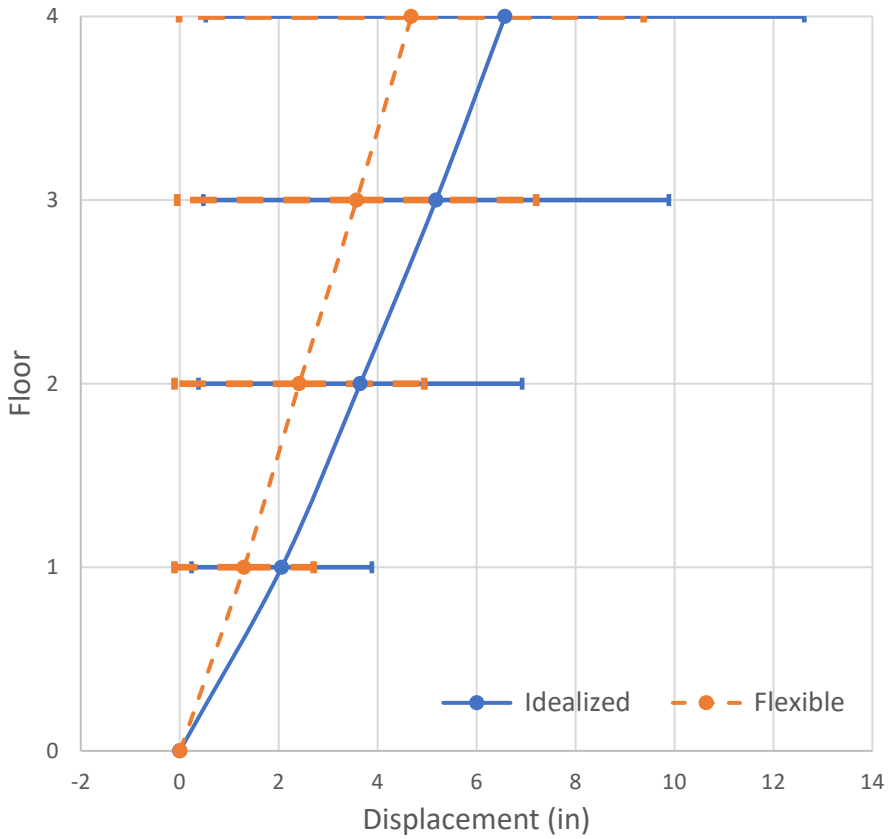

Figure 4.2-2 Average residual displacement for the SMF direction of the 4-story building.

Table 4.2-2 Difference in residual displacement (inch) for the SMF direction of the 4-story building.

Story	EQ1	EQ2	EQ3	EQ4	EQ5	EQ6	EQ7	EQ8	EQ9	EQ10	EQ11	Average
1	-2.0	-0.4	-2.9	-1.6	0.3	-0.9	0.8	-0.9	1.2	-0.2	-1.6	-0.8
2	-3.4	-0.4	-5.4	-2.3	0.6	-1.5	1.7	-1.7	1.4	-0.1	-2.4	-1.2
3	-5.1	-0.4	-7.5	-2.8	1.1	-1.7	2.7	-2.6	1.5	0.4	-3.2	-1.6
4	-7.0	-0.6	-8.9	-3.6	1.7	-1.0	3.6	-3.7	1.7	1.0	-4.0	-1.9

For the story drift, there is an increase in the drift of the 1st, 2nd, and 3rd stories, while the 4th story showed a decrease in story drifts as compared to the idealized foundation, as shown in Figure 4.2-3 and Table 4.2-3. EQ8 and EQ11 showed a reduction in drift, while the others showed

an increase in drift. The average increase in the drift of the first three stories ranged from 2% to 29%, and the decrease in the fourth story is 3%.

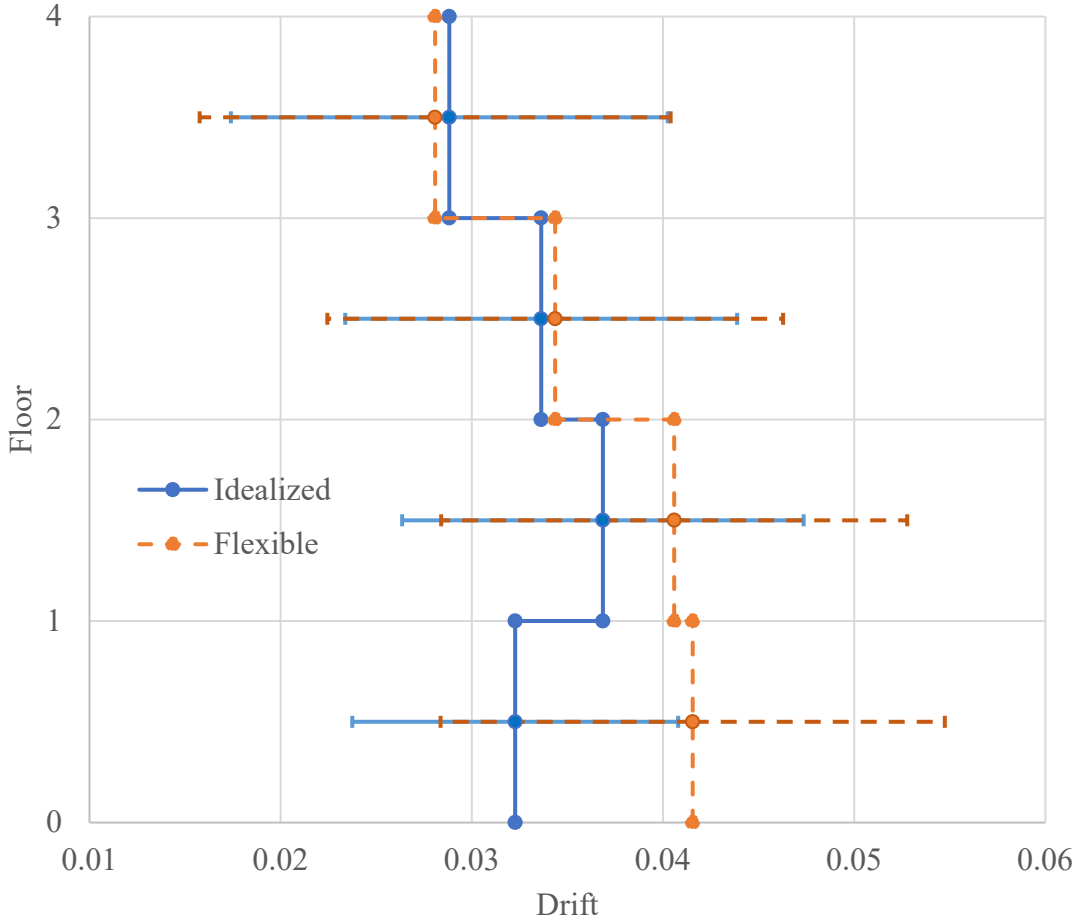

Figure 4.2-3 Average maximum drift for the SMF direction of the 4-story building.

Table 4.2-3 Average maximum drift for the SMF direction of the 4-story building.

Floor	Idealized		Flexible		Percentage Change	
	Average	Standard Deviation	Average	Standard Deviation	Average	Standard Deviation
0-1	0.0323	0.0085	0.0416	0.0132	29	55
1-2	0.0369	0.0105	0.0406	0.0122	10	16
2-3	0.0336	0.0102	0.0344	0.0119	2	16
3-4	0.0288	0.0114	0.0281	0.0123	-3	8

There is a reduction in the residual drift when modeling the foundation as shown in Figure 4.2-4. The reduction in the average residual drift ranged from $1.7*10^{-3}$ (at the fourth story) to

3.5*10^{-3} % (at the first story). For individual records, EQ5, EQ7, and EQ9 showed an increase in the residual drift with 5.4*10^{-3} as maximum increase happened at the first floor during EQ9. EQ10 showed a decrease in the first story drift and increase in the drift of the rest stories. The increase ranged from 0.8*10^{-3} (at the second floor) to 3.4*10^{-3} at the fourth floor, while the other earthquakes showed a decrease in the residual drift, as shown in Table 4.2-4.

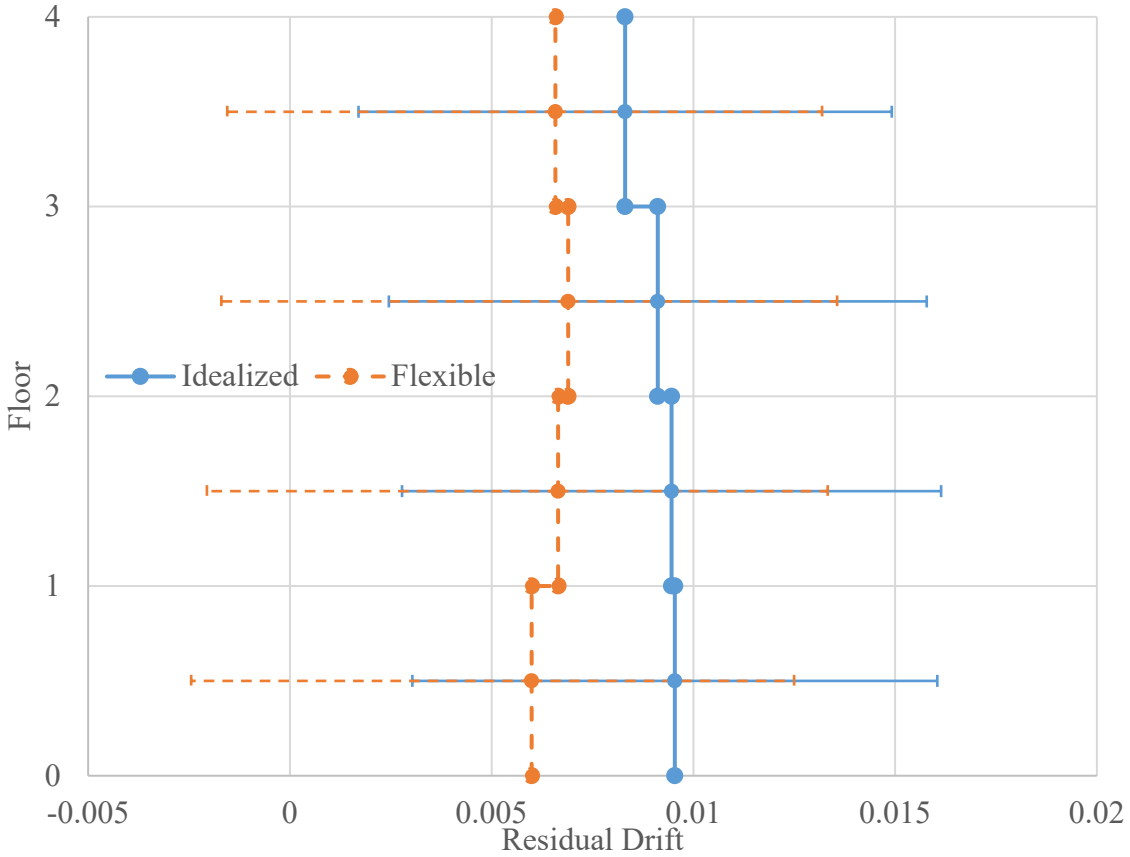

Figure 4.2-4 Average residual drift for the SMF direction of the 4-story building.

Table 4.2-4 Difference in residual drift for the SMF direction of the 4-story building (*10^{-3}).

Story	EQ 1	EQ 2	EQ 3	EQ 4	EQ 5	EQ 6	EQ 7	EQ 8	EQ 9	EQ 10	EQ 11	Average
0-1	-9.4	-1.7	-13.7	-7.6	1.2	-4.0	3.7	-4.3	5.4	-1.1	-7.5	-3.5
1-2	-8.4	-0.3	-14.4	-4.2	2.0	-4.0	5.4	-4.6	1.6	0.8	-4.9	-2.8
2-3	-9.7	-0.1	-12.8	-2.9	3.1	-1.2	5.8	-5.4	0.4	2.8	-4.6	-2.2
3-4	-11.4	-1.0	-8.6	-4.7	3.2	4.5	5.6	-6.5	1.1	3.4	-4.5	-1.7

Total acceleration increased at the base by 27% and decreased at the elevated floors. The decrease in the elevated floors acceleration ranged from 11% (at the fourth floor) to 19% (at the third floor), as shown in Figure 4.2-5. Table 4.2-5 shows the percentage change in the acceleration of the floors. All the earthquakes showed increase in the base acceleration except EQ4 showed zero change in the base acceleration for an individual record.

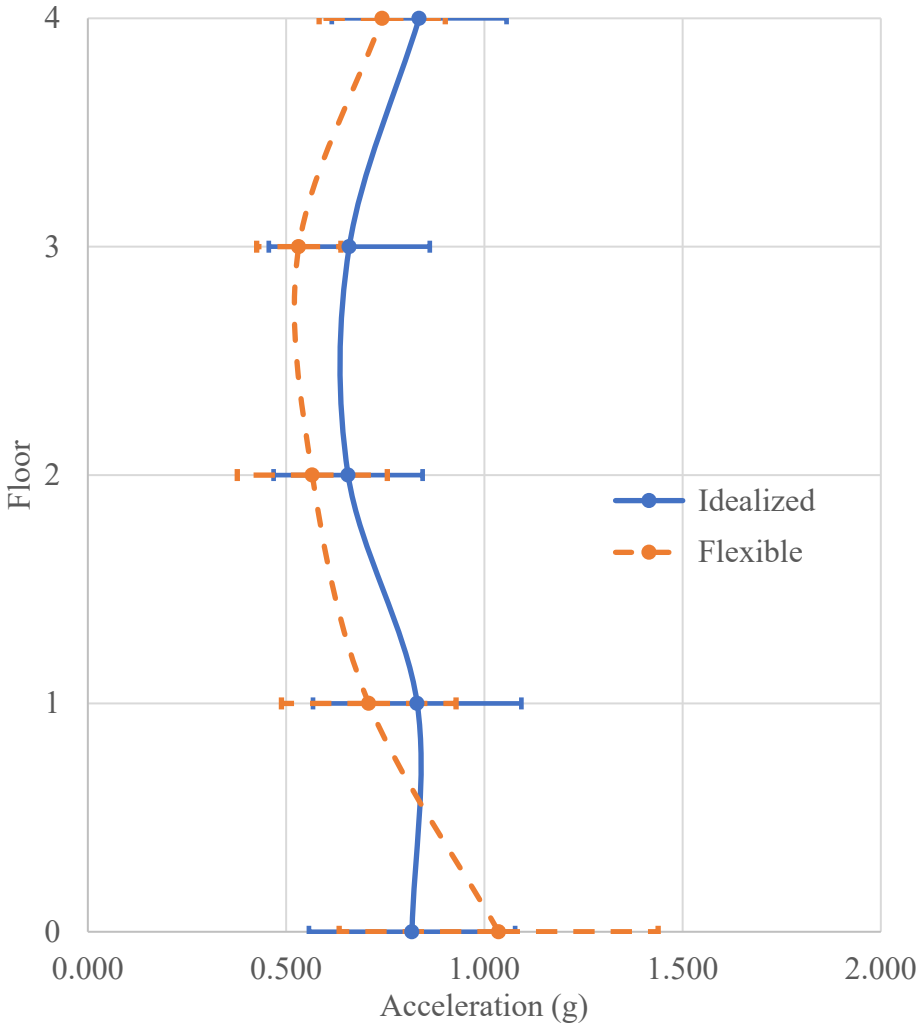

Figure 4.2-5 Average maximum total acceleration for the SMF direction of the 4-story building.

Table 4.2-5 Percentage change in maximum total acceleration for the SMF direction of the 4-story building.

Story	EQ 1	EQ 2	EQ 3	EQ 4	EQ 5	EQ 6	EQ 7	EQ 8	EQ 9	EQ 10	EQ 11	Average
0	24	16	54	0	1	5	46	18	20	24	66	27
1	-21	-28	-10	-22	0	-18	7	-19	-31	-17	10	-15
2	1	-29	-6	-22	-9	-23	-11	-31	-23	-5	9	-14
3	-22	-28	-4	-23	9	-23	0	-23	-44	4	-17	-19
4	-6	-22	-10	-16	1	-9	-1	-5	-34	-12	9	-11

For the elevated floors and base shear, overall, there is a reduction of shear in the range of 12% (at the base) to 25% (at the fourth floor), as shown in Figure 4.2-6 and Table 4.2-6. EQ7 and EQ10 showed an increase in the base shear by 1%. EQ11 did not show increase in the base shear, showed increase in the third and fourth floor shear by 1% and 16% respectively, and showed an increase in the second-floor shear by 19%. All other earthquakes showed a decrease in the elevated floors and base shear. A calculation was conducted to determine the allowable reduction in the ELF base shear in accordance with ASCE 7-16 section 19.2. The allowed reduction in ASCE 7-16 is 10% for the base shear, but the NRHA showed an average reduction of 12%.

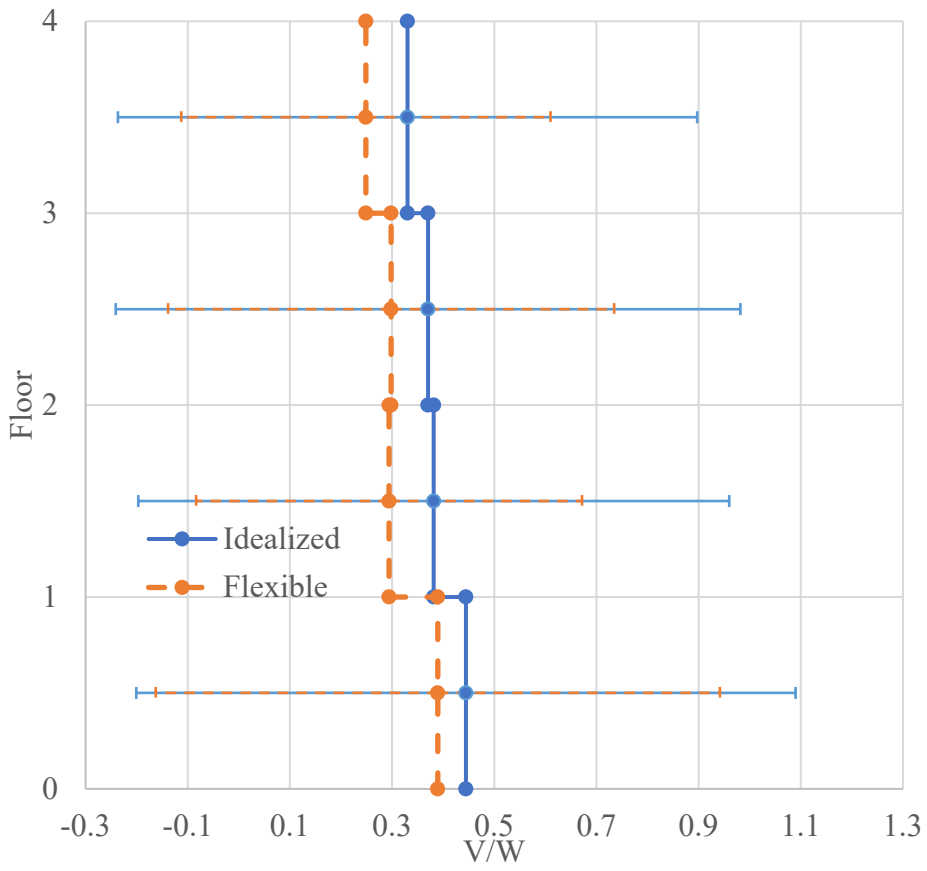

Figure 4.2-6 Average maximum floor shear and base shear for the SMF direction.

Table 4.2-6 Percentage change in maximum floor shear/weight for the SMF direction of the 4-story building.

Story	EQ1	EQ2	EQ3	EQ4	EQ5	EQ6	EQ7	EQ8	EQ9	EQ10	EQ11	Average
0-1	-12	-13	-6	-26	-8	-20	1	-15	-15	1	0	-12
1-2	-12	-20	-8	-17	-3	-17	-3	-2	-37	-1	-19	-23
2-3	-9	-16	-1	-27	-4	-17	-6	-5	-30	-11	1	-20
3-4	-6	-22	-11	-16	-4	-11	-6	-7	-37	-20	16	-25

For energy dissipation, certain RBS elements have been selected as shown in Figure 4.2-7. The energy dissipation has been calculated at those RBS springs to capture the general trend of the RBS springs behavior. The energy dissipation in those springs has decreased, as shown in Table 4.2-7. The maximum percentage reduction in the energy dissipation was 34% at RBS number

44002 which is located at the third floor. The reduction in the energy dissipation at the third and fourth floors was higher than the reduction at the first and second floors. The maximum rotation increased in some RBS springs by a maximum ratio of 14.4% and decreased in the others by a maximum ratio of 11.4%, as shown in Table 4.3-8. The energy dissipation decreased although the maximum rotation increased because the accumulation of plastic rotation (after RBS yielded) is less in the flexible case compared to the idealized case. Thereby the cumulative energy dissipation in the flexible case is lower than the idealized case. Also, the energy dissipation tracks the behavior of the RBS from the beginning till the end of the analysis, while the maximum rotation depends only on the cycle that produce the highest rotation. So, the cumulative energy dissipation in the flexible case is less because it depends on the all the cycles.

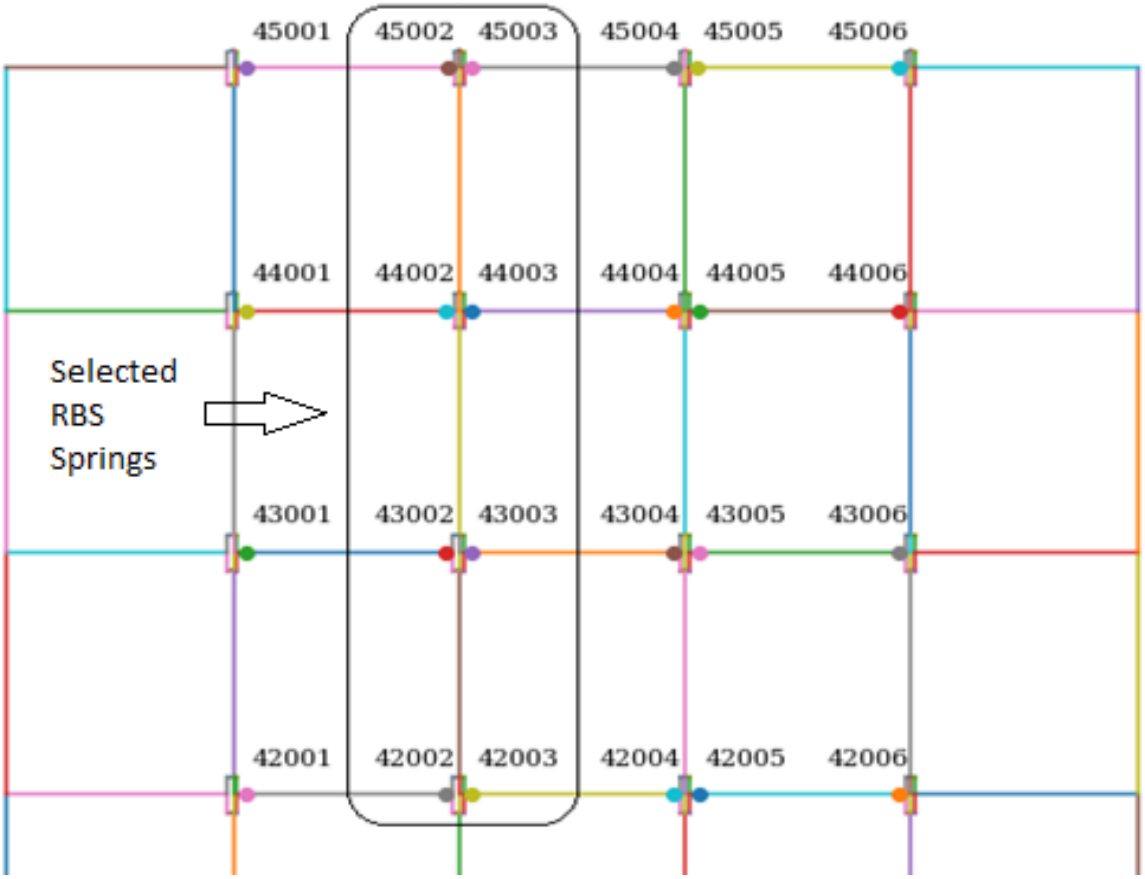

Figure 4.2-7 Selected RBS for energy calculation in the SMF direction of the 4-story building.

Table 4.2-7 Average energy dissipation at the selected RBS springs of the 4-story building.

RBS	Idealized		Flexible		Percentage Change	
	Average (kip*in)	standard deviation	Average (kip*in)	standard deviation	Average	standard deviation
42002	1735	1396	1684	1365	-3	-2
42003	1802	1611	1782	1528	-1	-5
43002	1105	866	975	843	-12	-3
43003	1119	872	1021	841	-9	-4
44002	606	616	401	463	-34	-25
44003	641	644	449	500	-30	-22
45002	194	231	133	168	-31	-27
45003	208	238	149	172	-29	-28

Table 4.2-8 Average of maximum rotation at the selected RBS springs of the 4-story building.

RBS	Idealized		Flexible		Percentage Change	
	Average (rad)	Standard Deviation	Average (rad)	Standard Deviation	Average	Standard Deviation
42002	0.0311	0.0133	0.0356	0.0161	14	21
42003	0.0319	0.0119	0.0365	0.0156	14	31
43002	0.0279	0.0128	0.0292	0.0155	5	21
43003	0.0290	0.0123	0.0300	0.0146	4	19
44002	0.0214	0.0131	0.0201	0.0151	-6	15
44003	0.0232	0.0125	0.0211	0.0143	-9	14
45002	0.0158	0.0139	0.0140	0.0150	-11	8
45003	0.0172	0.0137	0.0151	0.0143	-12	4

The column springs at the base were selected to evaluate the general behavior trend as shown in Figure 4.2-8. The energy dissipation at the selected column springs decreased by a maximum percentage of 90%, as shown in Table 4.2-9. Some of the column springs did not yield in the flexible case, while the same springs did yield in the idealized case. That is because of the footing rotational flexibility, which reduces the required rotation on the column springs. All the springs dissipated less energy in the flexible case for all earthquakes cases except spring 120201 and 120501 have dissipated more energy for EQ9. The standard deviation in the flexible case is very high because the column springs did not yield in the flexible case which makes the spread of the data very high, as shown in Table 4.2-10. At the same time, the maximum rotation in the column springs were decreased, as shown in Table 4.2-11.

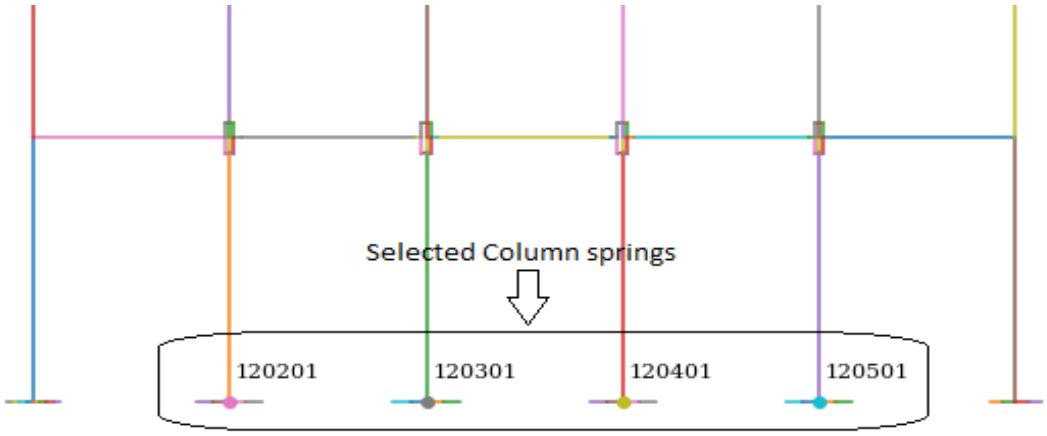

Figure 4.2-8 Selected column springs for the 4-story building.

Table 4.2-9 Energy dissipation at the selected column springs of the 4-story building.

Column	Idealized		Flexible		Percentage Change	
	Average (kip*in)	Standard Deviation	Average (kip*in)	Standard Deviation	Average	Standard Deviation
120201	367	285	111	196	-70	-31
120301	777	527	80	173	-90	-67
120401	777	527	82	174	-90	-67
120501	370	284	112	198	-70	-30

Table 4.2-10 Energy dissipation at the selected column springs of the 4-story building for each earthquake.

Idealized foundation (kip*ft)											
Column Spring	EQ 1	EQ 2	EQ 3	EQ 4	EQ 5	EQ 6	EQ 7	EQ 8	EQ 9	EQ 10	EQ 11
120201	79	19	45	18	0	24	62	11	40	20	17
120301	150	51	107	43	0	51	117	36	79	45	33
120401	150	51	107	43	0	51	117	36	79	45	33
120501	80	19	44	18	0	24	62	12	41	20	18
Flexible foundation (kip*ft)											
Column Spring	EQ 1	EQ 2	EQ 3	EQ 4	EQ 5	EQ 6	EQ 7	EQ 8	EQ 9	EQ 10	EQ 11
120201	0	0	34	0	0	0	42	0	0	26	0
120301	0	0	13	0	0	0	47	0	0	13	0
120401	0	0	14	0	0	0	47	0	0	14	0
120501	0	0	38	0	0	0	41	0	0	24	0

Table 4.2-11 Average of the maximum rotation at the selected column springs of the 4-story building.

Column Spring	Idealized		Flexible		Percentage of change	
	Average (rad)	Standard Deviation	Average (rad)	Standard Deviation	Average	Standard Deviation
120201	0.0119	0.0073	0.0047	0.0074	-61	1
120301	0.0130	0.0075	0.0027	0.0054	-79	-28
120401	0.0130	0.0075	0.0028	0.0054	-79	-28
120501	0.0120	0.0072	0.0053	0.0092	-56	27

4.2.2 BRBF

The results of the 4-story building dynamic analysis in the BRBF direction are presented in this section along with a comparison between idealized and flexible foundation. The results show a slight increase in the maximum displacement in range from 0.2 inch (at the first floor) to 1.1 inch (at the fourth floor), as shown in Figure 4.2-9. EQ2 showed a decrease in the maximum displacement for all the floors in range from 1% (at the fourth floor) to 6% (at the first floor), while all the other earthquakes showed an increase in the displacement for all the floors. EQ5 showed the highest increase in displacement with 20% at the fourth floor, as shown in Table 4.2-12.

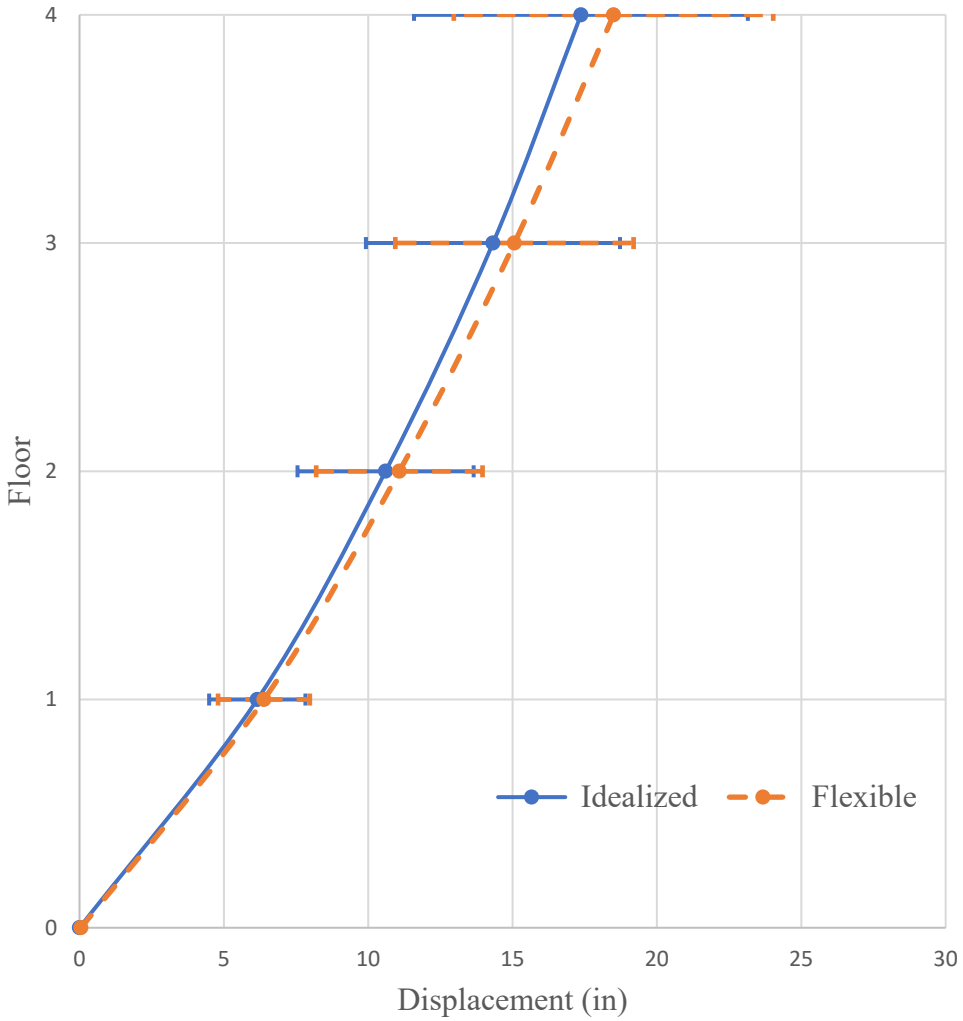

Figure 4.2-9 Maximum average displacement BRBF direction

Table 4.2-12 Difference in maximum story displacement (inch) at each floor for the BRBF direction of the 4-story building.

Story	EQ 1	EQ 2	EQ 3	EQ 4	EQ 5	EQ 6	EQ 7	EQ 8	EQ 9	EQ 10	EQ 11	Average
1	0.0	-0.5	0.1	0.4	0.6	0.1	0.5	0.2	0.2	0.3	0.6	0.2
2	0.2	-0.7	0.3	0.8	1.1	0.2	1.1	0.6	0.3	0.4	1.1	0.5
3	0.3	-0.6	0.4	1.1	1.7	0.5	1.6	1.0	0.3	0.4	1.7	0.7
4	0.5	-0.2	0.5	1.5	2.1	1.3	2.4	1.3	0.3	0.4	2.3	1.1

The change in the average residual displacement of the BRBF was small in range from zero (at the first floor) to 0.2 inch (at the four floor), as shown in Figure 4.2-10. Some earthquakes had

a higher difference in the residual displacement, as shown in Table 4.2-13. That indicate that the impact on the BRBF residual displacement of the 4-story building is negligible.

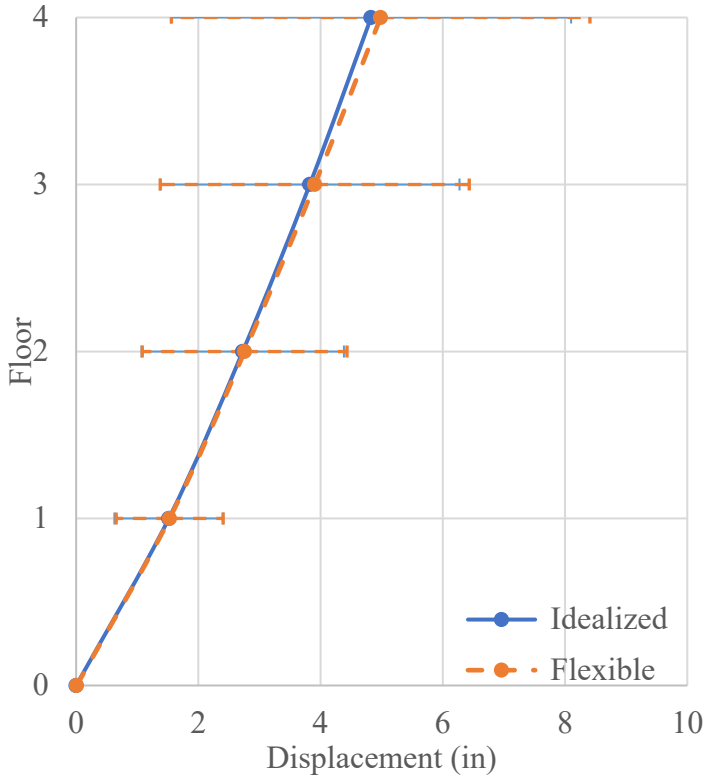

Figure 4.2-10 Average residual deformation in the BRBF direction of the 4-story building.

Table 4.2-13 Difference in residual displacement (inch) for the BRBF direction of the 4-story building.

Story	EQ 1	EQ 2	EQ 3	EQ 4	EQ 5	EQ 6	EQ 7	EQ 8	EQ 9	EQ 10	EQ 11	Average
1	-0.3	-0.2	-0.5	0.2	0.3	0.3	-0.2	0.1	0.3	0.1	0.1	0.0
2	-0.4	-0.3	-1.0	0.5	0.5	0.5	-0.4	0.2	0.5	0.0	0.2	0.0
3	-0.5	-0.2	-1.3	0.7	0.6	0.9	-0.7	0.3	0.8	-0.1	0.2	0.1
4	-0.5	-0.1	-1.6	1.1	0.7	1.3	-0.9	0.5	1.1	-0.2	0.1	0.2

There is an increase in the average maximum story drift, as shown in Figure 4.2-11. The increase ranged from $0.9*10^{-3}$ (at the first floor) to $2.4*10^{-3}$ (at the fourth floor). EQ7 had the maximum story drift increase by $6*10^{-3}$ at the fourth floor. All the earthquakes showed an increase in the drift except EQ2, which showed a decrease in the drift at the first and second floor by 2.3*

10^{-3} and $1.2*10^{-3}$ respectively and EQ1 at the first floor by $0.2*10^{-3}$, as shown in Table 4.2-14. Overall, the impact is small and can be neglect.

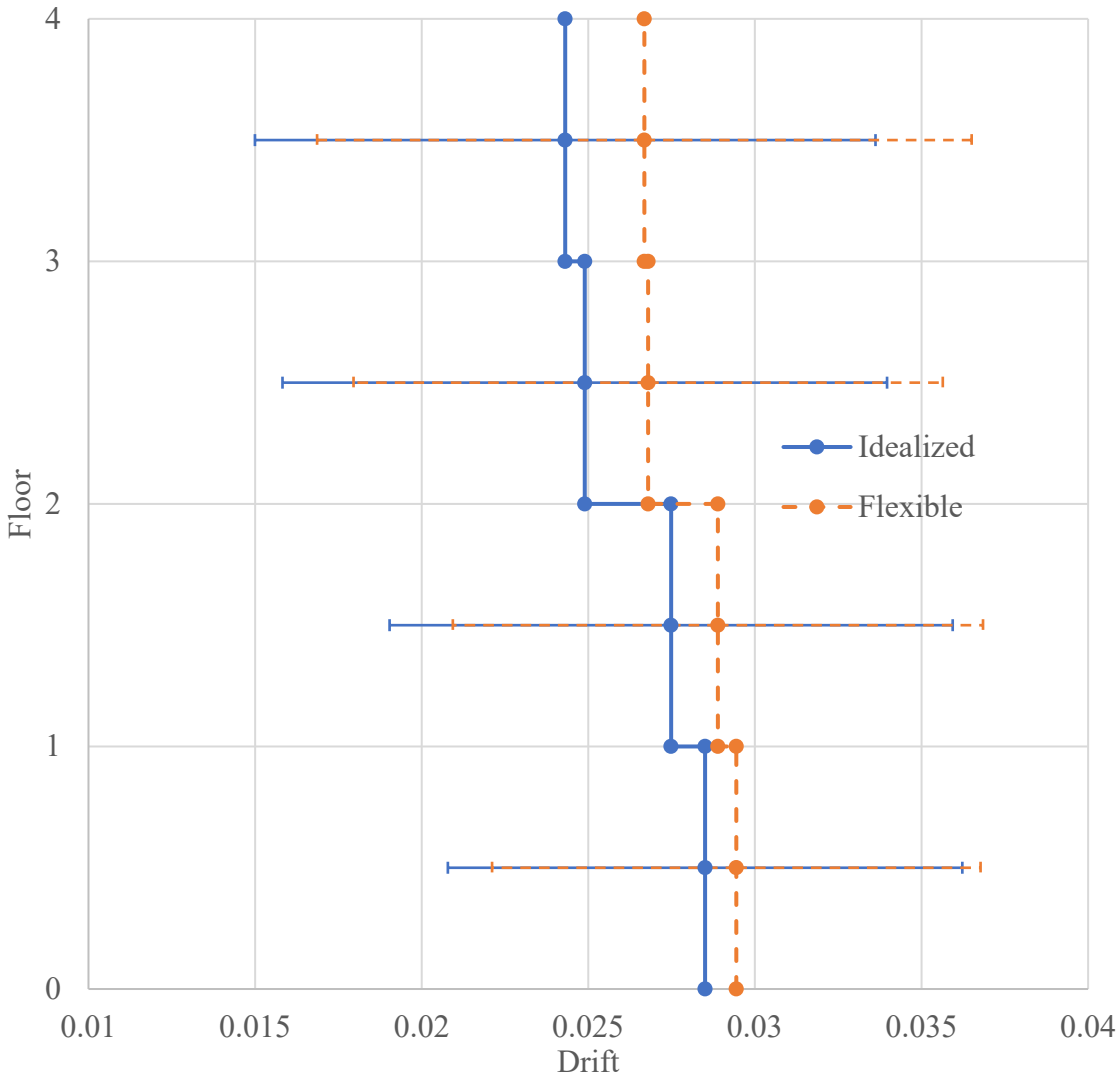

Figure 4.2-11 Average of the maximum drift for the BRBF direction of the 4-story building.

Table 4.2-14 Difference in maximum drift for the BRBF direction of the 4-story building (10^{*-3}).

Story	EQ 1	EQ 2	EQ 3	EQ 4	EQ 5	EQ 6	EQ 7	EQ 8	EQ 9	EQ 10	EQ 11	Average
0-1	-0.2	-2.3	0.4	1.9	2.6	0.4	2.2	1.0	0.6	1.2	2.6	0.9
1-2	0.9	-1.2	0.6	2.0	3.2	1.0	3.0	1.9	0.6	0.5	2.9	1.4
2-3	1.3	0.9	0.9	2.3	3.5	1.9	3.5	2.2	0.5	0.5	3.4	1.9
3-4	2.1	1.7	1.8	2.4	2.8	2.0	6.0	1.7	2.2	0.0	3.5	2.4

The residual drift did not change at the first floor and increased at the other floors in range from $0.1*10^{-3}$ (at the second floor) to $0.4*10^{-3}$ (at the fourth floor), as shown in Figure 4.2-12. Although the change in the average drift of the first story is zero, the change in the first story drift is not zero in the individual earthquakes, as shown in Table 4.2-15. Overall, the impact is small and can be neglect.

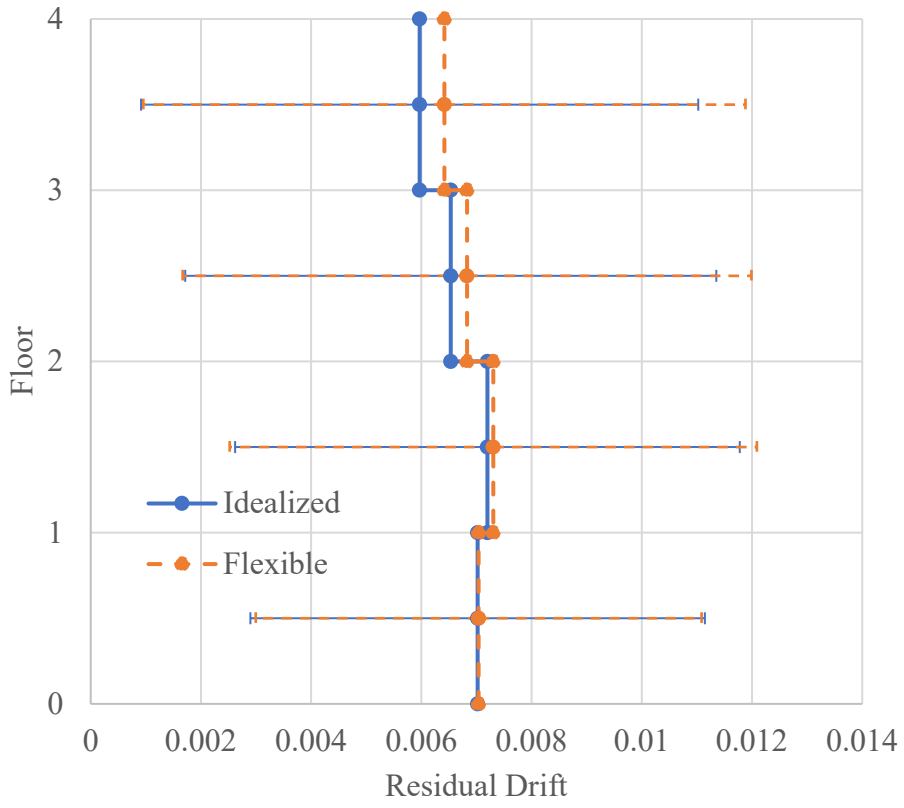

Figure 4.2-12 Average of the residual drift for the BRBF direction of the 4-story building.

Table 4.2-15 Difference in residual drift for the BRBF direction of the 4-story building ($*10^{-3}$).

Story	EQ 1	EQ 2	EQ 3	EQ 4	EQ 5	EQ 6	EQ 7	EQ 8	EQ 9	EQ 10	EQ 11	Average
0-1	-1.4	-1.0	-2.6	1.0	1.2	1.1	-0.9	0.6	1.2	0.2	0.6	0.0
1-2	-1.0	-0.3	-2.6	1.3	1.2	1.7	-1.3	0.5	1.6	-0.2	0.3	0.1
2-3	-0.3	0.3	-2.1	1.7	1.0	2.3	-1.5	0.7	1.7	-0.5	0.0	0.3
3-4	0.3	0.9	-1.6	2.0	0.7	2.5	-1.6	1.0	2.0	-0.7	-0.4	0.4

There was small change in the average maximum total acceleration of the elevated floors. The total acceleration at elevated floors decreased in the range from 1% and 2%, but the total acceleration at the base increased by 19%, as shown in Figure 4.2-13. The total base acceleration increased in all earthquakes except EQ4 and EQ6 where the base total acceleration decreased by 1%, as shown in Table 4.2-16. EQ3 showed the highest increase in the total base acceleration by 59%.

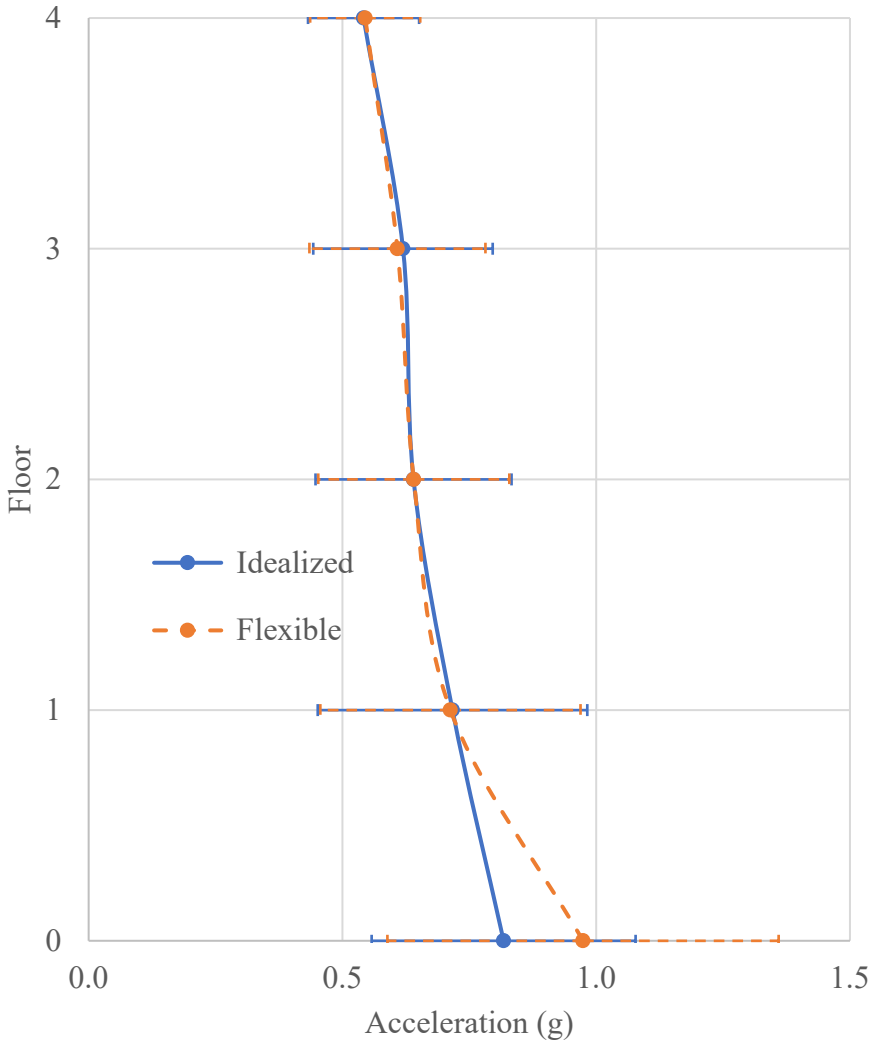

Figure 4.2-13 average maximum roof acceleration for the BRBF direction of the 4-story building.

Table 4.2-16 Percentage change in maximum total acceleration for the BRBF direction of the 4-story building.

Story	EQ 1	EQ 2	EQ 3	EQ 4	EQ 5	EQ 6	EQ 7	EQ 8	EQ 9	EQ 10	EQ 11	Average
0	18	4	59	-1	2	-1	11	16	18	15	50	19
1	3	-2	4	0	4	-3	-1	-5	-6	3	-1	-1
2	1	-5	1	4	1	-2	5	4	-1	1	-5	0
3	-2	-8	-2	-1	-2	1	5	-8	-1	-1	0	-2
4	0	2	3	-2	1	2	8	-2	4	-4	-4	1

There is a reduction in the average maximum base shear by 1% and an increase in the average maximum shear of the elevated floors in range between 1% and 4%, as shown in Figure 4.2-14. Some earthquakes showed an increase in the shear at the individual earthquake level, while others showed a reduction, as shown in Table 4.2-17. The allowed reduction in ASCE 7-16 is 10% for the base shear, but the NRHA showed an average reduction of 1%.

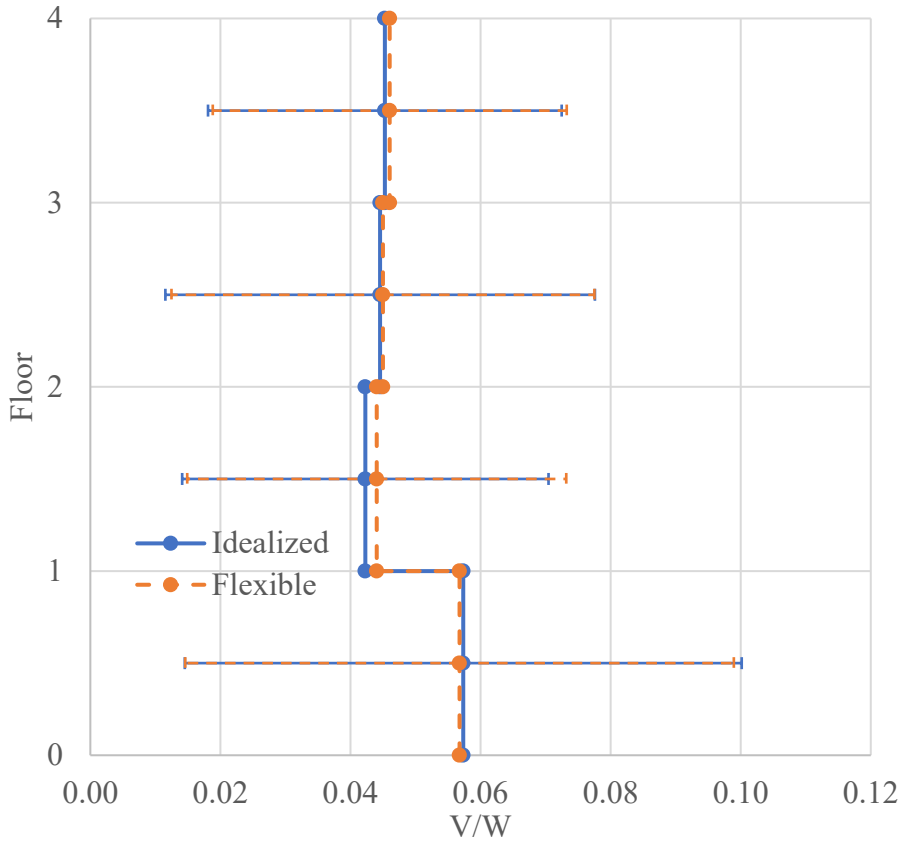

Figure 4.2-14 Average maximum shear force for the BRBF direction of the 4-story building.

Table 4.2-17 Percentage change in the maximum floor shear/ weight for the BRBF direction of the 4-story building.

Story	EQ 1	EQ 2	EQ 3	EQ 4	EQ 5	EQ 6	EQ 7	EQ 8	EQ 9	EQ 10	EQ 11	Average	Standard Deviation
0-1	0	-4	2	0	-3	-7	1	-4	-4	7	2	-1	-1
1-2	2	12	7	-13	8	5	23	-6	1	11	2	4	3
2-3	0	-7	-1	3	-1	-5	13	16	6	-6	0	1	-2
3-4	9	-4	7	6	9	-5	1	-3	4	0	0	2	0

To capture the general behavior of energy dissipation in the BRB elements, specific BRB elements have been selected as shown in Figure 4.2-15. The average energy dissipation calculations showed that the BRB elements dissipate less energy in the flexible foundation case, as shown in Table 4.2-18. The energy dissipation decreased during EQ1, EQ2, EQ9, EQ10, and EQ11 and increased during EQ4, EQ6, EQ7, and EQ8. The energy dissipation in the BRB in the 2nd and 4th floors decreased during EQ5 and the energy dissipation in the BRB in the 1st and 3rd floors increased. That indicates that the energy dissipation in the BRB depends on the nature of the earthquake. The maximum BRB strain increased in all floors, as shown in Table 4.2-19.

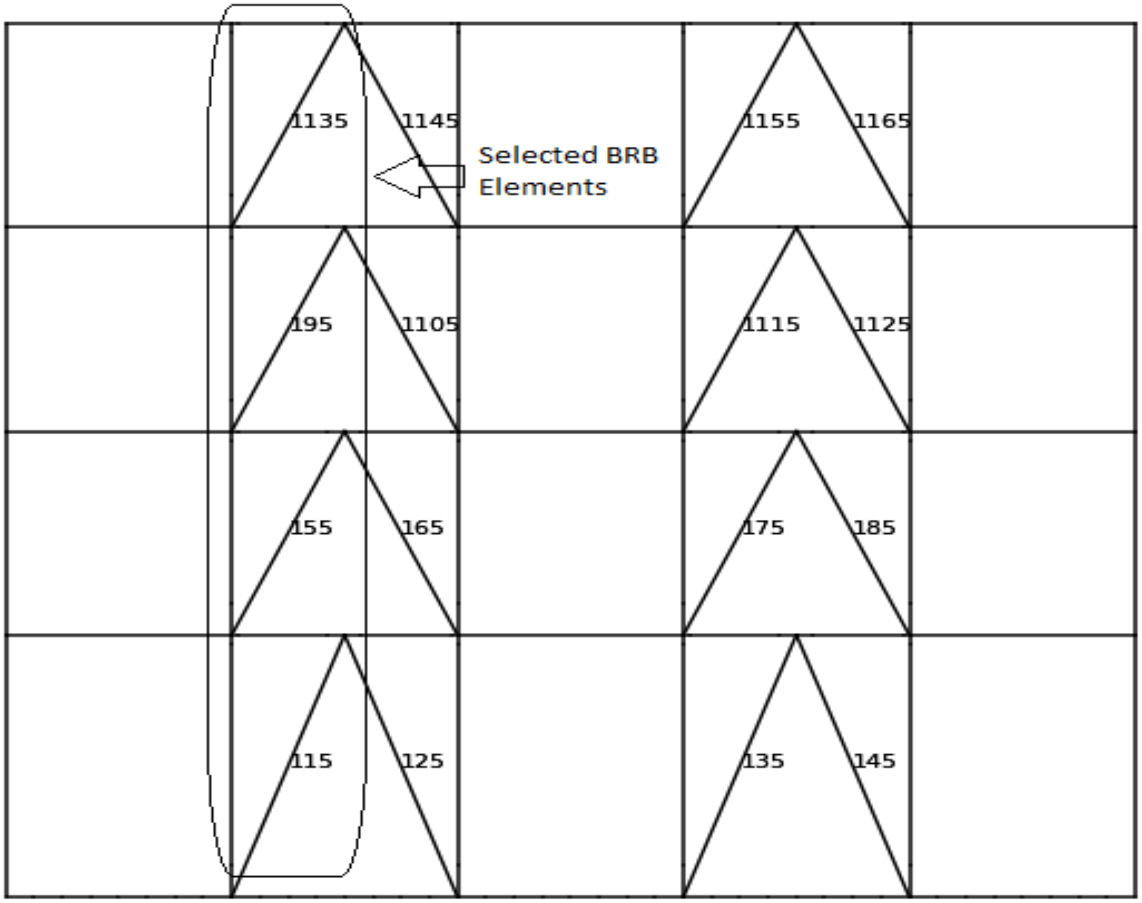

Figure 4.2-15 Selected BRB element for dissipated energy calculations.

Table 4.2-18 Percentage of change in the energy dissipation in the BRB elements of the 4-story building.

BRB	EQ 1	EQ 2	EQ 3	EQ 4	EQ 5	EQ 6	EQ 7	EQ 8	EQ 9	EQ 10	EQ 11	Average
115	-1	-10	1	4	3	3	4	5	-4	-4	-8	-1
155	-1	-8	0	9	-1	1	3	6	-1	-3	-5	-1
195	-2	-11	1	4	4	2	4	5	-4	-4	-8	-1
1135	-1	-9	0	8	-1	0	3	5	-1	-3	-6	-1

Table 4.2-19 Maximum strain at the selected BRB elements.

BRB	Idealized		Flexible		Change	
	Average	standard deviation	Average	Standard Deviation	Average	
115	0.0114	0.0031	0.0114	0.0029	0	-5
155	0.0117	0.0036	0.0120	0.0034	3	-6
195	0.0107	0.0039	0.0114	0.0038	7	-3
1135	0.0105	0.0040	0.0115	0.0043	9	8

4.3 8-Story Building Seismic Response

4.3.1 SMF

The results of the 8-story building dynamic analysis in the SMF direction are presented in this section along with a comparison between the idealized and flexible foundation. The results show a minor change in the average maximum absolute displacement ranging from -0.8 inch (at the eighth floor) to 0.8 inch (at the third floor), as shown in Figure 4.3-1 and Table 4.3-1. The reason for this minor change is the structure is flexible and the soil is stiff. Thereby the structure is controlling the seismic response of the building. The flexible case has a lower standard deviation. EQ2 showed the highest reduction in the maximum displacement. The behavior of this case is different from the behavior of the 4-story building, there was a reduction in the maximum displacement of the 4-story building.

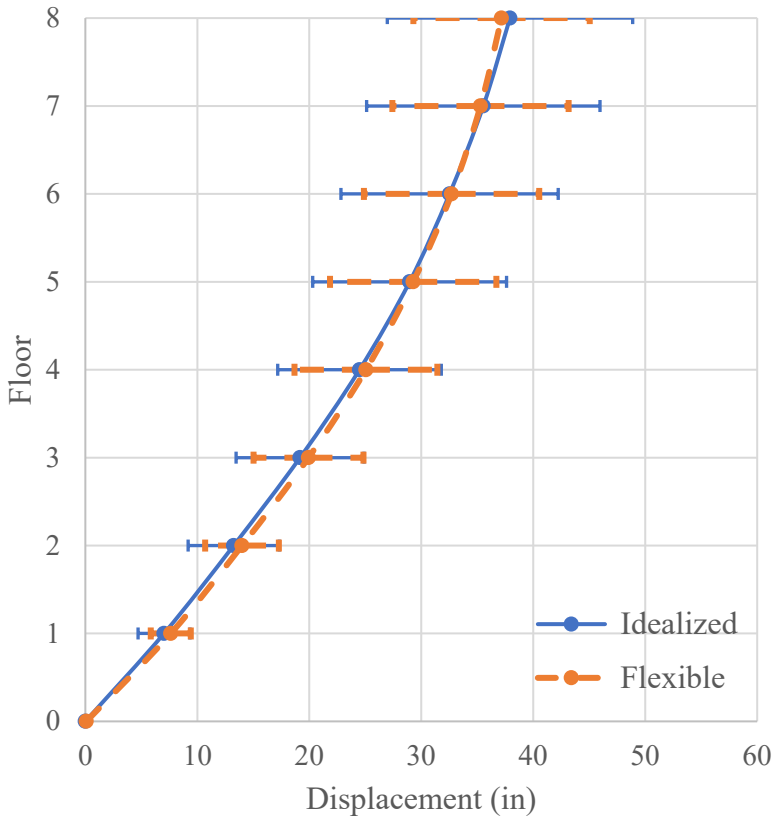

Figure 4.3-1 Average of the maximum displacement for the SMF direction of the 8-story building.

Table 4.3-1 Difference in maximum story displacement (inch) for the SMF direction of the 8-story building.

Story	EQ 1	EQ 2	EQ 3	EQ 4	EQ 5	EQ 6	EQ 7	EQ 8	EQ 9	EQ 10	EQ 11	Average
1	0.3	-1.8	1.4	0.8	0.8	1.7	0.4	0.3	0.5	1.0	1.2	0.6
2	0.3	-3.2	2.1	1.3	1.1	2.6	0.5	0.3	0.7	1.6	0.8	0.7
3	0.0	-4.4	2.7	2.2	1.4	3.2	0.3	0.2	1.2	2.0	-0.3	0.8
4	-1.0	-5.6	2.2	3.3	1.6	3.3	0.1	-0.1	1.7	2.0	-1.3	0.6
5	-1.1	-7.4	1.1	4.9	2.0	2.4	0.3	-0.4	2.1	1.7	-2.2	0.3
6	-0.5	-10.0	-0.1	6.8	2.4	2.5	0.6	-0.7	2.5	1.3	-2.9	0.2
7	-1.8	-12.6	-0.9	7.4	2.7	2.6	0.4	-0.8	2.7	1.0	-3.5	-0.3
8	-1.6	-14.7	-1.6	5.4	2.8	2.8	0.3	-0.9	2.7	0.7	-4.1	-0.8

The residual displacement decreased for the SMF direction in the range of 1.1 inch to 5.4 inch, as shown in Figure 4.3-2. The standard deviation of the flexible case is smaller than the idealized case. EQ4, EQ5, and EQ9 showed an increase in the residual displacement, while all other earthquakes showed a decrease in the residual displacement, as shown in Table 4.3-2. This behavior is similar to the behavior of the 4-story building, both buildings showed a reduction in the residual displacement.

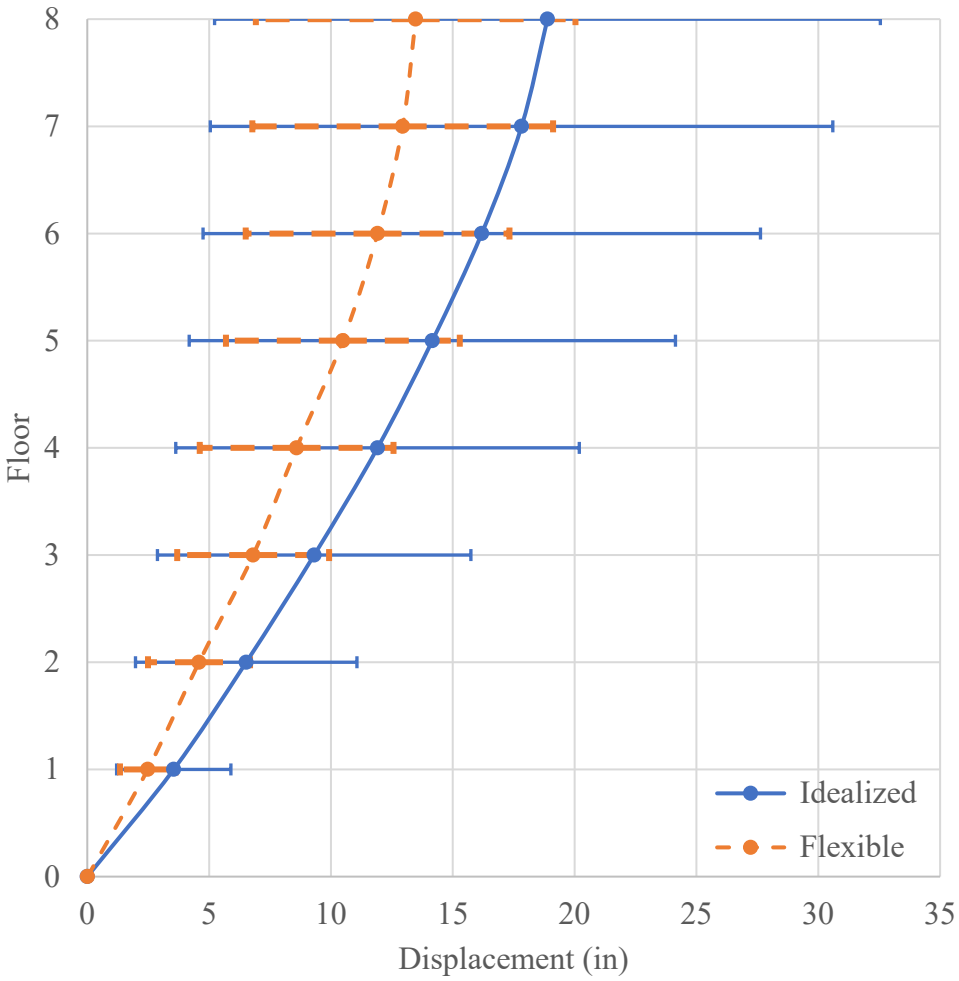

Figure 4.3-2 Average residual displacement for the SMF direction of the 8-story building.

Table 4.3-2 Difference in residual displacement (inch) for the SMF direction of the 8-story building.

Story	EQ 1	EQ 2	EQ 3	EQ 4	EQ 5	EQ 6	EQ 7	EQ 8	EQ 9	EQ 10	EQ 11	Average
1	-1.0	-6.5	-0.7	0.5	-0.7	-0.3	-1.1	-1.7	0.0	-0.6	0.4	-1.1
2	-1.6	-12.4	-1.2	1.0	-0.4	-0.9	-1.9	-3.5	0.2	-1.0	0.5	-1.9
3	-1.9	-17.2	-1.7	1.6	-0.2	-1.5	-2.6	-3.3	0.4	-1.3	0.3	-2.5
4	-2.3	-21.4	-2.0	2.5	0.3	-2.3	-2.9	-6.0	0.5	-1.5	-1.4	-3.3
5	-2.9	-25.6	-2.1	3.6	1.2	-3.2	-2.9	-5.6	0.8	-1.7	-2.0	-3.7
6	-3.7	-29.2	-2.0	3.6	2.0	-3.9	-2.8	-6.7	1.2	-1.9	-3.6	-4.3
7	-4.7	-33.3	-2.0	2.6	1.3	-4.4	-2.6	-5.9	1.6	-2.2	-4.0	-4.9
8	-5.9	-35.2	-2.2	1.1	2.0	-4.8	-2.4	-5.9	2.1	-2.4	-6.0	-5.4

For the maximum story drift, the change is different among the floors, as shown in Figure 4.3-3. The 1st and 2nd stories showed an increase in the maximum drift by $3*10^{-3}$ and $1*10^{-3}$, respectively. The rest of the floors showed a change in the maximum drift ranging from 0 to $-4*10^{-3}$, as shown in Table 4.3-3. The 8th floor showed the highest reduction in the maximum drift.

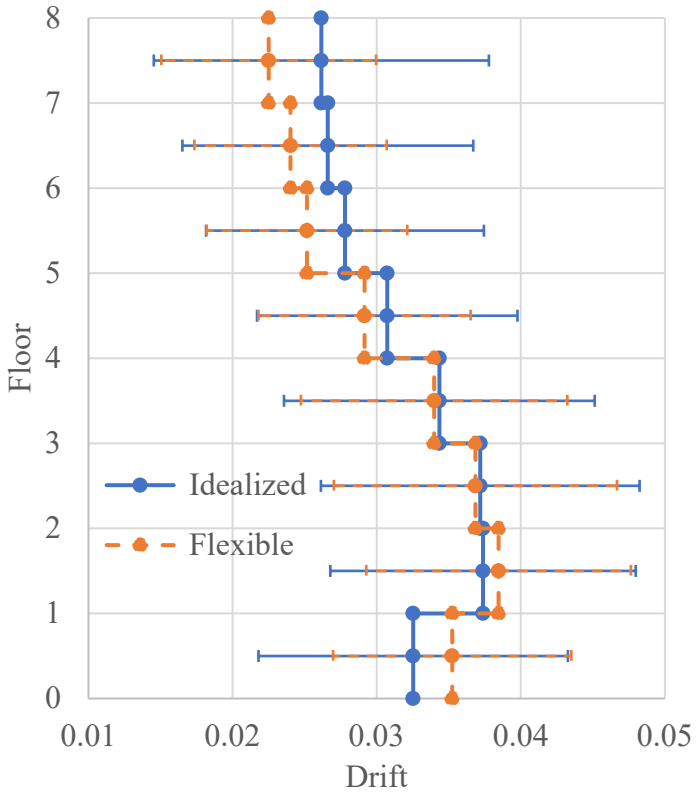

Figure 4.3-3 Average maximum drift for the SMF direction of the 8-story building.

Table 4.3-3 Difference in average maximum drift for the SMF direction of the 8-story building ($*10^{-3}$).

Story	EQ 1	EQ 2	EQ 3	EQ 4	EQ 5	EQ 6	EQ 7	EQ 8	EQ 9	EQ 10	EQ 11	Average
0-1	2	-8	6	4	3	8	2	1	2	5	6	3
1-2	0	-8	5	4	2	5	0	0	2	4	-2	1
2-3	-1	-7	1	5	2	3	-2	-4	3	1	-4	0
3-4	1	-7	-3	5	3	2	0	-2	3	0	-5	0
4-5	0	-11	-6	-4	3	1	0	1	2	0	-5	-2
5-6	-3	-13	-9	-5	2	1	2	-1	4	0	-6	-3
6-7	-9	-10	-6	-2	0	-1	2	-1	4	-1	-5	-3
7-8	-17	-11	-6	-5	0	-2	1	1	1	-1	-2	-4

There is a reduction in the residual drift as shown in Figure 4.3-4. The reduction in the average residual drift ranged from $2*10^{-3}$ to $5*10^{-3}$. For individual records, earthquakes like EQ3, EQ4, EQ5, EQ7, EQ8, and EQ9 showed increase in the residual drift for some floors and decrease in the residual deformation for other floors, while other earthquakes like EQ1, EQ2, and EQ10 showed a decrease in the residual drift for all stories, as shown in Table 4.3-4.

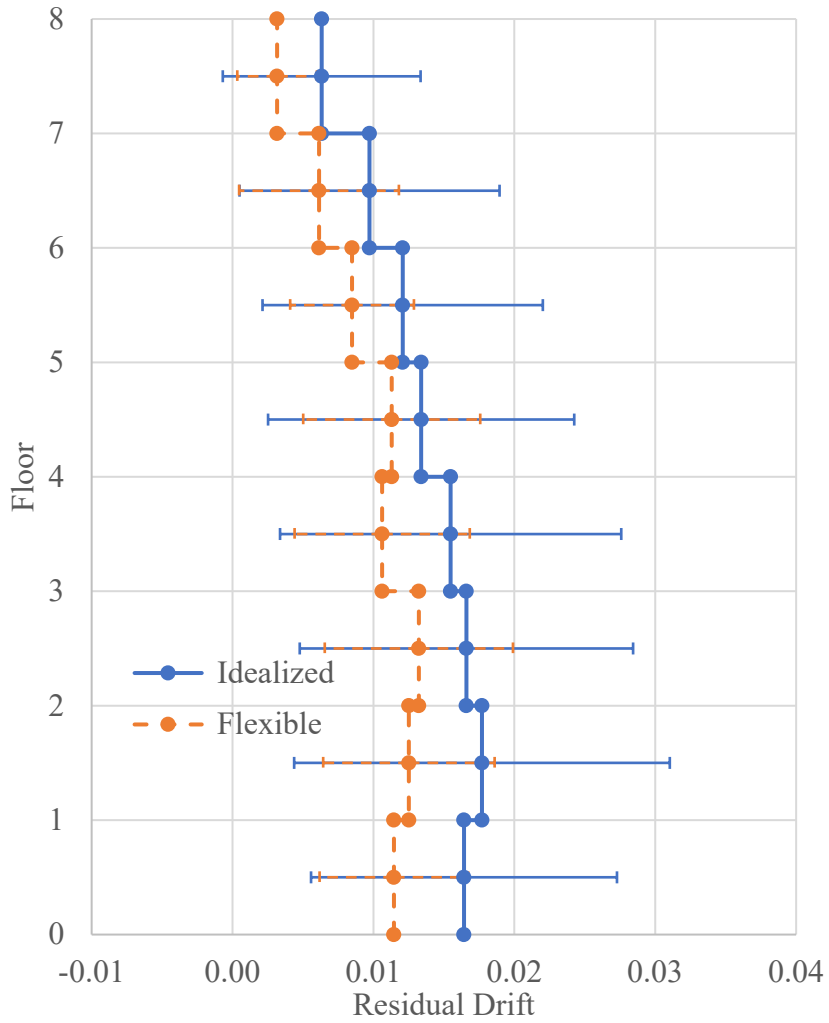

Figure 4.3-4 Average residual drift for the SMF direction of the 8-story building.

Table 4.3-4 Difference in residual drift for the SMF direction of the 8-story building (*10^{-3}).

Story	EQ 1	EQ 2	EQ 3	EQ 4	EQ 5	EQ 6	EQ 7	EQ 8	EQ 9	EQ 10	EQ 11	Average
0-1	-5	-30	-3	2	-3	-2	-5	-8	0	-3	2	-5
1-2	-3	-35	-3	3	2	-3	-5	-11	1	-2	0	-5
2-3	-2	-29	-3	4	1	-4	-4	1	1	-2	-1	-3
3-4	-2	-25	-2	5	3	-5	-2	-16	1	-1	-10	-5
4-5	-3	-25	0	7	5	-5	0	2	1	-1	-4	-2
5-6	-5	-21	0	0	5	-4	1	-6	2	-1	-10	-4
6-7	-6	-25	0	-6	-4	-3	1	5	2	-2	-2	-4
7-8	-7	-12	-1	-9	4	-2	1	0	3	-1	-12	-3

Total acceleration increased at the base by 71% and decreased at the elevated floors. The decrease in the elevated floors acceleration ranged from 2% to 4%, as shown in Figure 4.3-5.

Table 4.3-5 shows the percentage of change in the acceleration of the floors. All the earthquakes showed increase in the base acceleration for all individual records.

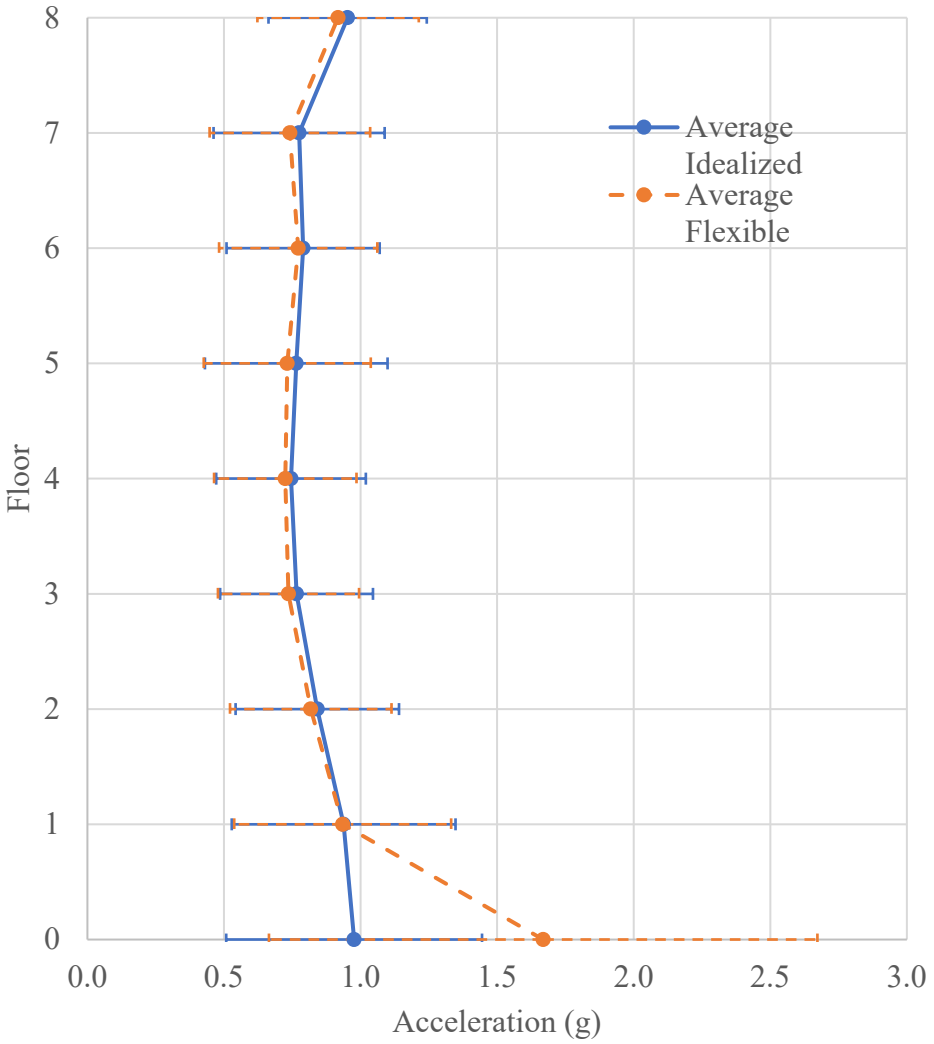

Figure 4.3-5 Average maximum acceleration for the SMF direction.

Table 4.3-5 Percentage change in maximum acceleration for the SMF direction of the 8-story building.

Story	EQ 1	EQ 2	EQ 3	EQ 4	EQ 5	EQ 6	EQ 7	EQ 8	EQ 9	EQ 10	EQ 11	Average
0	24	70	19	10	71	33	224	4	93	51	195	71
1	-5	4	-7	-7	23	-3	2	6	-4	-5	5	0
2	2	-6	1	-17	6	-6	6	4	-11	-3	-7	-3
3	-7	-3	-15	-5	4	-3	-3	11	-3	-5	-4	-4
4	0	4	4	-11	9	-7	0	-11	-12	7	-5	-3
5	-11	-2	-4	-5	-7	-8	-4	-2	-2	4	2	-4
6	4	-9	7	-5	-12	-12	-2	6	-6	-7	0	-2
7	-6	1	-8	-7	-8	2	0	-2	-9	-5	-4	-4
8	-8	-3	-2	-6	-14	-5	1	-2	-12	-1	5	-4

There is a reduction in the story shear forces in the range of 1% to 5%, as shown in Figure 4.3-6. EQ3 showed the highest increase in the base shear by about 5%, while EQ9 showed the highest reduction in the base shear by 14%, as shown in Table 4.3-6. The allowed reduction in ASCE 7-16 is 10% for the base shear, but the NRHA showed an average reduction of 3%.

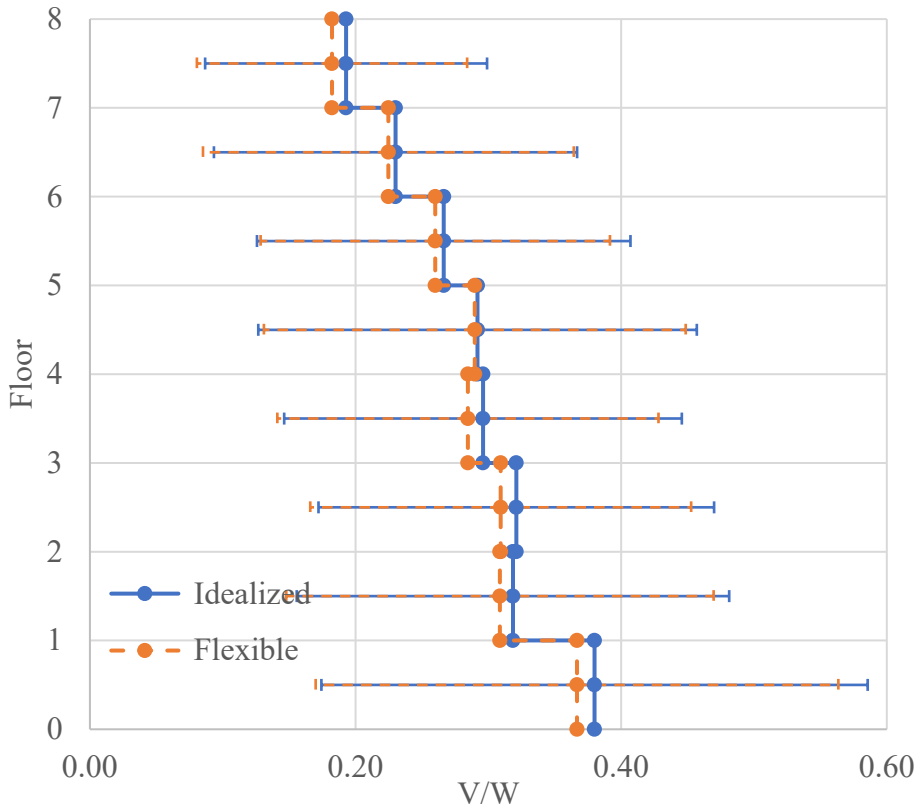

Figure 4.3-6 Average maximum floor shear and base shear for the SMF direction of the 8-story building.

Table 4.3-6 Percentage change in average floor shear for the SMF direction of the 8-story building.

Story	EQ 1	EQ 2	EQ 3	EQ 4	EQ 5	EQ 6	EQ 7	EQ 8	EQ 9	EQ 10	EQ 11	Average
0-1	4	-4	5	-6	0	-4	-6	3	-14	-2	-9	-3
1-2	-1	-6	-6	2	-5	-2	-5	-3	-2	-4	-4	-3
2-3	6	-5	1	-2	-6	-4	-6	-3	-5	-9	-6	-4
3-4	-4	-2	-9	-7	0	-3	-3	-3	-4	3	-6	-4
4-5	3	-3	0	0	1	-3	-1	13	-2	-2	-4	-1
5-6	0	0	-7	-6	7	-4	-2	10	-6	0	-4	-2
6-7	-5	-4	-5	-8	-4	0	6	-6	-5	-1	-4	-2
7-8	-8	-7	-5	-6	-14	-5	0	-2	-8	-3	-5	-5

For energy dissipation, certain RBS elements have been selected, as shown in Figure 4.3-7. The energy dissipation has been calculated at those RBS springs to capture the general trend of the RBS springs behavior. The energy dissipation in those springs has increased in some RBS springs in the range of 5% to 30%, especially the springs at the lower floors (1st, 2nd, and 3rd floor), and decreased in others in range of 4% to 43%, especially the springs at the top floors (4th, 5th, 6th, 7th, and 8th floor), as shown in Table 4.3-7. The maximum rotation increased in some RBS springs, especially the springs at the lower floors (1st, 2nd, and 3rd floor), in range of 2% and 8%, and decreased in other RBS springs, especially the springs at the top floors, in range of 1% to 32%, as shown in Table 4.3-8. That shows a greater demand in the lower floor hinges than the top floors hinges. The rotation at the foundation of the buildings imposes a rotation on the RBS which leads to increase in the energy dissipation in the lower floor springs.

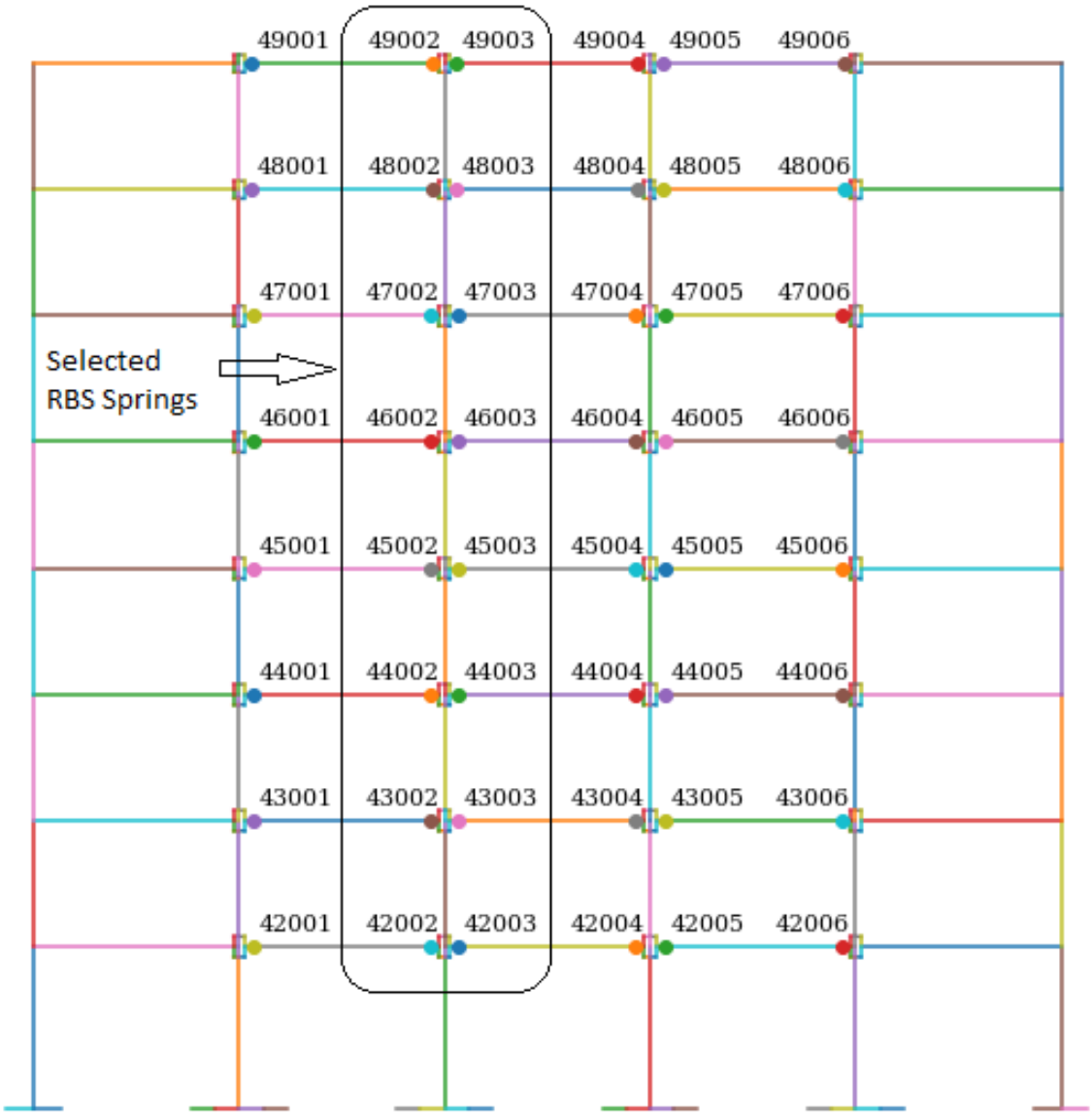

Figure 4.3-7 Selected RBS for energy calculation in the SMF direction of the 8-story building.

Table 4.3-7 Average energy dissipation at the selected RBS springs of the 8-story building.

RBS	Idealized		Flexible		Percentage Change	
	Average (kip*in)	Standard Deviation (kip*in)	Average (kip*in)	Standard Deviation (kip*in)	Average	Standard Deviation
42002	1861	868	2242	967	21	11
42003	1855	874	2402	1031	30	18
43002	1639	812	1725	838	5	3
43003	1666	823	1894	903	14	10
44002	1299	723	1245	679	-4	-6
44003	1353	735	1417	741	5	1
45002	946	550	900	566	-5	3
45003	994	580	1048	636	6	10
46002	789	610	674	606	-15	-1
46003	838	624	798	636	-5	2
47002	702	792	576	705	-18	-11
47003	747	793	668	722	-11	-9
48002	719	780	551	580	-23	-26
48003	782	841	630	625	-19	-26
49002	329	571	189	299	-43	-48
49003	346	568	212	304	-39	-47

Table 4.3-8 Average maximum rotation at the selected RBS springs of the 8-story building.

RBS	Idealized		Flexible		Percentage of change	
	Average (rad)	Standard Deviation (rad)	Average (rad)	Standard Deviation (rad)	Average	Standard Deviation
42002	0.03189	0.01261	0.03252	0.00889	2	-29
42003	0.03158	0.01329	0.03406	0.01027	8	-23
43002	0.03213	0.01261	0.03122	0.00981	-3	-22
43003	0.03196	0.01341	0.03287	0.01130	3	-16
44002	0.03030	0.01271	0.02883	0.01018	-5	-20
44003	0.03025	0.01358	0.03071	0.01153	2	-15
45002	0.02565	0.01140	0.02387	0.00866	-7	-24
45003	0.02591	0.01205	0.02573	0.00998	-1	-17
46002	0.02229	0.01018	0.01886	0.00732	-15	-28
46003	0.02304	0.01132	0.02090	0.00839	-9	-26
47002	0.01838	0.01175	0.01473	0.00877	-20	-25
47003	0.01934	0.01260	0.01666	0.00929	-14	-26
48002	0.01869	0.01294	0.01432	0.00814	-23	-37
48003	0.02062	0.01442	0.01675	0.00904	-19	-37
49002	0.01405	0.01413	0.00950	0.00807	-32	-43
49003	0.01564	0.01481	0.01082	0.00860	-31	-42

The column springs at the base were selected to evaluate the general behavior trend as shown in Figure 4.3-8. The energy dissipation at the specified column springs was decreased in the range of 47% to 54%, as shown in Table 4.3-9. Although all the base springs yielded in the flexible case, some of them dissipated a very small amount of energy in the flexible case, as shown in Table 4.3-10. All the springs have dissipated less energy in the flexible case, except spring 712051 which dissipated more energy for EQ10 and EQ11, as shown in Table 4.3-11Table 4.3-11. At the same time, the maximum rotation in the column springs was decreased, as shown in Table 4.3-12. The reduction in the energy dissipation in this case is less than the reduction in the 4-story

building because the foundation of the 8-story building is larger which leads to less reduction in the required rotation and becomes closer to the behavior of fixed support.

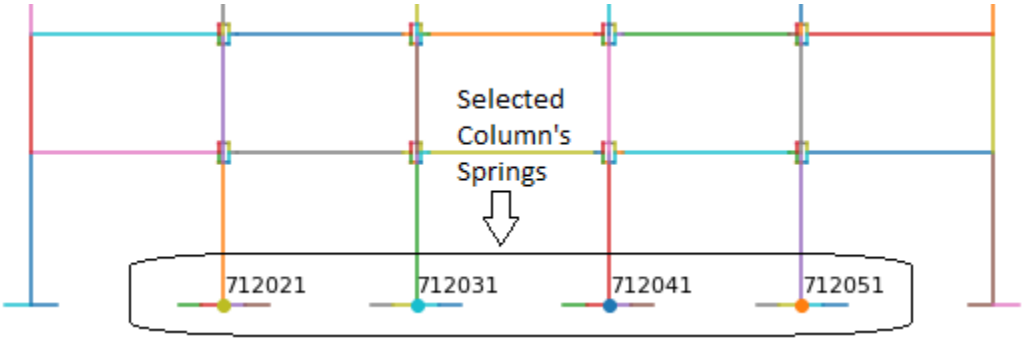

Figure 4.3-8 Selected column's springs for the SMF of the 8-story building.

Table 4.3-9 Energy dissipation at the selected column springs of the 8-story building.

Column springs	Idealized		Flexible		Percentage Change	
	Average (kip*in)	Standard Deviation (kip*in)	Average (kip*in)	Standard Deviation (kip*in)	Average	Standard Deviation
712021	735	577	356	304	-52	-47
712031	1288	969	598	472	-54	-51
712041	1288	969	627	494	-51	-49
712051	735	578	386	396	-47	-31

Table 4.3-10 Energy dissipation (kip*in) at the selected column springs of the 8-story building for each earthquake.

Idealized foundation											
Column Spring	EQ1	EQ2	EQ3	EQ4	EQ5	EQ6	EQ7	EQ8	EQ9	EQ10	EQ11
712021	1640	1352	986	1186	254	145	269	679	1307	215	49
712031	2807	2307	1759	2033	520	269	476	1129	2273	400	191
712041	2807	2307	1758	2033	520	269	476	1129	2273	400	191
712051	1641	1364	984	1188	259	150	264	685	1291	210	46
Flexible foundation											
Column Spring	EQ1	EQ2	EQ3	EQ4	EQ5	EQ6	EQ7	EQ8	EQ9	EQ10	EQ11
712021	747	722	678	333	1	268	2	646	411	97	7
712031	916	1049	1082	914	104	224	138	709	1267	178	2
712041	996	1027	1239	976	144	214	143	703	1273	179	2
712051	866	3	471	688	195	1	220	245	1251	224	87

Table 4.3-11 Percentage change in energy dissipation at the selected column springs of the 8-story building.

Column springs	EQ 1	EQ 2	EQ 3	EQ4	EQ 5	EQ 6	EQ 7	EQ 8	EQ 9	EQ 10	EQ 11	Average
712021	-54	-47	-31	-72	-100	85	-99	-5	-69	-55	-87	-52
712031	-67	-55	-38	-55	-80	-17	-71	-37	-44	-55	-99	-54
712041	-64	-55	-30	-52	-72	-20	-70	-38	-44	-55	-99	-51
712051	-47	-100	-52	-42	-25	-99	-17	-64	-3	7	90	-47

Table 4.3-12 Maximum rotation at the selected column springs of the 8-story building.

Column springs	Idealized		Flexible		Percentage Change	
	Average (rad)	Standard Deviation (rad)	Average (rad)	Standard Deviation (rad)	Average	Standard Deviation
712021	0.01622	0.01023	0.01004	0.00865	-38	-15
712031	0.01719	0.01027	0.01066	0.00739	-38	-28
712041	0.01719	0.01027	0.01094	0.00736	-36	-28
712051	0.01619	0.01027	0.01058	0.00828	-35	-19

4.3.2 BRBF

The results of the 8-story building dynamic analysis in the BRBF direction are presented in this section along with a comparison between the idealized and flexible foundation. The results show a slight increase in the maximum displacement in the range of 0 inch to 0.9 inch, as shown in Figure 4.3-9. The maximum increase in the displacement was seen at the first floor. EQ10 showed the highest decrease in the maximum displacement by 4.2 inch. EQ11 showed the highest increase in displacement by 4.5 inch, as shown in Table 4.3-13.

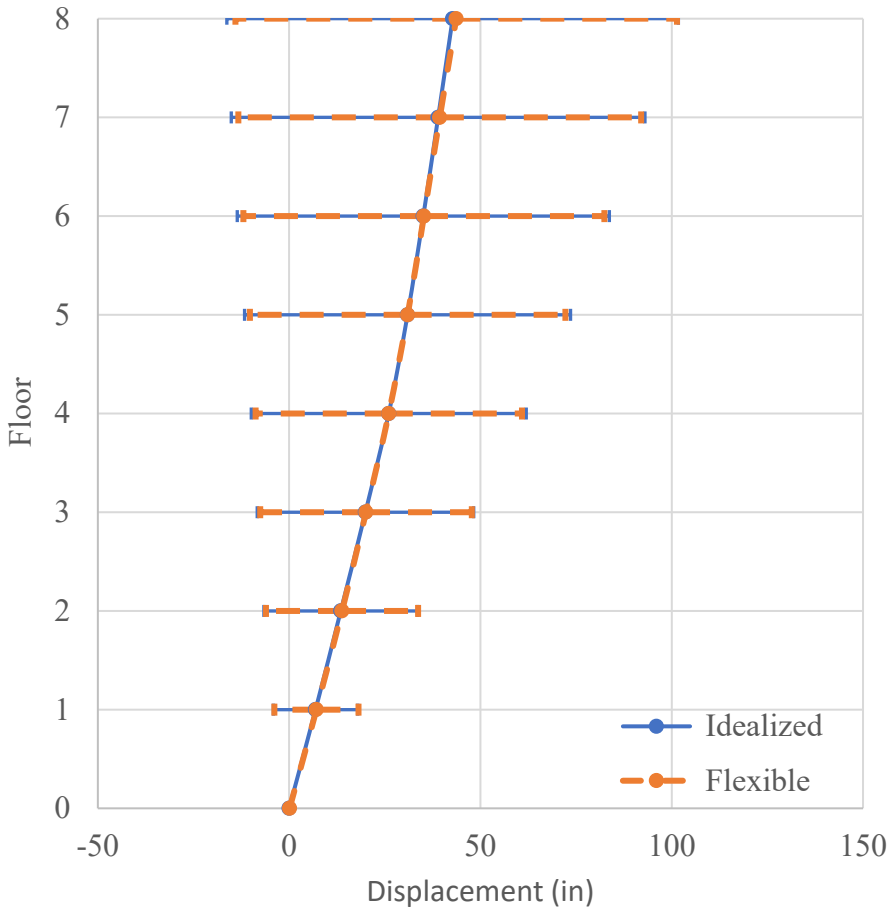

Figure 4.3-9 Average maximum displacement for the BRBF direction of the 8-story building.

Table 4.3-13 Difference in maximum displacement (inch) for the BRBF direction of the 8-story building.

Story	EQ 1	EQ 2	EQ 3	EQ 4	EQ 5	EQ 6	EQ 7	EQ 8	EQ 9	EQ 10	EQ 11	Average
1	0.3	0.2	0.1	0.0	0.4	0.1	0.5	0.2	0.2	0.2	0.3	0.2
2	0.3	0.3	0.5	-0.2	0.6	0.1	0.6	0.4	0.5	-0.2	0.7	0.3
3	-0.8	0.5	0.5	-0.3	0.6	0.0	0.5	0.5	0.8	-1.8	1.1	0.1
4	-1.3	0.7	0.4	0.0	0.6	-0.1	0.0	0.6	1.1	-3.5	1.6	0.0
5	-1.1	0.8	0.3	0.4	0.7	-0.1	-0.7	0.5	1.4	-4.2	2.3	0.0
6	-1.0	0.9	0.2	0.6	0.8	0.1	-0.8	0.3	1.5	-4.2	3.2	0.2
7	-1.3	0.9	0.9	0.7	0.9	0.8	0.3	0.1	1.3	-3.8	4.0	0.4
8	-1.6	3.2	1.9	0.9	0.8	1.6	1.2	-0.3	1.0	-3.0	4.5	0.9

The change in the average residual deformation of the BRBF was minimal, as shown in Figure 4.3-10. The average residual displacement decreased in all the floors in the range of 0 to 1.1 in but the residual displacement in individual earthquakes changed significantly. EQ11

showed the highest increase in roof residual displacement. EQ7 showed the highest increase in first floor residual displacement, as shown in Table 4.3-14. EQ10 showed the highest reduction in roof residual displacement 10.9 inch.

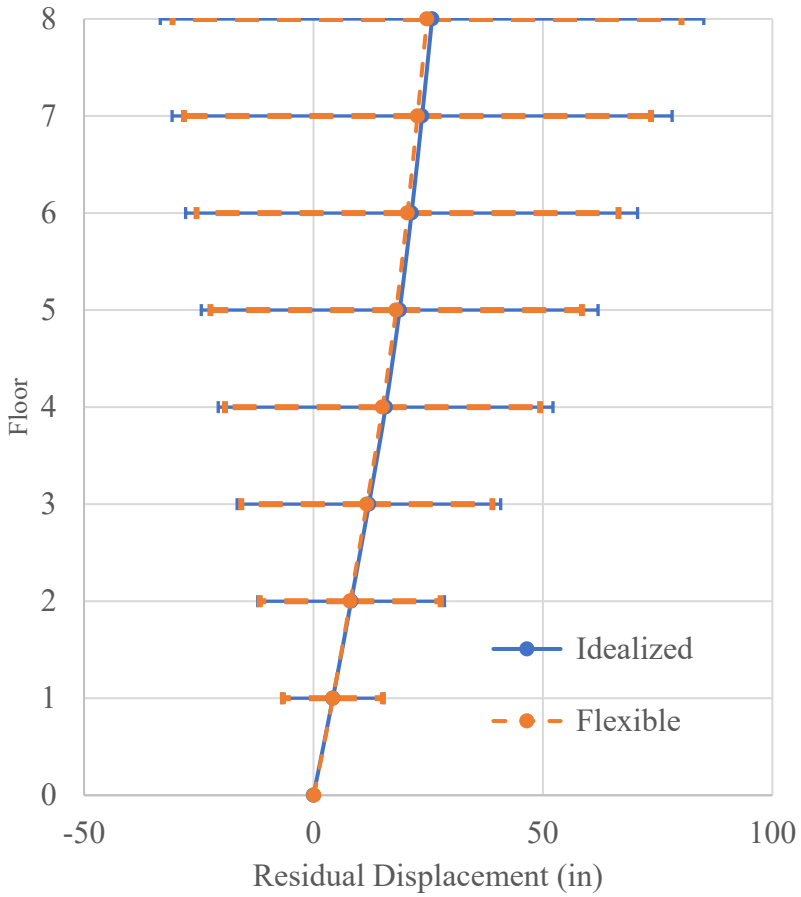

Figure 4.3-10 Average residual displacement for the BRBF direction of the 8-story building.

Table 4.3-14 Difference in the residual displacement (inch) for the BRBF direction for the 8-story building.

Story	EQ1	EQ2	EQ3	EQ4	EQ5	EQ6	EQ7	EQ8	EQ9	EQ10	EQ11	Average
1	-0.1	-0.3	-0.1	-0.5	0.2	0.1	1.3	-0.3	0.0	-0.5	0.1	0.0
2	-0.3	-0.6	-0.3	-1.0	0.1	0.2	2.3	-0.8	0.0	-2.1	0.4	-0.2
3	-0.7	-0.9	-0.5	-1.4	0.0	0.3	3.1	-1.3	0.2	-4.6	0.8	-0.5
4	-1.0	-1.1	-0.6	-1.6	0.0	0.4	3.6	-1.7	0.5	-7.2	1.4	-0.7
5	-1.2	-1.2	-0.6	-1.4	0.1	0.6	3.8	-1.9	0.7	-9.2	1.9	-0.8
6	-1.5	-1.4	-0.6	-0.9	0.1	1.0	3.6	-2.1	0.5	-10.9	2.4	-0.9
7	-2.0	-1.4	-0.4	0.0	0.2	1.2	3.1	-2.4	-0.1	-11.9	2.8	-1.0
8	-2.5	-1.5	-0.2	1.0	0.1	1.3	2.6	-2.7	-0.8	-12.6	3.2	-1.1

The change in the average maximum story drift is shown in Figure 4.3-11. The maximum story drift decreased in the third and fourth floors by 2% and 1% respectively and increased in other floors in the range of 1% and 5%, as shown in Table 4.3-15.

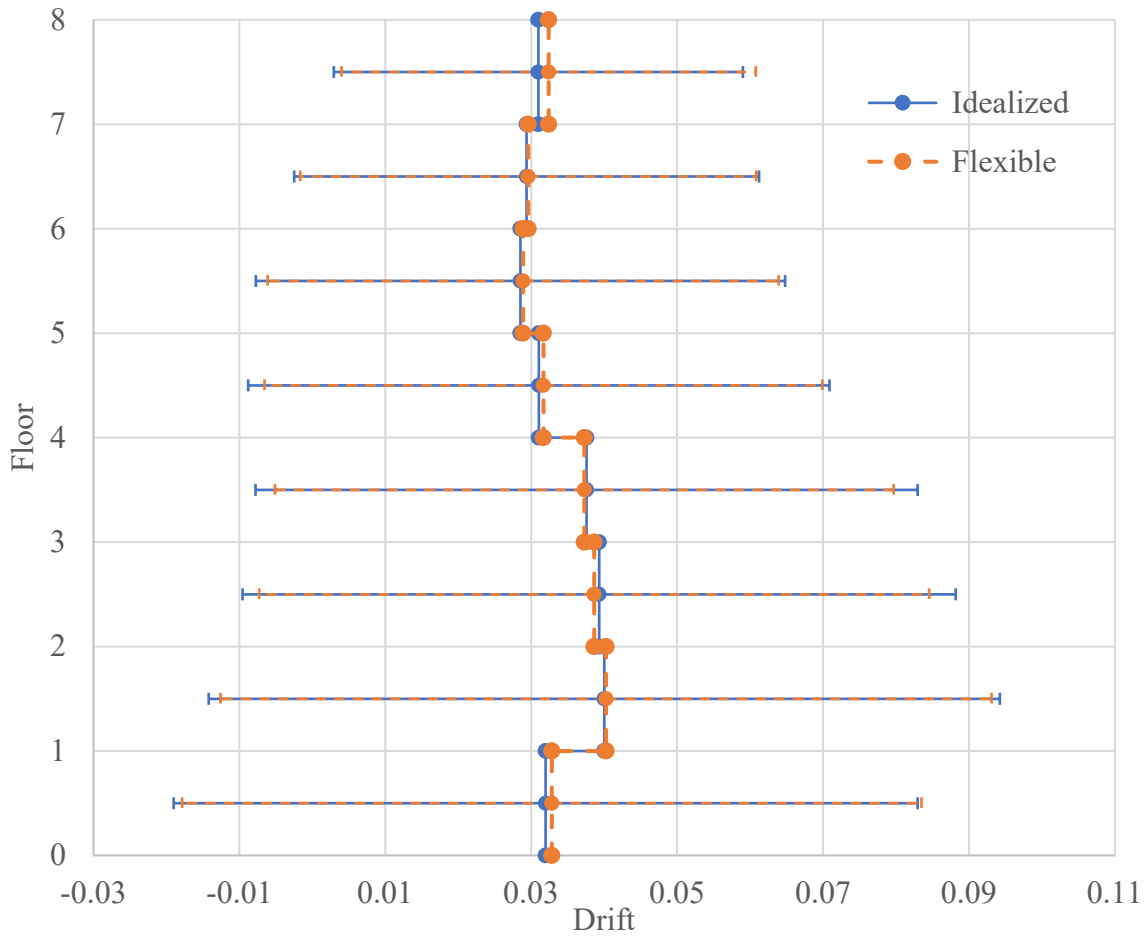

Figure 4.3-11 Average of the maximum drift for the BRBF direction of the 8-story building.

Table 4.3-15 Difference in maximum drift for the BRBF direction of the 8-story building (10^{-3}).

Story	EQ1	EQ2	EQ3	EQ4	EQ5	EQ6	EQ7	EQ8	EQ9	EQ10	EQ11	Average
0-1	1	1	0	0	2	0	2	1	1	0	1	1
1-2	-1	1	1	-1	1	0	0	1	2	-4	2	0
2-3	-2	1	0	0	0	-1	-2	1	2	-10	3	-1
3-4	-1	1	0	2	0	-1	-1	1	2	-10	3	0
4-5	1	1	0	2	0	1	0	0	2	-4	4	1
5-6	0	3	0	2	0	0	0	0	-1	-4	5	0
6-7	-2	2	4	1	1	-1	-2	0	-2	-1	4	0
7-8	0	4	2	1	-4	0	0	2	4	2	4	1

There is a reduction in the residual story drift as shown in Figure 4.3-12. The reduction in the average residual drift ranged from 3% to 7%, as shown in Table 4.3-16. But the individual earthquakes showed large variability, like EQ8 showed a reduction by 229% in the roof residual displacement. And EQ6 showed an increase by 1946% in the seventh-floor residual drift.

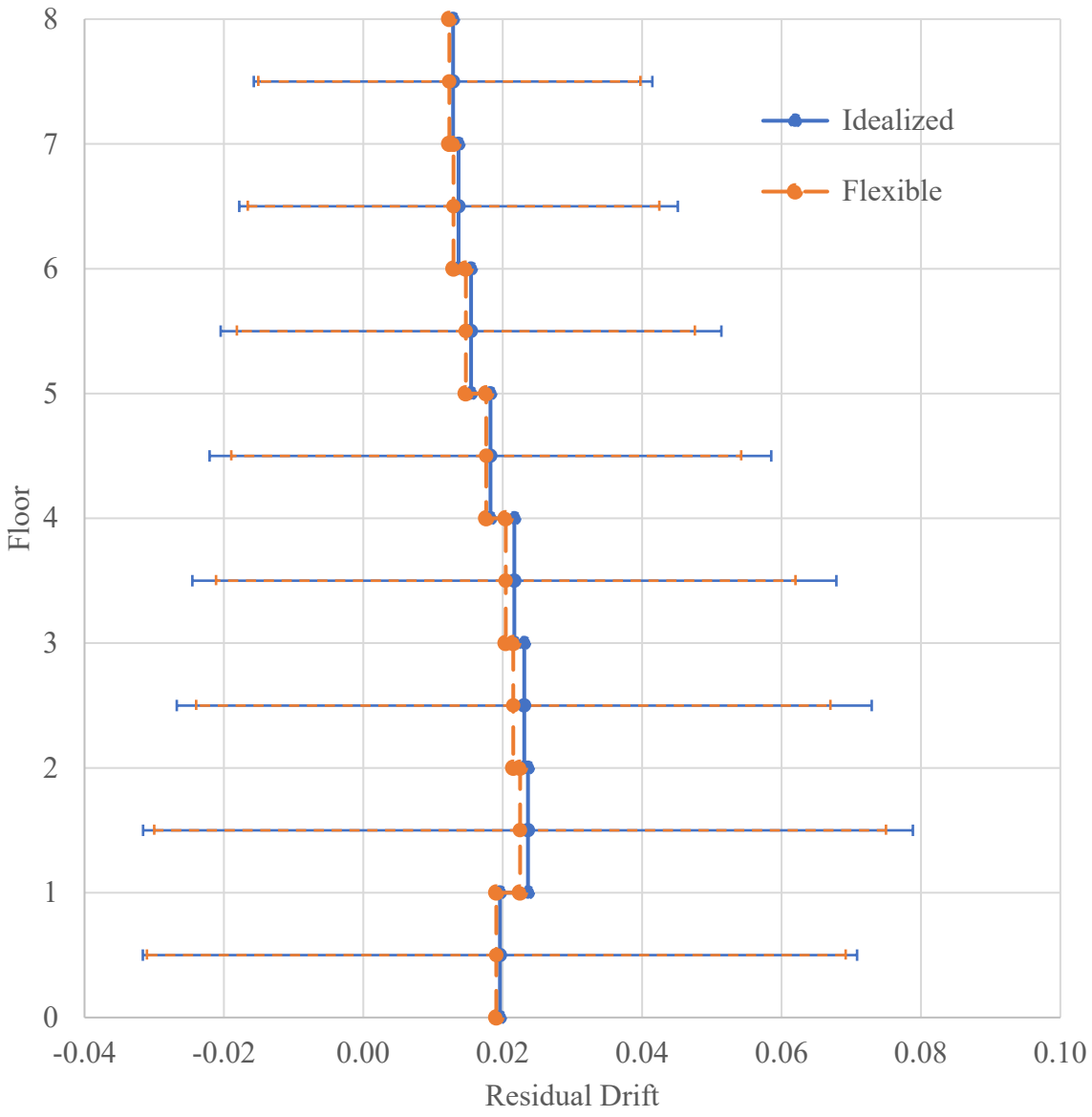

Figure 4.3-12 Average of the residual drift for the BRBF direction of the 8-story building.

Table 4.3-16 Difference in residual drift for the BRBF direction of the 8-story building (10^{-3}).

Roof	EQ1	EQ2	EQ3	EQ4	EQ5	EQ6	EQ7	EQ8	EQ9	EQ 10	EQ 11	Average
0-1	-1	-2	-1	-2	1	0	5	-2	0	-4	0	-1
1-2	-2	-2	-1	-3	0	1	6	-3	0	-9	2	-1
2-3	-2	-2	-1	-2	-1	0	4	-3	1	-15	3	-2
3-4	-2	-1	-1	-1	0	1	3	-2	2	-15	3	-1
4-5	-1	-1	0	1	1	1	1	-1	1	-12	3	-1
5-6	-2	-1	0	3	0	2	-1	-1	-1	-10	3	-1
6-7	-3	0	1	5	0	1	-3	-2	-3	-6	2	-1
7-8	-3	0	1	6	0	1	-3	-2	-4	-4	3	-1

Average total acceleration at the base increased by 48%, and average total acceleration at the elevated floors decreased in the range of 1% to 5%, as shown in Figure 4.3-13 and Table 4.3-17. The behavior in this case is similar to the behavior of the 4-story BRBF where the total acceleration only increased at the base.

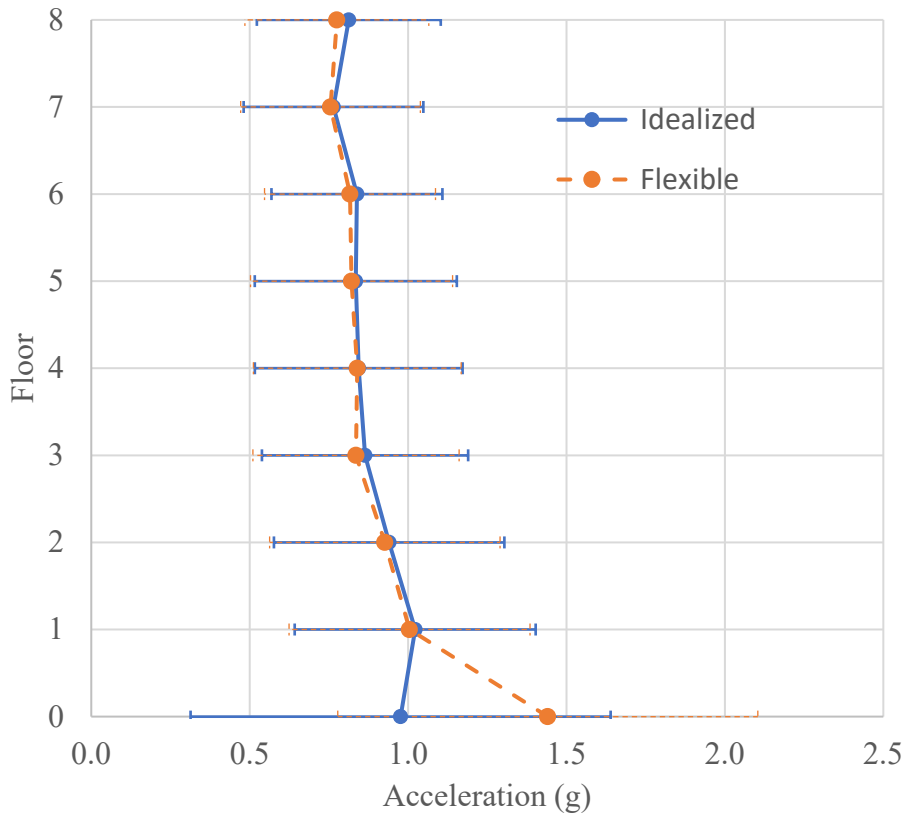

Figure 4.3-13 Average maximum roof acceleration for the BRBF direction of the 8-story building.

Table 4.3-17 Percentage change in the maximum acceleration at each floor for the BRBF direction of the 8-story building.

Story	EQ 1	EQ 2	EQ 3	EQ 4	EQ 5	EQ 6	EQ 7	EQ 8	EQ 9	EQ 10	EQ 11	Average
0	13	55	2	20	55	31	242	4	21	200	70	48
1	-3	3	-5	0	-11	-3	-4	-5	3	7	-2	-2
2	-3	4	2	-2	2	-6	-1	-1	-3	0	-1	-1
3	-3	-1	4	4	-20	-8	-12	1	-4	-1	2	-3
4	0	1	6	4	-10	-9	-5	-1	0	1	-1	-1
5	-2	-4	3	0	-3	-6	-9	0	1	1	1	-2
6	0	1	3	-3	-3	-2	-16	1	1	0	0	-3
7	1	1	-2	0	-3	7	-16	16	2	-1	1	-1
8	1	1	3	-1	-7	0	-22	-6	-9	0	1	-5

There is a slight change in the average maximum base and story shear, as shown in Figure 4.3-14. Some earthquakes showed an increase in the shear at the individual earthquake level, while others showed a decrease. EQ5 showed the highest increase in the base shear by 20%, as shown in Table 4.3-18. But the overall change in the average maximum shear is minimal. The allowed reduction in ASCE 7-16 is 10% for the base shear, but the NRHA showed an average reduction of 1%.

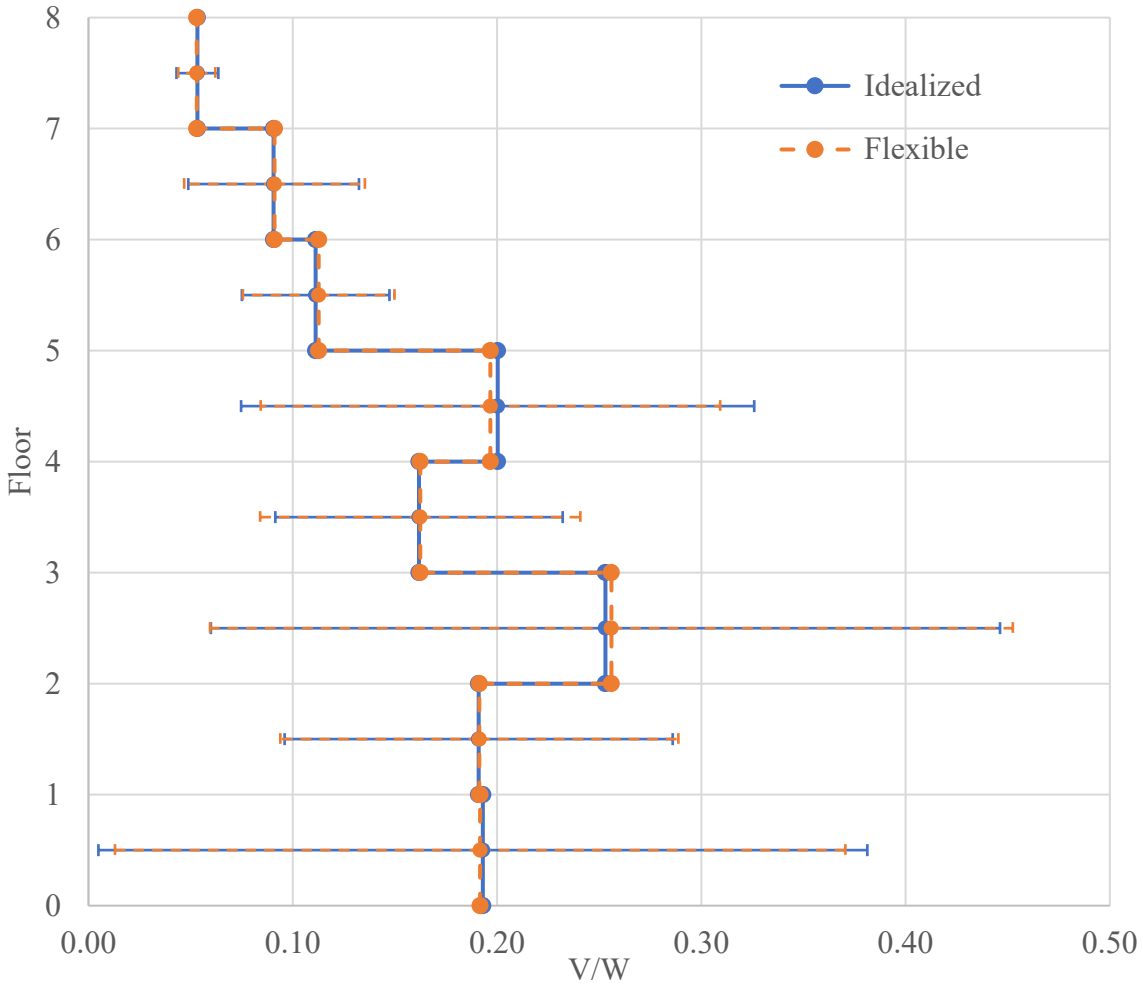

Figure 4.3-14 Average maximum shear force for the BRBF direction of the 8-story building.

Table 4.3-18 change in the base and floor shear for the BRBF direction of the 8-story building.

Story	EQ 1	EQ 2	EQ 3	EQ 4	EQ 5	EQ 6	EQ 7	EQ 8	EQ 9	EQ 10	EQ 11	Average
0-1	-2	0	-7	1	20	-1	10	-6	6	-4	-8	-1
1-2	1	0	-3	-1	0	1	2	-1	0	2	-2	0
2-3	-2	0	-4	-1	4	0	4	3	2	2	5	1
3-4	-2	-1	-1	0	-1	-7	-2	-1	-1	7	1	0
4-5	-5	4	1	-1	1	-8	2	-1	4	-8	6	-2
5-6	1	-1	-1	3	-1	-3	2	3	9	1	2	1
6-7	-4	2	-2	4	-2	1	-5	-2	6	3	-2	0
7-8	4	-1	0	3	-9	11	-4	-1	2	-6	-2	-1

To capture the general behavior of energy dissipation in the BRB elements, certain BRB elements have been selected as shown in Figure 4.3-15. The average energy dissipation

calculations showed that the BRB elements dissipate less energy in the flexible foundation case in the range of 0% to 7%, as shown in Table 4.3-19. The highest reduction occurred at the third floor, and the least change happened at the eighth floor (which is 0%). The behavior of the BRB elements in the 8-story building is similar to the behavior of the BRB elements in the 4-story building. The maximum BRB strain decreased in the lower floors (from 1st to 7th) and increased in the upper floors (8th), as shown in Table 4.3-20.

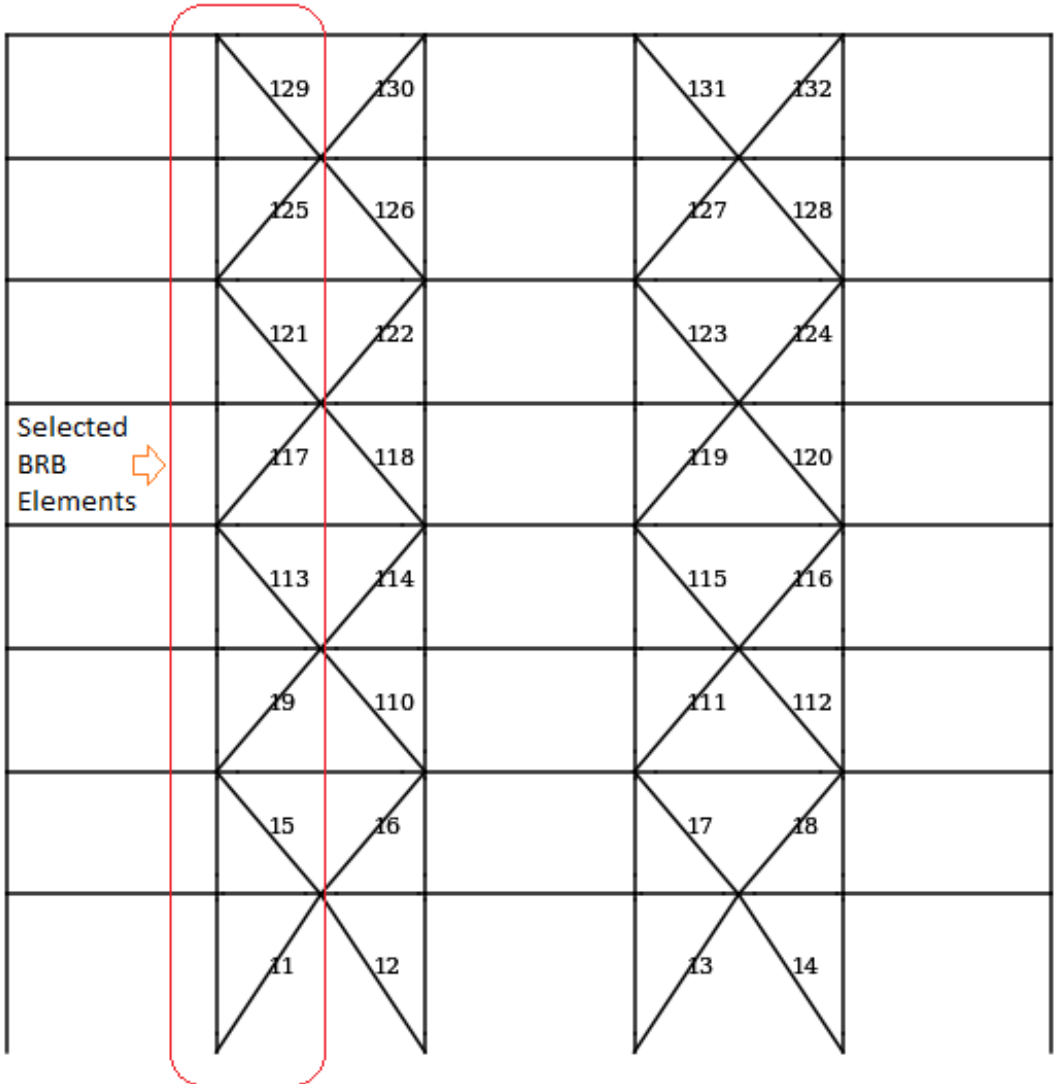

Figure 4.3-15 Selected BRB elements for dissipated energy calculations for the 8-story building.

Table 4.3-19 Percentage change in the energy dissipation in the BRB elements of the 8-story building.

BRB	EQ 1	EQ 2	EQ 3	EQ 4	EQ 5	EQ 6	EQ 7	EQ 8	EQ 9	EQ 10	EQ 11	Average
11	-22	-13	-3	-1	2	0	-6	-2	2	-5	-2	-5
15	-18	-10	-1	-1	0	4	-5	1	-1	-5	-5	-4
19	-13	-11	-1	-1	-5	6	-10	-2	-7	-8	-15	-7
113	6	-15	0	2	-2	-4	-8	-3	-4	-8	-9	-6
117	7	-12	4	9	-3	-11	-4	-9	3	-6	-10	-4
121	0	-7	2	7	4	-12	-6	-5	0	-5	3	-3
125	-5	1	11	1	-7	-10	2	-13	-2	-10	15	-3
129	1	5	5	2	-17	-3	5	-9	-4	-3	2	0

Table 4.3-20 Maximum strain at the selected BRB elements.

RBS	Idealized		Flexible		Percentage of change	
	Average	standard deviation	Average	standard deviation	Average	standard deviation
11	0.013559	0.021852	0.013145	0.020541	-3	-6
15	0.016677	0.022294	0.016372	0.021207	-2	-5
19	0.016645	0.020171	0.015730	0.018158	-5	-10
113	0.015269	0.018208	0.014491	0.016125	-5	-11
117	0.012219	0.015681	0.011987	0.014138	-2	-10
121	0.010513	0.013604	0.010222	0.012211	-3	-10
125	0.011362	0.011517	0.010819	0.010527	-5	-9
129	0.012558	0.009521	0.012655	0.009056	1	-5

4.4 16-Story Building Seismic Response

4.4.1 SMF

The results of the 16-story building dynamic analysis in the SMF direction are presented in this section along with a comparison between idealized and flexible foundation. The results showed an increase in the average maximum story displacement in the range of 0.4 inch to 3.4 inch, as shown in Figure 4.4-1 and Table 4.4-1. The behavior in this case is similar to the behavior of the 4-story building, while the 8-story building showed increase in the average maximum story displacement of the first six floors.

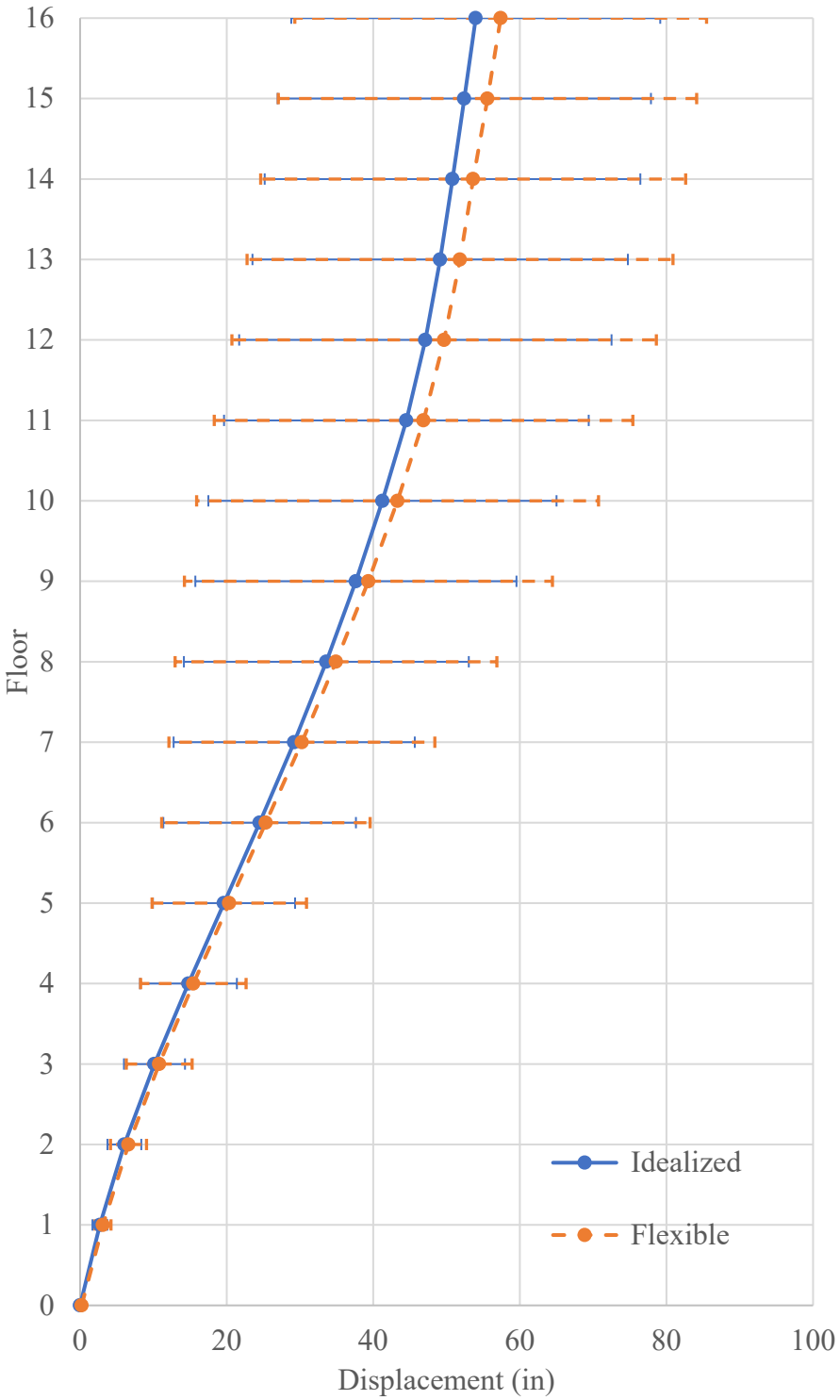

Figure 4.4-1 Average of the maximum displacement for the SMF direction of the 16-story building.

Table 4.4-1 Difference in maximum story displacement (inch) for the SMF direction of the 16-story building.

Story	EQ 1	EQ 2	EQ 3	EQ 4	EQ 5	EQ 6	EQ 7	EQ 8	EQ 9	EQ 10	EQ 11	Average
1	0.3	0.4	0.6	0.5	0.2	0.2	1.1	0.1	0.4	0.5	0.2	0.4
2	0.4	0.6	1.0	0.8	0.2	0.4	1.4	-0.1	0.6	0.7	0.3	0.6
3	0.5	0.7	1.6	1.1	0.2	0.6	1.6	-0.8	0.7	0.9	0.0	0.6
4	0.6	0.8	2.4	1.6	0.1	0.8	1.8	-2.2	0.7	0.9	-0.2	0.7
5	0.6	0.8	3.4	2.2	0.7	1.0	1.8	-4.0	0.7	1.1	-0.3	0.7
6	0.5	0.9	4.5	2.8	1.3	1.4	1.7	-5.3	0.5	1.4	-0.3	0.9
7	0.4	0.9	7.0	3.3	1.2	1.7	1.7	-6.5	0.4	1.6	-0.3	1.0
8	0.6	1.0	10.5	3.8	0.7	1.9	1.9	-7.5	0.2	1.8	-0.3	1.3
9	1.0	1.0	13.8	4.2	0.7	2.1	2.2	-7.9	0.0	1.9	-0.3	1.7
10	1.5	1.0	16.2	4.4	0.3	2.2	2.5	-7.4	0.0	2.2	-0.2	2.1
11	2.0	1.1	16.6	4.6	0.2	2.2	2.8	-6.6	0.0	2.9	0.0	2.3
12	2.6	1.2	16.4	4.7	0.0	2.5	3.2	-5.8	0.0	3.1	0.3	2.6
13	3.1	1.2	16.2	5.0	-0.1	2.6	3.3	-5.2	-0.1	3.3	0.5	2.7
14	3.6	1.3	16.0	5.2	-0.2	2.4	3.3	-4.8	-0.1	3.5	0.8	2.8
15	3.9	1.3	15.9	5.4	1.6	2.7	3.4	-4.3	-0.1	4.1	0.9	3.2
16	4.3	1.4	15.9	5.7	2.0	2.7	3.5	-3.7	0.0	4.7	1.0	3.4

Overall, the residual displacement increased for the SMF direction in the range of 0.1 inch to 2 inch, as shown in Figure 4.4-2 and Table 4.4-2. This behavior is different from the behavior of the 4- and 8-story buildings. Both showed a reduction in the residual displacement, while the 16-story building showed an increase in the residual displacement.

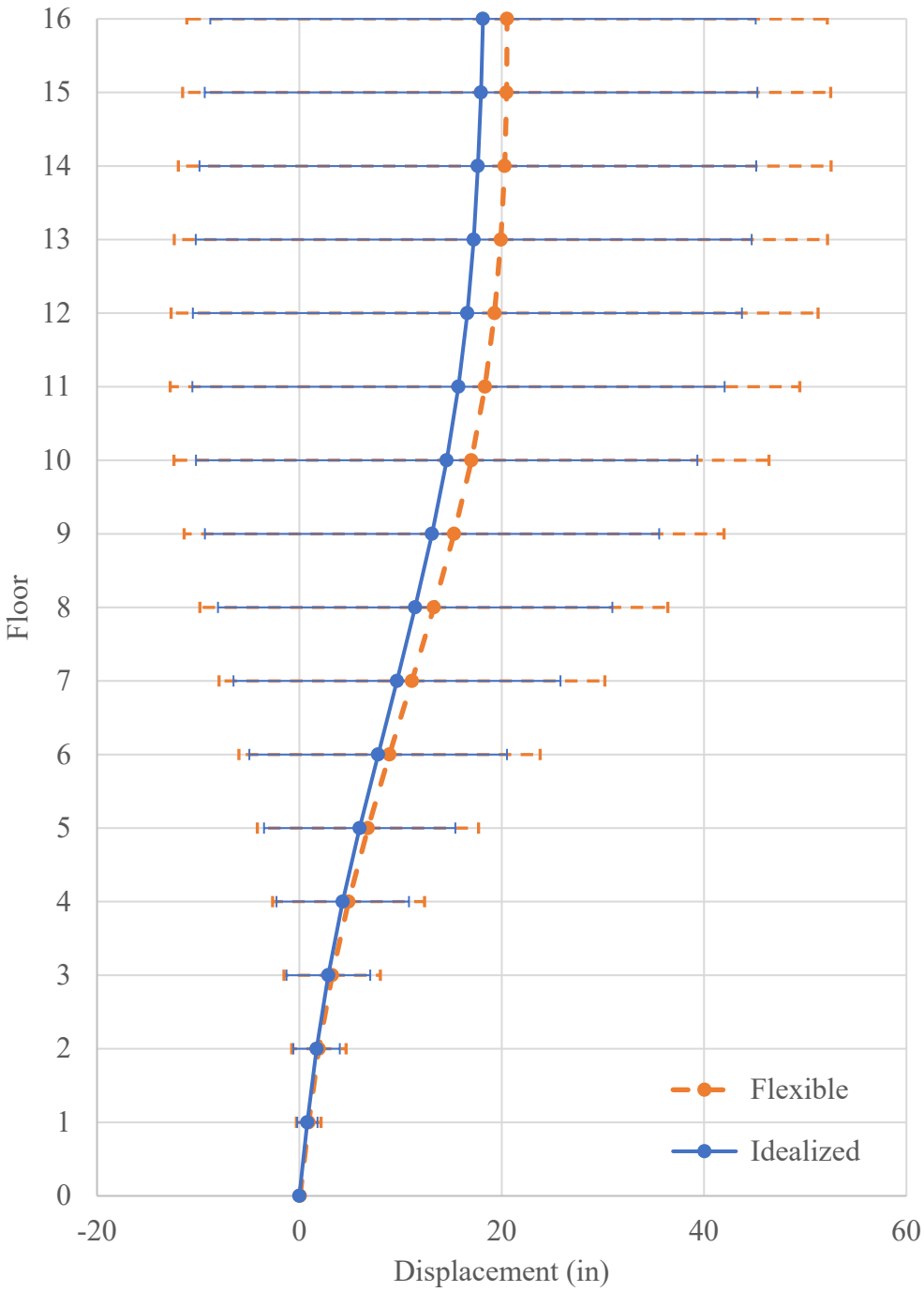

Figure 4.4-2 Average residual story displacement for the SMF direction of the 16-story building.

Table 4.4-2 Difference in residual story displacement (inch) for the SMF direction of the 16-story building.

Story	EQ1	EQ 2	EQ 3	EQ 4	EQ 5	EQ 6	EQ 7	EQ 8	EQ 9	EQ10	EQ11	Average
1	0.0	0.2	0.7	0.3	0.0	0.0	0.6	-0.3	0.1	0.2	-0.2	0.1
2	0.1	0.4	1.3	0.5	0.0	-0.2	0.8	-0.9	0.2	0.3	-0.3	0.2
3	0.2	0.6	2.4	1.0	0.0	-0.2	1.0	-1.7	0.4	0.4	-0.4	0.3
4	0.4	0.7	3.9	1.5	0.0	-0.2	1.2	-2.7	0.6	0.6	-0.5	0.5
5	0.7	0.9	6.0	2.1	0.0	-0.2	1.5	-3.9	0.8	0.7	-0.7	0.7
6	1.0	1.0	8.7	2.7	0.0	-0.2	1.6	-5.2	1.1	0.9	-1.0	1.0
7	1.3	1.0	11.8	3.3	0.0	-0.1	1.7	-6.3	1.4	1.0	-1.3	1.3
8	1.4	1.0	14.7	4.0	0.1	0.0	1.7	-7.2	1.7	1.2	-1.6	1.6
9	1.2	0.9	17.1	4.7	0.2	0.1	1.7	-7.9	2.1	1.3	-1.8	1.8
10	0.6	0.9	18.7	5.4	0.3	0.2	1.6	-8.2	2.5	1.4	-2.1	1.9
11	-0.5	0.9	19.6	5.9	0.5	0.3	1.5	-8.3	2.9	1.5	-2.3	2.0
12	-1.8	0.9	19.9	6.3	0.7	0.4	1.4	-8.2	3.1	1.6	-2.5	2.0
13	-3.3	0.9	20.0	6.5	0.9	0.4	1.4	-8.2	3.1	1.7	-2.5	1.9
14	-4.4	0.9	20.1	6.6	1.1	0.4	1.5	-8.1	3.1	1.8	-2.4	1.9
15	-4.6	0.8	20.0	6.7	1.2	0.4	1.6	-8.0	3.1	1.9	-2.3	1.9
16	-4.9	0.5	20.0	6.8	1.4	0.5	1.6	-7.8	3.1	2.0	-2.2	1.9

There is no change for the maximum story drift, as shown in Figure 4.4-3 and Table 4.4-3. Even in the individual earthquake records there was no change in the maximum drift except at the sixteenth floor there was a slight change in the maximum drift. That indicates that the drift is controlled mainly by the stiffness of the structure because it is less than the stiffness of the foundation in this case. This behavior is different from the behavior of the 4- and 8-story buildings. Both show increase in the bottom floors and a reduction in the top floors.

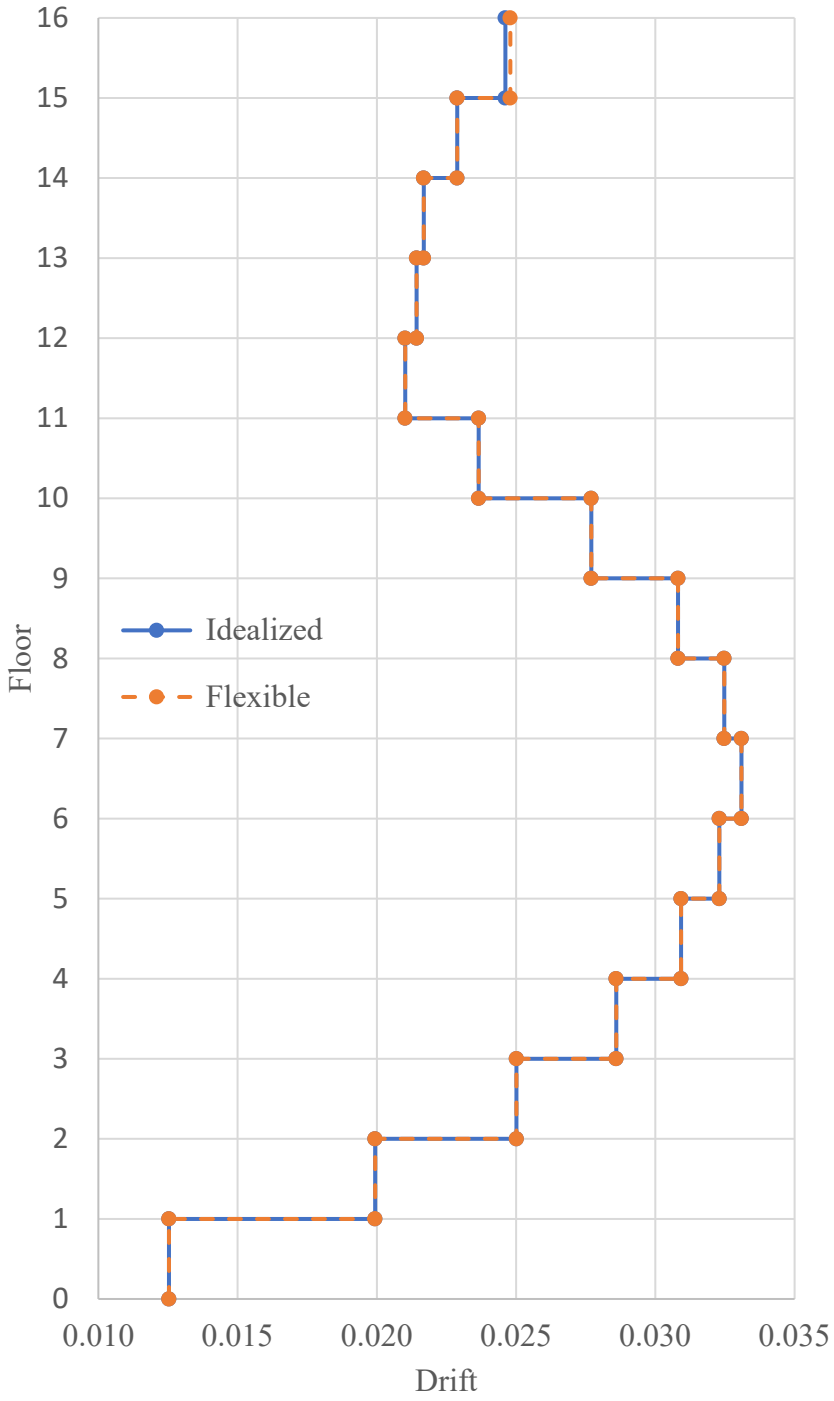

Figure 4.4-3 Average maximum drift for the SMF direction of the 16-story building.

Table 4.4-3 Difference in maximum drift for the SMF direction of the 16-story building ($*10^{-3}$).

Story	EQ1	EQ2	EQ3	EQ4	EQ5	EQ6	EQ7	EQ8	EQ9	EQ10	EQ11	Average
1	0	0	0	0	0	0	0	0	0	0	0	0
2	0	0	0	0	0	0	0	0	0	0	0	0
3	0	0	0	0	0	0	0	0	0	0	0	0
4	0	0	0	0	0	0	0	0	0	0	0	0
5	0	0	0	0	0	0	0	0	0	0	0	0
6	0	0	0	0	0	0	0	0	0	0	0	0
7	0	0	0	0	0	0	0	0	0	0	0	0
8	0	0	0	0	0	0	0	0	0	0	0	0
9	0	0	0	0	0	0	0	0	0	0	0	0
10	0	0	0	0	0	0	0	0	0	0	0	0
11	0	0	0	0	0	0	0	0	0	0	0	0
12	0	0	0	0	0	0	0	0	0	0	0	0
13	0	0	0	0	0	0	0	0	0	0	0	0
14	0	0	0	0	0	0	0	0	0	0	0	0
15	0	0	0	0	0	0	0	0	0	0	0	0
16	2	-1	0	0	-1	0	0	1	-1	1	0	0

The residual drift increased in range of $-0.4*10^{-3}$ to $1.8*10^{-3}$, as shown in Figure 4.4-4 and Table 4.4-4. This behavior is different from the behavior of the 4- and 8-story buildings. Both showed a reduction in the residual drift.

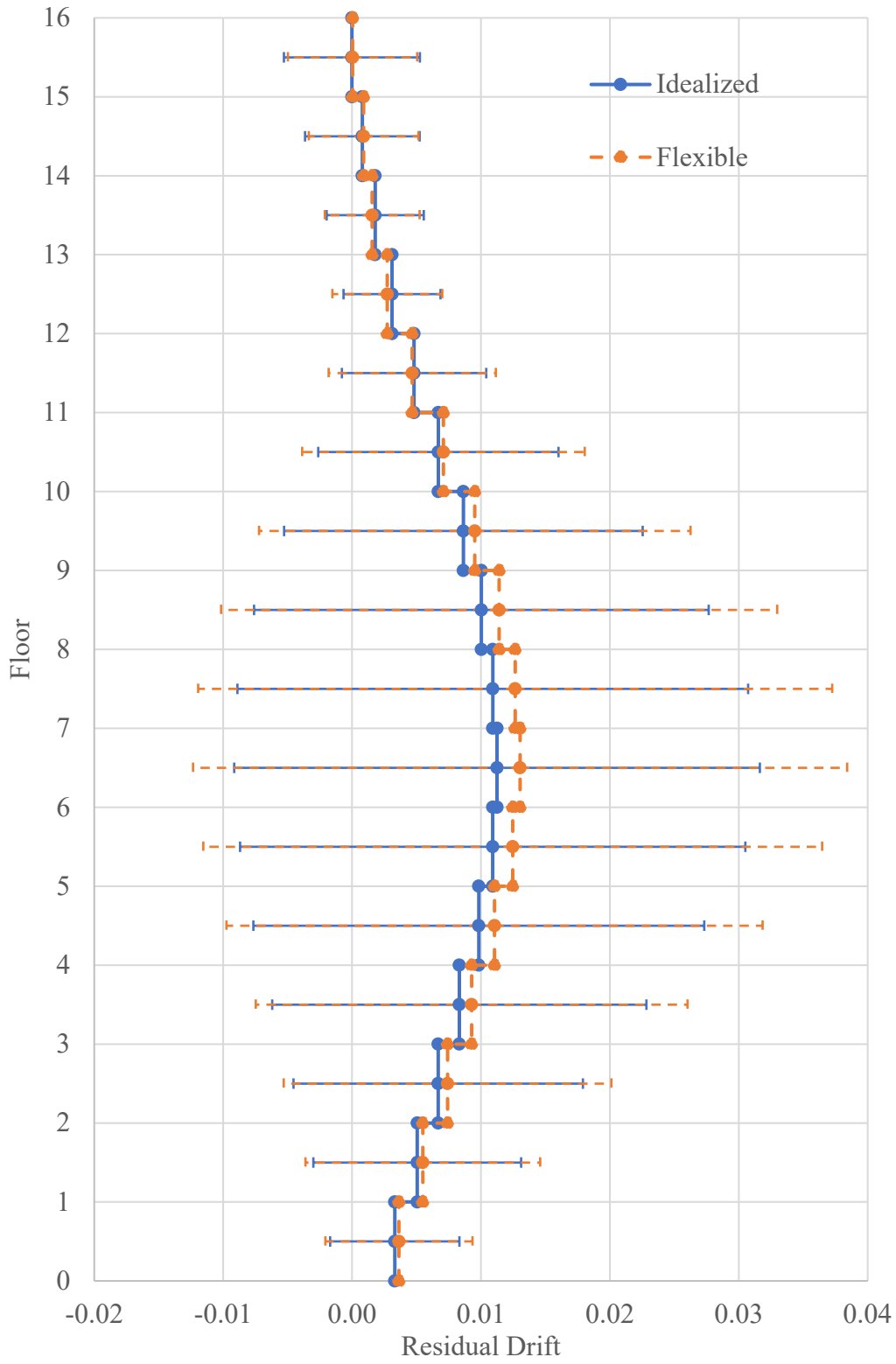

Figure 4.4-4 Average residual drift for the SMF direction of the 16-story building.

Table 4.4-4 Difference in residual drift for the SMF direction of the 16-story building (*10^{-3}).

Story	EQ1	EQ2	EQ3	EQ4	EQ5	EQ6	EQ7	EQ8	EQ9	EQ10	EQ11	Average
0-1	0.1	0.7	2.6	0.8	0.0	-0.4	1.4	-1.5	0.2	0.5	-1.0	0.3
1-2	0.4	1.0	4.1	1.7	0.1	-0.9	1.3	-3.4	0.6	0.6	-0.7	0.4
2-3	0.8	1.2	6.1	2.5	0.0	-0.1	1.4	-5.0	0.9	0.8	-0.7	0.7
3-4	1.1	1.1	8.9	3.3	-0.1	-0.1	1.4	-6.2	1.1	0.9	-1.0	1.0
4-5	1.4	0.8	12.6	3.6	-0.2	-0.1	1.3	-7.2	1.3	1.0	-1.2	1.2
5-6	1.8	0.5	16.4	3.6	-0.1	0.1	1.0	-7.4	1.6	1.0	-1.4	1.6
6-7	1.9	0.2	18.2	3.7	0.3	0.3	0.6	-6.6	2.0	0.8	-1.6	1.8
7-8	0.9	-0.1	17.4	3.9	0.6	0.6	0.1	-5.4	2.2	0.8	-1.7	1.7
8-9	-1.3	-0.3	14.1	4.1	0.7	0.8	-0.4	-3.9	2.4	0.7	-1.7	1.4
9-10	-3.8	-0.3	9.9	4.0	0.6	0.7	-0.5	-2.2	2.3	0.6	-1.6	0.9
10-11	-6.1	-0.1	5.2	3.2	1.2	0.7	-0.6	-0.4	1.9	0.6	-1.3	0.4
11-12	-8.0	0.2	1.8	2.1	1.0	0.3	-0.4	0.4	1.2	0.7	-0.8	-0.1
12-13	-8.7	0.2	0.7	1.2	1.0	0.1	0.0	0.4	0.4	0.7	-0.1	-0.4
13-14	-6.4	0.0	0.2	0.8	1.0	0.0	0.4	0.5	0.1	0.6	0.4	-0.2
14-15	-1.7	-0.7	-0.1	0.6	1.0	0.1	0.4	0.6	-0.1	0.5	0.5	0.1
15-16	-1.4	-1.5	-0.1	0.6	0.8	0.4	0.3	0.8	-0.2	0.4	0.5	0.1

Total acceleration increased at the base by 47% and at the elevated floors in the range of 1% to 19%, as shown in Figure 4.4-5 and Table 4.4-5. Comparing this behavior to the behavior of the 4- and 8-story buildings, the base acceleration increased in all the three cases, but the floor acceleration depends on the height (stiffness of the SMF) of the buildings. When the building height is low, the floor acceleration decreased, when the height of the building is intermediate, the change in floors acceleration is small, and when the building height is high, the floor accelerations increased.

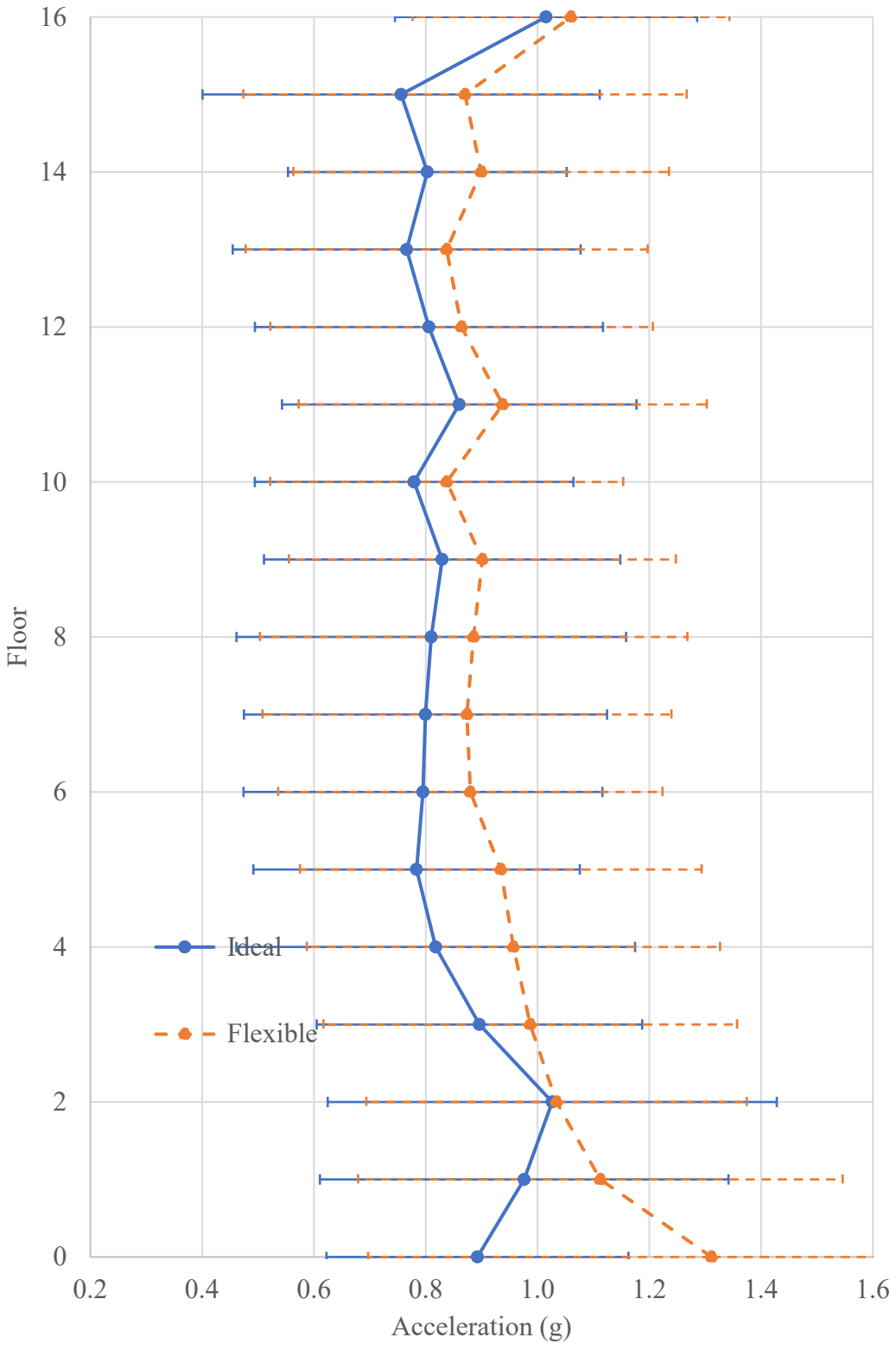

Figure 4.4-5 Average maximum acceleration for the SMF direction of the 16-story building.

Table 4.4-5 Percentage change in maximum acceleration for the SMF direction of the 16-story building.

Story	EQ1	EQ2	EQ3	EQ4	EQ5	EQ6	EQ7	EQ8	EQ9	EQ10	EQ11	Average
0	36	14	18	46	78	24	186	19	21	27	63	47
1	15	11	11	31	3	17	15	4	13	8	24	14
2	-16	10	6	33	4	3	-3	2	8	9	-11	1
3	5	8	7	23	-1	14	27	1	5	10	8	10
4	49	11	10	19	6	27	1	18	10	13	37	17
5	34	23	13	9	0	25	8	16	25	6	40	19
6	22	20	20	2	12	3	4	8	13	4	9	11
7	15	7	5	9	11	2	11	8	17	-1	16	9
8	18	4	14	12	0	20	5	2	14	0	13	9
9	25	14	6	9	0	7	-4	2	14	7	14	9
10	4	0	6	27	0	16	9	4	2	10	9	7
11	3	14	12	16	-1	25	2	5	-1	9	10	9
12	20	6	8	9	-1	7	4	13	1	5	5	7
13	5	12	2	10	4	6	10	16	-3	-2	37	9
14	17	13	3	-2	7	6	23	5	11	3	25	12
15	28	17	3	13	3	27	7	15	2	10	40	15
16	1	7	3	-1	3	6	2	6	3	6	11	4

Overall, there is a slight increase in the story and base shear in the range of 0% to 5%, as shown in Figure 4.4-6 and Table 4.4-6. The behavior in this case is different from the behavior of the 4- and 8-story buildings. The floor and base shear decreased in the 4- and 8-story buildings. The highest reduction occurred in the 4-story building. The allowed reduction in ASCE 7-16 is 10% for the base shear, but the NRHA showed an average increase of 1%.

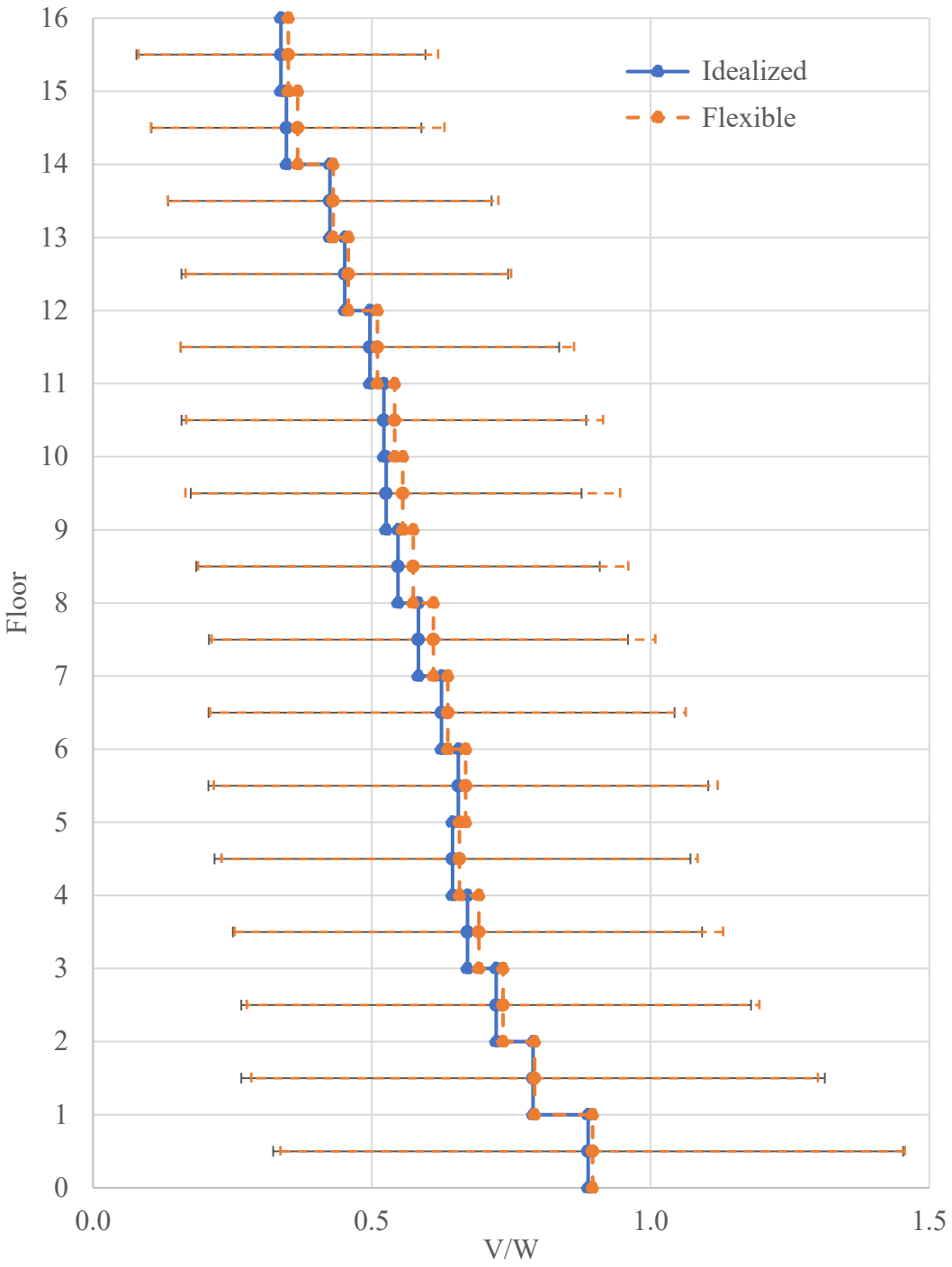

Figure 4.4-6 Average maximum floor shear and base shear for the SMF direction of the 16-story building.

Table 4.4-6 Percentage change in maximum floor shear for the SMF direction of the 16-story building.

Story	EQ 1	EQ 2	EQ 3	EQ 4	EQ 5	EQ 6	EQ 7	EQ 8	EQ 9	EQ10	EQ11	Average
0-1	1	0	0	2	1	-3	9	1	0	1	0	1
1-2	-3	0	4	1	1	-3	8	2	0	0	3	0
2-3	-2	2	4	-1	-2	1	8	0	0	4	5	2
3-4	5	2	0	0	0	1	4	-1	3	6	6	3
4-5	-2	2	0	-2	1	0	9	2	2	5	7	2
5-6	-1	3	1	-2	-2	2	11	2	4	3	3	2
6-7	2	3	1	1	3	2	0	-1	4	2	2	2
7-8	12	3	2	1	2	2	2	2	4	0	11	4
8-9	9	8	1	0	1	4	7	1	1	-1	12	5
9-10	1	7	4	-2	2	16	3	3	2	1	8	5
10-11	4	0	6	0	1	1	5	3	6	3	9	4
11-12	2	4	2	0	-1	5	2	3	-2	2	7	3
12-13	1	11	-1	1	2	0	10	1	0	-1	0	1
13-14	2	7	2	1	-2	2	0	2	-1	-2	3	1
14-15	14	0	0	2	2	1	12	5	0	2	4	5
15-16	2	7	3	-1	4	5	6	4	2	4	6	4

For energy dissipation, certain RBS elements have been selected as shown in Figure 4.4-7. The energy dissipation has been calculated at those RBS springs to capture the general trend of the RBS springs behavior. The energy dissipation has increased in some RBS springs by a maximum percentage of 9% and decreased in others by a maximum ratio of 6%, as shown in Table 4.4-7. The maximum rotation increased in some RBS springs by a maximum amount of 11% and decreased in other RBS springs by a maximum amount of 6%, as shown in Table 4.3-8. This change in energy dissipation is small compared to the change in energy dissipation in the 4- and 8-story buildings. The RBS energy dissipation has decreased by a maximum value of 34% in the 4-story building and decreased by a maximum value of 43% in some RBS in the 8-story building and increased by a maximum value of 21% in other RBS locations in the 8-story building.

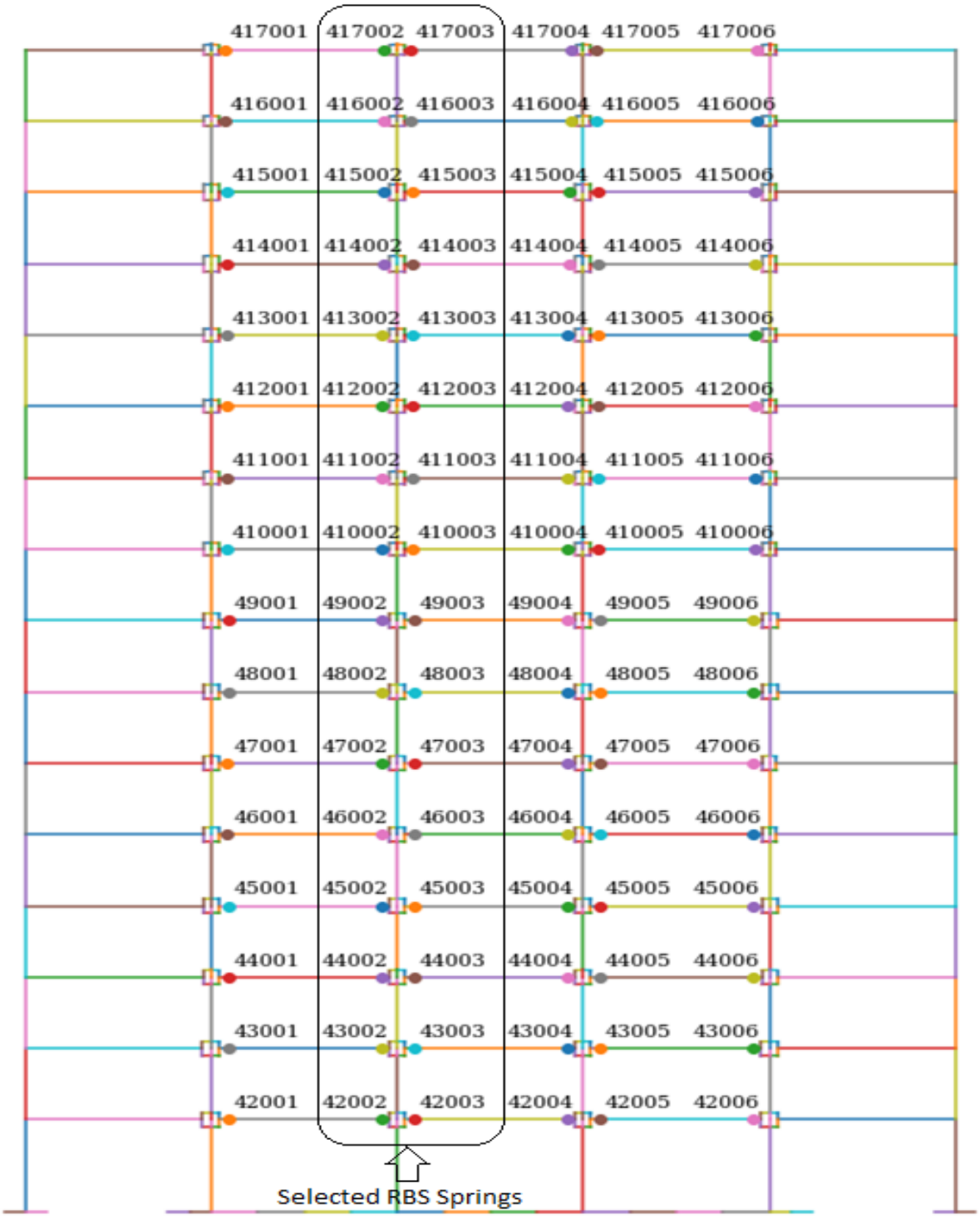

Figure 4.4-7 Selected RBS for energy calculation in the SMF direction of the 16-story building.

Table 4.4-7 Average energy dissipation at the selected RBS springs of the 16-story building.

RBS	Idealized		Flexible		Percentage Change	
	Average (kip*in)	Standard Deviation (kip*in)	Average (kip*in)	Standard Deviation (kip*in)	Average	Standard Deviation
42002	432	313	459	330	6	5
42003	405	309	444	321	9	4
43002	862	528	884	562	3	6
43003	858	532	901	575	5	7
44002	1260	869	1262	886	0	2
44003	1302	903	1327	932	2	3
45002	1471	1175	1455	1165	-1	-1
45003	1541	1223	1546	1218	0	0
46002	1420	1223	1383	1211	-3	-1
46003	1497	1259	1480	1248	-1	-1
47002	1389	1262	1351	1254	-3	-1
47003	1484	1298	1461	1289	-2	-1
48002	1291	1222	1220	1127	-6	-8
48003	1392	1254	1380	1247	-1	-1
49002	1225	1081	1228	1102	0	2
49003	1351	1121	1362	1145	1	2
410002	1037	821	1051	846	1	3
410003	1199	915	1227	950	2	4
411002	919	811	930	803	1	-1
411003	1098	962	1122	955	2	-1
412002	773	965	761	935	-2	-3
412003	960	1134	962	1111	0	-2
413002	679	1139	655	1118	-4	-2
413003	841	1316	826	1305	-2	-1
414002	742	1314	723	1312	-3	0
414003	873	1454	856	1459	-2	0
415002	723	1331	701	1319	-3	-1
415003	845	1465	824	1459	-3	0
416002	574	976	571	981	-1	1
416003	644	1081	637	1089	-1	1
417002	359	616	372	635	3	3
417003	392	676	402	691	2	2

Table 4.4-8 Average maximum rotation at the selected RBS springs of the 16-story building.

RBS	Idealized		Flexible		Percentage of change	
	Average (rad)	Standard Deviation (rad)	Average (rad)	Standard Deviation (rad)	Average	Standard Deviation
42002	0.0102	0.0074	0.0106	0.0078	4	5
42003	0.0100	0.0075	0.0107	0.0077	7	3
43002	0.0165	0.0116	0.0169	0.0124	3	7
43003	0.0165	0.0117	0.0171	0.0125	3	7
44002	0.0220	0.0169	0.0221	0.0183	1	8
44003	0.0222	0.0170	0.0225	0.0183	1	8
45002	0.0254	0.0217	0.0253	0.0236	0	9
45003	0.0259	0.0217	0.0260	0.0235	0	8
46002	0.0269	0.0254	0.0271	0.0283	1	11
46003	0.0276	0.0254	0.0279	0.0282	1	11
47002	0.0282	0.0270	0.0294	0.0326	4	21
47003	0.0290	0.0269	0.0303	0.0325	4	21
48002	0.0283	0.0272	0.0296	0.0323	5	19
48003	0.0292	0.0270	0.0307	0.0319	5	18
49002	0.0262	0.0245	0.0274	0.0275	5	12
49003	0.0272	0.0242	0.0287	0.0270	5	12
410002	0.0230	0.0186	0.0247	0.0211	7	13
410003	0.0243	0.0183	0.0263	0.0206	8	13
411002	0.0172	0.0121	0.0189	0.0135	10	12
411003	0.0187	0.0115	0.0207	0.0128	11	12
412002	0.0130	0.0086	0.0134	0.0089	3	4
412003	0.0148	0.0083	0.0153	0.0084	4	1
413002	0.0113	0.0080	0.0112	0.0087	-1	8
413003	0.0132	0.0079	0.0131	0.0084	-1	6
414002	0.0128	0.0087	0.0126	0.0097	-1	12
414003	0.0147	0.0081	0.0145	0.0087	-1	8
415002	0.0121	0.0079	0.0120	0.0093	-1	17
415003	0.0136	0.0073	0.0135	0.0082	0	11
416002	0.0153	0.0087	0.0154	0.0094	0	8
416003	0.0167	0.0085	0.0165	0.0090	-1	5
417002	0.0130	0.0085	0.0134	0.0095	3	11
417003	0.0144	0.0082	0.0147	0.0088	2	7

The column springs at the base were selected to evaluate the general behavior trend of the column springs as shown in Figure 4.4-8. The energy dissipation at the specified column springs decreased in a range of 0% to 14%, as shown in Table 4.4-9. All the springs dissipated less energy in the flexible case except spring 712031 which dissipated the same amount of energy. At the same time, the maximum rotation in the column springs was decreased in the range of 1% to 12%, as shown in Table 4.4-10. This behavior is similar to the behavior of column springs in the 4- and 8-story buildings, the highest reduction was in the 4-story building. The reduction is less in the 16-story building than the 4- and 8-story building because the foundation of the SMF in the 16-story building is raft, while the foundation is isolated footing in the 4- and 8-story building. The raft foundation adds less flexibility than the isolated foundation.

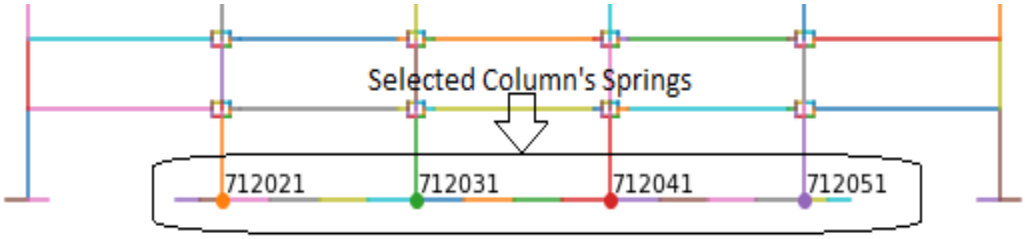

Figure 4.4-8 Selected column's springs.

Table 4.4-9 Energy dissipation at the selected column springs.

Column springs	Idealized		Flexible		Percentage Change	
	Average (kip*in)	Standard Deviation (kip*in)	Average (kip*in)	Standard Deviation (kip*in)	Average	Standard Deviation
712021	206	355	183	338	-11	-5
712031	145	250	145	256	0	2
712041	145	250	140	248	-4	-1
712051	208	357	178	321	-14	-10

Table 4.4-10 Maximum rotation at the selected column springs

Column springs	Idealized		Flexible		Percentage Change	
	Average (rad)	Standard Deviation (rad)	Average (rad)	Standard Deviation (rad)	Average	Standard Deviation
712021	0.002034	0.002827	0.001848	0.002673	-9	-5
712031	0.002185	0.003022	0.002159	0.003052	-1	1
712041	0.002186	0.003023	0.002125	0.002982	-3	-1
712051	0.002047	0.002844	0.001812	0.002547	-12	-10

4.4.2 BRBF

The 16-story building dynamic analysis results in the BRBF direction are presented in this section along with a comparison between the idealized and flexible foundation. The results show an increase in the maximum displacement in the range of 0.2 inch to 3.3 inch as shown in Figure 4.4-9 and Table 4.4-11. This behavior is similar to the behavior of the 4- and 8-story buildings, but the 8-story building showed a small increase in the maximum displacement.

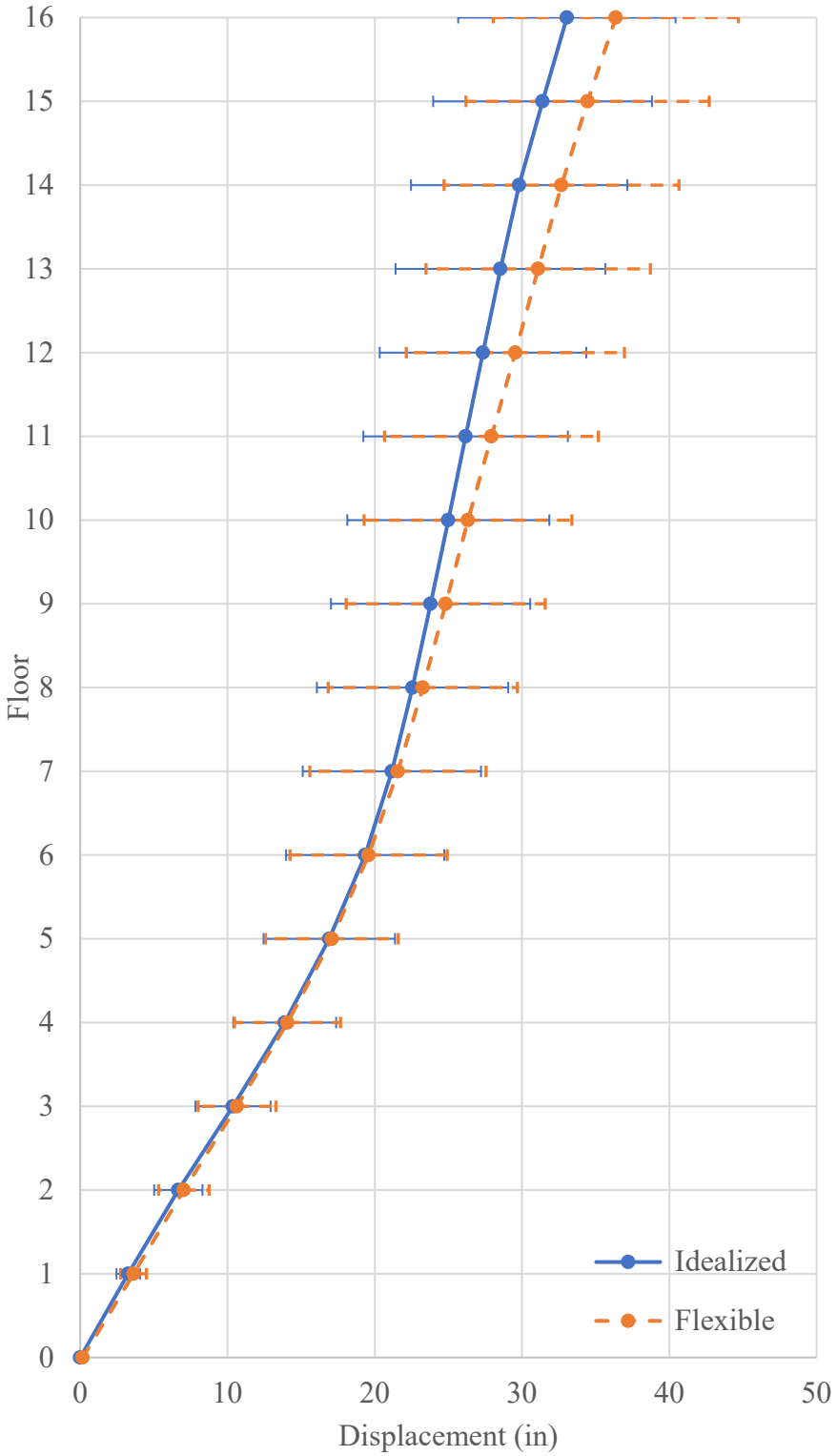

Figure 4.4-9 Average maximum displacement BRBF direction of the 16-story building.

Table 4.4-11 Difference in the maximum BRBF displacement (inch) of the 16-story building.

Story	EQ1	EQ2	EQ3	EQ4	EQ5	EQ6	EQ7	EQ8	EQ9	EQ10	EQ11	Average
1	0.4	0.4	0.1	0.8	0.4	0.2	0.2	-0.2	0.5	0.7	0.5	0.4
2	0.3	0.4	-0.1	1.3	0.6	0.2	0.2	-0.8	0.4	0.8	0.7	0.4
3	0.0	0.5	-0.3	1.8	0.9	0.0	0.1	-1.4	0.0	0.9	0.5	0.3
4	-0.3	0.6	-0.3	2.2	1.3	-0.3	0.0	-1.8	-0.5	1.0	0.3	0.2
5	-0.6	0.7	-0.3	2.6	1.6	-0.6	0.0	-2.0	-1.0	1.1	0.4	0.2
6	-0.7	0.8	-0.4	2.9	2.0	-0.6	0.0	-1.8	-1.4	1.2	0.6	0.2
7	-0.4	1.0	-0.5	3.3	2.3	-0.5	0.1	-1.6	-1.3	1.3	0.9	0.4
8	0.1	1.1	-0.5	3.6	2.9	-0.3	0.4	-1.3	-1.1	1.5	1.4	0.7
9	0.7	1.2	-0.3	3.8	3.6	-0.1	0.4	-1.1	-0.8	1.8	2.0	1.0
10	1.7	1.3	0.0	3.9	4.0	0.3	-0.2	-1.0	0.0	2.2	2.5	1.3
11	2.8	1.4	0.3	3.9	4.3	0.9	0.3	-0.8	0.6	2.8	2.8	1.8
12	4.0	1.5	0.6	3.8	4.7	1.5	1.1	-0.5	1.1	3.3	3.0	2.2
13	5.1	1.6	0.8	3.7	5.1	2.1	1.8	-0.4	1.8	3.6	2.9	2.6
14	6.2	1.8	0.9	3.5	5.3	2.5	2.7	-0.5	2.6	3.9	2.6	2.9
15	7.3	1.9	1.1	3.1	5.7	2.7	4.1	-0.5	3.1	4.4	0.9	3.1
16	8.3	1.6	1.3	2.0	6.1	2.9	5.5	-0.4	3.2	5.1	1.0	3.3

The change in the average residual displacement of the BRBF is shown in Figure 4.4-10. Overall, the residual story displacement increased in the range of 0.1in to 3.2in. Some earthquakes had a higher difference in the residual displacement, as shown in Table 4.4-12. The behavior of the 16-story building is similar to the behavior of the 4-story building, but the increase in the residual displacement of the 4-story building was less. The behavior of the 16-story building is different from the behavior of the 8-story building where a reduction in the residual displacement occurred. Both did not show change in the residual deformation. In the 16-story building, the residual displacement in the foundation (pile footing) was higher than the residual displacement in the foundations of the 4- and 8-story building (raft foundation).

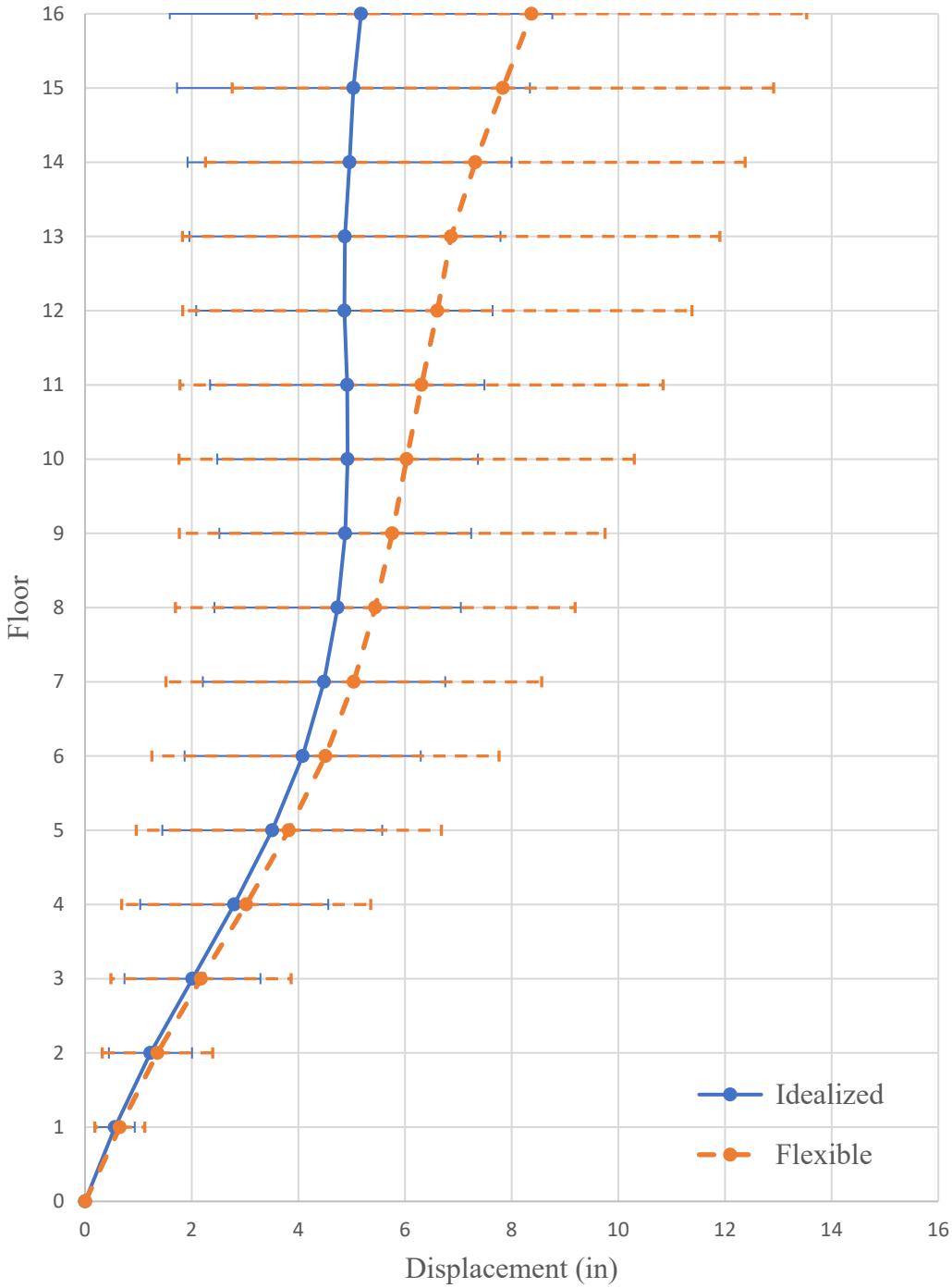

Figure 4.4-10 Average residual displacement of the BRBF direction of the 16-story building.

Table 4.4-12 Difference in residual displacement (inch) of the BRBF direction of the 16-story building.

Story	EQ 1	EQ2	EQ3	EQ4	EQ 5	EQ 6	EQ 7	EQ 8	EQ9	EQ1 0	EQ1 1	Averag e
1	-0.1	-0.2	-0.1	-0.1	0.7	0.0	0.0	0.0	0.3	-0.1	0.5	0.1
2	-0.2	-0.5	-0.1	-0.2	1.4	0.1	-0.2	0.0	0.5	-0.3	1.0	0.1
3	-0.3	-0.8	-0.2	-0.3	2.1	0.0	-0.4	0.0	0.8	-0.6	1.5	0.2
4	-0.3	-1.0	-0.2	-0.4	2.8	0.0	-0.6	0.0	1.4	-1.1	1.8	0.2
5	-0.1	-1.0	0.0	-0.5	3.5	0.0	-0.6	0.0	1.8	-1.6	2.0	0.3
6	0.2	-1.0	0.3	-0.7	4.0	0.1	-0.6	0.1	2.1	-2.0	2.3	0.4
7	0.7	-1.1	0.7	-0.9	4.3	0.2	-0.5	0.1	2.3	-2.2	2.5	0.6
8	1.2	-1.1	1.2	-1.2	4.6	0.3	-0.3	0.2	2.6	-2.3	2.6	0.7
9	1.9	-1.1	1.8	-1.6	4.9	0.6	-0.2	0.2	3.0	-2.4	2.6	0.9
10	2.6	-1.1	2.5	-2.0	5.2	1.0	0.1	0.3	3.3	-2.4	2.8	1.1
11	3.4	-0.7	3.2	-2.5	5.4	1.6	0.7	0.5	3.3	-2.4	2.9	1.4
12	4.3	0.4	4.0	-3.0	5.6	2.1	1.4	0.6	3.1	-2.4	3.1	1.7
13	5.0	0.8	4.7	-3.6	5.9	2.4	2.1	0.7	3.0	-2.4	3.3	2.0
14	5.7	0.6	5.4	-2.9	6.0	2.5	2.8	0.7	2.9	-1.6	3.7	2.4
15	6.4	0.5	6.2	-1.8	6.1	2.5	3.5	0.7	3.0	-0.6	4.2	2.8
16	6.8	0.3	6.1	-0.1	6.1	2.4	4.4	0.9	3.3	-0.1	4.9	3.2

The change in the average maximum drift is shown in Figure 4.4-11. There is a reduction in the maximum drift of the third and fourth stories by $-0.4*10^{-3}$, and there is no change in the maximum drift of the second and fifth story. The other stories showed an increase in the maximum story drift in a range of $0.4*10^{-3}$ to $1.4*10^{-3}$, as shown in Table 4.4-13.

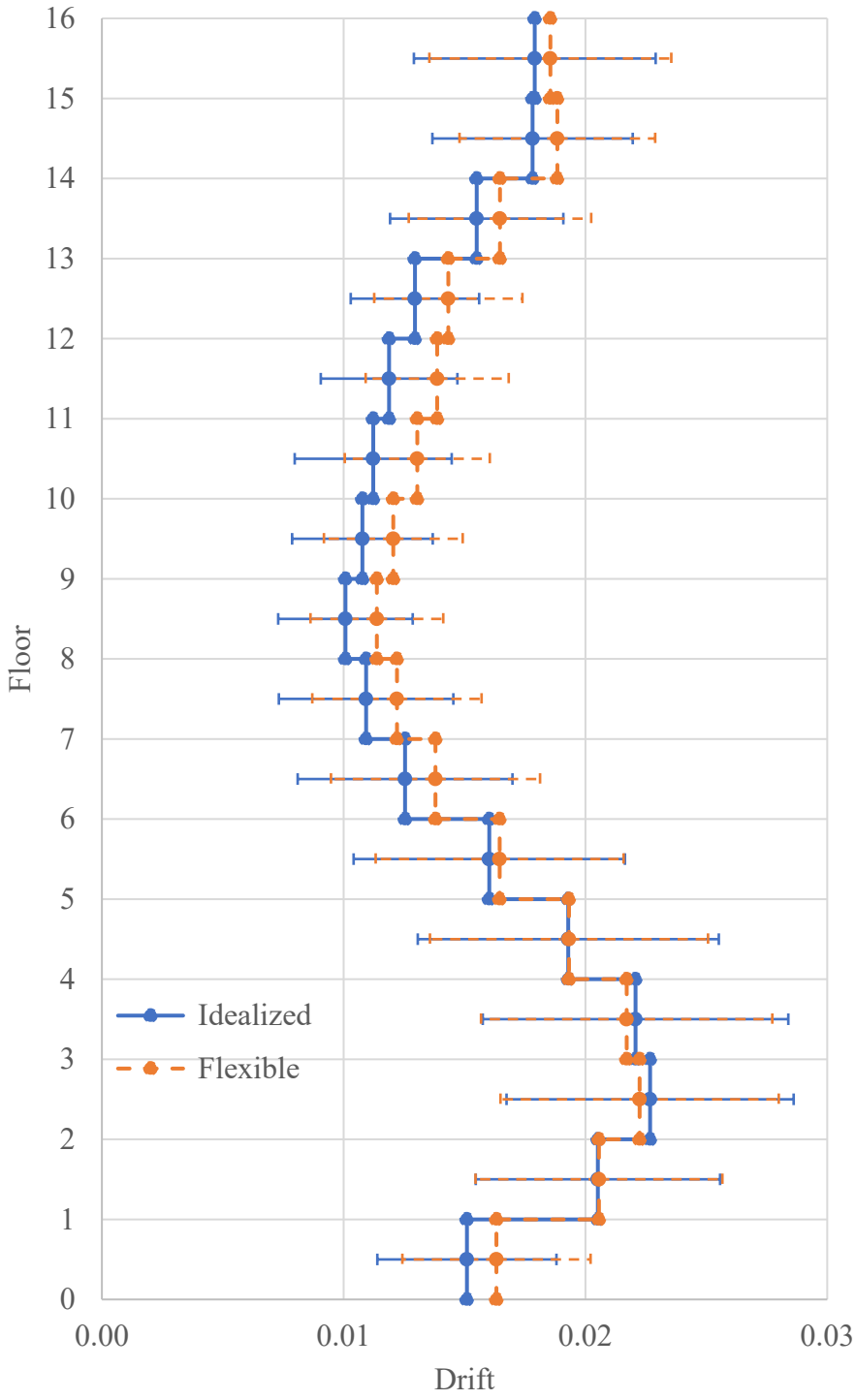

Figure 4.4-11 Average maximum drift of the BRBF direction of the 16-story building.

Table 4.4-13 Difference in maximum drift of the BRBF direction of 16-story building ($*10^{-3}$).

Story	EQ1	EQ2	EQ3	EQ4	EQ5	EQ6	EQ7	EQ8	EQ9	EQ10	EQ11	Average
0-1	1.3	1.2	-0.1	3.1	1.4	0.7	0.8	-1.2	1.9	2.4	2.0	1.2
1-2	-0.4	0.6	-1.3	3.1	1.4	-0.6	-0.2	-3.4	-0.5	1.0	0.7	0.0
2-3	-1.5	0.4	-0.5	2.7	1.9	-1.5	-0.4	-3.6	-2.8	0.6	-0.1	-0.4
3-4	-1.8	0.4	-0.2	2.6	2.1	-1.8	-0.6	-2.5	-2.8	0.4	0.0	-0.4
4-5	-1.4	0.6	-0.1	2.3	2.2	-1.0	-0.1	-0.7	-2.0	0.2	0.3	0.0
5-6	0.1	0.7	0.0	2.0	2.2	0.0	0.0	0.5	-1.3	-0.2	0.8	0.4
6-7	3.3	1.0	0.9	2.1	2.1	0.7	0.7	1.3	0.1	0.5	1.1	1.3
7-8	0.2	1.1	1.1	1.4	2.3	0.6	0.6	1.8	1.6	1.2	2.1	1.3
8-9	-0.2	0.3	0.5	2.3	2.5	0.7	-0.2	1.4	2.8	1.5	2.7	1.3
9-10	1.1	-0.8	-0.3	2.8	2.8	1.8	0.9	0.9	2.5	1.7	0.7	1.3
10-11	0.6	-1.0	-1.3	1.9	2.1	4.3	3.4	2.3	2.5	3.4	1.8	1.8
11-12	1.9	-1.6	1.2	1.5	2.3	5.1	3.3	2.2	1.2	2.1	2.7	2.0
12-13	3.1	-3.3	2.7	0.9	2.3	3.6	1.7	0.8	1.1	-1.0	3.3	1.4
13-14	1.9	-4.5	2.8	1.7	1.5	2.1	2.2	0.7	1.6	-1.6	2.1	1.0
14-15	2.3	-2.7	2.5	2.9	0.8	-0.5	3.4	0.4	1.8	-0.2	0.5	1.0
15-16	1.1	-1.3	1.0	3.5	0.7	-1.7	-0.5	0.7	3.4	-0.9	1.3	0.6

There is increase in the residual drift in the range of $0.4*10^{-3}$ to $2.4*10^{-3}$, as shown in Figure 4.2-12 and Table 4.4-14. The change in residual drift at the eleventh and twelfth floors is negative because the idealized foundation residual drift is negative. Most of the residual drift came from the residual deformation at the pile footing. Pile foundations showed higher displacement than the raft foundation.

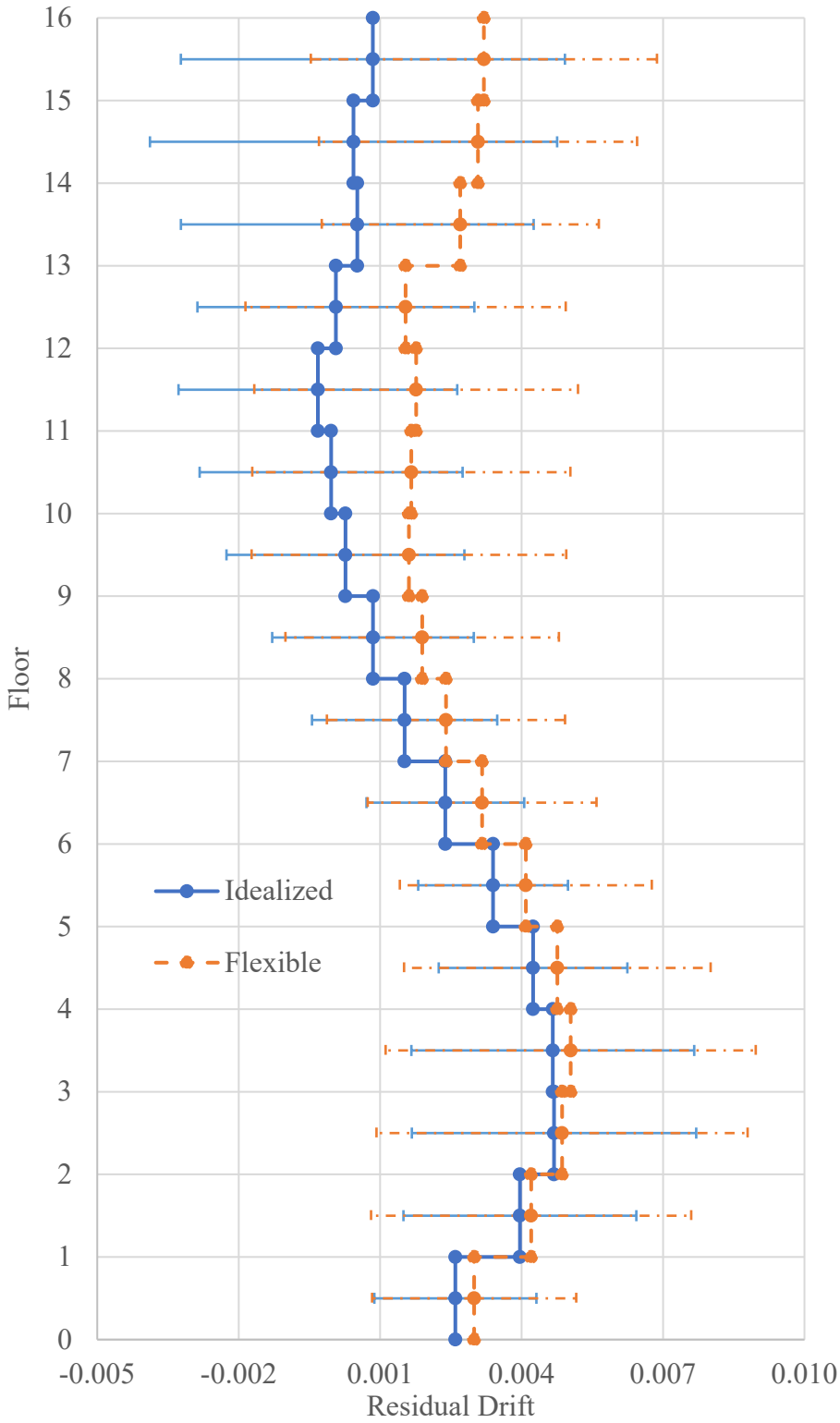

Figure 4.4-12 Average residual drift of the BRBF direction of the 16-story building.

Table 4.4-14 Percentage change in residual drift of the BRBF direction of the 16-story building.

Story	EQ1	EQ2	EQ3	EQ4	EQ5	EQ6	EQ7	EQ8	EQ9	EQ10	EQ11	Average
0-1	-0.4	-1.0	-0.4	-0.4	3.1	0.2	-0.1	0.1	1.5	-0.6	2.4	0.4
1-2	-0.8	-1.8	-0.3	-0.5	4.2	0.1	-1.1	0.1	0.9	-1.0	2.9	0.2
2-3	-0.5	-1.8	-0.4	-0.9	4.2	-0.1	-1.4	0.0	2.1	-2.0	2.7	0.2
3-4	-0.1	-1.1	0.0	-0.6	4.3	-0.3	-0.9	0.0	3.7	-3.0	2.1	0.4
4-5	1.0	-0.3	0.9	-0.3	4.1	0.3	-0.3	0.0	1.9	-3.0	1.3	0.5
5-6	2.2	0.0	1.7	-1.2	3.3	0.5	0.3	0.1	1.8	-2.3	1.3	0.7
6-7	2.6	-0.2	2.4	-1.5	1.9	0.6	0.7	0.2	1.7	-1.1	1.3	0.8
7-8	3.3	0.0	3.3	-1.8	1.4	0.7	0.7	0.4	1.7	-0.6	0.6	0.9
8-9	3.9	-0.1	3.6	-2.3	1.9	1.3	0.8	0.4	2.0	-0.5	0.3	1.0
9-10	4.4	0.0	3.9	-2.5	1.7	2.4	1.9	0.5	1.8	-0.2	0.9	1.3
10-11	4.7	2.1	4.4	-2.8	1.4	3.6	3.3	1.1	0.0	0.1	0.9	1.7
11-12	5.2	6.8	4.4	-2.9	1.4	2.9	4.3	0.9	-0.9	-0.1	1.0	2.1
12-13	4.5	2.2	4.6	-3.5	1.3	1.9	4.0	0.5	-0.8	0.4	1.3	1.5
13-14	4.4	-0.8	4.2	4.0	0.9	0.9	4.1	-0.2	-0.3	4.6	2.3	2.2
14-15	3.6	-0.8	4.7	6.9	0.6	-0.3	4.7	0.3	0.5	5.8	3.1	2.6
15-16	2.7	-0.9	-0.6	10.0	-0.3	-0.3	5.1	1.1	2.0	3.4	3.6	2.4

The change in total acceleration is shown in Figure 4.4-13. The base acceleration increased by 53% and the acceleration at the 1st, 3rd, 6th, and 7th floors increased in the range 2% to 3%. The total acceleration at the other floors decreased in the range of 1% to 5%, as shown in Table 4.3-16. The behavior in this case is similar to the behavior of the 4- and 8-story buildings where the base total base acceleration increased by a significant value and the total acceleration at the elevated floors changed slightly.

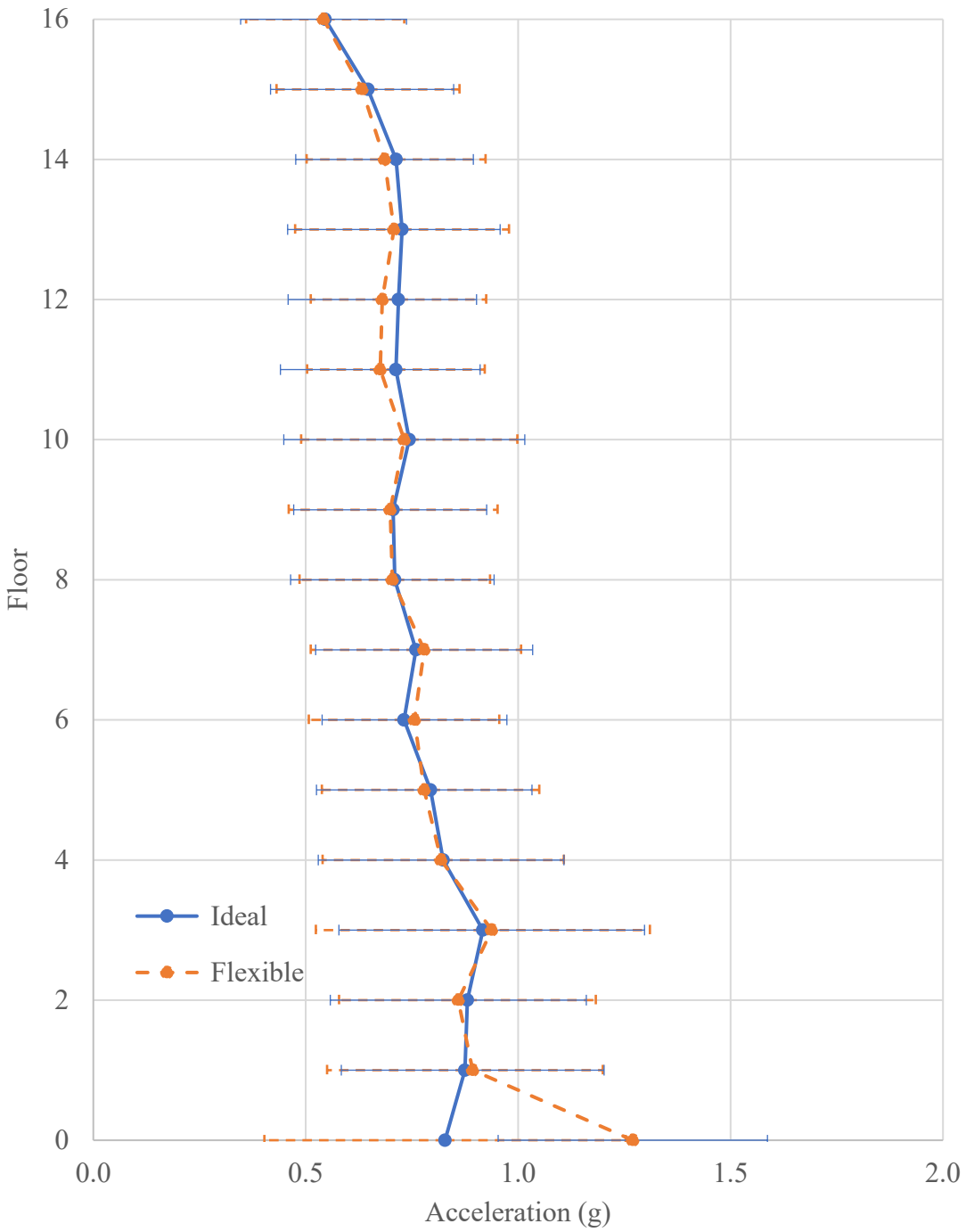

Figure 4.4-13 average maximum total story acceleration for the BRBF of the 16-story building.

Table 4.4-15 Percentage of change in maximum total story acceleration of the BRBF direction of the 16-story building.

Story	EQ1	EQ2	EQ3	EQ4	EQ5	EQ6	EQ7	EQ8	EQ9	EQ10	EQ11	Average
0	72	30	33	28	72	126	114	10	42	33	81	53
1	-13	1	1	-10	4	5	19	1	5	-2	9	2
2	3	0	-4	-11	-18	-4	-2	2	-6	1	4	-2
3	0	0	1	-5	-15	-2	11	7	8	5	-1	2
4	-1	0	-2	-16	11	-6	15	0	-5	11	-6	-1
5	-5	-2	-1	-8	-1	-2	3	-5	2	0	-6	-2
6	19	0	2	-4	-3	4	9	2	-3	4	6	3
7	10	-3	12	1	0	4	-2	0	-1	7	5	3
8	16	-4	-1	8	4	-1	-12	-6	-1	-3	1	-1
9	7	-5	0	-9	1	-17	13	-5	9	-6	-6	-1
10	1	-5	-7	5	6	6	-11	-3	3	7	-3	-2
11	-9	-8	7	-10	20	-17	-2	-4	-12	-3	0	-5
12	8	-18	-14	-5	-5	-11	-9	-1	-4	-1	6	-5
13	1	-4	-2	-5	6	-2	-9	0	4	-12	-5	-3
14	-4	-3	-8	-4	-3	-9	3	-3	0	-5	-9	-4
15	-9	-3	-7	2	4	-4	-8	-12	8	1	5	-2
16	3	-4	3	4	-4	1	-8	4	4	-3	-5	-1

The change in the average maximum base and floor shear is shown in Figure 4.4-14. The shear did not change in the 3rd, 10th, 14th, and 15th stories. The shear increased at the base and at the 9th, 11th,12th, 13th, and 16th in the range of 1% to 3%, while the shear at the other stories decreased in the range of 1% to 4%, as shown in Table 4.4-16. This behavior is similar to the behavior of the 4- and 8-story building where the story shear changed slightly. The allowed reduction in ASCE 7-16 is 10% for the base shear, but the NRHA showed an average increase of 1%.

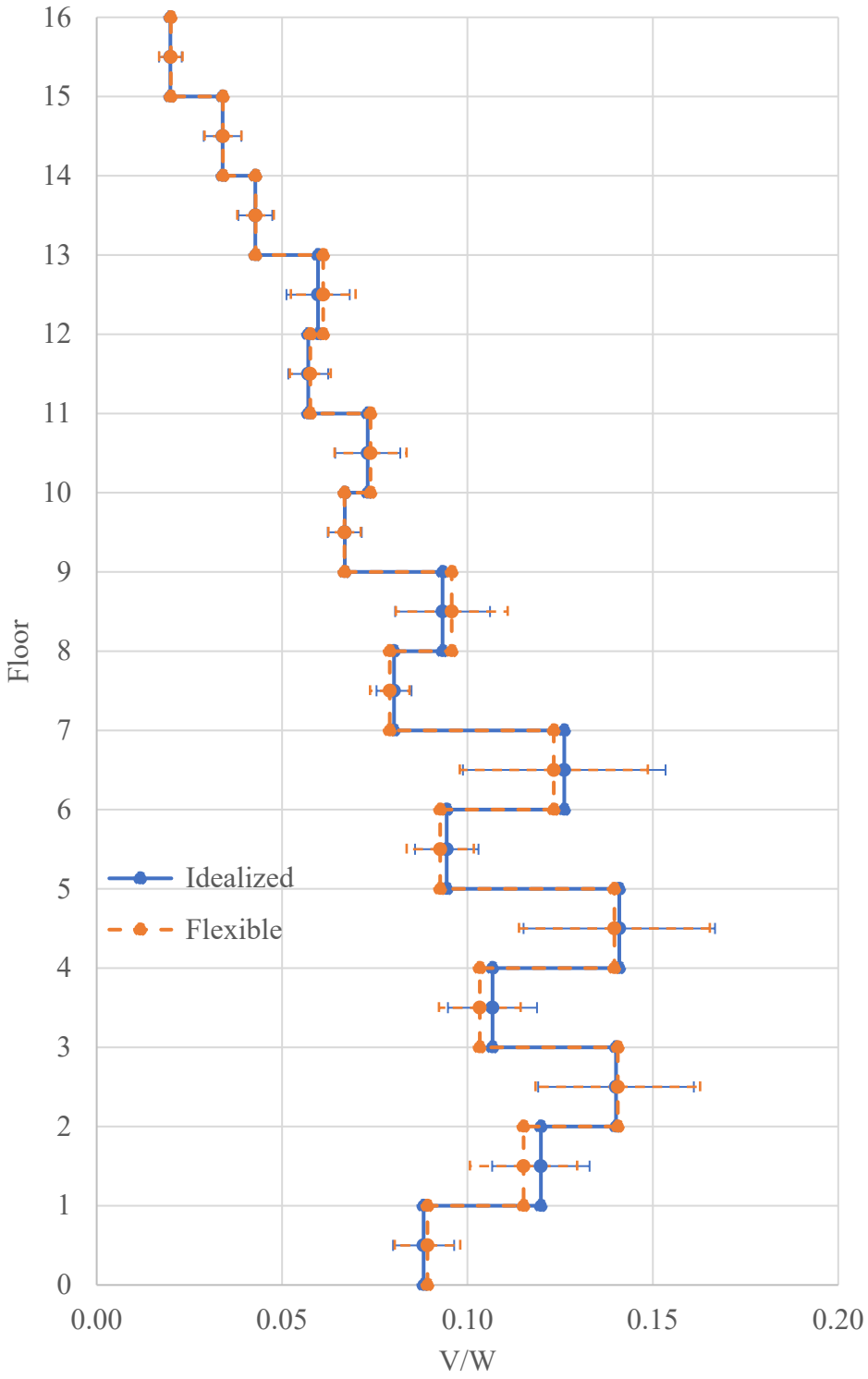

Figure 4.4-14 Average maximum story shear of the BRBF direction of the 16-story building.

Table 4.4-16 Percentage of change in maximum story shear of the BRBF direction of the 16-story building.

Story	EQ1	EQ2	EQ3	EQ4	EQ5	EQ6	EQ7	EQ8	EQ9	EQ10	EQ11	Average
1	7	-1	-5	6	8	3	-1	0	-8	2	1	1
2	-1	3	-4	-7	-1	-3	-5	-9	-5	-8	-7	-4
3	-2	-4	1	6	1	-3	-3	1	9	0	-5	0
4	-6	2	-6	-6	1	-8	-2	-10	-5	-4	6	-3
5	1	1	-3	1	2	-7	-3	0	-5	-2	4	-1
6	-3	-4	2	-4	2	-3	-3	-3	-1	-1	-5	-2
7	-4	0	0	1	2	-4	-4	-4	-8	-1	-1	-2
8	4	-1	-2	-3	1	-3	1	-2	0	-8	-3	-1
9	7	-1	2	2	2	0	3	3	5	1	-1	3
10	4	-1	-2	4	1	-2	-2	-2	0	-1	0	0
11	7	-7	-7	10	3	4	1	1	2	-6	1	1
12	-1	-5	4	-1	1	10	-2	1	-2	0	4	1
13	3	-6	5	-1	1	15	5	6	1	-7	1	2
14	4	-2	1	-3	-1	-1	-4	7	5	-5	-1	0
15	-4	-7	3	4	-3	-2	-4	3	9	0	4	0
16	2	-1	0	4	0	1	1	0	1	-2	0	1

To capture the general trend of the energy dissipation in the BRB elements, certain BRB elements have been selected as shown in Figure 4.4-15. The average energy dissipation calculations showed that the BRB elements dissipate less energy in the flexible foundation case in the range of 0% to 20%, as shown in Table 4.4-17. The reason for this reduction in energy dissipation is that most of the deformation is coming from the displacement of the foundation (piles). The vertical displacement of the piles reduces the demands on the BRB elements. The energy dissipation reduction in this case is higher than the energy dissipation reduction in the 4- and 8-story. The maximum BRB strain decreased in the lower floors (from 1st to 7th) and increased in the upper floors (from 8th to 16th), as shown in Table 4.4-18.

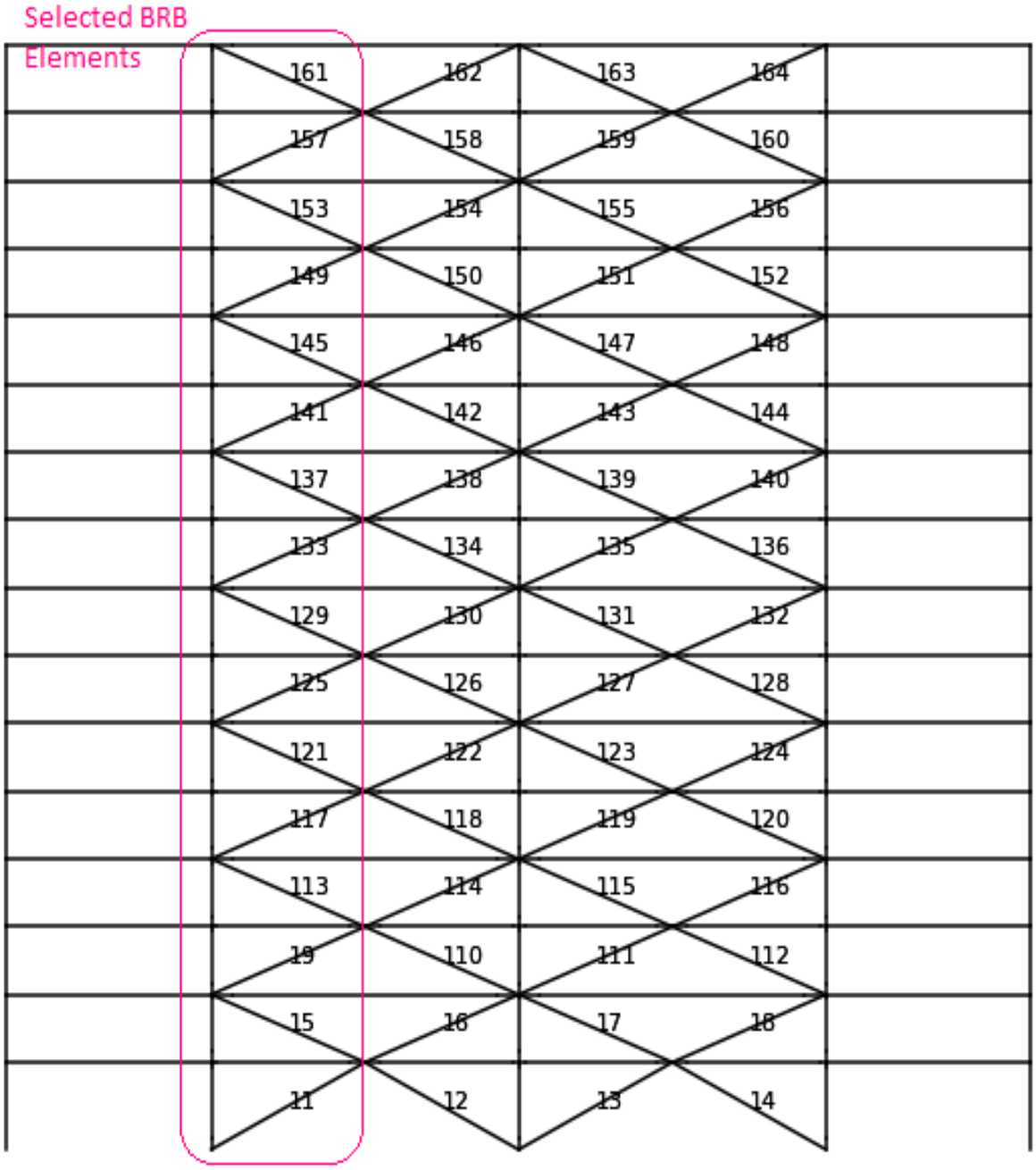

Figure 4.4-15 Selected BRB elements for dissipated energy calculations.

Table 4.4-17 Percentage change in the energy dissipation in the BRB elements of the 16-story building.

BRB	EQ 1	EQ 2	EQ 3	EQ 4	EQ 5	EQ 6	EQ 7	EQ 8	EQ 9	EQ 10	EQ 11	Average
11	-10	-9	-11	-1	-8	-19	-21	-13	-15	-12	-16	-12
15	-8	-6	-10	1	2	-16	-22	-11	-14	-6	-9	-9
19	-17	-17	-16	-6	0	-24	-17	-14	-19	-9	-14	-15
113	-21	-18	-17	-3	4	-22	-26	-15	-20	-8	-12	-15
117	-29	-31	-20	-12	6	-28	-20	-18	-21	-9	-21	-20
121	-32	-29	-23	-8	14	-23	-14	-13	-23	-9	-23	-20
125	-26	-34	-20	8	10	-17	-26	-14	-19	-11	-22	-19
129	-17	-5	-10	17	13	-8	-14	-3	-10	-23	-14	-11
133	-10	-26	-9	4	-11	-24	-15	-17	-11	-38	-7	-14
137	6	-22	-10	18	93	-18	-21	-31	-5	-43	10	-8
141	-7	-20	-1	3	19	-9	-26	-17	-2	-28	11	-8
145	-1	-18	13	-4	153	9	-13	-10	7	-29	17	0
149	-5	-20	9	-19	133	10	-14	-11	5	-26	11	-3
153	1	-12	2	-23	33	5	-9	8	6	-17	6	0
157	1	-7	1	-15	-12	-4	-9	7	0	-8	1	-1
161	0	-2	5	2	-15	-8	4	6	3	1	1	1

Table 4.4-18 Maximum strain at the selected BRB elements.

RBS	Idealized		Flexible		Percentage Change	
	Average	Standard Deviation	Average	Standard Deviation	Average	Standard Deviation
11	0.00759	0.00182	0.00719	0.00186	-6	2
15	0.00974	0.00243	0.00919	0.00253	-6	4
19	0.01107	0.00290	0.01009	0.00269	-10	-8
113	0.01024	0.00306	0.00931	0.00284	-10	-7
117	0.00925	0.00298	0.00846	0.00267	-9	-12
121	0.00718	0.00266	0.00661	0.00228	-9	-17
125	0.00564	0.00226	0.00556	0.00213	-1	-6
129	0.00446	0.00189	0.00469	0.00196	5	3
133	0.00417	0.00139	0.00453	0.00175	8	21
137	0.00393	0.00138	0.00410	0.00163	4	15
141	0.00442	0.00164	0.00479	0.00162	8	-1
145	0.00446	0.00144	0.00502	0.00176	11	18
149	0.00533	0.00146	0.00555	0.00195	4	25
153	0.00651	0.00179	0.00671	0.00211	3	15
157	0.00777	0.00221	0.00811	0.00249	4	11
161	0.00790	0.00255	0.00808	0.00263	2	3

4.5 Summary

In this chapter, the results of the NRHA were presented. Below is a comparison between the three buildings behavior. The idealized foundation case was considered as the reference. So the flexible foundation case increased or decreased relatively to the idealized case.

For the SMF:

- Maximum average total displacement increased in the three buildings. The highest increment is in the 4-story building, and the lowest increment is in the 8-story building.
- Total average residual displacement decreased in the 4- and 8-story buildings and increased in the 16-story building. The highest reduction occurred in the 4-story building.
- Maximum drift (1) increased in the first three floors of the 4-story building and decreased on the fourth floor, (2) increased in the first and second floors of the 8-story building and decreased in the floors from 3 to 8, and (3) did not change in the 16-story building.
- The residual drift decreased in the 4- and 8-story buildings and increased in bottom floors (from the 1st to the 12th) and decreased in the top floors (from the 13th to the 16th) of the 16-story building. The standard deviation decreased in the 4- and 8-story buildings which means variability of the residual displacement for individual earthquake reduced. The standard deviation increased in the 16-story building which means variability of the residual displacement for individual earthquake increased.
- Maximum total acceleration increased at the base of all three buildings; the highest increment occurred at the base of the 8-story building. Total floor acceleration decreased in the 4- and 8-story buildings and increased in the 16-story building.
- Base and story shear decreased in the 4- and 8-story building by 12% and 3% respectively and increased by a very small amount (1%) in the 16-story building.

- The energy dissipation decreased in the RBS of the 4-story building, decreased in some RBS of the 8- and 16-story buildings, and increased in others. The change in the energy dissipation in the RBS in the 16-story building is small, the maximum increase amount is 10%
- The energy dissipation in the column springs decreased in all three buildings. The highest reduction occurred in the 4-story building. That is because the foundation flexibility, which reduces the rotation in the column springs. Thereby this reduces the energy dissipation in the column base.

The foundations of the SMF in the 4- and 8-story building are isolated footings, and the 16-story building is a raft footing. The flexibility of the isolated footing is higher than the flexibility of the raft foundation. That is why the effect of SSI on the 4- and 8-story building is higher than the 16-story building. Also, when the vibration period of the building is very high the effect of the SSI is less because the response spectrum is almost flat at high values of vibration period. So, increasing the vibration period will have little effect in the base shear at that region.

Based on the results, it can be noticed that the response of the SMF in the 4- and 8-story building is enhanced by inclusion of SSI (less base shear, less energy dissipation in the structural elements, and less residual displacement). The effect on the response of the SMF of the 16-story building was less than the effect on the 4- and 8-story building, the base shear increased slightly and there is a slight increase in the residual displacement.

For the BRBF:

- Total maximum average displacement increased in all the three buildings. The highest increase occurred in the 16-story building and the lowest increase occurred in the 8-story building.

- Total average residual displacement increased slightly in the 4- story building, decreased slightly in the 8-story building, and increased in the 16-story building. The displacement in the foundation of the 16-story building (piles footing) is higher than the displacement in the foundation of the 4- and 8-story building (raft foundation).
- Maximum story drift increased in all the three buildings (except the 3rd and 4th floors in the 8- and 16-story building). However, the 4-story building showed the highest increase because the foundation is more flexible in the 4-story building than the 8- and 16-story buildings.
- The residual story drift did not change on the first floor and increased the rest floors of the 4-story building, decreased in the 8-story buildings, increased in the 16-story building. The standard deviation decreased in the 8-story buildings which means variability of the residual displacement for individual earthquake got reduced. The standard deviation increased in the 4- and 16-story buildings which means variability of the residual displacement for individual earthquake got increased.
- Maximum total acceleration increased at the base of all the three buildings but changed slightly at the elevated floors of all the three buildings.
- Base and story shears decreased in the 4- and 8-story buildings by a small amount (1%) and increased in the 16-story building by a small amount (1%).
- The energy dissipation in the BRB elements decreased in all the three buildings. However, the reduction in the energy dissipation in the BRB elements of the 16-story building is the highest because of the higher flexibility of the pile footing compared to the raft foundation; the maximum reduction is 20% in the 16-story building.

The BRB elements yield very fast because of the small area of the BRB core. Leading to a reduction in the stiffness of the structure. Thereby, the BRBF is controlling the seismic response

because when the foundation is stiffer than the structure, the effect of SSI is minimal. In the 16-story building, the foundation of the BRBF is pile footing. Because each group of piles is not connected to the adjacent groups of piles, the difference in the displacement is higher than the raft foundation (in the 4- and 8-story buildings) which in turn reduce the demand on the BRB elements. That is why the BRB on the 16-story building has higher reduction in energy dissipation than the 4- and 8-story buildings. Based on the results, it can be noticed that there is no enhancement in the displacements of the BRBF, but there is enhancement in the energy dissipation in the BRB elements. The enhancement when the foundations is not connected to each other (piles group of the 16-story building) is higher than the enhancement in the raft foundation (4- and 8-story building).

In conclusion, there is increasing and decreasing the seismic response quantities, but the amount of change is not very high to the degree that cause concern. So, it can be concluded that neglecting the soil-structure interaction is acceptable in the BRBF and SMF, especially in raft foundation case. But in the SMF of the 4-story building it is recommended to include the SSI because it leads to reduction in the floor shear.

Chapter 5 Summary, Conclusions, and Future Work

5.1 Summary

This work aims to investigate the effect of soil-structure interaction (soil flexibility) on the seismic response of traditional buildings. For that, a literature review is presented to understand the work that was already done in this discipline. The previous work showed that soil-structure interaction could be beneficial or detrimental to the seismic response or beneficial to a particular quantity and detrimental to another quantity.

For this work, three buildings (4-, 8-, and 16-story) were adopted to investigate the effect of soil-structure interaction on seismic response. Two types of lateral force resisting systems were used, a buckling restrained braced frame (BRBF) and a steel special moment frame (SMF). Three types of foundations were modeled, isolated footing, combined footing, and pile foundation. The foundation was modeled using a Beam-on-Nonlinear-Winkler-Foundation (BNWF) concept. The modeling was conducted in Open System for Earthquake Engineering Simulation (OpenSeesPy).

Nonlinear Response history analysis (NRHA) was conducted in each direction. A suite of earthquake records was selected for each building according to the ASCE 7-16 procedure. Building seismic response was evaluated by plotting the maximum displacement, residual displacement, maximum acceleration, maximum drift, residual drift, and maximum floor shear and compare the flexible foundation case to the idealized foundation case (baseline). The comparison between the idealized and the flexible foundation was presented in chapter 4.

For the SMF, the residual displacement was reduced in the flexible foundation case compared to the idealized foundation case for the 4- and 8-story buildings but increased in the 16-story building. The maximum displacement increased in the 4-, 8-, and 16-story buildings. In general, the base acceleration increased in all the three buildings, but the floor acceleration

decreased in the 4- and 8-story buildings and increased in the 16-story building. The base shear decreased in the 4- and 8-story buildings and increased by a very small amount in the 16-story building. The energy dissipation in the RBS springs increased in some springs and reduced in other springs for the three buildings, while the energy dissipation in the column springs decreased in the three buildings.

For the BRBF, the residual displacements changed slightly between the flexible foundation case and the idealized foundation case in the 4- and 8-story buildings but increased the 16-story building. Most of the displacements in the BRBF of the 16-story building came from the pile rocking. The BRBF foundation of the 4- and 8-story buildings is a raft footing and in the 16-story building is pile foundation. The maximum story displacement increased in the 4- and 16-story buildings and changed slightly in the 8-story building. In general, the change in the floor acceleration was small for all three buildings in the BRBF, the base acceleration increased for all three buildings. The base shear decreased by a small amount in the 4- and 8-story building and increased in the 16-story buildings. The energy dissipation in the BRBF elements decreased in all three buildings, and the highest reduction occurred in the 16-story building because of the pile rocking.

5.2 Conclusions

After processing the results, it was found that the effects of soil-structure interaction on seismic response of the 4-story building was higher than the effect on the 8- and 16-story buildings, and the impact on the SMF is higher than the BRBF, especially on the 4- and 8-story buildings. Overall, the soil-structure interaction enhanced the response of the SMF in the 4-story by reducing the base shear, the residual story displacement and the energy dissipation in the RBS and column base hinges. For the 8-story building, the enhancement was less than the enhancement in the 4-

story building. SSI reduced the base shear, residual displacement, and energy dissipation in the RBS and column base hinges in the SMF direction but by less than the reduction in the 4-story building. The reason for that is that the 8-story building is more flexible. Thereby the structure is controlling the seismic response more than the flexibility of the foundation. For the 16-story building, the enhancement was the least. SSI increased the residual displacement and did not affect the base shear and the energy dissipation in the RBS and the column springs.

In general, the effects of soil-structure interaction in the BRBF were less than the effect on the SMF. There was a very small change in the residual displacement, base share, and energy dissipation in the BRB elements. The reason for that is that the combined footing and the pile foundation were used, adding less flexibility to the system. Also, the BRB elements yield very early in the response, thereby controlling the seismic response of the BRBF. But in the 16-story building the increase in the residual displacement was high because the residual displacement in the pile foundation is high. The effect of SSI on the residual deformation of individual earthquake was significant.

In general, the amount of change is not very high to the degree that cause concern. So, it can be concluded that neglecting the soil-structure interaction is acceptable in the BRBF and SMF, especially in raft foundation case. But in the SMF of the 4-story building it is recommended to include the SSI because it leads to reduction in the floor shear.

5.3 Future Work

The results indicate a beneficial effect of soil-structure on the seismic response of buildings, especially in low-rise buildings. However, this discipline needs more research to fully understand the impact of soil-structure interaction on the seismic response of buildings.

- More research is needed to investigate the effect of soil properties on the seismic response of buildings.
- More research is needed to investigate the effect of variability in soil profile on the seismic response of buildings.
- More research is needed to investigate the effect of different sizes and types of footing on the seismic response of buildings.
- More experimental research is needed to verify the numerical models of soil-structure interaction that are used for determining the seismic response of buildings.
- More research is needed to investigate the effect of soil-structure interaction on soil behavior.
- Additional research needs to be completed related to other types of lateral force-resisting systems (e.g., shear walls).
- Comparing the results of direct analysis approach and substructure approach.
- Comparing the NRHA with codes equations for soil-structure interaction impact inclusion like ASCE 7-16 equations.
- Using pile foundation for the SMF of 16-story building and compare the results with raft foundation results.
- Using pile foundation in the BRBF of the 8-story building and compare the results to the raft foundation results.

References

ASCE. (2017a). *Minimum Design Loads and Associated Criteria for Buildings and Other Structures, ASCE/SEI 7-16*. American Society of Civil Engineers, New York, NY. https://doi.org/doi:10.1061/9780784414248

ASCE. (2017b). *Seismic Evaluation and Retrofit of Existing Buildings, ASCE/SEI 41-17*. American Society of Civil Engineers, New York, NY. https://doi.org/doi:10.1061/9780784414859

Dutta, S. C., Bhattacharya, K., & Roy, R. (2004). Response of low-rise buildings under seismic ground excitation incorporating soil–structure interaction. *Soil Dynamics and Earthquake Engineering*, *24*(12), 893-914. https://doi.org/https://doi.org/10.1016/j.soildyn.2004.07.001

Fatahi, B., Tabatabaiefar, H. R., & Samali, B. (2011). Performance Based Assessment of Dynamic Soil-Structure Interaction Effects on Seismic Response of Building Frames. In *GeoRisk 2011* (pp. 344-351). https://doi.org/doi:10.1061/41183(418)29

FEMA. (2009). *Evaluation of the FEMA P-695 Methodology for Quantification of Building Seismic Performance Factors.* National Institute of Standards and Technology, Gaithersburg, MD. https://doi.org/https://tsapps.nist.gov/publication/get_pdf.cfm?pub_id=915492

FEMA. (2018). *Example Application Guide for ASCE/SEI 41-13 Seismic Evaluation and Retrofit of Existing Buildings*. F. P-2006. https://www.hsdl.org/?view&did=831569

FEMA. (2020). *A Practical Guide to Soil-Structure Interaction* (FEMA P-2091, Issue. https://www.fema.gov/sites/default/files/documents/fema-p-2091-soil-structure-interaction.pdf

Gajan, S., Hutchinson, T., Kutter, B., Raychowdhury, P., Ugalde, J., & Stewart, J. (2008). Numerical Models for Analysis and Performance- Based Design of Shallow Foundations Subjected to Seismic Loading. *Pacific Earthquake Engineering Research Center, University of California, Berkeley, Report No. 2007/04*.

Gupta, A., & Krawinkler, H. (1998). *Seismic demands for the performance evaluation of steel moment resisting frame structures* Stanford University].

Harden, C., Hutchinson, T., Martin, G. R., & Kutter, B. L. (2005). *Numerical Modeling of the Nonlinear Cyclic Response of Shallow Foundations*. https://peer.berkeley.edu/sites/default/files/peer_504_c._harden_t._hutchinson_g._martin_b._kutter.pdf

Harris, J. L., & Speicher, M. S. (2015). *Special Moment Frames* (Assessment of First Generation Performance-Based Seismic Design Methods for New Steel Buildings, Issue.

Hokmabadi, A. S., Fatahi, B., & Samali, B. (2015). Physical Modeling of Seismic Soil-Pile-Structure Interaction for Buildings on Soft Soils. *International Journal of Geomechanics*, *15*(2), 04014046. https://doi.org/doi:10.1061/(ASCE)GM.1943-5622.0000396

Ibarra, L. F., & Krawinkler, H. (2005). *Global Collapse of Frame Structures under Seismic Excitations. John A. Blume Earthquake Engineering Center Technical Report 152. Stanford Digital Repository*. http://purl.stanford.edu/dj885ym2486

Ismail, S., Kaddah, F., & Raphael, W. (2020). Seismic soil structure interaction response of midrise concrete structures on silty sandy soil. *Jordan Journal of Civil Engineering*, *14*(1), 117-135. <Go to ISI>://WOS:000520509100010

Jennings, P. C., & Bielak, J. (1973). Dynamics of building-soil interaction. *Bulletin of the seismological society of America*, *63*(1), 9-48.

Lignos, D. (2008). *SIDESWAY COLLAPSE OF DETERIORATING STRUCTURAL SYSTEMS UNDER SEISMIC EXCITATIONS* STANFORD UNIVERSITY]. STANFORD UNIVERSITY. https://datacenterhub.org/resources/948/download/DLignos-PhD-Dissertation-DS-09-19-2008.pdf

Lu, Y., Hajirasouliha, I., & Marshall, A. M. (2016). Performance-based seismic design of flexible-base multi-storey buildings considering soil–structure interaction. *Engineering Structures*, *108*, 90-103.

Merritt, S., Uang, C.-M., & Benzoni, G. (2003). Subassemblage testing of Star Seismic buckling-restrained braces. *Test report, University of California, San Diego*.

Mylonakis, G., & Gazetas, G. (2000). SEISMIC SOIL-STRUCTURE INTERACTION: BENEFICIAL OR DETRIMENTAL? *Journal of Earthquake Engineering*, *4*(3), 277-301. https://doi.org/10.1080/13632460009350372

Newell, J., Uang, C.-M., & Benzoni, G. (2006). *Subassemblage testing of CoreBrace buckling-restrained braces (G Series). . Report No. TR-06/01, University of California, San Diego, 2006.*

NIST. (2012). *Soil-Structure Interaction for Building Structures.* https://tsapps.nist.gov/publication/get_pdf.cfm?pub_id=915495

Novak, M., & Hifnawy, L. E. (1983). Effect of soil-structure interaction on damping of structures. *Earthquake Engineering & Structural Dynamics*, *11*(5), 595-621. https://doi.org/https://doi.org/10.1002/eqe.4290110503

Popov, E. P., Blondet, M., & Stepanov, L. (1997). *Cyclic Testing of Four Full-Scale Steel Beam-Volumn Connections with "DOGBONES"*.

Raychowdhury, P. (2011). Seismic response of low-rise steel moment-resisting frame (SMRF) buildings incorporating nonlinear soil–structure interaction (SSI). *Engineering Structures*, *33*(3), 958-967. https://doi.org/https://doi.org/10.1016/j.engstruct.2010.12.017

Rocscience. (2018a). *Axially Loaded Piles Theory Manual*. https://www.rocscience.com/help/rspile/pdf_files/theory/RSPile_-_Axially_Loaded_Piles_Theory.pdf

Rocscience. (2018b). *Laterally Loaded Piles Theory Manual*. https://www.rocscience.com/help/rspile/pdf_files/theory/RSPile_-_Laterally_Loaded_Pile_Theory.pdf

Speicher, M. S., & Harris, J. L. (2018). Collapse Prevention seismic performance assessment of new buckling-restrained braced frames using ASCE 41. *Engineering Structures*, *164*, 274-289. https://doi.org/https://doi.org/10.1016/j.engstruct.2018.01.067

Speicher, M. S., & Harris, J. L. (2019). *Assessment of First Generation PerformanceBased Seismic Design Methods for New Steel Buildings, volume 4: Buckling-Restrained Braced Frames*. http://dx.doi.org/10.6028/NIST.TN.1863-4

Speicher, M. S., & Harris, J. L. (2020). Assessment of First Generation Performance-Based Seismic Design Methods for New Steel Buildings, Volume 4: Buckling-Restrained Braced Frames. *NIST Technical Note*, 4. https://doi.org/10.6028/NIST.TN.1863-4

Tabatabaiefar, S. H. R., Fatahi, B., & Samali, B. (2013). Seismic Behavior of Building Frames Considering Dynamic Soil-Structure Interaction. *International Journal of Geomechanics*, *13*(4), 409-420. https://doi.org/doi:10.1061/(ASCE)GM.1943-5622.0000231

Upadhyay, A., Pantelides, C. P., & Ibarra, L. (2019). Residual drift mitigation for bridges retrofitted with buckling restrained braces or self centering energy dissipation devices. *Engineering Structures*, *199*, 109663. https://doi.org/https://doi.org/10.1016/j.engstruct.2019.109663

Vivek, B., & Raychowdhury, P. (2020). Soil–Structure Interaction Study on 3D SMRFs of Indo-Gangetic Plain Using Resonant Vibration Tests. *Journal of Earthquake Engineering*, 1-23. https://doi.org/10.1080/13632469.2020.1822226

Appendix A: Isolated footing modeling routine

```
# -*- coding: utf-8 -*-
"""
Created on Fri Jun 19 14:23:21 2020

@author: Humam Al-Ghabawi
"""
import openseespy.opensees as ops
import openseespy.postprocessing.ops_vis as opsv
import matplotlib.pyplot as plt
from openseespy.postprocessing.Get_Rendering import *
from openseespy.opensees import *
import numpy as np
from IPython.core.pylabtools import figsize
wipe()
from units_Version2 import *
from math import *
model('Basic', '-ndm', 3, '-ndf', 6)
figsize(7,7);
inch=1
kip=1
sec=1
ft=12*inch
lbf=kip/1000
ksi=kip/(inch**2)
psi=lbf/(inch**2)
pcf=lbf/(ft**3)
psf=lbf/(ft**2)
in2=inch**2
in4=inch**4
cm=inch/2.54
PI=3.14
g=32.2*ft/(sec**2)
def NodeTag(Node):
    All_Nodes=getNodeTags()
    if Node not in All_Nodes:
        Inode=Node
    else:
        for i in range (10000000):
            Node+=1
            if Node not in All_Nodes:
                Inode=Node
                break
    return Inode

def EleTag(Element):
    All_Ele=getEleTags()
    if Element not in All_Ele:
        Ele=Element
    else:
        for i in range (10000000):
            Element+=1
            if Element not in All_Ele:
                Ele=Element
                break
    return Ele
'''
uniaxialMaterial('PySimple1', matTag, soilType, pult_Py, Y50_Py, Cd_Py, c=0.0)
Ndivision either 4, 6, 8,......

Kf -- Sliding Stiffness due to friction, in units of Force/unit length
Qf -- Sliding Capacity due to friction, in units of Force per unit Area (F/B**2)
Qf=Wg tan(phi) + Ab*C

qult--- ultimate bearing capacity of the footing (meyerhof bearing capacity), in units
of Force per unit Area (F/B**2),
kz--- stiffness of the bearing capacity, in units of Force/unit length

```

```
Pult_Py-- passive earth pressuer of the side soil, in units of Force per unit Length (F/B)
Kel_py-- stiffness of the passive earth pressuer of the side soil, in units of Force/unit

AreaSteel-- Area of flextural reinforcement per unit length, in**2/in
'''
def square_isolated(footTag, B, Ndivision,qult,kz,soiltype,Qf,Kf,Pult_Py, Kel_py,Connection_type,Main_node,stiff,soft,ConcreteTag,SteelTag,AreaSteel,Hf):
    kz=kz/B/B; Kf=Kf/B/B; Kel_py=Kel_py/B
    Xcoord=nodeCoord(Main_node)[0]; Ycoord=nodeCoord(Main_node)[1];
    Zcoord=nodeCoord(Main_node)[2]

################################################################################
#####----------------- Adding Nodes to the Footing -----------------------#####
################################################################################
    N_nodes=(Ndivision+1)**2     # number of nodes
    element_length=B/Ndivision
    Dg=7 # increasing in node digit
    nodeTag=footTag*10**Dg+1
    MainNode=footTag*10**Dg+Ndivision/2*(Ndivision+2)+1
    node_1=nodeTag
    all_nodes=[]
    nodeTagS=footTag*10**Dg+1+10**(Dg-1) # second layer of nodes
    node_1_S=nodeTagS  # second layer of nodes
    all_nodes_S=[]     # second layer of nodes
    for Y in range (Ndivision+1):
        Ycoord1=Ycoord-0.5*B+Y*element_length
        for X in range (Ndivision+1):
            Xcoord1=Xcoord-0.5*B+X*B/Ndivision
            coord=(Xcoord1, Ycoord1, Zcoord)
            coordS=(Xcoord1, Ycoord1, Zcoord)
            #print('nodeTag=',nodeTag)
            node(nodeTag, *coord)
            node(nodeTagS, *coordS)    # second layer
            all_nodes+=[nodeTag]
            all_nodes_S+=[nodeTagS]   # second layer
            if Xcoord1==Xcoord and Ycoord1==Ycoord:
                store_this_node1=nodeTag   # store the nodes that has the same position as footTag
            #print("ok",nodeTag,Xcoord1, Ycoord, Zcoord1)
            nodeTag+=1
            nodeTagS+=1
################################################################################
#####----------------------- Add Springs ------------------------------#####
################################################################################
    if soiltype=='clay': # qzType = 1 Backbone of q-z curve approximates Reese and O'Neill's (1987) relation for drilled shafts in clay.
        qzType=1
        kfar=0.525
        Ce=0.708 # for T-Z
        Ce_Py=8  # for P-Y
    elif soiltype=='sand': # qzType = 2 Backbone of q-z curve approximates Vijayvergiya's (1977) relation for piles in sand.
        qzType=2
        kfar=1.39
        Ce=2.05 # for T-Z
        Ce_Py=0.542 # for P-Y
#############################################################
#####-------- Add QZ and TZ springs at the cornor nodes--###
#############################################################
    # find Qult for the nodes @ cornors, and (ki=kz*tributary area)
    Qult_corner=qult*(element_length/2)**2 # force at the cornor springs
    # print('Qult_corner=',Qult_corner)
    ki=kz*(element_length/2)**2  # add the material
    Z50=kfar*Qult_corner/ki      # add the material
    matTagQZ=footTag+1000                  # add the material
    uniaxialMaterial('QzSimple1', matTagQZ, qzType, Qult_corner, Z50,0.1,0)  # add the
```

```
        material
128     nodes_e_s=Ndivision+1
129     # print('nodes_e_s=',nodes_e_s)
130     #
        corner_nodes=[node_1,footTag*10**7+(nodes_e_s),footTag*10**7+(nodes_e_s**2-Ndivision)
        ,footTag*10**7+(nodes_e_s**2)]
131     # #print('corner_nodes=',corner_nodes)
132     Qsliding=(Qf)*(element_length/2)**2   # adding T-Z springs
133     Ksliding=(Kf)*(element_length/2)**2   # adding T-Z springs
134     Z50_sliding=Ce*Qsliding/Ksliding           # adding T-Z springs
135     matTagTZ=footTag+2000                 # add the material
136     uniaxialMaterial('TzSimple1', matTagTZ, qzType, Qsliding,Z50_sliding)
137
        corner_nodes=[node_1,footTag*10**Dg+(nodes_e_s),footTag*10**Dg+(nodes_e_s**2-Ndivisio
        n),footTag*10**Dg+(nodes_e_s**2)]
138     #print('corner_nodes=',corner_nodes)
139     incre=footTag*10**Dg+1+10**(Dg-1)-1
140     # print('incre=',incre)
141     # second layer
142
        corner_nodes_S=[node_1_S,incre+(nodes_e_s),incre+(nodes_e_s**2-Ndivision),incre+(node
        s_e_s**2)]
143     # print('corner_nodes_S=',corner_nodes_S)
144     # add zero length element @ the corner nodes
145     eleTag=node_1+5*10**5
146     for i in range(4):
147         node_i=corner_nodes_S[i]
148         node_j=corner_nodes[i]
149
            element('zeroLength',eleTag,node_i,node_j,'-mat',matTagTZ,matTagTZ,matTagQZ,'-dir
            ',1,2,3)
150         # print('QZ_Corner=',eleTag)
151         eleTag+=1
152     eleTagPY=node_1+6*10**5
153 ############################################################
154 #####----------- Add QZ and TZ springs at the side nodes--###
155 ############################################################
156     node_sides=[]
157     start=corner_nodes[0]+1
158     end=corner_nodes[1]
159     for i in range (start,end):
160         node_sides+=[i]
161     start=corner_nodes[0]+nodes_e_s
162     end=corner_nodes[2]-nodes_e_s+1
163     for i in range (start,end,nodes_e_s):
164         node_sides+=[i]
165     start=corner_nodes[1]+nodes_e_s
166     end=corner_nodes[3]-nodes_e_s+1
167     for i in range (start,end,nodes_e_s):
168         node_sides+=[i]
169     start=corner_nodes[2]+1
170     end=corner_nodes[3]
171     for i in range (start,end):
172         node_sides+=[i]
173     #print('node_sides=',node_sides)
174     # find Qult for the nodes @ sides------ second layer
175     Qult_side=qult*(element_length*element_length/2)
176     # print('Qult_side=',Qult_side)
177     ki=kz*(element_length*element_length/2)  # add the material
178     Z50=kfar*Qult_side/ki      # add the material
179     matTagQZ+=100                 # add the material
180     uniaxialMaterial('QzSimple1', matTagQZ, qzType, Qult_side, Z50,0.1,0)  # add the
        material
181     Qsliding=(Qf)*(element_length*element_length/2)   # adding T-Z springs
182     Ksliding=(Kf)*(element_length*element_length/2)   # adding T-Z springs
183     Z50_sliding=Ce*Qsliding/Ksliding           # adding T-Z springs
184     matTagTZ+=100                 # add the material
```

```
185       uniaxialMaterial('TzSimple1', matTagTZ, qzType, Qsliding,Z50_sliding)
186       node_sides_S=[]  # second layer
187       start=corner_nodes_S[0]+1
188       end=corner_nodes_S[1]
189       for i in range (start,end):
190           node_sides_S+=[i]
191       start=corner_nodes_S[0]+nodes_e_s
192       end=corner_nodes_S[2]-nodes_e_s+1
193       for i in range (start,end,nodes_e_s):
194           node_sides_S+=[i]
195       start=corner_nodes_S[1]+nodes_e_s
196       end=corner_nodes_S[3]-nodes_e_s+1
197       for i in range (start,end,nodes_e_s):
198           node_sides_S+=[i]
199       start=corner_nodes_S[2]+1
200       end=corner_nodes_S[3]
201       for i in range (start,end):
202           node_sides_S+=[i]
203       #print('node_sides=',node_sides)
204       # add zero length element @ the sides nodes
205       for i in range(len(node_sides)):
206           node_i=node_sides_S[i]
207           node_j=node_sides[i]
208
              element('zeroLength',eleTag,node_i,node_j,'-mat',matTagTZ,matTagTZ,matTagQZ,'-dir
              ',1,2,3)
209           # print('QZ_Side=',eleTag)
210           eleTag+=1
211   ############################################################
212   #####----------- Add QZ and TZ springs at the internal nodes--###
213   ############################################################
214       # find Qult for the nodes @ middle
215       Qult_middle=qult*(element_length)**2
216       # print('Qult_middle=',Qult_middle)
217       ki=kz*(element_length)**2  # add the material
218       Z50=kfar*Qult_corner/ki      # add the material
219       matTagQZ+=100                 # add the material
220       uniaxialMaterial('QzSimple1', matTagQZ, qzType, Qult_middle, Z50,0.1,0)  # add the
          material
221       Qsliding=(Qf)*(element_length*element_length)    # adding T-Z springs
222       Ksliding=(Kf)*(element_length*element_length)    # adding T-Z springs
223       Z50_sliding=Ce*Qsliding/Ksliding           # adding T-Z springs
224       matTagTZ+=100                  # add the material
225       uniaxialMaterial('TzSimple1', matTagTZ, qzType, Qsliding,Z50_sliding)
226       Node_list=list(set(all_nodes)-set(node_sides)-set(corner_nodes))
227       Node_list=sorted(Node_list)
228       # print('Node_list=',Node_list)
229       # find Qult for the nodes @ middle----- second layer
230       Node_list_S=list(set(all_nodes_S)-set(node_sides_S)-set(corner_nodes_S))
231       Node_list_S=sorted(Node_list_S)
232       # print('Node_list_S=',Node_list_S)
233       # add zero length element @ the middle nodes
234       for i in range(len(Node_list)):
235           node_i=Node_list_S[i]
236           node_j=Node_list[i]
237
              element('zeroLength',eleTag,node_i,node_j,'-mat',matTagTZ,matTagTZ,matTagQZ,'-dir
              ',1,2,3)
238           # print('QZ_Internal=',eleTag)
239           eleTag+=1
240       # fix the second layer nodes
241       for i in (all_nodes_S):
242           fix(i,1,1,1,1,1,1)
243   ############################################################
244   #####----------- Add PY springs at the side nodes--###
245   ############################################################
246       pult_Py=(Pult_Py)*(element_length)    # adding P-Y springs
```

```
    Kel_PY=(Kel_py)*(element_length)   # adding P-Y springs
    Y50_Py=Ce_Py*pult_Py/Kel_PY           # adding P-Y springs
    matTagPY=footTag*100+3000                # add the material
    Cd_Py=1
    uniaxialMaterial('PySimple1',matTagPY,qzType, pult_Py, Y50_Py, Cd_Py)
    for i in range(1,Ndivision):
        node_i=node_1_S+i
        node_j=node_1+i
#       print('node_i=',node_i,'node_j=',node_j)
        element('zeroLength',eleTagPY,node_i,node_j,'-mat',matTagPY,'-dir',2) # at the
        sides
        # print('pult_Py2=',pult_Py)
        eleTagPY+=1
    pult_Py=(Pult_Py)*(element_length/2)   # adding P-Y springs
    Kel_PY=(Kel_py)*(element_length/2)   # adding P-Y springs
    Y50_Py=Ce_Py*pult_Py/Kel_PY           # adding P-Y springs
    matTagPY+=1                # add the material
    Cd_Py=1
    uniaxialMaterial('PySimple1',matTagPY,qzType, pult_Py, Y50_Py, Cd_Py)
    for i in (0,Ndivision):
        node_i=node_1_S+i
        node_j=node_1+i
#           print('node_i=',node_i,'node_j=',node_j)
        element('zeroLength',eleTagPY,node_i,node_j,'-mat',matTagPY,'-dir',2) # at the
        corners
        # print('pult_Py2=',pult_Py)
        eleTagPY+=1
    pult_Py=(Pult_Py)*(element_length)   # adding P-Y springs
    Kel_PY=(Kel_py)*(element_length)   # adding P-Y springs
    Y50_Py=Ce_Py*pult_Py/Kel_PY           # adding P-Y springs
    matTagPY+=1                # add the material
    Cd_Py=1
    uniaxialMaterial('PySimple1',matTagPY,qzType, pult_Py, Y50_Py, Cd_Py)
    for i in range(1,Ndivision):
        node_i=node_1_S+Ndivision*i+i
        node_j=node_1+Ndivision*i+i
#           print('node_i=',node_i,'node_j=',node_j)
        element('zeroLength',eleTagPY,node_i,node_j,'-mat',matTagPY,'-dir',1) # at the
        sides
        # print('pult_Py1=',pult_Py)
        eleTagPY+=1
    pult_Py=(Pult_Py)*(element_length/2)   # adding P-Y springs
    Kel_PY=(Kel_py)*(element_length/2)   # adding P-Y springs
    Y50_Py=Ce_Py*pult_Py/Kel_PY           # adding P-Y springs
    matTagPY+=1                # add the material
    Cd_Py=1
    uniaxialMaterial('PySimple1',matTagPY,qzType, pult_Py, Y50_Py, Cd_Py)
    for i in (0,Ndivision):
        node_i=node_1_S+Ndivision*i+i
        node_j=node_1+Ndivision*i+i
#       print('node_i=',node_i,'node_j=',node_j)
        element('zeroLength',eleTagPY,node_i,node_j,'-mat',matTagPY,'-dir',1) # at the
        corners
        # print('pult_Py1=',pult_Py)
        eleTagPY+=1
##############################################################################
#######----------------- Add Rigid Beams between nides ------------------######
##############################################################################
    FootingType='stiff'
    if FootingType=='Flexible':
        # Define cross-section for nonlinear columns
        # ------------------------------------
        #  some parameters
        colWidth = element_length
        colDepth = Hf
        cover = 3
        As = AreaSteel*element_length/3
```

```
310             # some variables derived from the parameters
311             y1 = colWidth / 2.0
312             z1 = colDepth / 2.0
313             J=element_length*Hf*(element_length**2+Hf**2)/12
314             G=3795/2/1.2*ksi
315             GJ=G*J
316             secTag=footTag
317             section('Fiber', secTag, '-GJ', GJ)
318             # Create the concrete core fibers
319             patch('rect', ConcreteTag, 10, 10, -y1, cover-z1, y1, z1)
320             # Create the concrete cover fibers (top, bottom, left, right)
321             patch('rect', ConcreteTag, 10, 1, -y1, -z1 , y1, z1-cover)
322             # Create the reinforcing fibers (left, middle, right)
323             layer('straight', SteelTag, 3, As, y1, -z1+cover, -y1, cover-z1)
324             layer('straight', SteelTag, 3, As, y1, z1-cover, -y1, z1-cover)
325             integrationTag=footTag
326             beamIntegration('Legendre', integrationTag, secTag, 5)
327         elif FootingType=='stiff':
328             E_mod=3734; G_mod=11500; Jxx=10
329             Area=element_length*40
330             Iy=(element_length*40**3)/12
331             Iz=Iy
332         # add elastic beam column in the first direction
333         transfTag=200+footTag
334         vecxz=(0,0,1)
335         geomTransf('PDelta', transfTag, *vecxz)
336         eleTag=node_1+2*10**6
337         i_node=node_1-1
338         j_node=i_node+1-1
339         for i in range (Ndivision+1):
340             i_node=i_node+1
341             j_node=i_node+1
342             for j in range (Ndivision):
343                 eleNodes=(i_node,j_node)
344                 eleTag=EleTag(eleTag)
345                 if FootingType=='Flexible':
346                     # numIntgrPts=5;
347                     # element('nonlinearBeamColumn', eleTag, *eleNodes, numIntgrPts,
                        secTag, transfTag)
348                     # element('dispBeamColumn', eleTag, *eleNodes, transfTag, integrationTag)
349                     element('forceBeamColumn', eleTag, *eleNodes, transfTag, integrationTag)
350                 elif FootingType=='stiff':
351                     element('elasticBeamColumn', eleTag, *eleNodes, Area, E_mod, G_mod,
                        Jxx, Iy, Iz, transfTag)
352                 eleTag+=1
353                 #print('i_node,j_node=',i_node,j_node)
354                 i_node=i_node+1
355                 j_node=i_node+1
356         # add elastic beam column in the second direction
357         transfTag=300+footTag
358         vecxz=(0,0,1)
359         geomTransf('Linear', transfTag, *vecxz)
360         eleTag=node_1+3*10**6
361         for i in range (Ndivision+1):
362             i_node=node_1+i*1
363             j_node=i_node+Ndivision+1
364             for j in range (Ndivision):
365                 eleNodes=(i_node,j_node)
366                 if FootingType=='Flexible':
367                     # numIntgrPts=5;
368                     # element('nonlinearBeamColumn', eleTag, *eleNodes, numIntgrPts,
                        secTag, transfTag)
369                     # element('dispBeamColumn', eleTag, *eleNodes, transfTag, integrationTag)
370                     element('forceBeamColumn', eleTag, *eleNodes, transfTag, integrationTag)
371                 elif FootingType=='stiff':
372                     element('elasticBeamColumn', eleTag, *eleNodes, Area, E_mod, G_mod,
                        Jxx, Iy, Iz, transfTag)
```

```
            eleTag+=1
            #print('Second=',i_node,j_node)
            i_node=i_node+Ndivision+1
            j_node=i_node+Ndivision+1
    if Connection_type=='pined':
        eleTag=5550
        for i in range (1,100):
            All_Elements=getEleTags()
            if eleTag in All_Elements:
                eleTag+=1
            if eleTag not in All_Elements:
                break
        element('zeroLength', eleTag, MainNode, Main_node, '-mat',
        stiff,stiff,stiff,soft,soft,stiff , '-dir', 1,2,3,4,5,6)
    elif Connection_type=='fixedX':
        eleTag=5550
        for i in range (1,100):
            All_Elements=getEleTags()
            if eleTag in All_Elements:
                eleTag+=1
            if eleTag not in All_Elements:
                break
        element('zeroLength', eleTag, MainNode, Main_node, '-mat',
        stiff,stiff,stiff,stiff,soft,stiff , '-dir', 1,2,3,4,5,6)
    elif Connection_type=='fixedY':
        eleTag=5550
        for i in range (1,100):
            All_Elements=getEleTags()
            if eleTag in All_Elements:
                eleTag+=1
            if eleTag not in All_Elements:
                break
        element('zeroLength', eleTag, MainNode, Main_node, '-mat',
        stiff,stiff,stiff,soft,stiff,stiff , '-dir', 1,2,3,4,5,6)
    elif Connection_type=='fixed':
        eleTag=5550
        for i in range (1,100):
            All_Elements=getEleTags()
            if eleTag in All_Elements:
                eleTag+=1
            if eleTag not in All_Elements:
                break
        element('zeroLength', eleTag, MainNode, Main_node, '-mat',
        stiff,stiff,stiff,stiff,stiff,stiff , '-dir', 1,2,3,4,5,6)
##############################################################################
#######------- Add Rigid Diaphram to the Footing ------------------##########
##############################################################################
    Main_nodeList=[MainNode]
    SlaveNodes=list(set(all_nodes)-set(Main_nodeList))
    perpDirn=3
    rigidDiaphragm(perpDirn, Main_node, *SlaveNodes)
```

Appendix B: Raft footing modeling routine

```
# -*- coding: utf-8 -*-
"""
Created on Fri Jun 19 14:23:21 2020

@author: Humam Al-Ghabawi
"""
import openseespy.opensees as ops
import openseespy.postprocessing.ops_vis as opsv
import matplotlib.pyplot as plt
from openseespy.postprocessing.Get_Rendering import *
import openseespy.postprocessing.Get_Rendering as opsplt
from openseespy.opensees import *
import numpy as np
from IPython.core.pylabtools import figsize
from units_Version2 import *
from math import *
model('Basic', '-ndm', 3, '-ndf', 6)
wipe()
'''
this code is an update for
https://opensees.berkeley.edu/wiki/images/f/fc/ShallowDocumentation.pdf

uniaxialMaterial('PySimple1', matTag, soilType, pult_Py, Y50_Py, Cd_Py, c=0.0)
Ndivision either 4, 6, 8,......

Kf -- Sliding Stiffness due to friction, in units of Force per unit Area (Kf)
Qf -- Sliding Capacity due to friction, in units of Force per unit Length (F/B)
Qf=Wg tan(phi) + Ab*C

qult--- ultimate bearing capacity of the footing, in units of Force per unit Area
(F/B**2)
kz--- stiffness of the bearing capacity, in units of Force per unit Length (F/B)

Pult_Py-- passive earth pressuer of the side soil, in units of Force per unit Length
(F/B)
Kel_py-- stiffness of the passive earth pressuer of the side soil, in units of Force
per unit Length (F/B)
'''
def Combined_Footing_BRB(footTag,B,L,Ndivision,qult,kz,soiltype,Qf,Kf_L,Kf_B ,Pult_Py,
Kel_py_L,Kel_py_B,Main_node1,Main_node2,Main_node3,Main_node4,Main_node5,Main_node6,stiff
,soft,Hf):#,ConcreteTag,SteelTag,AreaSteel,Hf):

################################################################################
#####---------------- Adding Nodes to the Footing ----------------------#####
################################################################################
    Footing_Nodes=[]
    Elements_Befor_Springs=getEleTags()

    X1=nodeCoord(Main_node1)[0];Y1=nodeCoord(Main_node1)[1];Z1=nodeCoord(Main_node1)[2]
    X2=nodeCoord(Main_node2)[0];Y2=nodeCoord(Main_node2)[1];Z2=nodeCoord(Main_node2)[2]
    X3=nodeCoord(Main_node3)[0];Y3=nodeCoord(Main_node3)[1];Z3=nodeCoord(Main_node3)[2]
    X4=nodeCoord(Main_node4)[0];Y4=nodeCoord(Main_node4)[1];Z4=nodeCoord(Main_node4)[2]
    X5=nodeCoord(Main_node5)[0];Y4=nodeCoord(Main_node5)[1];Z4=nodeCoord(Main_node5)[2]
    X6=nodeCoord(Main_node6)[0];Y4=nodeCoord(Main_node6)[1];Z4=nodeCoord(Main_node6)[2]
    Z2=Z1
    '''
    Determine the direction X or Y
    '''
    if X1==X2 and X1==X3 and X1==X4:
        direction='Y'
        # L=2*B+abs(Y4-Y1)
    elif Y1==Y2 and Y1==Y3 and Y1==Y4:
        direction='X'
        # L=2*B+abs(X4-X1)
    print('L=',L)
    print('Side friction',footTag,'=',Qf*B*L)#+Pult_Py*B)
    print('Vertical Load',footTag,'=',qult*B*L)
```

```
    '''
    Add the cornor nodes
    '''
    dlist=[]
    node1=footTag*1000000+1
##############################################
    if direction=='Y':
        node1X=nodeCoord(Main_node1)[0]-B/2
        node1Y=nodeCoord(Main_node1)[1]# the edge dimention
        Node=node1
        for i in range(Ndivision+1):
            d1=B/2
            dx=d1/Ndivision
            x=nodeCoord(Main_node1)[0]-(B/2)+(i*dx)
            Y1=node1Y
            dlist+=[dx]
            D=nodeCoord(Main_node2)[1]-nodeCoord(Main_node1)[1] # distance between
            columns
            d=D/(2*Ndivision)
            dlist+=[d]
            for j in range(2*Ndivision):
                node(Node,x, Y1,Z1)
                Footing_Nodes+=[Node]
                Node_Second=int('20'+str(Node))
                node(Node_Second,x,Y1,Z2); fix(Node_Second,1,1,1,1,1,1)
                X1=nodeCoord(Node)[0]; Y1=nodeCoord(Node)[1]; Z1=nodeCoord(Node)[2];
                Y1=Y1+d
                Node=Node+1
            D=nodeCoord(Main_node3)[1]-nodeCoord(Main_node2)[1]
            d=D/2/Ndivision
            dlist+=[d]
            for j in range(2*Ndivision):
                node(Node,x, Y1,Z1)
                Footing_Nodes+=[Node]
                Node_Second=int('20'+str(Node))
                node(Node_Second,x, Y1,Z2); fix(Node_Second,1,1,1,1,1,1)
                X1=nodeCoord(Node)[0]; Y1=nodeCoord(Node)[1]; Z1=nodeCoord(Node)[2];
                Y1=Y1+d
                Node=Node+1
            D=nodeCoord(Main_node4)[1]-nodeCoord(Main_node3)[1]
            d=D/2/Ndivision
            dlist+=[d]
            for j in range(2*Ndivision):
                node(Node,x, Y1,Z1)
                Footing_Nodes+=[Node]
                Node_Second=int('20'+str(Node))
                node(Node_Second,x, Y1,Z2); fix(Node_Second,1,1,1,1,1,1)
                X1=nodeCoord(Node)[0]; Y1=nodeCoord(Node)[1]; Z1=nodeCoord(Node)[2];
                Y1=Y1+d
                Node=Node+1
            D=nodeCoord(Main_node5)[1]-nodeCoord(Main_node4)[1]
            d=D/2/Ndivision
            dlist+=[d]
            for j in range(2*Ndivision):
                node(Node,x, Y1,Z1)
                Footing_Nodes+=[Node]
                Node_Second=int('20'+str(Node))
                node(Node_Second,x, Y1,Z2); fix(Node_Second,1,1,1,1,1,1)
                X1=nodeCoord(Node)[0]; Y1=nodeCoord(Node)[1]; Z1=nodeCoord(Node)[2];
                Y1=Y1+d
                Node=Node+1
            D=nodeCoord(Main_node6)[1]-nodeCoord(Main_node5)[1]
            d=D/2/Ndivision
            dlist+=[d]
            for j in range(2*Ndivision+1):
                node(Node,x, Y1,Z1)
                Footing_Nodes+=[Node]
```

```
                Node_Second=int('20'+str(Node))
                node(Node_Second,x, Y1,Z2); fix(Node_Second,1,1,1,1,1,1)
                X1=nodeCoord(Node)[0]; Y1=nodeCoord(Node)[1]; Z1=nodeCoord(Node)[2];
                Y1=Y1+d
                Node=Node+1
        for i in range(Ndivision):
                d1=B/2
                dx=d1/Ndivision
                x=nodeCoord(Main_node1)[0]+(i+1)*dx
                Y1=node1Y
                D=nodeCoord(Main_node2)[1]-nodeCoord(Main_node1)[1]
                d=D/(2*Ndivision)
                dlist+=[d]
                for j in range(2*Ndivision):
                    node(Node,x, Y1,Z1)
                    Footing_Nodes+=[Node]

                    Node_Second=int('20'+str(Node))
                    node(Node_Second,x, Y1,Z2); fix(Node_Second,1,1,1,1,1,1)

                    X1=nodeCoord(Node)[0]; Y1=nodeCoord(Node)[1];
                    Z1=nodeCoord(Node)[2];
                    Y1=Y1+d
                    Node=Node+1

                D=nodeCoord(Main_node3)[1]-nodeCoord(Main_node2)[1]
                d=D/2/Ndivision
                dlist+=[d]
                for j in range(2*Ndivision):
                    node(Node,x, Y1,Z1)
                    Footing_Nodes+=[Node]

                    Node_Second=int('20'+str(Node))
                    node(Node_Second,x, Y1,Z2); fix(Node_Second,1,1,1,1,1,1)

                    X1=nodeCoord(Node)[0]; Y1=nodeCoord(Node)[1];
                    Z1=nodeCoord(Node)[2];
                    Y1=Y1+d
                    Node=Node+1

                D=nodeCoord(Main_node4)[1]-nodeCoord(Main_node3)[1]
                d=D/2/Ndivision
                dlist+=[d]
                for j in range(2*Ndivision):
                    node(Node,x, Y1,Z1)
                    Footing_Nodes+=[Node]

                    Node_Second=int('20'+str(Node))
                    node(Node_Second,x, Y1,Z2); fix(Node_Second,1,1,1,1,1,1)

                    X1=nodeCoord(Node)[0]; Y1=nodeCoord(Node)[1];
                    Z1=nodeCoord(Node)[2];
                    Y1=Y1+d
                    Node=Node+1

                D=nodeCoord(Main_node5)[1]-nodeCoord(Main_node4)[1]
                d=D/2/Ndivision
                dlist+=[d]
                for j in range(2*Ndivision):
                    node(Node,x, Y1,Z1)
                    Footing_Nodes+=[Node]

                    Node_Second=int('20'+str(Node))
                    node(Node_Second,x, Y1,Z2); fix(Node_Second,1,1,1,1,1,1)

                    X1=nodeCoord(Node)[0]; Y1=nodeCoord(Node)[1];
                    Z1=nodeCoord(Node)[2];
```

```
                        Y1=Y1+d
                        Node=Node+1

                    D=nodeCoord(Main_node6)[1]-nodeCoord(Main_node5)[1]
                    d=D/2/Ndivision
                    dlist+=[d]
                    for j in range(2*Ndivision+1):
                        node(Node,x, Y1,Z1)
                        Footing_Nodes+=[Node]

                        Node_Second=int('20'+str(Node))
                        node(Node_Second,x, Y1,Z2); fix(Node_Second,1,1,1,1,1,1)

                        X1=nodeCoord(Node)[0]; Y1=nodeCoord(Node)[1];
                        Z1=nodeCoord(Node)[2];
                        Y1=Y1+d
                        Node=Node+1

    ###########################################################################
    #####------------------------ Add Springs -------------------------------#####
    ###########################################################################

        if soiltype=='clay': # qzType = 1 Backbone of q-z curve approximates Reese and
        O'Neill's (1987) relation for drilled shafts in clay.
            qzType=1
            kfar=0.525
            Ce=0.708 # for T-Z
            Ce_Py=8  # for P-Y
        elif soiltype=='sand': # qzType = 2 Backbone of q-z curve approximates
        Vijayvergiya's (1977) relation for piles in sand.
            qzType=2
            kfar=1.39
            Ce=2.05 # for T-Z
            Ce_Py=0.542 # for P-Y

    ###########################################################################
    #####-------------- Add QZ and TZ springs at the cornor nodes-------------###
    ###########################################################################
        '''
        B is parallel to X
        L is parallel to Y
        stiffness of B works when the translation is parallel to Y
        stiffness of L works when the translation is parallel to X
        '''
        kz=kz/B/L
        Kf=Kf_B/B/L
        Kf_L=Kf_L/B/L
        # Kel_py=Kel_py/B

        Q=0
        friction=0
        dy=abs(nodeCoord(node1)[1]-nodeCoord(node1+1)[1])


        # find Qult for the nodes @ cornors, and (ki=kz*tributary area)
        Qult_corner=qult*0.5*dx*0.5*dy # force at the cornor springs
        # print('dx*dy=',dx,dy)


        ki=kz*0.5*dx*0.5*dy  # add the material
        Z50=kfar*Qult_corner/ki      # add the material
        matTagQZ=footTag+50000                  # add the material
        uniaxialMaterial('QzSimple1', matTagQZ, qzType, Qult_corner, Z50,0.1,0)  # add
        the material


        Qsliding=(Qf)*0.5*dx*0.5*dy   # adding T-Z springs
```

```
254         Ksliding=(Kf)*0.5*dx*0.5*dy  # adding T-Z springs
255         Z50_sliding=Ce*Qsliding/Ksliding           # adding T-Z springs
256         matTagTZ=footTag+51000                  # add the material
257         uniaxialMaterial('TzSimple1', matTagTZ, qzType, Qsliding,Z50_sliding)
258         friction+=Qsliding
259
260
261         # add zero length element @ the corner nodes
262         eleTag=node1+5*10**5
263         for i in
            (node1,node1+10*Ndivision,node1+(10*Ndivision+1)*(2*Ndivision+1)-1-10*Ndivision,n
            ode1+(10*Ndivision+1)*(2*Ndivision+1)-1):
264
265             node_i=int('20'+str(i))
266             # print('node_j=',i)
267             node_j=i
268
                element('zeroLength',eleTag,node_i,node_j,'-mat',matTagTZ,matTagTZ,matTagQZ,'
                -dir',1,2,3)
269             # print('Qult_corner,',eleTag,'=',Qult_corner)
270             Q+=Qult_corner
271             eleTag+=1
272     ##########################################################################
273     #####-------------- Add QZ and TZ springs at the side nodes--------------######
274     ##########################################################################
275
276         Side_Nodes=[]
277         for i in range (node1+1, node1+10*Ndivision):
278             Side_Nodes+=[i]
279         for i in range
            (node1+(10*Ndivision+1)*(2*Ndivision+1)-10*Ndivision,node1+(10*Ndivision+1)*(2*Nd
            ivision+1)-1):
280             Side_Nodes+=[i]
281
282         for i in Side_Nodes:
283
                dy=(abs(nodeCoord(i)[1]-nodeCoord(i-1)[1])+abs(nodeCoord(i)[1]-nodeCoord(i+1)
                [1]))*0.5
284             # print(i,',dx*dy=',dx,'*',dy)
285             # print(abs(nodeCoord(i)[0]-nodeCoord(i-1)[0]))
286             # print(abs(nodeCoord(i)[0]-nodeCoord(i+1)[0]))
287             # find Qult for the nodes @ sides------ second layer
288             Qult_side=qult*dx*0.5*dy
289
290
291             ki=kz*dx*0.5*dy  # add the material
292             Z50=kfar*Qult_side/ki      # add the material
293
294             matTagQZ+=10000                 # add the material
295             uniaxialMaterial('QzSimple1', matTagQZ, qzType, Qult_side, Z50,0.1,0)  #
                add the material
296
297
298             Qsliding=(Qf)*dx*0.5*dy   # adding T-Z springs
299             Ksliding=(Kf)*dx*0.5*dy   # adding T-Z springs
300             Z50_sliding=Ce*Qsliding/Ksliding           # adding T-Z springs
301             matTagTZ+=10000                 # add the material
302             uniaxialMaterial('TzSimple1', matTagTZ, qzType, Qsliding,Z50_sliding)
303             friction+=Qsliding
304
305
306             # add zero length element @ the sides nodes
307
308             node_i=int('20'+str(i))
309             node_j=i
310
                element('zeroLength',eleTag,node_i,node_j,'-mat',matTagTZ,matTagTZ,matTagQZ,'
```

```
            -dir',1,2,3)
311         # print('Qult_side,',eleTag,'=',Qult_side)
312         Q+=Qult_side
313         eleTag+=1
314
315     ##########################################################################
316     #####---------- Add QZ and TZ springs at the internal nodes------------#####
317     ##########################################################################
318         for i in range (2*Ndivision-1):
319
320             start=node1+(10*Ndivision+1)*(1+i)
321             end=start+(10*Ndivision)
322
323             for i in range (start,end+1):
324                 if i==start:
325                     dy=abs(nodeCoord(i)[1]-nodeCoord(i+1)[1])*0.5
326                 elif i==end:
327                     dy=abs(nodeCoord(i)[1]-nodeCoord(i-1)[1])*0.5
328                 else:
329
                        dy=(abs(nodeCoord(i)[1]-nodeCoord(i-1)[1])+abs(nodeCoord(i)[1]-nodeCo
                        ord(i+1)[1]))*0.5
330
331
332                 # find Qult for the nodes @ middle
333                 Qult_middle=qult*dx*dy
334
335                 # print(i,',dx*dy=',dx,'*',dy)
336
337                 ki=kz*dx*dy  # add the material
338                 Z50=kfar*Qult_corner/ki      # add the material
339                 matTagQZ+=10000                 # add the material
340                 uniaxialMaterial('QzSimple1', matTagQZ, qzType, Qult_middle,
                    Z50,0.1,0)  # add the material
341
342                 Qsliding=(Qf)*dx*dy   # adding T-Z springs
343                 Ksliding=(Kf)*dx*dy   # adding T-Z springs
344                 Z50_sliding=Ce*Qsliding/Ksliding           # adding T-Z springs
345                 matTagTZ+=10000                  # add the material
346                 uniaxialMaterial('TzSimple1', matTagTZ, qzType, Qsliding,Z50_sliding)
347                 friction+=Qsliding
348
349
350                 # add zero length element @ the middle nodes
351                 node_i=int('20'+str(i))
352                 node_j=i
353
                    element('zeroLength',eleTag,node_i,node_j,'-mat',matTagTZ,matTagTZ,matTag
                    QZ,'-dir',1,2,3)
354                 # print('Qult_middle,',eleTag,'=',Qult_middle)
355                 Q+=Qult_middle
356                 eleTag+=1
357
358
359     ##########################################################################
360     #####---------------- Add PY springs at the side nodes--------------------#####
361     ##########################################################################
362         # print('Q=',Q)
363         # print('friction=',friction)
364         Kel_pyB=Kel_py_B/B
365         matTagPY=int('91'+str(node1))                  # add the material
366         for i in (node1,node1+(10*Ndivision+1)*(2*Ndivision+1)-1-10*Ndivision):
367             pult_Py=(Pult_Py)*(dx*0.5)    # adding P-Y springs
368
369             Kel_PY=(Kel_pyB)*(dx*0.5)    # adding P-Y springs
370             Y50_Py=Ce_Py*pult_Py/Kel_PY            # adding P-Y springs
371             matTagPY+=1
```

```
372             Cd_Py=0
373             uniaxialMaterial('PySimple1',matTagPY,qzType, pult_Py, Y50_Py, Cd_Py)
374             node_i=int('20'+str(i))
375             node_j=i
376             element('zeroLength',eleTag,node_i,node_j,'-mat',matTagPY,'-dir',2) # at
                the sides
377             eleTag+=1
378
379         Side_Nodes=[]
380         for i in range (2*Ndivision-1):
381             start=node1+(10*Ndivision+1)*(1+i)
382             Side_Nodes+=[start]
383
384         for i in (Side_Nodes):
385             pult_Py=(Pult_Py)*(dx)    # adding P-Y springs
386             Kel_PY=(Kel_pyB)*(dx)    # adding P-Y springs
387             Y50_Py=Ce_Py*pult_Py/Kel_PY           # adding P-Y springs
388             matTagPY+=1                 # add the material
389             Cd_Py=0
390             uniaxialMaterial('PySimple1',matTagPY,qzType, pult_Py, Y50_Py, Cd_Py)
391             node_i=int('20'+str(i))
392             node_j=i
393             element('zeroLength',eleTag,node_i,node_j,'-mat',matTagPY,'-dir',2) # at
                the sides
394             eleTag+=1
395
396
397     ################
398         Kel_pyL=Kel_py_L/L
399         for i in (node1,node1+10*Ndivision):
400             dx=dy
401             pult_Py=(Pult_Py)*(dy)    # adding P-Y springs
402             Kel_PY=(Kel_pyL)*(dy)    # adding P-Y springs
403             Y50_Py=Ce_Py*pult_Py/Kel_PY           # adding P-Y springs
404             matTagPY+=1                 # add the material
405             Cd_Py=0
406             uniaxialMaterial('PySimple1',matTagPY,qzType, pult_Py, Y50_Py, Cd_Py)
407             node_i=int('20'+str(i))
408             node_j=i
409             element('zeroLength',eleTag,node_i,node_j,'-mat',matTagPY,'-dir',1) # at
                the sides
410             eleTag+=1
411
412         Side_Nodes=[]
413         for i in range (node1+1, node1+10*Ndivision):
414             Side_Nodes+=[i]
415
416         for i in (Side_Nodes):
417
                dy=(abs(nodeCoord(i)[1]-nodeCoord(i-1)[1])+abs(nodeCoord(i)[1]-nodeCoord(i+1)
                [1]))*0.5
418             pult_Py=(Pult_Py)*(dy)    # adding P-Y springs
419             Kel_PY=(Kel_pyL)*(dy)    # adding P-Y springs
420             Y50_Py=Ce_Py*pult_Py/Kel_PY           # adding P-Y springs
421             matTagPY+=1                 # add the material
422             Cd_Py=0
423             uniaxialMaterial('PySimple1',matTagPY,qzType, pult_Py, Y50_Py, Cd_Py)
424             node_i=int('20'+str(i))
425             node_j=i
426             element('zeroLength',eleTag,node_i,node_j,'-mat',matTagPY,'-dir',1) # at
                the sides
427             eleTag+=1
428
429         # Springs_Elements=list(set(getEleTags())-set(Elements_Befor_Springs))
430     ##########################################################################
431     #######----------------- Add Rigid Beams between nodes ------------------######
432
```

```
#############################################################################
    FootingType='stiff'
    #  some parameters
    colWidth = max(dlist)
    colDepth = Hf

    if FootingType=='Flexible':
        # Define cross-section for nonlinear columns

        cover = 3
        As = AreaSteel*colWidth/3

        # some variables derived from the parameters
        y1 = colWidth / 2.0
        z1 = colDepth / 2.0

        J=element_length*Hf*(element_length**2+Hf**2)/12
        G=3795/2/1.2*ksi
        GJ=G*J
        secTag=footTag
        section('Fiber', secTag, '-GJ', GJ)
        # Create the concrete core fibers
        patch('rect', ConcreteTag, 10, 10, -y1, cover-z1, y1, z1)
        # Create the concrete cover fibers (top, bottom, left, right)
        patch('rect', ConcreteTag, 10, 1, -y1, -z1 , y1, z1-cover)
        # Create the reinforcing fibers (left, middle, right)
        layer('straight', SteelTag, 3, As, y1, -z1+cover, -y1, cover-z1)
        layer('straight', SteelTag, 3, As, y1, z1-cover, -y1, z1-cover)

        integrationTag=footTag
        beamIntegration('Legendre', integrationTag, secTag, 5)

    elif FootingType=='stiff':
        # add elastic beam column in the first direction
        Area=colWidth*colDepth
        E_mod=3650; G_mod=E_mod/2/1.2;
        Iy=(colWidth*colDepth**3)/12
        Iz=Iy;
        Jxx=Iy*2
        Avy=colWidth*colDepth
        Avz=colWidth*colDepth

    transfTag=20000+footTag
    vecxz=(0,0,1)
    geomTransf('Linear', transfTag, *vecxz)

    for i in range (2*Ndivision+1):
        start=node1+(10*Ndivision+1)*(i)
        end=start+(10*Ndivision)

        for i in range (start,end):
            eleTag=int('13'+str(i))
            i_node=i
            j_node=i_node+1
            eleNodes=(i_node,j_node)

            if FootingType=='Flexible':
                # numIntgrPts=5;
                # element('nonlinearBeamColumn', eleTag, *eleNodes, numIntgrPts,
                secTag, transfTag)
                element('dispBeamColumn', eleTag, *eleNodes, transfTag,
                integrationTag)

            elif FootingType=='stiff':
                element('ElasticTimoshenkoBeam', eleTag,*eleNodes, E_mod, G_mod,
                Area, Jxx, Iy, Iz, Avy, Avz, transfTag)
```

```
                    # element('elasticBeamColumn', eleTag, *eleNodes, Area, E_mod,
                    G_mod, Jxx, Iy, Iz, transfTag)
                eleTag+=1

        # add elastic beam column in the Second direction

        for i in range (10*Ndivision+1):
            start=node1+i
            end=start+(10*Ndivision+1)*(2*Ndivision)-(10*Ndivision+1)

            for i in range (start,end+1,10*Ndivision+1):

                i_node=i
                j_node=i_node+10*Ndivision+1
                eleNodes=(i_node,j_node)

                if FootingType=='Flexible':
                    # numIntgrPts=5;
                    # element('nonlinearBeamColumn', eleTag, *eleNodes, numIntgrPts,
                    secTag, transfTag)
                    element('dispBeamColumn', eleTag, *eleNodes, transfTag,
                    integrationTag)

                elif FootingType=='stiff':
                    element('ElasticTimoshenkoBeam', eleTag,*eleNodes, E_mod, G_mod,
                    Area, Jxx, Iy, Iz, Avy, Avz, transfTag)

                    # element('elasticBeamColumn', eleTag, *eleNodes, Area, E_mod,
                    G_mod, Jxx, Iy, Iz, transfTag)
                # rigidLink('beam', i_node, j_node)
                eleTag+=1

        eleTag+=1
        footTag=node1-1+(10*Ndivision+1)*(Ndivision)+1
        element('zeroLength', eleTag, footTag, Main_node1, '-mat',
        stiff,stiff,stiff,soft,soft,stiff , '-dir', 1,2,3,4,5,6)


        eleTag+=1
        footTag=node1-1+(10*Ndivision+1)*(Ndivision)+1+2*Ndivision
        element('zeroLength', eleTag, footTag, Main_node2, '-mat',
        stiff,stiff,stiff,stiff,soft,stiff , '-dir', 1,2,3,4,5,6)


        eleTag+=1
        footTag=node1-1+(10*Ndivision+1)*(Ndivision)+1+2*Ndivision*2
        element('zeroLength', eleTag, footTag, Main_node3, '-mat',
        stiff,stiff,stiff,stiff,soft,stiff , '-dir', 1,2,3,4,5,6)

        eleTag+=1
        footTag=node1-1+(10*Ndivision+1)*(Ndivision)+1+2*Ndivision*3
        element('zeroLength', eleTag, footTag, Main_node4, '-mat',
        stiff,stiff,stiff,stiff,soft,stiff , '-dir', 1,2,3,4,5,6)

        eleTag+=1
        footTag=node1-1+(10*Ndivision+1)*(Ndivision)+1+2*Ndivision*4
        element('zeroLength', eleTag, footTag, Main_node5, '-mat',
        stiff,stiff,stiff,stiff,soft,stiff , '-dir', 1,2,3,4,5,6)

        eleTag+=1
        footTag=node1-1+(10*Ndivision+1)*(Ndivision)+1+2*Ndivision*5
        element('zeroLength', eleTag, footTag, Main_node6, '-mat',
        stiff,stiff,stiff,soft,soft,stiff , '-dir', 1,2,3,4,5,6)

    ##########################################################################
    #######------------------- Add Rigid Diaphram  ----------------------######
    ##########################################################################
```

```
551         # print('Footing_Nodes=',Footing_Nodes)
552         Master_Node=[Footing_Nodes[0]]
553         Slave_Nodes=list(set(Footing_Nodes)-set(Master_Node))
554         perpDirn=3
555         rigidDiaphragm(perpDirn, Master_Node[0], *Slave_Nodes)
556     '''
557     set Q-Z materail for q-z spring
558     kz=Vertical Global Stiffness of the foundation for a unit subgrade reaction of the
        middle region, in units of
559     Force per unit Length (F/L)
560     '''
561
562     # example for using the routine
563     def soil_stiffness(B,L,c,Hf,Df,soil_density): # this routine is cosistent for
564                                                   # isolated and raft footing and has to be
565                                                   # called before calling the footing
                                                      routine
566                                                   # the stiffness quations is from
                                                      https://opensees.berkeley.edu/wiki/images/f
                                                      /fc/ShallowDocumentation.pdf

567         prop=dict()
568
569         E_soil=500*c # in kip/in^2
570         Poissons_ratio=0.5  # Assumed
571         G=E_soil/2/(1+Poissons_ratio)  # shear modulus
572
573
574         Kz_prime=G*L/(1-Poissons_ratio)*(0.73+1.54*(B/L)**0.75)
575
576         ez=(1+0.095*(Df/B)*(1+1.3*(B/L)))*(1+0.2*((2*L+2*B)*Hf/L/B)**0.67)  # H foundation
            thikness
577
578         Kz=Kz_prime*ez
579         prop['Kz']=(Kz)
580
581
582
            Ky_prime_B=G*L/(2-Poissons_ratio)*(2+2.5*(B/L)**0.85)+(G*L/(0.75-Poissons_ratio))*(0.
            1*(1-B/L))
583         ey_B=(1+0.15*(2*Df/L)**0.5)*(1+0.52*((Df-0.5*Hf)*16*(L+B)*Hf/(L*B**2))**0.4)
584
585         Ky_B=Ky_prime_B*ey_B
586         prop['Ky_B']=(Ky_B)
587
588         Ky_prime_L=G*L/(2-Poissons_ratio)*(2+2.5*(B/L)**0.85)
589         ey_L=(1+0.15*(2*Df/B)**0.5)*(1+0.52*((Df-0.5*Hf)*16*(L+B)*Hf/(B*L**2))**0.4)
590
591         Ky_L=Ky_prime_L*ey_L
592         prop['Ky_L']=(Ky_L)
593
594         Qf=c #force/Area
595         prop['Qf']=(Qf)
596
597         kp=1 # because friction angle= 0
598         P_passive=0.5*soil_density*kp*(Df**2-(Df-Hf)**2)
599         prop['P_passive']=(P_passive)
600         return prop
601
602     kip=1
603     inch=1
604     ft=1#12*inch
605     ksi=kip/inch**2
606     ksf=0.006944*ksi
607     m=39.37*inch
608
609     kN=0.225*kip
```

```
kPa=kN/m/m




Es=29000
E_stiff=Es*10**8
stiff=1
uniaxialMaterial('Elastic',stiff,E_stiff)
E_soft=0
soft=2
uniaxialMaterial('Elastic', soft, E_soft)

ConcreteTag=13; fpc=-4.5*ksi; epsc0=-0.004; fpcu=-3.5; epsU=-0.014
uniaxialMaterial('Concrete01', ConcreteTag, fpc, epsc0, fpcu, epsU)
# STEEL
# Reinforcing steel
fy = 60*ksi;  # Yield stress
E = 29000*ksi;  # Young's modulus
SteelTag=14
uniaxialMaterial('Steel01', SteelTag, fy, E, 0.01)
AreaSteel=0.3*in2/inch



# Main_node1=6;           Main_node2=7;          Main_node3=8;            Main_node4=9;
#
node(Main_node1,0,0,15*ft);node(Main_node2,0,30*ft,15*ft);node(Main_node3,60*ft,0,15*ft);
node(Main_node4,0,90*ft,15*ft);

Main_node1=2;           Main_node2=3;              Main_node3=4;
Main_node4=5;             Main_node5=6;           Main_node6=7
node(Main_node1,0,0,0);node(Main_node2,0,20*ft,0);node(Main_node3,0,40*ft,0);node(Main_no
de4,0,60*ft,0);node(Main_node5,0,80*ft,0);node(Main_node6,0,100*ft,0)

footTag=1
Ndivision=2
Df=88*inch
Hf=88*inch
c=110*kPa # undrained shear strength
soil_density=120*kN/m/m/m
soiltype='clay'

B=int(15*ft);qult=11.203*ksf
L=int(2*B+nodeCoord(Main_node4)[1]-nodeCoord(Main_node1)[1])
Prop=soil_stiffness(B,L,c,Hf,Df,soil_density)
print('soil_stiffness=',Prop)
kz=Prop['Kz']; Qf=Prop['Qf']; Kf_L=Prop['Ky_L'];Kf_B=Prop['Ky_B'];
Pult_Py=Prop['P_passive']; Kel_py_L=Prop['Ky_L'];Kel_py_B=Prop['Ky_B'];
Combined_Footing_BRB(footTag,B,L,Ndivision,qult,kz,soiltype,Qf,Kf_L,Kf_B ,Pult_Py,
Kel_py_L,Kel_py_B,Main_node1,Main_node2,Main_node3,Main_node4,Main_node5,Main_node6,stiff
,soft,Hf)
################################################################################

fig = plt.figure()                  # ploting the nodes to be sure of numbering
ax = fig.add_subplot(1,1,1)
#ax = plt.axes(projection='3d')
plt.ylim(0, 100*ft)
plt.xlim(-B/2,B/2)
# plt.ylabel('West (y)')
for nodes in (getNodeTags()):              # for adding the nodes number
    Node_Coord=nodeCoord(nodes)
    if Node_Coord[2]==0:
        plt.plot(Node_Coord[0], Node_Coord[1],marker='o')
        plt.text(Node_Coord[0], Node_Coord[1], str(nodes)) #label elements


```

```
plt.show()

# ##############################################################################


# transfTag=22
# vecxz=(-1,0,0)
# geomTransf('Linear', transfTag, *vecxz)

# Area=10; E_mod=29000*10**3; G_mod=11500; Jxx=10; Iy=2500; Iz=2500


# element('elasticBeamColumn', 1, 2,6, Area, E_mod, G_mod, Jxx, Iy, Iz, transfTag)
# element('elasticBeamColumn', 2, 3,7, Area, E_mod, G_mod, Jxx, Iy, Iz, transfTag)
# element('elasticBeamColumn', 3, 4,8, Area, E_mod, G_mod, Jxx, Iy, Iz, transfTag)
# element('elasticBeamColumn', 4, 5,9, Area, E_mod, G_mod, Jxx, Iy, Iz, transfTag)

# Display Model
plot_model()


# apply the load
timeSeries('Linear', 1)
pattern('Plain', 1, 1)
#--- add load
Load=-20164.1/4;Direction=3
loadValues=(0,0,Load,0,0,0)
load(Main_node1, *loadValues)
load(Main_node2, *loadValues)
load(Main_node3, *loadValues)
load(Main_node4, *loadValues)
####################################################
createODB("footingTest","test1")

# Define Static Analysis
constraints('Transformation')
# constraints('Penalty', 10**14, 10**14)
numberer('RCM')         # renumber dof's to minimize band-width (optimization), if you want to
system('UmfPack')       # how to store and solve the system of equations in the analysis (large model: try UmfPack)
#test('EnergyIncr', 1.0e-10, 100)       # determine if convergence has been achieved at the end of an iteration step
test('NormDispIncr', 1.0e-5, 70)
# test('RelativeEnergyIncr',1.0e-7,30,1)
#test('RelativeNormDispIncr', 1.0e-10,10000,1)
algorithm('RaphsonNewton')          # use Newton's solution algorithm: updates tangent stiffness at every iteration

NstepsGrav=100
integrator('LoadControl', 1/NstepsGrav) # determine the next time step for an analysis
analysis('Static')

# perform the analysis

# data = np.zeros((NstepsGrav+1,2))

Applied_Load=[]
u=[]
for j in range(NstepsGrav):
    analyze(1)
    # data[j+1,0] = nodeDisp(nodeTag1,2)
    # data[j+1,1] = getLoadFactor(1)*Load

    u.append(-nodeDisp(Main_node2,Direction))
    Applied_Load.append(-getLoadFactor(1)*Load*4)
# print('data=',data)
```

```
734
735 plt.plot(u,Applied_Load)
736 plt.xlabel('Horizontal Displacement of node 1 (in)')
737 plt.ylabel('Applied_Load')
738
739 plt.show()
740 # print('Applied_Load=',Applied_Load)
741
742 print('Node ',Main_node1,'=',[round(num, 2) for num in nodeDisp(Main_node1)])
743 print('Node ',Main_node2,'=',[round(num, 2) for num in nodeDisp(Main_node2)])
744 print('Node ',Main_node3,'=',[round(num, 2) for num in nodeDisp(Main_node3)])
745 print('Node ',Main_node4,'=',[round(num, 2) for num in nodeDisp(Main_node4)])
746
747 # print(Springs_Elements)
748 # for i in (Springs_Elements):
749 #     print('column',i,'=',[round(num, 2) for num in eleForce(i)])
750 wipeAnalysis()
751 wipe()
```

Appendix C: Pile foundation modeling routine

```
# -*- coding: utf-8 -*-
"""
Created on Wed Dec 16 12:48:52 2020

@author: Humam Al-Ghabawi
"""
import openseespy.opensees as ops
import openseespy.postprocessing.ops_vis as opsv
import matplotlib.pyplot as plt
from openseespy.postprocessing.Get_Rendering import *
from openseespy.opensees import *
import numpy as np
from IPython.core.pylabtools import figsize
from units_Version2 import *
from footing2 import *
from math import *
from modal2 import *
from nonlinear_fiber_section import*
wipe()
model('Basic', '-ndm', 3, '-ndf', 6)
figsize(7,7);
def NodeTag(Node):
    All_Nodes=getNodeTags()
    if Node not in All_Nodes:
        Inode=Node
    else:
        for i in range (10000000):
            Node+=1
            if Node not in All_Nodes:
                Inode=Node
                break
    return Inode

def EleTag(Element):
    All_Ele=getEleTags()
    if Element not in All_Ele:
        Ele=Element
    else:
        for i in range (10000000):
            Element+=1
            if Element not in All_Ele:
                Ele=Element
                break
    return Ele

def TZ(c,density,depth):
    Overburden=depth*density
    Psi=c/Overburden
    if Psi<=1:
        Alpha=0.5*Psi**(-0.5)
    if Psi>1:
        Alpha=0.5*Psi**(-0.25)
    TZ=Alpha*c
    return TZ

def Piles(ShaftTag,Node_Master,L2,nElePile,qult_Qz,z50_Qz, qult_Tz,z50_Tz, density,
Y50_Py,c,transfTag, d,Loction):#,ColMatTagAxial):
    first_Layer_Nodes=[]
    second_Layer_Nodes=[]
    LateralForce=0
    XCoord=nodeCoord(Node_Master)[0]
    YCoord=nodeCoord(Node_Master)[1]
    ZCoord=nodeCoord(Node_Master)[2]
    Node=Node_Master
    NodeS=NodeTag(Node)
    node(NodeS, XCoord, YCoord, ZCoord)
    first_Layer_Nodes+=[Node_Master]
```

```
        second_Layer_Nodes+=[NodeS]
        #-------------------------------------------------------
        #  pile geometry and mesh
        #-------------------------------------------------------
        # pile element length
        eleSize = (L2)/nElePile
        # print('eleSize=',eleSize)
        # number of total pile nodes
        nNodePile =  1 + nElePile
        for i in range(2,nNodePile+1):
            zCoord = eleSize * (i-1)
            # print('zCoord=',zCoord)
            if zCoord <= L2:
                NodeF=NodeTag(Node)
                node(NodeF, XCoord, YCoord, ZCoord-zCoord)
                first_Layer_Nodes+=[NodeF]

                NodeS=NodeTag(Node)
                node(NodeS, XCoord, YCoord, ZCoord-zCoord)
                second_Layer_Nodes+=[NodeS]

        # spring node fixities
        for i in (second_Layer_Nodes):
            fix(i, 1,1,1, 1,1,1)
        ##########################################################################
        #####------------ Adding Springs to the Toe, Qz & Py ------------#########
        ##########################################################################
        matTagQz=int('110'+str(ShaftTag)+str(Loction))
        uniaxialMaterial('QzSimple1', matTagQz, 2, qult_Qz, z50_Qz) #, 0.0, 0.0
        EleTag(ShaftTag)
        eleTag=EleTag(ShaftTag) #int('33'+str(ShaftTag)+'00')
        Inode=second_Layer_Nodes[nElePile]
        Jnode=first_Layer_Nodes[nElePile]
        matTagPy=int(str(Loction)+'220'+str(ShaftTag))
        Depth=abs(nodeCoord(Inode)[2])
        Np=min(9,(3+density*Depth/c+0.5*Depth/d))
        pult_Py1=Np*c*d
        Depth=abs(nodeCoord(Inode)[2])-eleSize/2
        Np=min(9,(3+density*Depth/c+0.5*Depth/d))
        pult_Py2=Np*c*d
        pult_Py=(pult_Py1+pult_Py2)/2*eleSize/2
        # pult_Py=density*Depth*d*eleSize/2
        # print('pult_PyToe=',pult_Py)
        # print('density*Depth*d*eleSize1 Toe=',density,Depth,d,eleSize/2)
        uniaxialMaterial('PySimple1', matTagPy, 2, pult_Py, Y50_Py, 1)
        LateralForce+=pult_Py
        element('zeroLength', eleTag, Inode,Jnode , '-mat', matTagPy,matTagPy,matTagQz,
        '-dir', 1,2,3)
        ##########################################################################
        #####------- Adding Springs to the other nodes, Tz & Py ------------######
        ##########################################################################
        matTagPy=int(str(Loction)+str(ShaftTag)+'2210')
        matTagTz=int(str(Loction)+str(ShaftTag)+'5500')
        # uniaxialMaterial('TzSimple1', matTagTz, 2, qult_Tz*eleSize, z50_Tz, 0.0)
        for i in range (1,nNodePile-1):
            eleTag+=1
            eleTag=EleTag(eleTag)
            Inode=second_Layer_Nodes[i]
            Jnode=first_Layer_Nodes[i]
            matTagPy+=1
            Depth=abs(nodeCoord(Inode)[2])+eleSize/2
            Np=min(9,(3+density*Depth/c+0.5*Depth/d))
            pult_Py1=Np*c*d
            qult_Tz1=TZ(c,density,Depth)
            Depth=abs(nodeCoord(Inode)[2])-eleSize/2
            Np=min(9,(3+density*Depth/c+0.5*Depth/d))
            pult_Py2=Np*c*d
```

```
            qult_Tz2=TZ(c,density,Depth)
            pult_Py=(pult_Py1+pult_Py2)/2*eleSize
            # pult_Py=density*Depth*d*eleSize
            # print('pult_Py2=',pult_Py)
            # print('density*Depth*d*eleSize2=',density,Depth,d,eleSize)
            uniaxialMaterial('PySimple1', matTagPy, 2, pult_Py, Y50_Py, 1)
            LateralForce+=pult_Py
            matTagTz+=1
            qult_Tz=(qult_Tz1+qult_Tz2)/2*(d*4)
            uniaxialMaterial('TzSimple1', matTagTz, 2, qult_Tz*eleSize, z50_Tz, 0.0)
            element('zeroLength', eleTag, Inode,Jnode , '-mat', matTagPy,matTagPy,matTagTz,
            '-dir', 1,2,3)
        ########################################################################
        #####------- Adding Springs to the top node, Tz & Py ------------######
        ########################################################################
        matTagPy=int(str(Loction)+'251'+str(ShaftTag))
        Depth=abs(nodeCoord(Node)[2])
        Np=min(9,(3+density*Depth/c+0.5*Depth/d))
        pult_Py1=Np*c*d
        # qult_Tz1=TZ(c,density,Depth)
        Depth=abs(nodeCoord(Node)[2])+eleSize/2
        Np=min(9,(3+density*Depth/c+0.5*Depth/d))
        pult_Py2=Np*c*d
        qult_Tz2=TZ(c,density,Depth)
        pult_Py=(pult_Py1+pult_Py2)/2*eleSize/2
        # pult_Py=density*Depth*d*eleSize/2
        # print('pult_Py3=',pult_Py)
        # print('density*Depth*d*eleSize3=',density,Depth,d,eleSize/2)
        uniaxialMaterial('PySimple1', matTagPy, 2, pult_Py, Y50_Py, 1)
        LateralForce+=pult_Py
        matTagTz=int(str(Loction)+'560'+str(ShaftTag))
        qult_Tz=(qult_Tz2+qult_Tz2)/2*(d*4)
        uniaxialMaterial('TzSimple1', matTagTz, 2, qult_Tz*eleSize, z50_Tz, 0.0)
        eleTag+=1
        eleTag=EleTag(eleTag)
        Inode=second_Layer_Nodes[0]
        Jnode=first_Layer_Nodes[0]
        element('zeroLength', eleTag, Inode,Jnode, '-mat', matTagPy,matTagPy,matTagTz,
        '-dir', 1,2,3)
        # print('LateralForce=',LateralForce)
        ########################################################################
        #####-------------- Adding Drilled Shaft elements ------------------######
        ########################################################################
        FootingType='stiff'
        eleTag=int('454'+str(ShaftTag)+'00')
        Area=d*d
        E_mod=3650; G_mod=E_mod/2/1.2;
        Iy=(d*d**3)/12
        Iz=Iy;
        Jxx=Iy*2
        Avy=d*d
        Avz=d*d
        eleTag=int('454'+str(ShaftTag)+'00')
        for i in range (nElePile):
            eleTag=EleTag(eleTag)
            Inode=first_Layer_Nodes[i]
            Jnode=first_Layer_Nodes[i+1]

            if FootingType=='Flexible':
                Wfiber_section_3D(eleTag,ColMatTagAxial,d,tw,bf,tf,G,J,transfTag,Inode,Jnode)
            elif FootingType=='stiff':
                element('ElasticTimoshenkoBeam', eleTag, Inode,Jnode , E_mod, G_mod, Area,
                Jxx, Iy, Iz, Avy, Avz, transfTag)
                # element('elasticBeamColumn', eleTag, Inode,Jnode , Area, E_mod, G_mod,
                Jxx, Iy, Iz, transfTag)
            eleTag+=1
        # print('first_Layer_Nodes=',first_Layer_Nodes)
```

```
    # print('second_Layer_Nodes=',second_Layer_Nodes)
    fix(first_Layer_Nodes[nElePile], 0,0,0, 0,0,1)


def PileGroup(PileCapTag,Node_Master,B, L2,nElePile,qult_Qz,z50_Qz, qult_Tz,z50_Tz,
density, Y50_Py,c,d,stiff,soft):#,ColMatTagAxial):
#################################################################################
#####----------------- Adding the pile Cap nodes ----------------------######
#################################################################################
    PileCapNodes=[]
    NumPile=3 #Number of piles in one row
    segmant_length=B/(NumPile-1)

    for i in range (NumPile):
        for j in range (NumPile):
            PileNode=NodeTag(Node_Master)
            XCoord=nodeCoord(Node_Master)[0]-B/2+segmant_length*j
            YCoord=nodeCoord(Node_Master)[1]-B/2+segmant_length*i
            ZCoord=nodeCoord(Node_Master)[2]
            node(PileNode, XCoord, YCoord, ZCoord)
            PileCapNodes+=[PileNode]
            if XCoord==nodeCoord(Node_Master)[0] and YCoord==nodeCoord(Node_Master)[1]:
                mainNode=PileNode
                # print('mainNode=',mainNode)
#################################################################################
#####----------------- Adding the pile Cap Beams ----------------------######
#################################################################################
    E_mod=3734; G_mod=11500; Jxx=100;
    Area=segmant_length*48
    Iy=(segmant_length*48**3)/12
    Iz=Iy
    transfTag=5353+PileCapTag
    vecxz=(0,0,1)
    geomTransf('Linear', transfTag, *vecxz)
    eleTag=PileCapTag

    for i in range (NumPile): # Adding Beams parrallel to X axis
        for j in range (NumPile-1):
            ID=i*NumPile+j
            i_node=PileCapNodes[ID]
            j_node=PileCapNodes[ID+1]
            eleTag=EleTag(PileCapTag)
            eleNodes=(i_node,j_node)
            element('elasticBeamColumn', eleTag, *eleNodes, Area, E_mod, G_mod, Jxx,
            Iy, Iz, transfTag)
            eleTag+=1

    for i in range (NumPile): # Adding Beams parrallel to Y axis
        for j in range (NumPile-1):
            ID=j*NumPile+i
            i_node=PileCapNodes[ID]
            j_node=PileCapNodes[ID+NumPile]
            eleTag=EleTag(PileCapTag)
            eleNodes=(i_node,j_node)
            element('elasticBeamColumn', eleTag, *eleNodes, Area, E_mod, G_mod, Jxx,
            Iy, Iz, transfTag)
            eleTag+=1

#################################################################################
#####----------------------- Adding the piles -------------------------######
#################################################################################
    transfTag=333+PileCapTag
    geomTransf('Linear', transfTag, 1,0,0)
    NumPile=3
    if NumPile==3:
        for i in range(NumPile*NumPile):
            NodeMaster=PileCapNodes[i]
```

```
            Piles(PileCapTag,NodeMaster,L2,nElePile,qult_Qz,z50_Qz, qult_Tz,z50_Tz,
            density, Y50_Py,c,transfTag, d,i)#,ColMatTagAxial)

    elif NumPile==2:
        NodeMaster=PileCapNodes[0]
        Piles(PileCapTag,NodeMaster,L2,nElePile,qult_Qz,z50_Qz, qult_Tz,z50_Tz,
        density, Y50_Py,c,transfTag, d,1)#,ColMatTagAxial)

        NodeMaster=PileCapNodes[2]
        Piles(PileCapTag,NodeMaster,L2,nElePile,qult_Qz,z50_Qz, qult_Tz,z50_Tz,
        density, Y50_Py,c,transfTag, d,2)

        NodeMaster=PileCapNodes[6]
        Piles(PileCapTag,NodeMaster,L2,nElePile,qult_Qz,z50_Qz, qult_Tz,z50_Tz,
        density, Y50_Py,c,transfTag, d,3)

        NodeMaster=PileCapNodes[8]
        Piles(PileCapTag,NodeMaster,L2,nElePile,qult_Qz,z50_Qz, qult_Tz,z50_Tz,
        density, Y50_Py,c,transfTag, d,4)
##############################################################################
#####---------- Connect the structure with the Drilled Shaft ----------######
##############################################################################
    eleTag=EleTag(eleTag)
    element('zeroLength', eleTag, mainNode,Node_Master,
    '-mat',stiff,stiff,stiff,stiff,soft,stiff , '-dir',1,2,3,4,5,6)
    # element('zeroLength', eleTag, mainNode,Node_Master,
    '-mat',stiff,stiff,stiff,stiff,stiff,stiff , '-dir',1,2,3,4,5,6)
    ##############################################################################
    #######------------------- Add Rigid Diaphram  ----------------------######
    ##############################################################################
    Master_Node=[mainNode]
    Slave_Nodes=list(set(PileCapNodes)-set(Master_Node))
    perpDirn=3
    rigidDiaphragm(perpDirn, Master_Node[0], *Slave_Nodes)

##############################################################################
#####------------------ example of using the routine. ------------------######
##############################################################################
Es=29000
E_stiff=Es*10**8
stiff=1
uniaxialMaterial('Elastic',stiff,E_stiff)
E_soft=0
soft=2
uniaxialMaterial('Elastic', soft, E_soft)

Node_Master=7
node(Node_Master, 0, 0, 0)
PileCapTag=1;B=150*inch

transfTag=333
geomTransf('Linear', transfTag, 1,0,0)

c=0.016
L2=31*ft;d=30*inch; nElePile=22;
qult_Qz=(9*c*d**2)*kip; z50_Qz=0.013*d#0.008*d
qult_Tz=(0.5*c*d*4); z50_Tz=0.0031*d #0.025
Y50_Py=2.5*0.005*d
density=110*pcf

PileGroup(PileCapTag,Node_Master,B, L2,nElePile,qult_Qz,z50_Qz, qult_Tz,z50_Tz,
density, Y50_Py,c, d,stiff,soft)
# Piles(PileCapTag,Node_Master,L2,nElePile,qult_Qz,z50_Qz, qult_Tz,z50_Tz, density,
Y50_Py,c,transfTag, d,1)
plot_model()
```

```
# apply the load
timeSeries('Linear', 1)
pattern('Plain', 1, 1)

Load=2106*2;Direction=3
if Direction==1:
    loadValues=(Load,0,0, 0,0,0)
elif Direction==2:
    loadValues=(0,Load,0, 0,0,0)
elif Direction==3:
    loadValues=(0,0,Load, 0,0,0)
elif Direction==4:
    loadValues=(0,0,0, Load,0,0)
elif Direction==5:
    loadValues=(0,0,0, 0,Load,0)
elif Direction==6:
    loadValues=(0,0,0, 0,0,Load)

loadValues=(0,159.65*2,-2106*2,-4493.44*2,0,0)
load(Node_Master, *loadValues)
# fix(Node_Master,0, 1,1,1,1,1)
#####################################################
createODB("Pile","test1")
# Define Static Analysis
constraints('Transformation')
# constraints('Penalty', 10**14, 10**14)
numberer('RCM')          # renumber dof's to minimize band-width (optimization), if you want to
system('SparseGeneral')     # how to store and solve the system of equations in the analysis (large model: try UmfPack)
#test('NormDispIncr', 0.0001, 100)
test('NormDispIncr',1.0e-4, 50)   #test('NormDispIncr', 1e-9, 100)
#test('EnergyIncr', 1.0e-10, 100)       # determine if convergence has been achieved at the end of an iteration step
algorithm('ModifiedNewton')
#algorithm('NewtonLineSearch')          # use Newton's solution algorithm: updates tangent stiffness at every iteration
#set NstepGravity 10;       # apply gravity in 10 steps
#set DGravity [expr 1./$NstepGravity];  # first load increment;

NstepsGrav=100
integrator('LoadControl', 1/NstepsGrav) # determine the next time step for an analysis
analysis('Static')

Applied_Load=[]
u=[]
for j in range(NstepsGrav):
    ok=analyze(1)
    # data[j+1,0] = nodeDisp(nodeTag1,2)
    # data[j+1,1] = getLoadFactor(1)*Load
    u.append(nodeDisp(Node_Master,Direction))
    Applied_Load.append(getLoadFactor(1)*Load)
# print('data=',data)
# print('Applied_Load=',Applied_Load)
plt.plot(u,Applied_Load)
plt.xlabel('Horizontal Displacement of node 1 (in)')
plt.ylabel('Applied_Load')
plt.show()
plot_model("nodes")
print('nodeDisp(Node,Direction)=',nodeDisp(Node_Master))
wipe()
plot_deformedshape(Model="Pile",LoadCase="test1", tstep=2.0, scale=100, overlap="yes")

```